STUDIES ON SOME LARGE PORE ZEOLITES : SYNTHESIS, MODIFICATION AND CHARACTERIZATION

A Thesis Submitted to
UNIVERSITY OF PUNE
for the degree of
DOCTOR OF PHYLOSOPHY
(IN CHEMISTRY)

BY
R. A. ABDULLA
CATALYSIS DIVISION
NATIONAL CHEMICAL LABORATORY
PUNE - 411 008, INDIA

MAY 1998

TO MY

BELOVED PARENTS
AND
GRANDMOTHER

CETRTIFICATE

Certified that the work incorporated in the thesis entitled "Studies on some large pore zeolites : Synthesis , modification and Characterization " submitted by Smt. Mohammad Rakhshan. A. Abdulla , for the degree of Doctor of Philosophy was carried out by the candidate under my supervision in the National Chemical Laboratory , Pune. Such material as has been obtained from other sources has been duly acknowledged in the thesis.

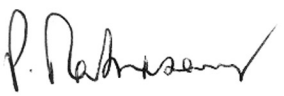

Dr. P. Ratnasamy
(Research Guide)

ACKNOWLEDGEMENT

I would like to express my gratitude to my research guide Dr. P. Ratnasamy for his valuable guidance and most of all for providing me an opportunity to work at NCL.

I am deeply indebted to Dr. S. G. Hegde for his stimulating discussions, selfless dedication as well as constant professional help. I am equally indebted to Dr. S. Sivasankar for his valuable guidance, cooperation and constant moral support, which gave me the necessary inspiration to fulfil my task. Without their support it would have been impossible for me to complete my research work successfully.

I take this opportunity to thank Dr. B. S. Rao, Dr. (Mrs) A. J. Chandwadkar, Dr. R. N. Bhat and Dr. Prabhat Singh for their cooperation and help. I sincerely thank Prof. Gore, Mr. D. P. Sabde and Mr. Satish Kuriyavar for their whole-hearted cooperation and help that made it possible to complete my research work. I am also thankful to Mr. K. Ramakrishnan, and Mr. T. A. B. Mulla for their assistance and all members of the catalysis division for their willingness to help whenever required.

My most heartfelt thanks are due to aunty and uncle Iqbal for their encouragement and help. Those who have helped me in different ways are far too numerous to mention by name but I would like them to accept my sincere thanks. I am also indebted to my parents and all my family members for their cooperation and encouragement.

My special word of thanks is due to my husband for his whole-hearted encouragement and cooperation. I sincerely thank Dr. A. V. Ramaswamy, Head - Catalysis Division and Dr. P. Ratnasamy, Director - National Chemical Laboratory for allowing me to submit this work in the form of a thesis.

ANJUM

CONTENTS

CHAPTER -1

GENERAL INTRODUCTION

CHAPTER I

GENERAL INTRODUCTION

1 . 1 INTRODUCTION :

Zeolites form an extraordinary, diverse and interesting class of inorganic polymers. They have continued to fascinate scientists for decades due to the immense opportunities they offer for research. They have benefitted the chemical industry equally, in numerous ways. Recently, their range of application has widened considerably, more noticeably as heterogeneous catalysts, catalyzing a number of organic reactions.

Zeolites are crystalline hydrated alumino-silicates, possessing a rigid framework based on an infinitely extending three-dimensional network of SiO_4 and AlO_4 tetrahedra , linked through oxygen atoms. Within this framework are present well-defined channels and cavities of specific dimensions rendering them microporous. The negative charge on the AlO_4 tetrahedron is compensated by cations, resulting in an electrically neutral framework. The crystallographic unit cell of a zeolite may be represented as $M_{2x/n}\{(Al_2O_3)_x.(SiO_2)_4\}.zH_2O$, where `M' represents exchangeable cation of `n' valency generally from group I or II, rare earth ions or an organic species and `z' gives the number of water molecules[1,2] .

Zeolites are classified according to their morphological characteristics[3,4,5,6], crystal structure[3,4,7] (Table 1.1) , effective pore diameter[3,4,8], chemical composition[3,4,9] and natural occurrence[3,4] :

The primary building unit (PBU) of the zeolite structure is a tetrahedron of four oxygen atoms surrounding a central Si or Al atom. These tetrahedra are connected

TABLE 1.1 : Classification of Zeolites according to structure type .

Sl. No.	Structure type	Main species	Iso structural species
1.	Analcime group : (interconnected 4- and 6– membererd rings)	Analcime	Leucite, Pollucite, Viseite, Wairakite.
2.	Natrolite group : (4-1 membered rings)	Natrolite	Laubanite, Mesolite, Metanatrolite
3.	Chabazite group : (parallel 6 - or double 6 – membered rings)	Chabazite	Linde D, herschelite, Linde R
4.	Phillipsite group : (approximately parallel 4 – membered rings)	Phillipsite	Harmotome, ZK - 19, Na - P_1 , Linde W
5.	Heulandite group : (characteristic configuration with 4 -5 membered rings)	Heulandite	Clinoptilolite
6.	Mordenite group : (each tetrahedra of the framework belongs to at least one 5-membered ring)	Mordenite	Na – D, Zeolon, ZSM – 21, ZSM – 35, ZSM - 38, ptilolite
7.	Faujasite group : (frameworks based on polyhedral cages of cubic or near cubic symmetry)	Faujasite	Linde X, Linde Y, ZSM–20 , ZK- 4, ZK-21, ZK-22, N- A, Alpha
8.	Laumonite group :	Laumonite	Leonhardite
9.	Pentasil group :	ZSM-5, ZSM-11	
10.	Clathrate group :	Melanophlogite, ZSM- 39	

through their shared oxygen atoms to give rise to a wide range of secondary building units (SBU). These SBUs in turn, interconnect to give polyhedra which combine in different ways to form a variety of 3-D structures of zeolites, as shown in Fig 1.1.

1.2 ZEOLITE SYNTHESIS :

Synthetic zeolites are normally crystallized from aqueous alkaline gels containing sources of silica, alumina and cations. Crystallization may take hours or weeks and is generally carried out hydrothermally in the temperature range of ~333 to 473K under autogenous pressure and static / stirred conditions. The nature of the product is controlled by kinetic factors and small changes in the conditions can alter the product.

The first step in zeolite synthesis essentially involves the dissolution/depolymerization of aluminium and silicon species to form aluminate and silicate ions, which then couple with the template and/or inorganic cations to form a gel by condensation/polymerization. The chemical transformations steps involved in zeolite crystallization have been summarized by Sand[10] .

Crystallization of a zeolite generally occurs from a molecularly inhomogenous system i.e., the reactive gel. Based on experimental evidence, two theories have been postulated to explain the crystallization mechanism in zeolite formation : i) The solid-solid phase transformation and ii) Solution-solid phase transformation[11]. The exact nature of the mechanism will depend upon the reactants, method of mixing and other synthesis conditions. The following factors have a major influence on the crystallization of zeolites.

1.2.1 Gel silica/alumina ratio :

This factor imposes constraints on the framework composition of the zeolite produced . For many catalytic applications like cracking and isomerization, zeolites with

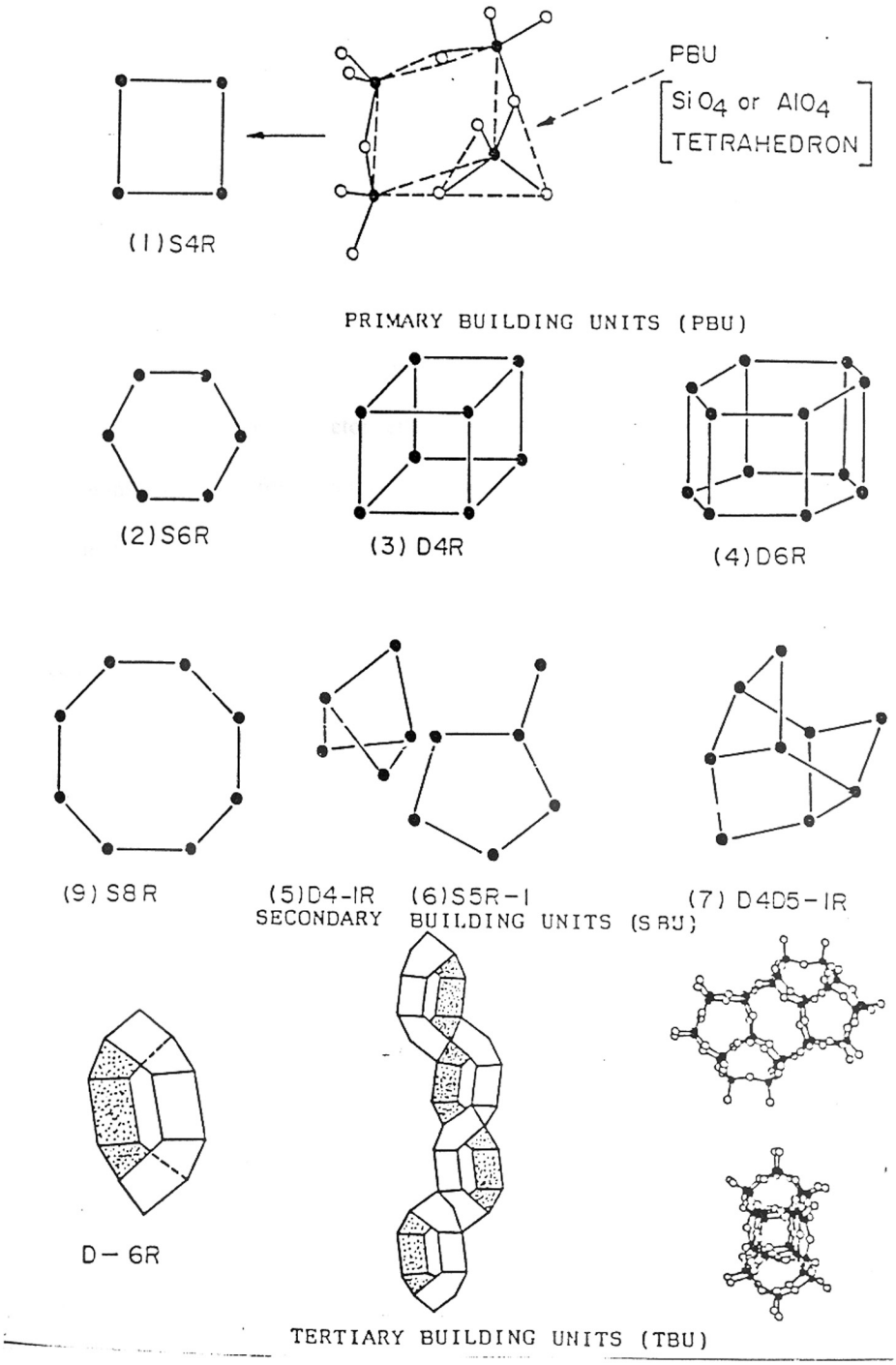

Fig. 1.1 : Primary, Secondary and Tertiary building units (PBU, SBU and TBU) leading to three dimensional zeolite framework.

increased silica/alumina ratios are useful, whereas, for many adsorption and ion-exchange processes, zeolites with decreased silica/alumina ratios serve the purpose. Thus, the ideally desired silica/alumina ratio of a zeolite chosen for a specific application can be obtained by adjusting the ratio in the synthesis mixture within tolerable limits, so that a vast deviation does not result in the final structure obtained.

1.2.2 Hydroxide ion concentration / pH :

This is another important factor affecting zeolite synthesis. The hydroxide ion serves as a complexing agent for silicon and aluminium. Its concentration in the reacting gel affects the rate of hydrolysis of the molecular/polymeric species present therein. It can also induce a change in the crystalline phase and composition produced. Increased OH^- ion concentration decreases the nucleation time as well as the yield of the crystalline material. However, proper balancing of crystallinity, induction period and phase purity can be achieved through proper control of the OH^- concentration alone[12].

It should be noted that the total hydroxide content of the system does not relate directly to its pH. Thus pH is rather the free OH^- content of a crystallizing system; hence, pH changes during the course of crystallization.

1.2.3 Presence of inorganic cations :

Presence of inorganic cations to a great extent determines the formation of specific structures, as well as influencing crystallinity, morphology and final yield of the product[4]. Addition of increasing amounts of alkali results in a decrease in nucleation time [13-16]. Also, the adjustment of the cation content in the gel can be done to inhibit the intergrowth of one zeolite with another[17]. Besides, certain cations may act as templates and direct the formation of specific structures[18]. The $SiO^- M^+$ interaction is also known to have a

structure stabilizing effect[19].

1.2.4 Presence of organic amines and/or quarternary ammonium ions :

These agents are important for the crystallization of many of the known zeolite molecular sieve structures. The use of organic species in synthesis gels was initiated by Barrer[19] in the sixties. These organic species get trapped inside the pores of the zeolite after crystallization and act as structure directing templates, besides being void fillers. The organic species can interact physically with the gel components and thereby alter the gelling process, solubility of the various species, ageing characteristics, crystallization time, transport properties and interactive energies. It can also interact chemically to alter or buffer the pH of the crystallizing gel[20]. A guest species that is an especially good fit to the topology of the zeolite pores is referred to as a template. The addition of templates to the synthesis gels of aluminium rich zeolites results in the crystallization of more silica-rich structures[19,21,22]. Besides, they may act as donors of hydroxyl ions, organize water molecules, stabilize some structures, balance the framework charge and/or alter the morphology of the product crystals. Although, the organic cation has the primary structure directing role, secondary effects due to the presence of the inorganic cations cannot be ruled out[16,23].

1.2.5 Effect of water content :

The water content influences the transport properties within the gel and the viscosity of the gel. The water content of the gel may also sometimes be responsible for directing certain zeolite structures, in conjunction with the cations present in the gel[17,24] .

1.2.6 Temperature :

Temperature can alter the zeolite phase obtained. Most zeolite structures often crystallize over a narrow range of temperatures. The induction period decreases, whereas the crystallization rate increases with increase in temperature.

1.2.7 Duration of crystallization :

This is an important parameter from the point of view of obtaining the desired metastable phase singly without any impurities of the other stable phases or intergrowths, as well as to get maximum crystallinity of the desired metastable phase. Thus it becomes important to optimize duration of crystallization as a parameter in the synthesis of many zeolite molecular sieves.

1.2.8 Source of raw-materials :

The source of raw materials and their formulation treatment is often found to influence the product obtained[25]. This factor may also affect the induction period and the crystallization rate as well as the crystal size and/or morphology of the product obtained.

1.3 PHYSICO-CHEMICAL CHARACTERIZATION :

Zeolites possess a variety of unique characteristics which are cumulatively responsible for putting them in an altogether different class of inorganic compounds. These characteristics not only enable the zeolite to be used for a wide range of applications, but also often form the basis for the various techniques used to characterize individual zeolites. These physico-chemical properties are discussed in this section.

1.3.1 Crystalline nature :

This property imparts characteristic powder diffraction patterns to the zeolite molecular sieves, which are finger prints of their structure. The structure is 3D with specific morphology, symmetry, particle size, unit cell size, specific pore size and channel systems of molecular dimensions.

1.3.2 Sorption properties :

The presence of pore systems of varying pore sizes with molecular dimension, enables the zeolites to selectively adsorb certain molecules preferentially over others. Hence, zeolites can be used as selective adsorbents. In zeolites, the intracrystalline surface area usually constitutes about 97% of the total surface area and values of a few hundred m^2/g are known. This factor and the large void volume coupled with the electrostatic fields leads to the extremely high sorption capacity of zeolites.

Diffusion also plays a key role in molecular shape selective catalysis. The rates of diffusion can significantly affect activity and selectivity of zeolite catalysts[26]. Barrer[27] has thoroughly reviewed the major features of diffusion in zeolites. Zeolitic catalysts exhibit three different types of diffusion phenomena, namely configurational Knudsen and Bulk diffusion. These have been described by Barrer[28].

1.3.3 Thermal and hydrothermal properties :

The geometry of the crystalline network is the major factor in its thermal stability. Zeolites can withstand the very high temperatures that are needed for the regeneration of catalysts. A zeolite to be used as a catalyst is considered to be thermally stable if its structure remains unaltered upto at least 1073 to 1273 K. Thermal stability of a zeolite

can be improved by increasing the Si/Al ratios[29], dealumination[30,31,32] or by ion-exchange with poly-valent cations[29].

1.3.4 Ion exchange :

Zeolites may manifest a variety of ion-exchange characteristics. The presence of well defined channels and cavities of uniform sizes within zeolites allows intracrystalline water to be occluded readily, thus making the charge compensating cations mobile. Therefore, they are readily exchangeable with different mono- or multivalent cations. The ion-exchange property of zeolites is a function of the amount of aluminium (or other trivalent ion) present in the zeolite lattice. This property also depends upon the size and charge of the exchanging cation, concentration of the exchanging solution, temperature at which the exchange is carried out, solvent used, structure of the zeolite and location of the cation site.

1.3.5 Acidity and basicity :

Substitution of Al for Si in the zeolite framework generates a negative charge on the framework. This charge is compensated by extra framework exchangeable cations. When the charge compensating cation is a proton, a bridging -OH group Si(OH)Al is generated and the zeolite framework exhibits the capacity to act as a Bronsted acid[33,34] (proton donor). On dehydration, Lewis acid sites are created. Dissociation energy calculations[33] have shown that between the bridging and terminal hydroxyl groups the former are more acidic than the latter. This conclusion is supported by the lower vibrational frequency of the bridging hydroxyl groups[34].

Acidity becomes a very important parameter during catalytic reactions over zeolites. It can be tuned as per the needs by various pre- and post-synthesis methods. Several

methods based on titration and adsorption/desorption, spectroscopy and catalytic tests have been used to determine the strength of both types of acid sites[35-37].

The application of basic properties of zeolites in adsorption as well as catalysis has recently been reported by some workers[38-42]. The extent of charge on the oxygen atom determines the basic strength of the zeolite. Barthomeuf et al[42]. have shown that the actual basic strength of a zeolite not only depends on its chemical composition, but also, on the structural environment of the framework oxygen.

Besides the conventional acidic and basic zeolites, we also have zeolites exhibiting practically neutral behaviour. These are the isomorphously substituted titano- and vanado-silicates, where the tetravalent metal ion imparts complete or partial neutrality to the zeolite framework[43]. They have proved to be important oxidation catalysts. In addition, neutral, pure silica isomorphs are also known for many zeolite structures.

1.3.6 Shape selectivity :

The intracrystalline surface area of zeolites is an inherent part of the crystal structure and hence they are topologically well-defined. The zeolite pores are of molecular dimensions and most of the catalytic sites are confined within these pores. As a result, the zeolites are able to restrict or prevent the passage of organic moities based on size or steric effects. This property of zeolites is referred to as shape selectivity. Four main types of shape selectivities and their basic concepts have been described by many authors[44-51]. Chen[52] has summarized the impact of shape selective zeolite catalysts on petroleum and petrochemical industry.

The effective pore size of zeolites can be determined by sorption of hydrocarbons with increasing kinetic diameter. However, the presence of mesopores as well as

variations in crystal size and shape can cause distinct differences in adsorption behaviour. Therefore, factors like constraint index, spaciousness index and distribution of various isomers in products, etc have been used to determine the extent of shape selectivity quantitatively[53-57].

1 .3 . 7 Catalytic properties :

Catalytic properties of zeolites and molecular sieve materials are very much dependent on both their physical as well as chemical features. The physical aspect is known to greatly influence shape selectivity[58], confinement[59] and diffusion[60] properties. The chemical aspect determines the nature of the active centers and the ability to catalyze acidic, basic or redox type reactions.

Zeolites have major advantages over conventional heterogeneous catalysts in many applications involving acid, acid-base, oxidation, reduction and polyfunctional catalysts. They have high thermal, hydrothermal and chemical stabilities; they possess well defined micropore and secondary pore systems, ion-exchange properties and are non-corrosive in nature. They can be easily rendered bifunctional as well as modified in several other different ways. These properties coupled with the ease of regeneration of their initial activities makes zeolites attractive as catalysts and adsorbents.

There are however, certain major disadvantages encountered with zeolite catalysts. These have been recently reviewed by Perot and Guisnet [61]. Two of the disadvantages are their deactivation by irreversible adsorption of secondary products and pore size restrictions to the bulkier molecules.

1.4 MODIFICATIONS IN ZEOLITES :

One of the greatest advantages of zeolite molecular sieves is the ease with which their properties can be tuned using different techniques, leading to the formation of modified zeolites which can be used more advantageously than the parent zeolite material.

Modification implies that a given material is tailored by appropriate treatments in order to change its physical properties such as its structural features, surface area, crystallinity and pore size, as well as its inherent properties like acidity, shape selectivity, catalytic properties etc. Quite often, a zeolite obtained by direct hydrothermal synthesis is not useful for catalytic applications unless either or some of its above mentioned properties are modified suitably.

Modified zeolites are finding new applications as heterogeneous catalysts in many organic reactions in the liquid phase and at moderate temperatures [62]. This is mainly due to their being solid catalysts, resulting in easy separation and product work-up. Besides, zeolites are nontoxic and regenerable. Modifications in zeolites can be brought about mainly by direct synthesis methods and post-synthesis methods .

1.4.1 Modifications by direct synthesis :

The most commonly encountered modification by direct synthesis is the one where compositional changes in the reactants give crystalline products with varying Si/Al ratios, varying crystal size, etc. Besides changing the Si/Al ratio, the crystalline product obtained can be altered to some extent by factors like the type of raw material used, ratio between reaction components, ageing conditions, crystallization temperature and the use of seed crystals. Providing a fluoride medium to the reaction mixture substitutes F^- for OH^- resulting in a decrease in acidity [63,64]. However, the most significant modification by direct

synthesis is isomorphous substitution.

Isomorphous substitution has attracted a lot of attention during the last few years. Modification of zeolites by isomorphous substitution gives rise to materials with new properties which may have potential for novel catalytic applications. The most important isomorphous substitution is the replacement of the framework T-atom of the zeolite molecular sieve by other bi-, tri- and tetravalent metal ions like Be/B/Ga/Fe/Ti/V etc. In principle, the following replacements can be brought about in zeolites by isomorphous substitution [65].

1) One guest molecule by another; this type of substitution has no significance as far as catalytic applications are concerned.

2) One cation by another; this replacement is useful in making bifunctional catalysts.

3) One element by one of its isotopes; this type of substitution is important in characterization of zeolite materials.

4) Replacement of one element in tetrahedral position by another; this last type of replacement is very important in substituting different elements into zeolite frameworks.

Goldsmith[66] was the first to report the isomorphous substitution of Si^{4+} by Ge^{4+} in the lattice. The possibility of isomorphous substitution and the stability of that particular metal ion in the zeolite tetrahedral framework was originally predicted by Pauling's theory[67] and subsequently reviewed in many articles[68-72]. According to Pauling criterion, the metal ion is stable in the tetrahedral framework when S is in the range $0.414 > S > 0.225$, where S = rc/ro, (ro is the radius of the oxygen ion and rc is the cation radius). However, some metal ions like Fe^{3+}, Ti^{4+}, Ga^{3+} and V^{4+}, for which the value of the Pauling criterion falls out of this range have been successfully substituted into the zeolite tetrahedral framework due to their stability in tetrahedral environments.

In the recent years, with the use of organic templating agents, a large number of elements like B/Fe/Ga/Ti[73,77], have been incorporated into the zeolite framework by direct hydrothermal synthesis and shown to result in materials with novel catalytic properties. A recent review of isomorphous substitution in zeolites by primary (or direct) synthesis methods speculates on the potential impact of such substances on catalysis[77]. Isomorphous substitution modifies the strength of the Bronsted acid sites. The relative Bronsted acidity of the zeolite molecular sieves is found to increase in the order :

$$SiOH < B(OH)\ Si < Fe(OH)\ Si < Ga(OH)\ Si < Al(OH)\ Si^{78}$$

Besides alumino- and the other metallic silicates, $AlPO_4$s, SAPOS and MeAlPOs form another important class of isomorphous substituted molecular sieves. The alumino-phosphates i.e., $ALPO_4$s are molecular sieves wherein Si^{4+} from the framework is replaced by P^{5+}. They were first reported by Wilson et al.[79] in 1982. Recent additions to the $AlPO_4$ family which include extra large-pore molecular sieves like VPI-5[80], MCM-9[81] and JDF-20[82]. Metalloaluminophosphate (MeAlPOs), where a metal ion like Co/Fe/Mg/Mo etc. replaces Al partially or completely in the $AlPO_4$ framework, have also been synthesized[83]. Recently, a new gallophosphate christened Cloverite[84] has been reported.

Silicoaluminophosphates (SAPOs) are molecular sieves where Si^{4+} replaces P^{5+} and $Al^{3+} + P^{5+}$ in the AlPO framework[85]. SAPOs exhibit cation exchange and mild-to-weak acidic properties. As in the case of $AlPO_4$s, SAPOs too exhibit excellent thermal and hydrothermal stabilities[86,87].

The techniques which are used to ascertain the substitution of a metal ion in a zeolite framework and to determine the degree of substitution are described in section 1. 5.

1.4.2 Post synthesis modifications :

Post synthesis modifications in zeolites become important when a zeolite with the desired physico-chemical properties cannot be obtained by direct hydro-thermal synthesis. In such cases, the hydrothermally synthesized parent zeolite molecular sieves can be modified further to varying degrees in a number of ways :

A. ion exchange

B. metal loading

C. modification into high-silica zeolites

A. Ion exchange :

In the pioneering work by Barrer[4], it was proved that the molecular sieving properties of a zeolite can be profoundly changed if the zeolite is modified by ion-exchange. Since then ion-exchange has been established as a standard method of tailoring zeolite molecular sieves so as to meet the best requirements of a particular separation. The exchangeable K^+ or Na^+ cations in the zeolite framework can be stoichiometrically replaced with other mono, di or trivalent cations (eg. La/Ca/Ba and Li) giving rise to varying sorption capacities. Ion-exchange may also be brought about via solid-solid reaction between the zeolite and the given salt or oxide in dry or hydrothermal conditions[88,89]. Besides cation exchange, rare earth exchange is another modification brought about mainly in fluid Cracking Catalysts for octane enhancement and good gasoline selectivity.

B. Metal loading :

Zeolite containing catalysts can be loaded with metals in several ways like ion-exchange of the zeolite from solution, impregnation from solution, sorption from gas

phase and comulling during catalyst formulation with a solid metal component or its solution. Metal loading, leading to catalytically active components in zeolites is particularly necessary for many industrial reactions like hydrogenation or oxidations. Metals generally desirable for introduction in the zeolite containing catalysts include Ni/Co/ Pt/Pd/Ag/Mo/Cr/W.

C . **Modifications into high - silica zeolites :**

High silica zeolites with large pores and cavities are attractive materials for catalytic applications in a variety of industrial processes, because of their high hydrothermal stability, hydrophobicity, strong acidity and particularly good resistance to deactivation[90]. Unfortunately, not all types of known zeolite structures can be obtained as high-silica zeolites by direct hydrothermal synthesis. Hence it often becomes necessary to modify them into high silica zeolites by post synthesis methods. Therefore thermal, hydrothermal and chemical methods or a combination of some/all of these have been used to increase the Si/M ratios in previously synthesized zeolites by subsequent modifications. All these techniques essentially involve the dealumination process. The term dealumination is used in zeolite chemistry to describe the extraction of framework aluminum.

C . 1 Thermal and hydrothermal modifications :

As the name suggests, this type of modification is brought about by subjecting an ammonium exchanged zeolite to thermal treatment in the presence of steam, resulting in the expulsion of tetrahedral aluminum from the framework into non-framework positions. This results in the high-temperature hydrolysis of Si-O-Al bonds, leading to the formation of non-framework aluminium species while increasing the framework Si/Al ratio and decreasing the unit cell size (Fig1.2)[91-94]. Thus, are obtained the ultrastable zeolites, having fewer ion

A. i) DEALUMINATION

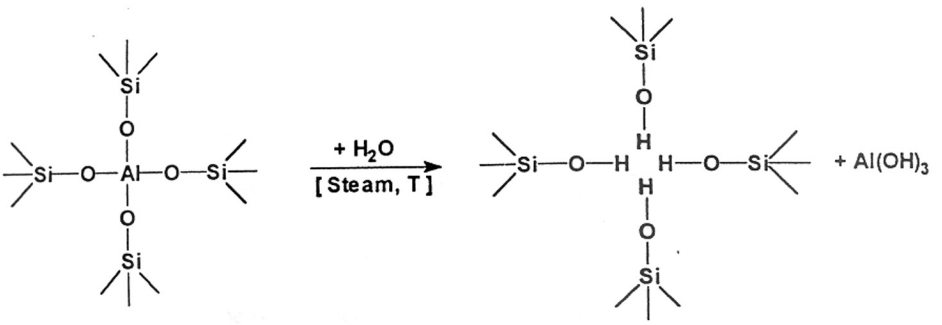

ii) $Al(OH)_3 + H^+ [Y] \longrightarrow Al(OH)^+_2 [Y] + H_2O$

B. ii) STABILIZATION

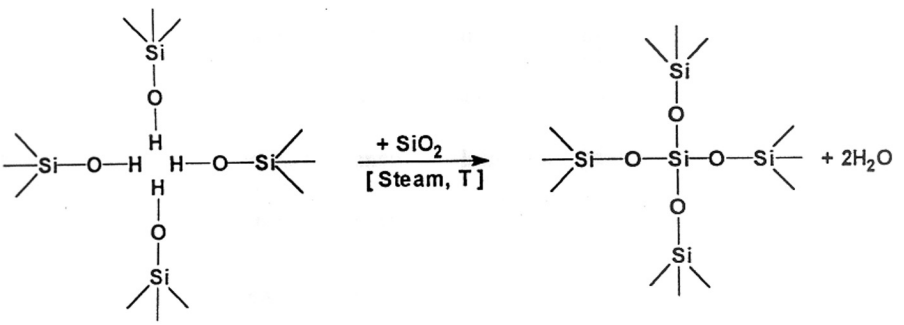

Fig. 1.2 : Mechanism of dealumination in zeolite type –Y

exchange as well as Bronsted acid sites are obtained. Such differences in acidity have a noticeable impact on the catalytic activity and selectivity of the modified zeolites.

C . 2 Chemical modifications

Dealumination to varying degrees can be brought about by various chemical reagents, depending upon the treatment used. It may be carried out by reacting the zeolite with a suitable reagent in solution phase or by passing the reagent in the gas phase at high temperature. Another type of chemical modification consists of grafting a given compound on the outer surface of the zeolite crystallites or the inner pores by chemical reaction with external or internal -OH groups, respectively. Depending upon the reagent used, dealumination may be accomplished both with or without silicon enrichment. Dealumination without silicon enrichment may be brought about by hydrothermal treatment[90] followed by acid leaching with mineral acids or chelating agents like EDTA, acetyl acetone, amino acid derivatives, etc. This results in extraction of framework Al^{3+} which is accompanied by the formation of framework defects arising out of the vacancies left by the extracted Al^{3+}. It also often gives rise to extra-framework aluminium species (EXFAL) in non-framework positions, which too contribute to modified catalytic activity.

The process of dealumination with silicon enrichment minimizes these limitations to a great extent. There are many techniques available for Al-replacement by Si. Two of these are : Chemical Vapour Deposition (CVD) using $SiCl_4$; and the use of salts like ammonium hexafluorosilicate $(NH_4)_2SiF_6$.

The treatment of zeolites, with ammonium hexafluorosilicate (AFS) solution, under controlled conditions of pH and temperature brings about dealumination effectively with simultaneous insertion of silicon to a certain extent[95,96]. These two methods thus result in

significantly lesser number of framework defects, and essentially involve a structure healing process, giving rise to modified high-silica zeolites with improved crystallinity. Silicon insertion by AFS treatment occurs in the following manner:

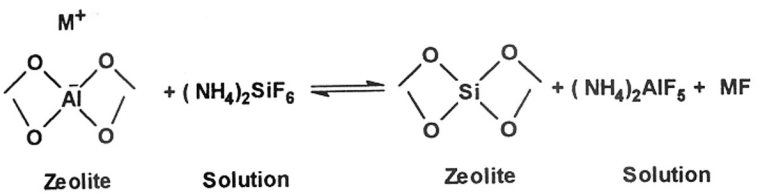

(1)

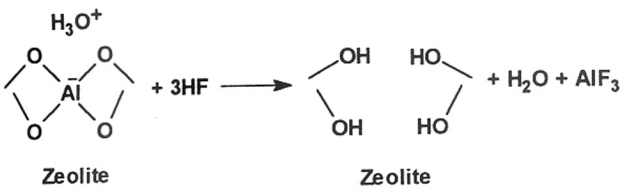

(2)

All these dealumination procedures have certain advantages and disadvantages, the method adopted depends upon the requirements.

1.5 TECHNIQUES FOR ZEOLITE CHARACTERIZATION :

1.5.1 X-ray diffraction :

X-ray powder diffraction is the single most important technique used to characterize zeolites. It furnishes vital information regarding phase purity, uniqueness of the structure, isomorphous substitution, degree of crystallinity and also makes possible the estimation of unit cell parameters[97,98]. When isomorphous substitution occurs, the extent of incorporation of the isomorphous element is correlated with the unit cell expansion or contraction. Modern methods have used ab initio calculations and Reitveld analyses to solve zeolite structure using powder X-ray patterns[99-103].

1 . 5 . 2 Thermal analysis :

This technique provides information regarding the thermal behaviour of zeolites. It is used extensively in the study of kinetics and dehydration of zeolites and also for studying the oxidative combustion of occluded organics in zeolites[104]. Besides this, other physico-chemical changes like the desorption of adsorbed water, dehydroxylation leading to the formation of Lewis sites during thermal treatment, phase transformation or structure collapse occurring during thermal treatment (if any), are all indicated in the thermoanalytical curves[105,106]. DTA curves provide qualitative and quantitative information about the energy of activation and enthalpy of the zeolite systems.

1 . 5 . 3 Adsorption measurements :

The ability of the zeolites to adsorb only selected molecules inside the channels and cavities enables adsorption measurements to be a useful tool in providing information about their void volume, crystal size, degree of crystallinity, acidity, diffusion limitations and pore blockages if any. Besides, sorption studies also help in determining specific interactions between the sorbate and sorbents as well as the strength of such interactions[107]. Various thermodynamic parameters such as entropy, heat and free energy of sorption can also be estimated with the help of sorption measurements.

1 . 5 . 4 Ion exchange :

The ion exchange property of metallosilicate zeolites originates from framework MO^{-}_{2} groups bonded with SiO_2 groups. Hence the ion-exchange capacity of a zeolite can be taken as a direct quantitative evidence for the presence of M^{3+} ions in tetrahedral positions[108] in the zeolite lattice. Therefore, ion-exchange capacity exhibited by zeolites becomes a simple and handy tool for characterization by providing evidence for the

incorporation of the metal ion in a zeolite framework.

1.5.5 Temperature programmed desorption (TPD) of ammonia :

The estimation of acid strength distribution in zeolites is carried out by this technique. It is used to characterize weak, medium and strong acid sites. The amount of ammonia released above 753K is normally considered to represent very strong acid sites. The presence of different types of acid sites have been reported by several workers[109,110].

1.5.6 Infra red spectroscopy :

This is one of the most sensitive tools for the investigation of the structural features of zeolites, the isomorphous substitution in them, their acidity, and the nature of zeolite-adsorbate interactions[111-113]. Zeolites may be characterized by infra red spectroscopy yielding valuable information in the vibrational mode region (400-1300 cm^{-1}). Various structure sensitive as well as structure insensitive vibrations (in the framework region) have been assigned by Flanigen[111]. Later, systematic investigations of the framework vibrations of many zeolites were reported. Isomorphous substitution of various elements into the zeolite framework shifts the OH^- vibrations as well as the asymmetric and symmetric framework vibrations, to higher or lower wave numbers in case of lighter and heavier elements, respectively[113]. In most of the metal substituted alumino silicates, a characteristic band due to Si-O-T (or >Si-O-T=O) asymmetric vibrations is seen around 960 cm^{-1}. The intensity of this band is correlated[114] with the amount of T-atom of the isomorphous element incorporated into the zeolite lattice. IR spectroscopy can also distinguish large pore zeolites from small and medium pore ones on the basis of OH stretching vibrations[115]. This technique is also used to estimate the acid sites by the adsorption of various basic probe molecules like ammonia, pyridine and benzene and to measure the acidity qualitatively as well as quantitatively.

1.5.7 Nuclear magnetic resonance spectroscopy :

High resolution solid state NMR spectroscopy using Magic angle spinning (MAS) has become a powerful method to characterize zeolite materials[116-122]. Till now about twenty different NMR active nuclei have been studied. Much attention has been focussed towards ^{29}Si and ^{27}Al MAS NMR in order to investigate the nature of Si and Al ordering in the zeolite framework[123], as well as the crystallographically equivalent and nonequivalent Si[124] and Al[125] ions in various sites. Further, information such as framework Si/Al ratios[126], coordination number of Si[127] and Al[128] and spectral correlations with Si-O-T bond angles[129] and Si-O bond lengths[130] can also be obtained.

Newly developed techniques like 2D NMR can be used to establish connectivities in the solid state[131]. ^{1}H-^{29}Si cross-polarization technique[132] provides semiquantitative information regarding silanol groups. High resolution liquid NMR (^{29}Si and ^{27}Al) helps detect the various silicate and aluminosilicate species leading to the identification of SBU's. $^{13}CP/MAS$ NMR helps locate and determine the configuration of organic templates[133-138], type of intermediates formed during catalytic reactions and the nature of the adsorbed species present on the zeolite surface[139]. ^{1}H MAS NMR has been used to study zeolite acidity[140,141], arising out of the various types of protons.

1.6 APPLICATIONS OF ZEOLITES :

The largest application of zeolites so far has been as catalysts in catalytic cracking for oil refining and major petrochemical processes. Besides, they are used as ion-exchangers, in detergents formulation, descicants and as selective adsorbents in separation processes. Other applications are in non-linear optical materials, electron or ion conductors and as agents for nuclear waste treatment. Recently, zeolites have been advantageously replacing conventional catalysts for catalyzing a number of organic reactions, providing

innovative technologies for various chemical processes, in the manufacture of organic fine chemicals useful in dyesttuff, pharmaceutical, drugs and fertilizer industries. This is mainly because, they enable the avoidance of the use of hazardous chemicals, besides assuring of a clean and friendly environment, as well as being more viable economically. The industrially important petrochemical and petroleum conversion processes based on shape selective zeolites are presented in Table 1.2.

The varied applications of zeolites are mainly attributed to their inherent features, namely, acidity, shape selectivity, feasibility of tailoring the number and strength of acid centres and finally, the doping with metals which renders bifunctionality to these catalysts.

1.7 ABOUT SOME LARGE PORE ZEOLITES :

High silica, large pore zeolites have recently been attracting attention from the scientific community world wide due to their immense technological potential in catalyzing various hydrocarbon reactions. However, not all large pore zeolites can be synthesized directly as high silica materials and therefore need to be modified post-synthetically. Consequently, the synthesis and catalytic application of large pore molecular sieves has become a significant trend in zeolite catalysis. As a result, several large pore materials have been reported recently (Table 1.3). However, most of the above are phosphate based. The high silica, large pore materials which are strictly zeolites are of greater utility and are fast gaining importance as industrial catalysts. Some of them are described below and their physico-chemical properties are presented in Table 1.4.

Table 1 . 2 : Industrial petroleum conversion/petrochemical processes based on shape selective zeolites[142]

Name of Process	Purpose
SELECTO FORMING	Octane boosting
M-FORMING	- do -
CATALYTIC CRACKING	- do -
MDDW	Distillate dewaxing
MLDW	Lube dewaxing
M_2 -FORMING, CYCLAR	Gas to aromatics
MOGD	Light defins to gasoline and distillate
MTG	Methanol to gasoline
MTO	Methanol to light defins
MVPI, MLPI, MHTI, XYLOFINING*	Xylene isomerization
MTDP	Toluene disproportionation
MEB, ALBENE*	Ethyl benzene synthesis
PARA SELECTIVE REACTIONS	p-xylene synthesis
	p-ethyl toluene synthesis

* Developed at the National Chemical Laboratory, Pune and in commercial operation.

Table 1.3 : The typical large pore zeolites / zeotypes.

Material	Ring Size	Year Discovered	Synthesis Media	Inorganic framework composition	Channels / pores
Cacoxenite	20- TO_4 ring		naturally occuring	Al, Fe, P	14.2 Å pore dameter
$AlPO_4$ - 8 (AET)	14- TO_4 ring	1982	*n* – dipropylamine template	Al , P	1D channel
			tetrabutylammoniu m / *n* –		
VPI - 5 (VFI)	18 - TO_4 ring	1988	dipropylamine template	Al , P	13 Å channel diameter hexagonal arrangement of ID channel system
Cloverite (CLO)	20 - TO_4 ring	1991	(a) quiniclidinium template (b) F^- rather than OH^- as mineraliser	Ga , P	Largest aperture of window is 13 Å 3-D cavities
JDF – 20	20 - TO_4 ring	1992	(a) triethylamine template	Al , P	3-D channel system hydroxyl groups protruding into channel system
UTD – 1	14 – TO_4 ring	1996	(b) glycol solvent $[(C_p^*)_2Co]OH$	Si , Al	1-D channel system 7.5 x 10 Å

Table **1.4 : Synthetic large pore zeolites and some of their properties**

Zeolites	Unit Cell Composition	U.C. Vol. $(Å)^3$	Pore opening (Å)	Pore Vol. ml/g
X (1 - 1.5)	Na_{86} [Al_{86} SiO_{106} O_{384}]. n H_2O	15600	7.4	0.38
Y (3.0 - 6.0)	Na_{86} [Al_{56} SiO_{136} O_{384}]. 260 H_2O	15000	7.4	0.28
Mordenite (9 - 30)	Na_8 [Al_8 Si_{40} O_{96}]. 24 H_2O	2974	6.7 x 7.0	0.165
L-type (5.7 - 7.0)	K_6 Na_3 [Al_9 Si_{27} O_{72}]. 21 H_2O	2205	7.1	0.24
Ω (5 - 12)	Na_4 K_6 [Al_{10} Si_{26} O_{72}]. 28 H_2O	2150	7.5	0.23
ZSM - 20 (8 - 10)	Na_{16} [Al_{16} Si_{80} O_{192}]. n H_2O	4550	7.4	0.31
ZSM - 12 (50 - 300)	$Na_{0.5}$ [$Al_{0.5}$ $Si_{27.5}$ O_{56}]. 4 H_2O	-	5.7 x 6.1	0.15
Beta (20 - 200)	Na_4 [Al_4 Si_{60} O_{128}]. 193 H_2O	4094	7.3 x 6.0	0.21
BC_6 (8 – 10)	Na_{18} [Al_{18} Si_{78} O_{192}]. n H_2O	10000	7.4 x 0.8	-
SAPO – 5	Na_m [Al_{10} P_{11} Si_3 O_{48}]. 8 H_2O	-	7.3	0.18
SAPO – 37	Na_{20} [Al_{76} P_{92} Si_{28} O_{384}].240 H_2O	-	7.4	0.28
VPI – 5	Na_{11} [Al_{16} P_{17} Si_3 O_{192}]. n H_2O	2533	12.1	0.31

1.7.1 Zeolite Beta :

Zeolite Beta was first synthesized in 1967, by Wadlinger et al.[143]. Its crystal structure was resolved recently[144,145]. It is a highly intergrown hybrid of two distinct but closely related polymorphs A & B (Fig 1. 3). The high stacking fault densities give rise to complex X-ray powder diffraction patterns containing both broad and sharp peaks. The low resolution model of the pore structure of zeolite beta is shown in Fig 1.3C. This model explains both its high stacking disorder and excellent sorption capacities.

Models of either form can be built by stacking together layers of the same basic plane, that is either the left (L) or the right (R) plane. So for example LLLL or RRRR stacking arrangement (Fig. 1.3 A, B) results in chiral left or right - handed helical structure or polymorph A. An LRLR arrangement on the other hand, results in the achiral structure of Polymorph B (Fig. 2c).

Zeolite beta has several unique and interesting features. It is the only high silica zeolite to have fully three-dimensional, 12-membered ring pores with two different types of channel systems. It is the only large pore zeolite to possess chiral pore intersections. Unlike other zeolites, it is the only zeolite to have a near-random degree of stacking faults and adsorbs equal amounts of n-hexane and cyclohexane with a sorption capacity of about 0.23 ml. g^{-1}.

On account of its rigid three-dimensional network of large pores with high framework SiO_2/Al_2O_3 ratios, it is a potential catalyst in many hydrocarbon processes of industrial importance [146-152].

Therefore, numerous publications have appeared on beta concerning improved synthesis methods and mechanism of formation[153], isomorphous substitution[154,155] and acidic

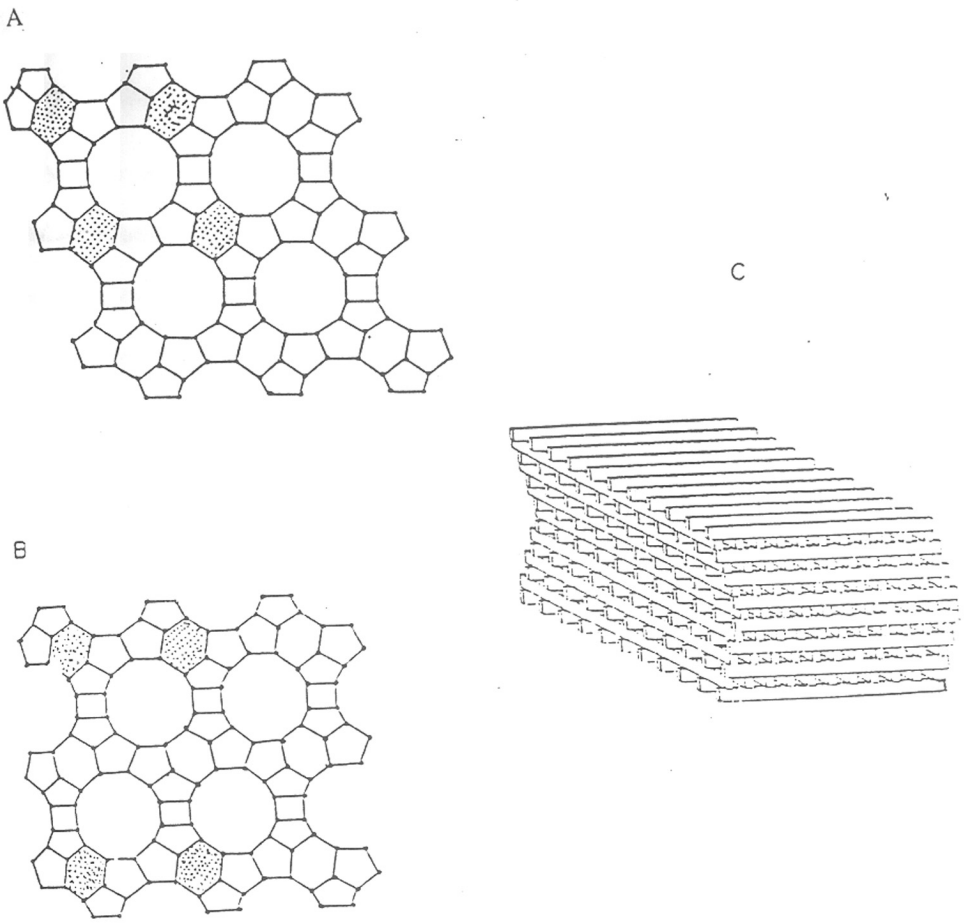

Fig. 1.3 : Projection along [100] of polymorph A and polymorph B of zeolite beta. Low resolution model of the zeolite beta pore structure showing an interpenetrating arrangement of channels (C)

and basic properties[156-159]

1.7.2 Mordenite :

Mordenite is one of the naturally occurring oldest known, most siliceous zeolite mineral with a nearly constant SiO_2/Al_2O_3 ratio of 10. It has been investigated in most detail and achieved industrial application quite early in the history of zeolite catalysis. The framework structure was determined by Meier[160]. Its pore structure is unidimensional and consists of non-intersecting parallel channels as shown in Fig 1.4 and 1.5. Chains of 4 and 5 membered rings are crosslinked by the sharing of neighbouring oxygens. The dehydrated zeolite has a two dimensional channel system, in which the smaller molecules can diffuse through, but the larger molecules, have to diffuse through the one dimensional larger channels and may be subjected to diffusion blocks produced by crystal stacking faults in the c-direction or the presence of amorphous material or cations in the channels. Mordenite exists in two forms, namely : small port and large port; distinguishable by the adsorption properties but not by their X-ray diffraction patterns.

The unique features of its structure lend distinctive characteristics to mordenite like the development of the unidimensional channels upon dehydration. The preponderance of energetically favoured 5-membered rings account for the extraordinary thermal stability of mordenite. Similarly, the highly siliceous nature offers additional stability to the mordenite framework enabling it to be modified in different ways to suit varying applications[161-163]. Mordenite has proved to be a useful catalyst in various reactions involving selective alkylation, hydrocracking and isomerization of hydrocarbons[164-168].

1.7.3 Faujasite (Y) :

This is another commercially important and widely used large pore zeolite. The

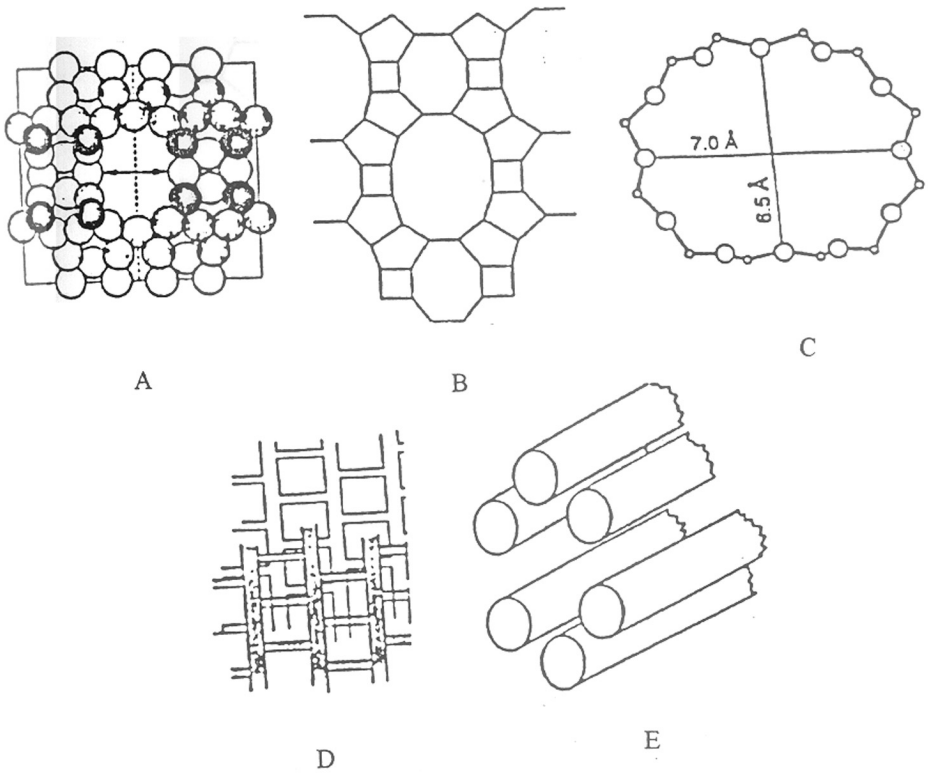

Fig. 1.4 : Mordenite Structure. A) Cross-Section. B) Mordenite framework projected down c-axis. C) 12– Ring viewed along [010]. D) Schematic two dimensional channels. E) Simplified visualization of mordenite like large-pore system as an assembly of parallel tubes.

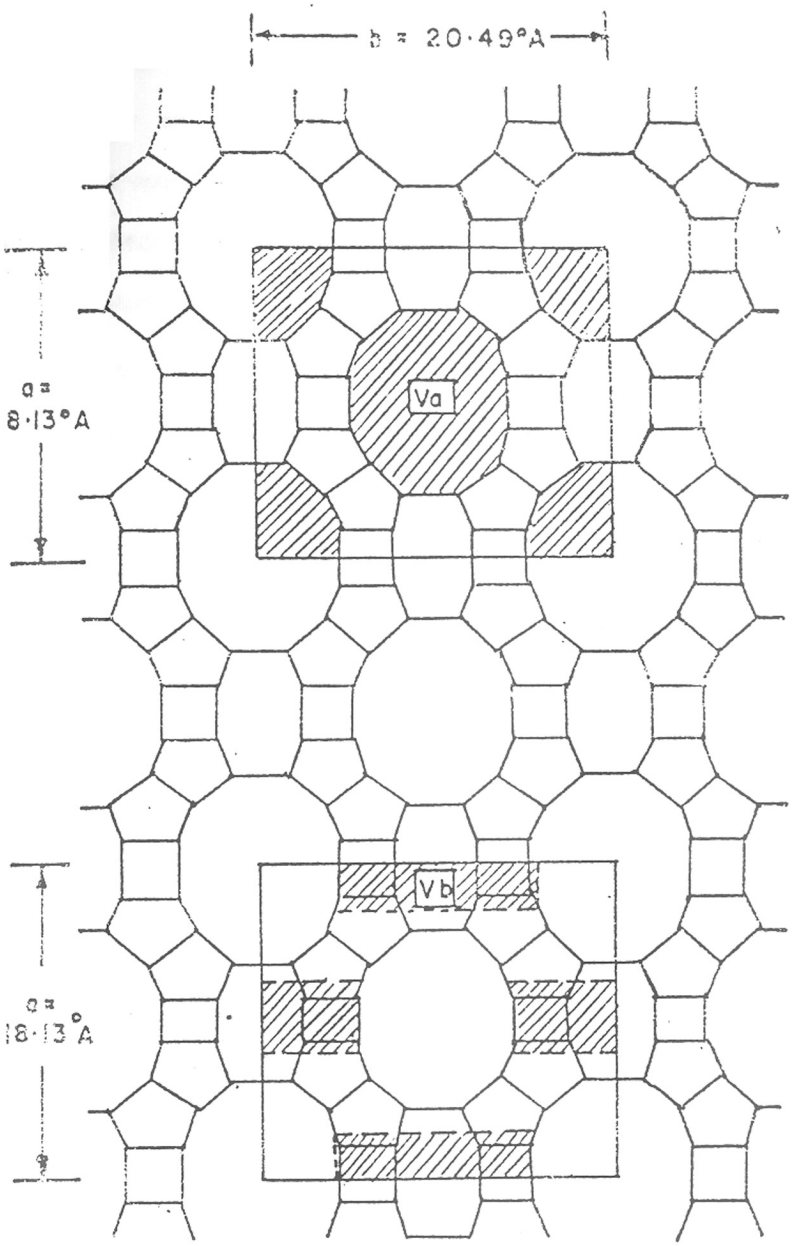

Fig. 1.5 : Schematic diagram of a cross section of Mordenite. The two volumes possible for adsorption are indicated by Va and Vb.

synthetic type-Y zeolites have framework structures similar to that of the natural mineral Faujasite, although they are a distinct species with characteristic properties. The structure of Y-zeolites consists of a negatively charged, three-dimensional framework of SiO_4 and AlO_4 tetrahedra, joined to form an array of truncated octahedra (ß-cages/sodalite cages), which in turn are joined at the octahedral faces by hexagonal prisms resulting in tetrahedral stacking , creating α-cages or super cages with a diameter of 13 A°. These super cages are connected through 12-membered rings (7.4 A° diameter) to form the large-pore system of the zeolite. Besides, the structure also comprises of a small-pore system made up of sodalite cages and the connecting hexagonal prisms (Fig 1.6).

The characteristic feature of the Y-zeolites is that in the dehydrated form, charge balancing protons occupy certain preferred positions in the zeolite and form two types of acidic hydroxyl groups; α-cage hydroxyls which are very acidic and directly accessible to adsorbates and ß-cage hydroxyls, which are less acidic but mobile enough to interact with the α-cage restricted adsorbates. In the hydrated form, the ions and the water molecules in the super-cages are sufficiently mobile so as to permit ion-exchange as well as reversible dehydration and sorption[169]. The three dimensional large pore system enables adsorption of many different species. This is the major reason why these zeolites have found wide application in catalysis. Y type zeolites and their various modified forms are widely used as catalysts in various hydrocarbon conversion reactions. Their use as fluid cracking catalysts for octane enhancing is an important application. Therefore, literature on the preparation and properties of faujasite type-Y zeolite is continously expanding[169-171].

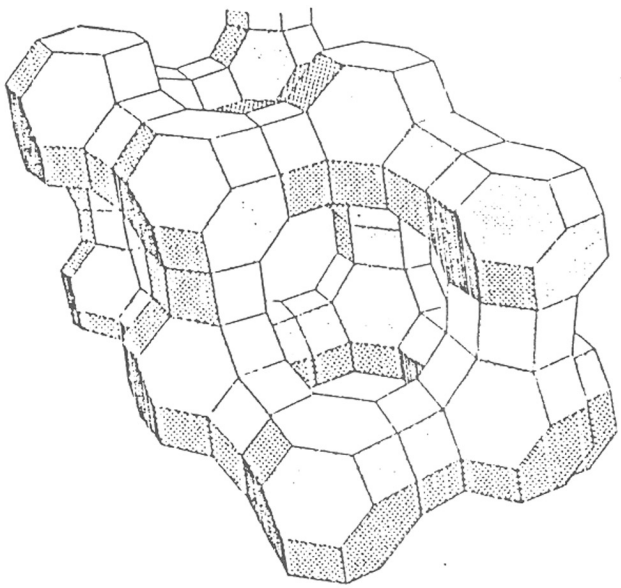

Fig. 1.6 : Cage-like structure of Faujasite Y.

1.8 SCOPE OF THE THESIS :

The foregoing review of the literature reveals that the large pore zeolites are emerging as important catalysts for many reactions. Among many such zeolites, zeolite beta stands out because of its remarkable structural features. It is an intergrown hybrid of two structural isomers A and B; structure A is chiral (left or right handed) and B is achiral. There is no energetic difference betweeen these three possibilities; so a real sample will consist of an intimate mixture of all three isomorphs and has no net chiral character. If we could crystallize one particular form (left or right handed) of A, then the resulting zeolite would be chiral and could be used as an enantio-selective catalyst. On the other hand if we could crystallize form B, which is more stable compared to A, It could also lead to a more useful catalyst.

The present work is an attempt, towards modifications of beta keeping the above points in view.The following studies were carried out:

1. Zeolite beta was modified by direct hydrothermal synthesis by isomorphous substitution of Ga^{3+} and Be^{2+} in place of Al^{3+} in the lattice.
2. It was also modified by acid leaching/silation action through $(NH_4)_2SiF_6$ treatment.
3. The modified forms were characterized by XRD, SEM, TG-DTA, FTIR, MAS-NMR and adsorption methods.
4. Zeolite mordenite was modified by direct hydrothermal synthesis by isomorphous substitution of Ga^{3+} in place of Al^{3+} in the lattice, and degallation by $(NH_4)_2SiF_6$ and characterized by various methods.
5. The catalytic properties of these materials were studied in m-xylene isomerization and benzene alkylation by long chain alkenes. The former is a test reaction for activity and shape selectivity, whereas the latter reaction is important from an ecological angle as linear alkylbenzenes can be obtained in the absence of anhydrous HF.

The thesis consists of five chapters including this introductory ***chapter 1*** describing

the basics of zeolite chemistry.

In ***Chapter 2*** are presented the details of all the experimentation undertaken during the present studies.

Chapter 3 contains the results of the physico-chemical characterization of [Ga]-and [Be]-beta and a novel *gallosilicate mordenite* material.

Chapter 4 presents the results of the test reaction viz. meta-xylene isomerization.

In ***Chapter 5*** the results of alkylation of benzene to produce linear alkylbenzenes using long chain olefins are presented. Various, modified large pore zeolites were used in this reaction.

In the end, the summary of the thesis is presented.

REFERENCES :

1. Breck , D.W., *J. Chem. Edn.*, **41** (1964) 678.
2. Turkevich , J., *Catal. Rev.***1** (1968) 1.
3. Breck, D.W., in "Zeolite Molecular Sieves", Wiley Publ. New York, (1974).
4. Barrer, R.M., in "Hydrothermal Chemistry of Zeolites", Acad.Press, New York, (1982).
5. Meier, W. M. and Olson, D.H., in "Atlas of Zeolite Structure Types", 2nd Edn. Butterworths, London, (1987).
6. Bragg, W. L., in "The Atomic Structure of Minerals", Cornell Univ. Press, Ithaca New York , (1937).
7. Meier,W. M., in "Molecular Sieves", Soc.Chem.Ind., London, (1968) 10.
8. Sand, L.B., in "Econ. Geol" (1967) 191.
9. Flanigen, E. M., in "Proceedngs of the fifth international zeolite conference", Ed. L.V.C. Rees, Heydon, London, (1980) 760.
10. Sand, L.B., *Pure and Applied chemistry*, **52** (1980) 125.
11. a) Kerr, G.T., *J. Phys. Chem.*, **70** (1966) 104.
    b) Kerr, G.T. , *J.Phys.Chem*, **72** (1968) 1385.
12. Domine, D. and Quobex, J., " Molecular Sieves'', Ed.Barrer, R. M., Soc.Chem.Ind. , (1968) 78.
13. Eur. Patent 15, 702 (1980).
14. Camblor, M. A. and Peréz - Pariente, J., *Zeolites*,**11** (1991) 202
15. Lillernd, K. P. and Raeder, J. H., *Zeolites*, **6** (1986) 474.
16. Flanigen, E. M., in "Molecular Sieves", Eds. Meier,W.M., Uytterhoeven, J. B., ACS Advances in Chem.Series, **121** (1973) 119.
17. Ueda, S., Nishimara, M. and Koizumi, M. in "Zeolite synthesis : Structure, Techniques and Applications", Eds. Brazaj, B., et al., Elsevier, Amsterdam, (1985) 105.
18. Keijsper, J. J. and Post, M. F. M., "ACS Symp. Series, Am. Chem. Soc.", Washington D. C., (1989) 28.
19. Barrer, R. M. and Penny P. J.,*J. Chem.Soc.*, (1961) 971.

20. Iler R. K., in "The Chemistry of Silica :Solubility, Polymerization, Colloid and Surface Properties And Biochemistry", Wiley, New York, (1979).
21. U.S. Patent 3, 314, 752 (1967).
22. U.S. Patent 3, 306, 922 (1967).
23. Barrer, R. M. and Sieber, W. *J.Chem. Soc. Dalton Trans.* (1977) 1020.
24. Belov, N. V., in "Crystal Chemistry of Large Cation Silicates", Eds.Flanigen, E.M., et.al., Consultants Bureau, N.Y. Academy of Science Press, Moscow, **91** (1961) 34.
25. Meier,W. M., in "Molecular Sieves", Soc.Chem.Ind., London, (1968)chap.II.
26. Eberly, Jr. P. E., in "Zeolite Chemistry and Catalysis", ACS. Symp. Series, **171** (1976) 392.
27. Barrer, R. M., in "Adv. Chem. Ser.", **102** (1971) 1.
28. Barrer, R. M., in "Adsorption of Liquids and Gases by Solids".
29. Breck, D. W., in "Zeolite Molecular Sieves", Wiley, New York, (1974) 449.
30. Kerr, G.T., *J. Phys. Chem.*, **73** (1969) 2780.
31. Beaumont, R. and Barthomeuf, D., *J.Catal.*, **30** (1973) 288.
32. Beaumont, R.and Barthomeuf, D., *J.Catal.*, **26** (1972) 1780.
33. Mortier, W. J., Saur, J., Lercher, J. A. and Noller, H., *J.Phys. Chem.*, **88** (1985) 905.
34. Hegde, S. G., Kumar, R., Bhat, R. N. and Ratnaswamy, P., *Zeolites*, **9** (1989) 231.
35. Van Hoof, J. H. C. and Roelofsen, J.W., "Studies In Surface Science And Catalysis", **58** (1991) 241.
36. Karge, H. G., in "Studies In Surface Science And Catalysis", **65** (1991) 133.
37. Jacobs, P. A., in"Carbogenic Activity of Zeolites", Elsevier, Amsterdam, (1977) 33.
38. Sidernoko, Y. N., Gallich , P. N., Gatyrya, V. S., Ilin, V.G. and Neimark, I.E., *Dokl. Akad. Nauk, USSR,* **173** (1967) 132.
39. Yashima, T., Sato, K., Hayasaka , T. and Hara , N., *J. Catal.*, **26** (1976) 303.
40. Ono, Y., "Studies In Surface Science And Catalysis", **5** (1980) 19.
41. Unland, M. L. and Barker, G. E., in "Catalysis of Organic Reactions",Ed. Moser, W. R., Marcel Dekker Inc. New York, Chem. Ind. Ser., **5** (1981) 51.

42. Barthomeuf, D., "Studies In Surface Science And Catalysis", **65** (1991) 157. & References cited there in.

43. Peregoi, G., Bellusi, G., Corno, C., Taramasso, M., Buonomo, F.and Esposito, A. "Studies in Surface Science And Catalysis", **28** (1986) 129.

44. Chen, N. Y. and Weisz, P. B., "Chem. Engg. Progr. Symp. Ser.", **63** (1967) 86.

45. Csicsery, S. M., "ACS Monogr.", **171** (1976) 680.

46. Derouane, E.G., in "Interrelation Chemistry", Eds. Whittingham, M. S. and Jacobson, A. J., Acad. Press, New York, (1982) 101.

47. Venuto, P. B., "Adv. Chem. Ser.", **102** (1971) 260.

48. Chen, N. Y., in "Shape Selective Catalysis In Industrial Applications", Eds. Garwood, W. E. and Dwyer, F.G., Marcel Dekker Inc., New York, (1989).

49. Derouane, E. G. and Gabelica, Z.,*J. Catal.*, **65** (1980) 486.

50. Weisz, P. B., "Studies In Surface Science And Catalysis" , **47A** (1981) 3.

51. Csiccery, S. M., *J. Catal.*, **23** (1971) 124.

52. Chen, N. Y. and Garwood, W. E., "*Catal. rev-sci. Engg.*", **28** (1986) 1.

53. Frillette,V. J., Haag W. O. and Lego, R. M., *J. Catal.*, **67** (1981) 218.

54. Martens, J. A., Teilson, M., Jacobs,P. A. and Weitkamp, J., Zeolites,**4** (1984) 98.

55. Weitkamp, J. Ernst, S., Jacobs, P.A.and Karge, H. G., "Erdoel.Khole-Erdgaspetrochem", **39** (1984) 13.

56. Dewing, J. J., *J. Mol. Catal.*, **61** (1990) 173.

57. Chen, N. Y. and Garwood, W. E., "*Catal. rev-sci. Engg.*", **28** (1986) 1.

58. Weisz, P. B., *Pure and Applied Chemistry*, **52** (1980) 2091.

59. Derouane. E. G., Andre, J. M., Lucas, A. A., *J. Catal.*, **110** (1988) 58.

60. Vedrine, J.C., in "Zeolite Chemistry And Catalysis.", Eds. Jacobs, P. A., et.al., Elsevier, Amsterdam, (1991) 25.

61. Perot, G., Guinset , M., *J. Mol.Catal,* **61** (1990) 173.

62. Van, Bekkum, H. and Kouwenhove, H.W.,"Red.Trav. Chim.Pays-Bas", **108** (1989) 283

63. Li, R. S., Zhang, W. Y., Lai, D. R. and Wei, Q., *Appl. catal.*, **71** (1991) 185.

64. a) Guth, J. L., Kessler, H. and Wei, R., *Pure and Appl. Chem.*, **58** (1986) 1389.
b) Guth, J. L., Kessler, H., Higel, J. M., Lamblin, J. M., Patrin, J. and Wey, R., in "Zeolite Synthesis", Eds. Occelli, M.L. and Robson, H. E., ACS Symp. Series, **198**, (1989) 176.

65. Flanigen, E. M., in "Proceedngs of the fifth international zeolite conference", Ed. L.V.C. Rees, Heydon, London, (1980)chap.VI.

66. Goldsmith, J. R., *Miner. Mag.*, **29** (1952) 952.

67. Pauling, L. in "The Nature of Chemical Bond", Goskhi Mizdat, Moscow.

68. Ione, K.G. and Vostrikova, L. A., *Russ. Chem. Rev.*, **56 (3)** (1987) 231.

69. Ione, K. G., Vostrikova, L. A., and Mastikhin, V. M., *J. Mol. Catal.*, **31** (1985) 355.

70. Taramasso, G., Perego, G. and Notari, B., in "Proceedings Vth International Zeolite Conference", Napoli, Eds. Rees, L.V.C., Heydon, London, (1980) 27.

71. Tielen, M., Geelen, M. and Jacobs, P. A., *Acta.Phys. Chem.*, **31** (1985) 1

72. Xure, X. and Wenquin, P. in "Studies in Surface Science And Catalysis",**24** (1985) 27.

73. Flanigen, E. M., in "Proceedngs of the fifth international zeolite conference", Ed. L.V.C. Rees, Heydon, London, (1980) 419.

74. U.S.Patent 4,410501., (1983), assigned to ENI.

75. Chu, C. T-W and Chang, C. D., *J Phys. Chem.*, **89** (1985) 1569.

76. Taramasso, M. Perego,G. and Notari, B., U.S.Patent 4, 410501., (1983), assigned to ENI.

77. Goldsmith, J. R., *Miner. Mag.*, **29** (1952) 952.

78. Meier,W. M., in "Molecular Sieves", Soc.Chem.Ind., London, (1968) 240.

79. Wilson, S. T., Lok, B. M., Messina, C. A., Cannan, T. R. and Flanigen, E. M., *J. Am. Chem. Soc.*, **104** (1982) 1146.

80. Davies, M.E., Saldariagga, C., Mentes, C., Gross, J., Rowden, C., *Nature*, **331** (1988) 968.

81. Derouane, E. G., Valyoisik, E. W. and Van Ballmoos, R., European Patent Appl. 1, 46,384 (1984).

82. Jones, R. H, Thomas, J. M., Chen, J., et.al., *J. Solid State Chem*, **102** (1993) 204.

83. Wilson, S. T. and Flanigen, E. M., "ACS. Symp. Series", **298** (1988) 871.

84. Esterman, M., McCusker, L.B., et.al., *Nature,* **352** (1991) 320.

85. Lok, B. M., Messina,C. A., Patten, R. L., Cannan, T. R. and Flanigen, E. M., U.S. Patent 4, 440, 871 (1981).

86. Ben Taarit, Y., in "Zeolite Microporous Solids:Synthesis, Structure And Reactivity", Eds. Derouane, E. G. et.al. NATO, **ASI Series**, Kluwer Academic Publishers, (1991) 291.

87. Vedrine, J. C., in "Guidelines For Mastering The Properties Of Molecular Sieves", Eds. Barthomeuf, D., et.al., NATO,ASI Series B, Physics, **221,** Plenum (1990) 291.

88 Kucherov, A. V. and Slinkin, A. A., *Zeolites*, **6** (1986) 175, and **7** (1987) 43.

89 Kucherov, A. V., Slinkin, A. A., Beyer, G. K. and Bordley, G., *J.Chem. Soc., Faraday Trans.I*, **85** (1989) 3087 and 3095.

90 Scherzer, J., in "Catalytic Materials : Relation between Structure and Reactivity", Eds. Whyte, T. E. Jr., et.al., ACS Series, Am. Chem. Soc., Washington D.C., **248** (1984) 154.

91 Kerr, G.T., *J.Phys.Chem.,* **71** (1967) 4155.

92 Kerr, G.T., "Adv. Chem. Series", **121** (1973) 219.

93 Eyer, H.K. and Belenzkaya, I."Catalysis by Zeolites",Eds.Imelik,B.,et.al., Amsterdam, (1980) 203.

94 Chang , C. H. U.S. *Patent* 4,273,753 (1981).

95. Skeels, G.W. and Breck, D.W.,"Proceedings, VIth International Zeolite Conference", Reno, Nevada, (1983).

96. Breck, D. W., Blass, H. and Skeels, G. W., U.S. Patent 4,503,023 (1985).

97. Balmoos. Van, R. , in "Collection of Stimulated XRD Powder Patterns of Zeolites", Butterworths, London, (1984) .

98. Meier,W. M., in "Molecular Sieves", Soc.Chem.Ind., London, (1968) 283.

99. Pluth, J. J., Smith, J. V. and Bennett, J. M. , ***Acta. Crystallogr.,*** **C42**(1986)283

100. Charnell, J. F. , *J. Cryst. Growth*, **8** (1971) 271.

101. Rietveld, H. M., *J. Appl. Crystallogr.*, **2** (1969) 2.

102. Derouane,E. G., Detremmerie, S., Gabelica, Z. and Blom, N., *Appl.Catal,***1**(1981) 20.

103. Barrer, R. M. and Langloy, D. A., *J. Chem. Soc,* (1958) 3804.

104. Ligia Siena de Saldarriga, Saldarrage, C. and Davies, M.E., *J. Am. Chem. Soc.*, **109** (1987) 109.

105. Gal, I. G., Tankovie, O., Makis, S., Raoovanor, P. and Tadorivic, M., *Trans. Faraday Soc.*, **67** (1971) 999.

106. Bremer, H., Morke, W., Scodel, R.,ogt, F.,*Adv. In. Chem. Ser.*, **121** (1973) 249.

107. Naddenriep, R. J., *Colloid Interface Science*, **28** (1968) 293.

108. Szostak, R., in Molecularc Sieves ; "Principles of Synthesis and Identification", Van Nostrand Reinhold, New York, Ch.1

109. Topsoe, N., Penderson , R. K. and Derouane, E.G., *J. Catal.*, **70** (1981) 41.

110. Borade, R. B., Hegde, S. G., Kulkarni, S. B. and Ratnaswamy, P. *Appl. Catal.*, **13** (1984) 27.

111. Flanigen, E. M. and Khatami, H., in "Molecular Sieve Zeolites - 1", ACS Monograph, Eds. Szymanski, H. A., **101** (1971) 201.

112. Flanigen, E. M., in *Zeolite Chemistry and Catalysis*, ACS Monograph, Eds. Rabo, J. A., et.al., **171** (1976) 180.

113. Kutz, N. in "Heterogenous Catalysis -II", Eds. Shrpiro, B. L., (1984) 121.

114. Perego, G., Bellusi, G., Corno, C., Taramasso, M., Buonomo, F and Eposite A., in "New Developments in Zeolite Science and Technology", Eds. Murakami,Y. et.al., Elsevier, Amsterdam, (1986) 129.

115. Ward, J. W., "Zeolite Chemistry and Catalysis", Ed. Rabo, J. A., et.al., ACS Monograph, **171** (1976) 80.

116. Jacobs, P. A. and Von Ballmoos., *J. Phys. Chem.*, **86** (1982) 3050.

117. Chu, C. T-W and Chang , C. D., *J. Phys. Chem.* **89** (1985) 1569.

118. Topsoe, N.Y., Pederson, K. and Derouane, E. G., *J. Catal*, **70** (1981) 41.

119. Anderson, M. W. , Klinowski, J., *Zeolites*, **6** (1986) 455.

120. Klinowski, J., Progress in "NMR Spectroscopy", Eds. Emsley, J. W., et.al. Pregamon Press, GB, **17** (1984) 237.

121. Thomas, J. M. and Klinowski, J., "Advances in Catalysis", **33** (1985) 199 .

122. Engelhardt, G. and Michell, DD., "High Resolution Solid State NMR of Silicates and Zeolites", John Wiley, New York, (1987).

123 a) Lippmaa, E., Magi, M. , Samason, A. Engelhardt, G. and Grimmer, A. R., *J. Am. Chem. Soc.* , **102** (1983) 4889 .

b) Lippmaa, E., Magi, M., Samason, A. Tarmak, M. and Engelhardt, G., *J. Am. Chem. Soc.*, **103** (1981) 4992.

124. Fyfe, C. A., Gobbi, G. C., Klinowski, J., Thomas, J. M. and Ramdas, S., *Nature*, (London), **296** (1982) 530.

125. Fyfe, C. A., Gobbi, G.C., Hartman, J. K., Klinowski, J. and Thomas, J. M., *J. Phys. Chem"*, **86** (1982) 1247.

126. Engelhardt, G., Lohose, U., Lippmaa, E., Tarmak, M. and Magi, M., Z. Anorg. Allg. Chem, **482** (1981) 49 .

127. Mastikhin, V. M. and Zamarev, K. I., *Z. Phys. Chemie*, (Neue Folge), **152** (1987) 332.

128. Muller, D., Gessner, W., Behrens, H. J. and Cheler, G. ,*Chem. Phys. Lett.*, **79** (1981) 59.

129. Thomas, J. M., Fyfe, C. A., Ramdas, S., Klinowski, J. and Gobbi, G. C., *J.Phys. Chem.*, **86** (1982) 3061.

130. Ramdas, S. and Klinowski, J., *Nature*, (London), **308** (1984) 521.

131. Fyfe, C. A., Grondey, H., Feng , Y. and Kokotailo, G. T., *Chem. Phys. Lett*, **173** (1990) 211.

132. Bodart, P., Nagy, J. B., Debres, G., Gabelica, Z. and Jacobs, P. A., *J. Phys. Chem.* **90** (1986) 5183.

133. Engelhardt, G., Jancke, H., Hoebbel, D. and Wieker, W., *Z. Chem.*, **14** (1974) 109.

134. McCormick, A. V., Bell, A.T. and Radke, C. J., *Zeolites*, **7** (1987) 183.

135. Van der Berg, J. P., de Jong-Versloot, P. C., Keijsper, J and Post, M. F. M., "Innovation in Zeolite Materials Science", Eds. Grobet, P. J. et.al., Elsevier, Amsterdam, (1988) 85.

136. McCormick, A. V., Bell, A.T. and Radke, C. J., "New Development in Zeolite Science and Technology",Eds.Murakami,Y., et.al. , Elsevier, Amsterdam, (1986) 247.

137. Thangaraj, A. and Kumar, R., *Zeolites*, **10** (1990) 117.

138. Boxhoorn, G.,Van Santen, R. A., Van Erp, W.A., Huis and Clague, D., *J. Chem. Soc Chem. Commun.*, (1982) 264.

139. a) Anderson, M. W. and Klinowski, J. *Nature*, (London), **339** (1989) 200 .
b) Anderson, M. W. and Klinowski, J. *J. Am. Chem. Soc*, **112** (1990) 10.

140. Freude, D.,Hunger,M. and Pfeifer, H.,*Z. Phys. Chemie* (Neue Folge), **152** (1987) 429.

141. Scholle, K. F. M. G. J., Veeman, W. S. Post, J. G. and Van Hoof, *Zeolites*, **3** (1983) p. 214.

142. NCL. Annual Report 1989-90.

143. Wadlinger, R. L., Kerr, G. T. and Rosinki, E. J., U.S. Pat. 3, 308, 069 (1967) .

144. Newsam, J. M., Treacy, M. M. J., Koetsier, W. T. and De Gruyter, C.B., "Proc. Royal. Soc. Lond.", **A420**, (1988) p 375- 405.

145. Higgins, J. B., La Pierre, R. B., Schlenker, J. L., Rohrman, A.C., Wood, J. D., Kerr, G. T. and Rohrbaugh, W. J., *Zeolites*, **8** (1988) 446 .

146. Young, L. B. Eur. Pat. Appl., 30, 084 (1981).

147. Tobias, M. A., U.S. Pat 3, 728, 408 (1973).

148. La Pierre, R. B. and Patridge, R. D., Eur. Pat. Appl. **94**, (1983), 827

149. La Pierre, R. B, Patridge,R D., Chen, N.Yand Wong, S.S. U.S.Patent.4,501,926 (1986).

150. Martens,J.A,..Perez -Pariente, J. and Jacobs, P.A., Acta. Phys. Chem , **31**(1985)487

151. Martens, J. A. Perez-Pariente, J., Sastre, E., Corma, A. and Jacobs, P.A., Appl. *Catal.* **45** (1988) 85.

152. Leu, L-J, Hou, L-Y, Kang, B-C, Li, C. C., Wu, S-T. and Wu, J-C., *Appl. Catal*, **69** (1991) 49.

153. Lchse, U., Altrichter, B., Fricke, R., Polz, W., Schreiver, F., Garkisch, Ch., and Jancke, K., *J. Chem . Soc. Faraday trans.* **93** (1997) 505- 512 .

154. Camblor, M. A., Constantini, M., Corma, A., Esteve, P., Gilbert, L., Martinez, A., Valencia, S., *Appl . Catal.*, **A 133** (1996) 485.

155. Chien Shu - Hua, Ho. Jang - Cheng . "Stud . Surf. Sci . Catal.", **97** (1996) 533.

156. Guisnet, M., Ayrault, P., Countanceau, C., Alveraz, M., and Datka. J., *J .Chem.Soc. Faraday Trans.* **93(8)** (1997) 1661.

157. Beck L. W., and Haw. J. F., *J. Phys. Chem.* **99** (1995) 1076.

158. Yang C., and Xu.Q., *Zeolites*, **19** (1997) 404 .

159. Shen, J. P., Ma, J., Guo, J., Jinag, D. Z. and Min, E. Z. *Chinese Chem. Letts.*, **5(12)** (1994)1075.

160. Meier, W. M., *Z.Krist.*, **115** (1961) 439.

161. Florela, C., Jona, B., *J. Porous materials.* **2(1)** (1995) 2534.

162. Helmut Stach and Jochen Janchen ; *Zeolite*, **12** (1992) 152.

163. Chumbale, V. R, Chandwadkar, A. J, and Rao, B. S; *Zeolites*, **12** (1992) 63.

164. Burbioge, B.W., Keen, I. M. and Eyles, M. K., 2nd "Intern. Conf. MOI. Sieves. Zeols." Warcester, Mass. (1970).

165. Mobil Oil Corp., U. K. Patent 1,022, 687 (1966) .

166. Norman, G. H., Shigemura, D.S. and Hopper, J. R., *Ind.Engg.Chem. Prod. Res. Dev.* **15** (1976) 41.

167. Norton Int. Corp., U. K. Patent 1,008,596 (1965).

168. Shell International , Dutch Patent 6,807,837 (1968).

169. Jia, M., H. Lechert and H. Forster ; *Zeolites*, **12** (1992) 32.

170. Janin, A., M. Maacha, J. C. Lavalley, J. F. Joly, et. al ., *Zeolites*, **11** (1991) 391.

171. Liu Da - Song, Bao Shu Lin, Xu . Qin - Hua ; *Zeolites*, **18(2/3)** (1997) 162.

172. Venuto, P.B., *Microporous Materials*, **2** (1994) 364.

CHAPTER -2

EXPERIMENTAL

CHAPTER II

EXPERIMENTAL

2.1 INTRODUCTION :

This chapter describes all the experimental techniques used in the present studies on *modifications in large pore zeolites* namely beta and mordenite. The details of the procedures adopted for syntheses, modifications, physicochemical characterization and evaluation of the catalytic activity of these materials are presented .

2.2 PART-A, MODIFICATIONS BY DIRECT SYNTHESIS :

The modification by direct hydrothermal synthesis was carried out by isomorphous substitution of Ga^{3+} and Be^{2+} cations. Hydrothermal synthesis was carried out using different compositions in stainless steel autoclaves of 150 ml. capacity (Fig 2.1) at various temperatures under autogenous pressure in static conditions. Prior to use, the autoclaves were thoroughly cleaned in a boiling solution of strong alkali (NaOH) to prevent contamination from any impurities and to minimise seeding effects, if any. All the synthesis procedures described here are based upon preliminary investigations which involved experimenting with different synthesis parameters like varying molar compositions, order of mixing the reactants, variation in reaction temperatures, etc. Figures 2.2 and 2.3 depict the sequence of addition that was adopted to achieve substantial crystallinity in the products. Thus, the zeolites used in the present study were obtained under optimized conditions of synthesis and were highly crystalline and consisted of the purest phase of the desired zeolite framework.

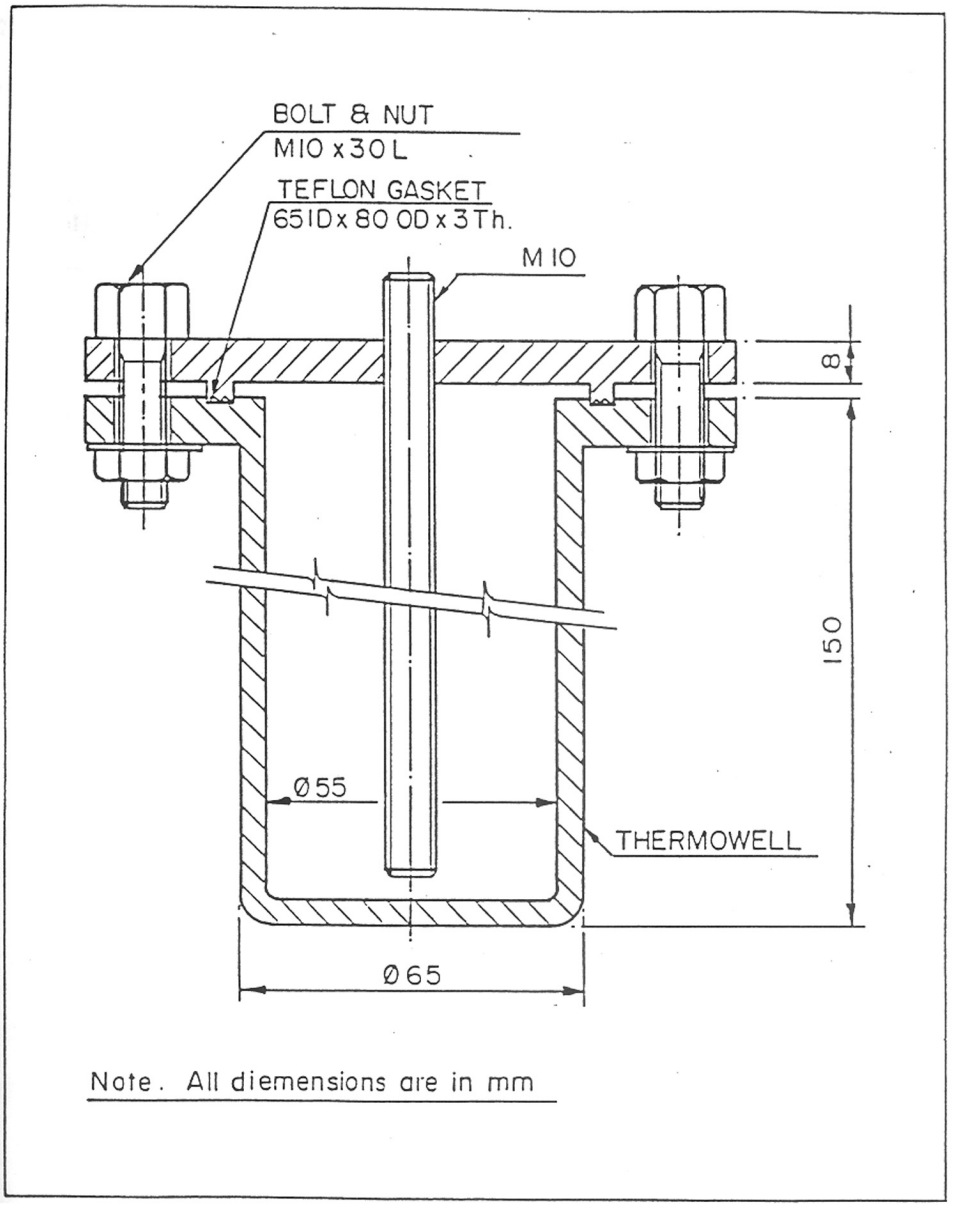

Fig. 2.1 : Stainless steel (316) autoclave with teflon gasket for hyrothermal synthesis.

Fig.2.2 : Flow Sheet For The Synthesis Of Various Isomorphs Of Zeolite Beta

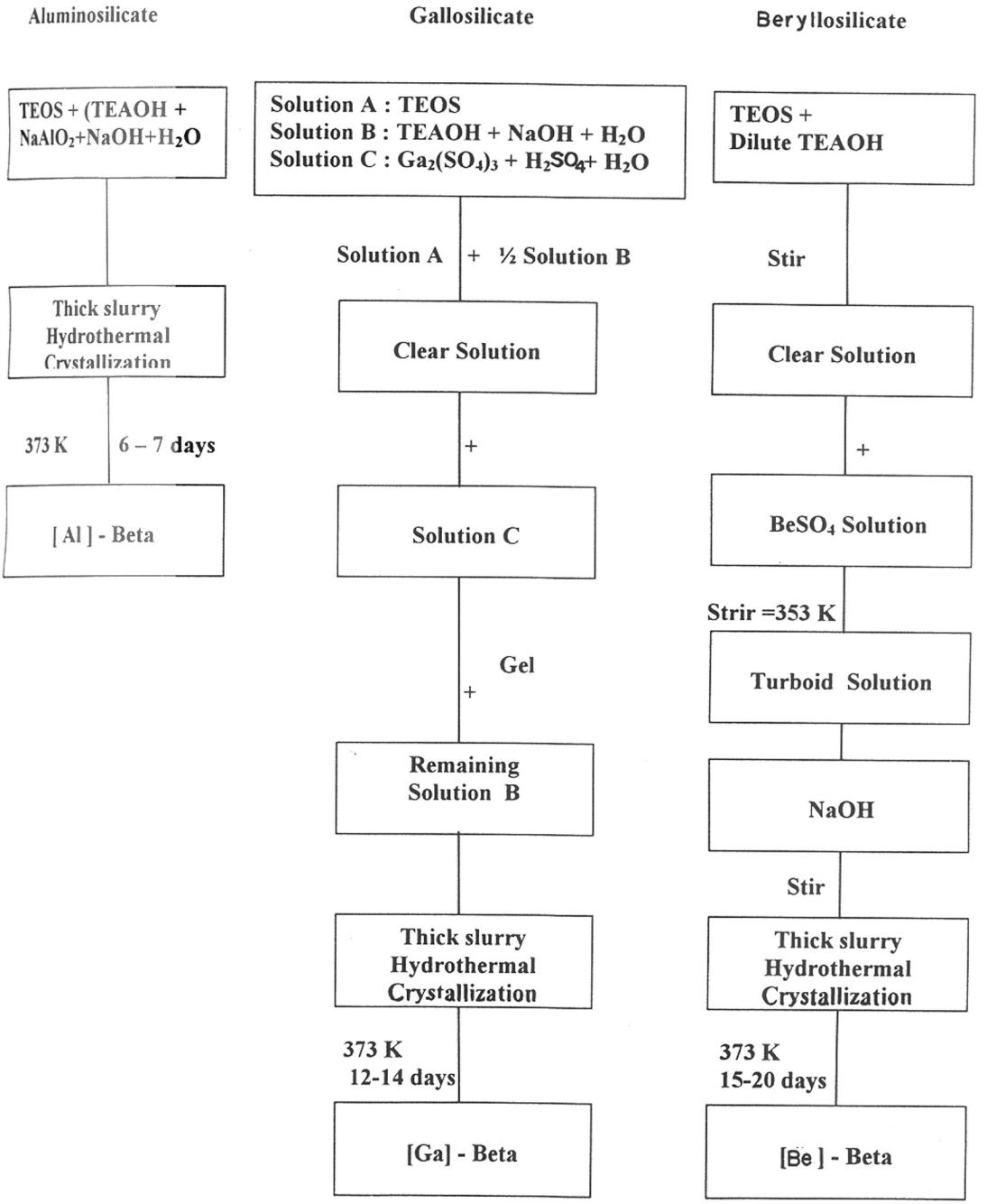

Fig . 2.3 : Flow Sheet for the Synthesis of Isomorphs of Mordenite

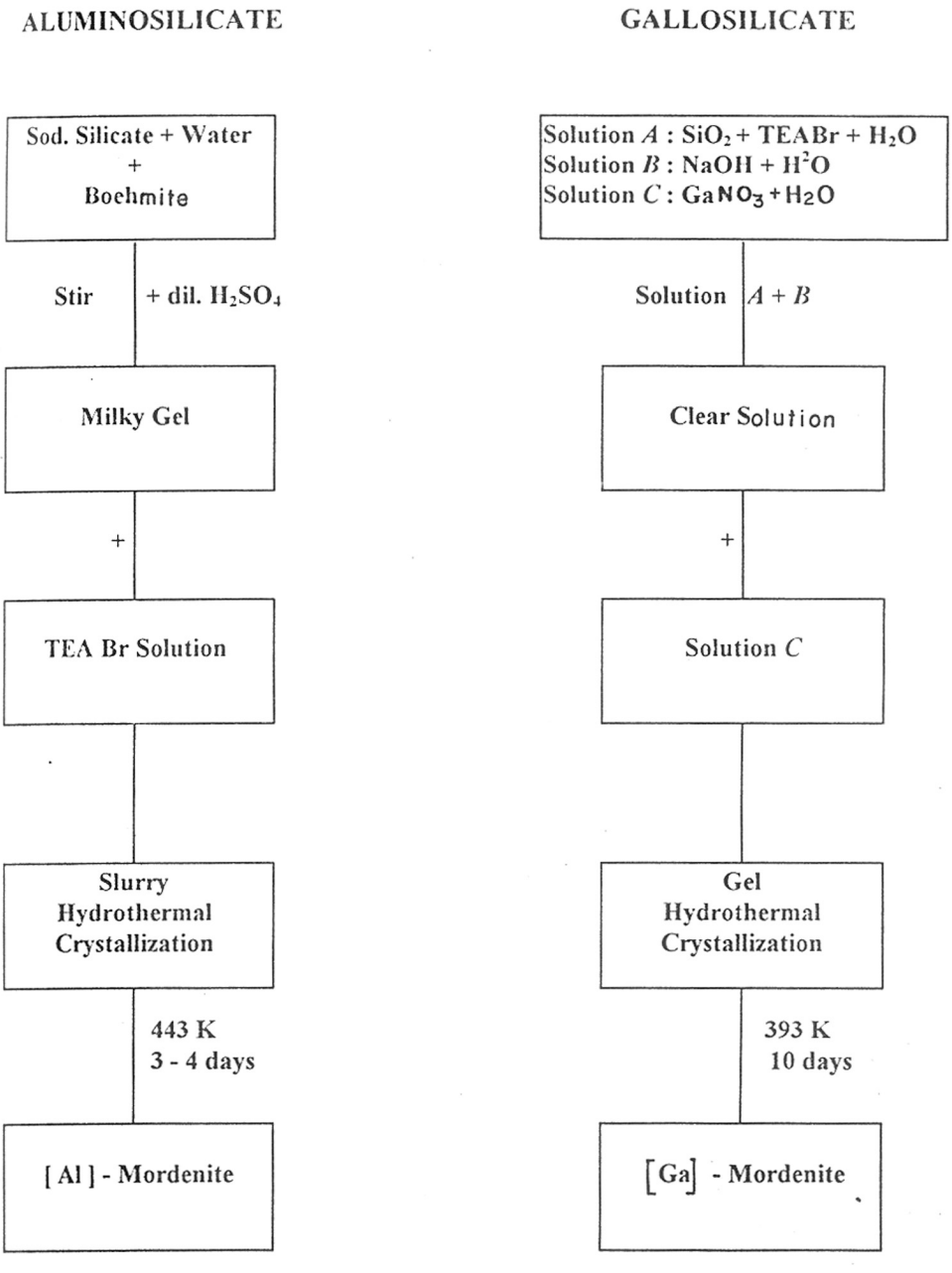

2.2.1 Synthesis of [A1]-beta :

In a typical preparation procedure, 0.1g Sodium hydroxide (NaOH, AR. LobaChemie, Bombay), 1.55g sodium aluminate ($NaAlO_2$) and 36.8g tetraethylammonium hydroxide (TEAOH, 40%, Aldrich) were mixed with 48.8g deionized water. To this homogenous mixture was added gradually 42.5g tetraethyl orthosilicate (TEOS, 98% Fluka) taken in a polythene beaker with constant stirring (using a magnetic stirrer-cum-hot plate) at a temperature between 343 to 353K. Stirring was continued till the ethanol resulting from the hydrolysis had apparently evaporated (approximately 4 to 5 hours), and a reactive gel was obtained with the molar composition : $60SiO_2 : Al_2O_3 : 5 (TEA)_2 O : 3Na_2O : 1500 H_2O$.

The gel was then transferred into a thoroughly cleaned autoclave, closed tightly and heated in a static oven at 393K. After 6-7 days, the autoclave was removed and quenched in cold water. The solid was filtered and washed thoroughly with deionized water and dried at 373K .

2.2.2 Synthesis of [Ga]-beta :

The synthesis of [Ga]-beta zeolite was carried out hydrothermally from the system $(TEO)_2O$-SiO_2-Ga_2O_3-Na_2O-H_2O at 393K. Samples A, B, and C were prepared by mixing appropriate quantities of tetraethyl orthosilicate (TEOS, Aldrich), sodium hydroxide (AR grade), sulphuric acid (98%,AR), galliumsulfate (AR, ALFA), 40% aqueous tetraethylammonium hydroxide (TEAOH, ALFA), and distilled water. The gel compositions were as follows:

Sample A : $30.0SiO_2 : Ga_2O_3 : 18.22 (TEA)_2O : 2.98Na_2O : 0.3 H_2SO_4 : 575.0 H_2O$;

Sample B : $60.0SiO_2 : Ga_2O_3 : 36.33 (TEA)_2O : 5.95Na_2O : 0.14 H_2SO_4$: 1147.0 H_2O;

and Sample C : $150SiO_2 : Ga_2O_3 : 90.8\ (TEA)_2O : 14.84\ Na_2O : 0.06\ H_2SO_4 : 2867\ H_2O$

The reacting gel was prepared as follows : (for sample, A) 3.01g $Ga_2(SO_4)_3$ was dissolved in 18.5 ml (0.1 N) H_2SO_4 by warming on a hot plate until a clear solution was obtained. To this, a solution containing 18.25g of TEAOH, 15ml H_2O, and 0.47g NaOH was added dropwise under continuous stirring at 333K. In another container, 42.5g TEOS was taken, and to this a solution containing 18.25g TEAOH, 15ml H_2O, and 0.46g NaOH was added dropwise under continuous stirring at 333K. To this solution, tha $Ga_2(SO_4)_3$-containing the solution prepared earlier was added dropwise under continuous stirring at 333K. All additions were done very slowly over a period of 3 h and stirring was continued for further 5 h after completing addition. The milky solution thus obtained had a pH of 12.5. It was then allowed to crystallize in a stainless-steel autoclave (250 ml) at 393K under static conditions. A pure crystalline product was obtained after 13 days. Tha solid material thus obtained was filterd, washed with deionized water, and dried at 393K. The solid was further calcined in a flow of dry air by slowly increasing the temperarture to 700K and maintaning it for 24 h to obtain the sodium form.

A similar synthesis procedure was adopted to prepare [Ga]-beta with two other SiO_2/Ga_2O_3 ratios after making appropriate changes in the quantities of the reactants taken. The molar composition of the three solid samples (Na-[Ga]-beta) by wet chemical analysis method on anhydrous basis was,

Sample A : $20SiO_2 : Ga_2O_3 : 0.02Na_2O$;

Sample B : $56SiO_2 : Ga_2O_3 : 0.02Na_2O$;

Sample C : $113SiO_2 : Ga_2O_3 : 0.01Na_2O$

2.2.3 Synthesis of [Be]-beta :

In a typical preparation, 73.0g of tetraethyl ammonium hydroxide diluted with 60 ml deionized water was gradually added to 85.0g tetraethyl orthosilicate taken in a polythene beaker of 500 ml capacity. To this was added 0.70g beryllium sulfate ($BeSO_4$, AR, Aldrich) dissolved in 20 ml of water. Addition was done very slowly under vigorous stirring on a magnetic stirrer-cum-hot plate. After partial addition (approx. 1/4th of the total quantity of beryllium sulfate solution), stirring was done simultaneously with heating, the temperature being maintained at 353K. Addition of beryllium sulfate was completed over a period of one hour. The contents were allowed to stir for one more hour. Finally, a solution of 1.62g sodium hyroxide in 17ml deionized water was added gradually. After all these additions were complete, stirring and heating were continued for 5-6 hours, till the liberated ethanol had apparently completely evaporated. The reacting gel had the molar composition of $60SiO_2$:BeO:36.33 $(TEA)_2O$:5.95 NaO_2 : $1147H_2O$. The resulting thin slurry was transferred to a stainless steel autoclave and allowed to crystallize at 373 K for two weeks. The autoclave was then taken out, quenched in cold water, the content filtered, washed thoroughly and dried at 373K for 6 hours.

[Be]-beta with different beryllium contents were synthesized by varying the amount of beryllium sulfate in the synthesis gel.

2.2.4 Synthesis of [A1]-mordenite :

Synthesis of [A1]-mordenite was carried out using sodium silicate (water glass, 28 % SiO_2), tetraethyl ammonium bromide (TEABr, AR, Aldrich), Boehemite (Catapal B) and sulfuric acid (98%). In a typical synthesis procedure, 50g of deionized water was added to 64.53g sodium silicate under stirring. 1.38g boehemite was slowly added to this solution

under stirring. Addition of a solution of 0.86g of sulfuric acid in 50g water to this solution resulted in the formation of a milky gel. Stirring was continued for one more hour. The composition of the gel in terms of moles of oxides was : $30SiO_2$: Al_2O_3 : 3TEABr : $7.5Na_2O$: $1054H_2O$. The gel was then transferred to a stainless steel autoclave and kept in a static oven at 443 K for 3-5 days. The autoclave was then removed from the oven and quenched in cold water. The resultant white material was filtered, washed and dried at 393 K in air for 8 hours.

2.2.5 Synthesis of [Ga]-mordenite :

A slurry of 14.87g of microfine (0.007 μ) silicon dioxide (90.88% SiO_2, 9.8% H_2O) in 50g water and a solution of 4.73g of TEABr dissolved in 25g of water were mixed together, to obtain solution [A] which was kept stirring. Solution [B] was prepared by dissolving 4.50g NaOH in 300g of water and added to the above solution [A]. The resultant gel was kept stirring for one hour. Solution [C] was then obtained by dissolving 5.02g gallium (III) nitrate (99.9% Aldrich) in 30.94 g of water and transferred dropwise to the above stirring gel comprising of the solutions [A] and [B]. The mixture was allowed to stir for one hour at room temperature to get a homogenous gel and then transferred to a stainless steel autoclave. Its composition in terms of moles of oxides was as follows:$30SiO_2$: Ga_2O_3 : 3 TEABr : 7.50 Na_2O :1054 H_2O .

The autoclave was kept in an oven at 413K for seven days. The autoclave was then removed and quenched in cold water. The crystalline white solid product was filtered, washed and dried in an air oven at 393K for 10 hours.

2.2.6 Pretreatment procedure :

All the zeolite molecular sieves synthesized above contained organic templates inside the channels. In order to characterize and use these zeolites in catalytic reactions, it is necessary to remove the organic material from the zeolite pores and to convert them into the hydrogen form. To accomplish this, the following procedure was adopted.

The as-synthesized material was placed in a silica boat, in a tubular furnace. The Al-analogs of zeolites beta and mordenite were slowly heated to 793K, and Ga- and Be- analogs to 673K in flowing nitrogen (100 ml/min) for 8 hours, then in flowing air for further four hours before being raised to 723K and 700K respectively, and kept for another 6 hours. to completely remove the organics. This treatment gave the Na- forms of the said zeolites.

The calcined material was refluxed thrice in 5M aqueous ammonium acetate solution (20 ml /g zeolite, at 368K for 6 hours). After each exchange, the material was filtered, washed thoroughly with deionized water and dried at 393K. The resultant ammonium form was calcined at 793K (Al-analogs) and 673K (Ga-/Be-analogs) respectively. This pretreatment yielded the catalytically active hydrogen form of all the zeolites.

2.3 PART-B, POST-SYNTHESIS MODIFICATIONS :

Chemical modification.

This section describes the various techniques that have been used to modify the zeolites used in the present studies.

2.3.1 Demetallation by acid leaching :

The NH_4^+- form of the [M]-beta with Si : M (M = Ga and Be) ratios of 56 and 55

respectively was used in this experiment. 2g of the sample was treated with 20 ml of 0.1N HNO_3, for 2 hours at room temperature. The mixture was then heated at 313K for 3 hours. It was then filtered, washed thoroughly with deionized water and dried at 383K for 3-4 hours. This mild treatment brought about demetallation without any significant loss in the crystallinity of the sample. However, treatment with higher concentrations of HNO_3 or heating at higher temperatures resulted in a tremendous loss in crystallinity of the material. The samples were calcined and characterized according to the procedure described in the earlier section. Degallation of the NH_4^+- form of [Ga]-mordenite was carried out similarly.

2.3.2 Demetallation of (NH_4)-Be-beta using ammonium fluorosilicate :

The NH_4^+- form of [Be]-beta (2g, $SiO_2/M=55$) was suspended in an aqueous solution of ammonium acetate, (40ml, 10M) at 348K. To this suspension, a 0.75 M solution of $(NH_4)_2 SiF_6$. (1g; dissolved in 7.5 ml deionized water) was added at a precisely controlled rate of 0.003 moles per minute per mole of metal present in the zeolite. To achieve this the fluorosilicate solution was passed at a steady rate of 0.1 - 0.2 ml/min, under reflux. The temperature of the slurry was maintained at 353 K. These conditions of temperature, concentration and addition rate were necessary to control the pH of the system at 6. The ammonium acetate solution acted as a buffer. Addition was completed over a period of 3 - 4 hours; after which the reaction mixture was further digested for another 2-4 hours. The sample was then filtered and washed thoroughly with hot water. It was dried at 383K for 6 hours. The sample was subsequently calcined according to the procedure described in section 2.2.

2.3.3 Demetallation of [TEA]-Be-beta using ammonium fluorosilicate :

A new procedure was adopted to remove the organic template [TEA] from [TEA]-Be-beta zeolite, which can also remove Be cations and insert Si cations into the lattice simultaneously. The [TEA]-Be-beta sample (5g) was put into 100 ml 0.1N ammonium acetate solution, ammonium hexaflurosilicate (0.75 M) was added drop wise while stirring at 25 °C. After stirring for 4 h, it was filtered and washed with deionised water, then the sample was treated with 100 ml 0.1N aqueous potassium chloride solution at 90 °C for 4 h, filtered and washed with deionised water. This K^+ ion-exchange was repeated three times. Then the sample was calcined to remove the remaining organic matter at 703 K in air for 6 h. It was further exchanged with NH_4NO_3 solution to convert it into the NH_4^+- form.

2.3.4 : Modification of Y zeolite (Faujasite) :

Commercial NaY zeolites supplied by PQ Corporation, USA were exchanged with ammonium ions and/or rare earth (RE) ions and were used to prepare the catalysts. The ion-exchange procedures for NH_4^+ and RE-ions are given below.

A. NH_4^+ - Ion exchange :

The Na^+ ions present in the Na-Y zeolite were partially exchanged with NH_4^+ ions by refluxing at 353 K with a 5 wt.% of solution of NH_4NO_3 in water for 12 hours. The volume of solution used for the exchange was 10 ml/g of the zeolite. The zeolite was than filtered, washed with warm deionized water thoroughly, dried at 383K for 12 hours and calcined at 773 K for 6 hours, to obtain the H-form of the zeolite.

B. Rare Earth (RE) – ion exchange :

RE ion-exchange was carried out using a 5 wt. % $RECl_3$ solution adopting a

procedure similar to the NH_4^+- ion-exchange procedure. Similarly, multiple exchanges were carried out to obtain greater exchange levels. The $RECl_3$ was supplied by Indian Rare Earth Ltd., Udhyogmandal, and its composition (as oxide form) was : 1-2 wt.% CeO_2, 35-40 wt.% Nd_2O_3, 10-12 wt.% Pr_3O_{11}, 4-6 wt.% Sm_2O_3, 40-50 wt.% $La_2O_3/Y_2O_3/$ etc. The RE-exchanged zeolite was finally calcined at 773K for 6 hours.

2.3.5 : Modification of mordenites

The dealuminated mordenite samples were prepared from a commercial H-mordenite [HM(1)] obtained from Norton, USA. The dealumination was carried out by a combination of hydrothermal and chemical methods.

About 20g of the commercial (H-mordenite) was taken in a silica boat and kept in a horizontal tubular (5 cm. id) furnace. The furnace was heated to 473K and water injected into it at a rate of 6 ml per hour. The temperature was raised to 923K over a period of 1 hour. The sample was maintained at 923K in a continuous flow of steam for 4 hours. The furnace was allowed to cool and the zeolite taken out.

The steamed zeolite was next extracted with 6N HCl for 1 hour at 353-358K in order to remove the extra framework Al_2O_3 formed during the steaming procedure. After the extraction, the zeolite was filtered out, washed thoroughly and dried at 383K.

The dealuminated samples were prepared by carrying out the dealumination procedure once [HM(2)] and twice[HM(3)], to bring about greater dealumination in the successive samples.

The chemical analyses of the NH_4^+-Y and REY was done using wet chemical methods (section 2.4.1). The surface areas of the samples were determined using the t-plot method. This modification (section 2.3.4 and 2.3.5) was done primarily for using the samples as catalysts in the alkylation of benzene with long chain olefins, mentioned in chapter V.

2.4 CHARACTERIZATION :

2.4.1 Chemical analysis :

An accurately weighed, known amount of sample in the range 200-300 mg was taken in a platinum crucible, covered with a lid and ignited over a Bunsen flame for approximately 2-3 hours. The sample was then cooled in a desiccator and weighed. The weight of the sample before and after ignition gave the loss due to occluded water and organics (calculated as % LOI). The anhydrous weight of the sample was calculated on the basis of % LOI. The anhydrous sample was moistened with 2-3 drops of deionized water. To this was added 20 ml, 1:1 HF (40% wt/vol, electronic grade, Loba Chemie Bombay) along with 2-3 drops of concentrated sulfuric acid (98%, AR). The contents of the crucible were digested on a hot plate and evaporated to near dryness very gently. This treatment was repeated two more times to ensure complete removal of Si as H_2SiF_6. The residue was again ignited over a Bunsen flame for 3-4 hours (till constant weight was obtained), cooled in a descicator and weighed. The loss in weight was determined to get the silicon content of the sample. The residue left behind contained oxides of Na/Al/Ga/Be, etc. It was fused with potassium pyrosulfate, dissolved in deionized water and the solution made up to a known volume in a standard volumetric flask. The solution was then analysed by ICP (Jobin Yvon, JYU-38 VHR) and Atomic Absorption Spectroscopy (Hitachi Z-8000) for estimating Na/Al/ Ga/Be, etc.

2.4.2 X-Ray Diffraction :

The samples synthesized during the course of this work under different conditions and different crystallization time, were analysed for qualitative and quantitative phase identification by X-ray powder diffraction (Rigaku model D/MAX III VC, Japan). The most

crystalline sample of each zeolite framework type was taken as the reference sample, for the quantitative phase identification.

Silicon was used as an internal standard for calibrating the 2θ values. The unit cell parameters were calculated for the calcined samples from x-ray diffraction patterns obtained at a scanning speed of 0.25 min^{-1}.

2.4.3 Scanning and Transmission Electron Microscopy :

The morphology of all the as-synthesized zeolite gallosilicate and beryllosilicate samples were investigated using a scanning electron microscope (JEOL JSM-5200). The samples were dusted on alumina and coated with a thin gold film by sputtering to prevent the formation of surface charging and damage of the zeolite material by the electron beam. In all the analyses, an uniform thickness of ~ 0.10 mm was maintained.

For transmission eletron microscopy, samples were dispersed ultrasonically in isopropylalcohol for several seconds. A drop of this suspension was then placed on a carbon film supported over a TEM specimen grid. The samples thus prepared were dried and then examined with an electron microscope (model 1200EX, Jeol, Japan 120 KV) both in bright and dark field modes. The lattice parameter calibration with grid film mode showed the accuracy of measurements to be better than ±1%.

2.4.4 Sorption studies :

The sorption experiments for water and hydrocarbons were carried out by gravimetric methods. A conventional McBain spring balance assembly was used as shown in figure 2.4. The zeolite was pressed into a pellet (weighing approximately 18 mg), attached to a sensitive quartz spring of sensitivity, S = 70 $cm.g^{-1}$. The sample was activated at 673K under

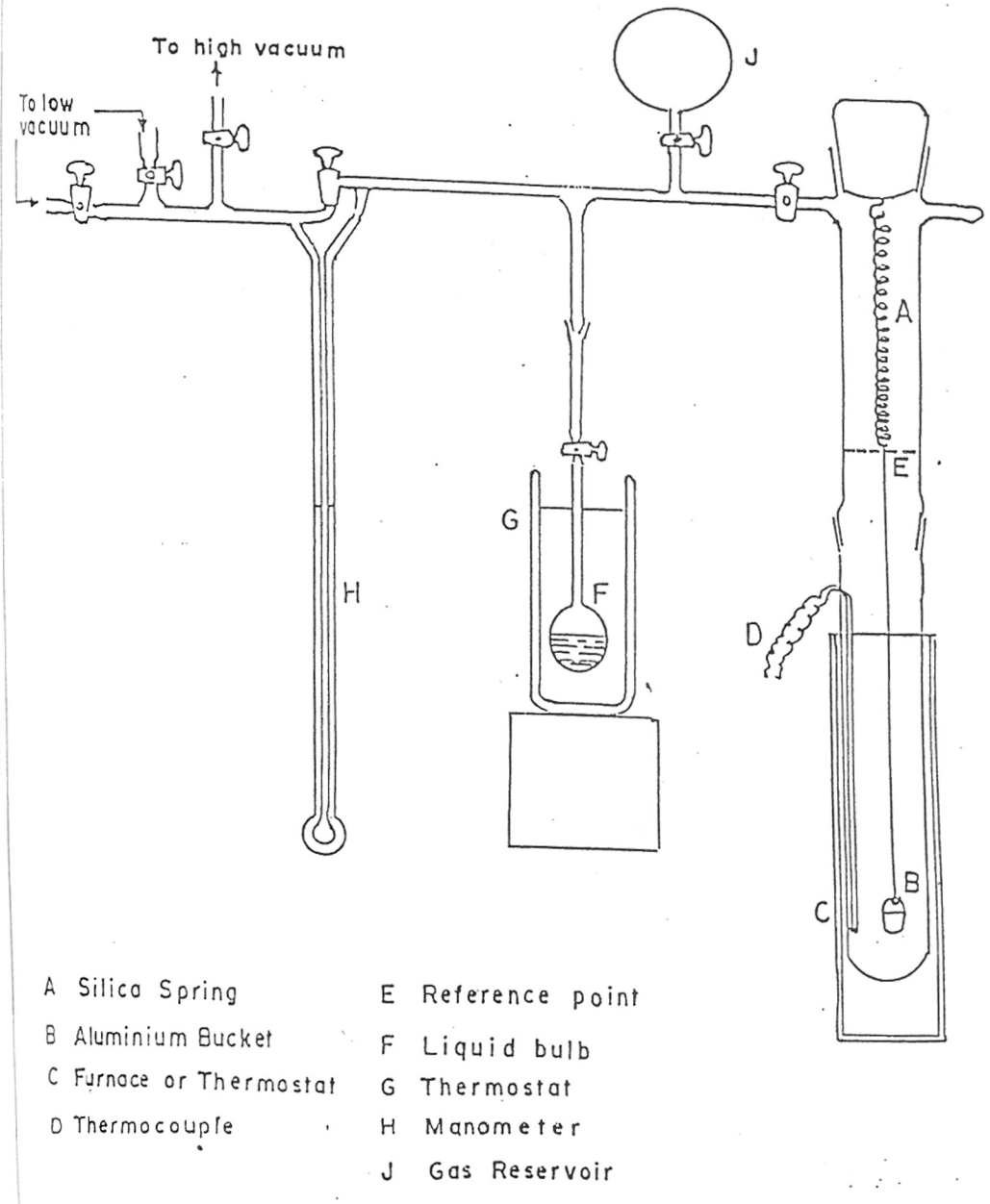

Fig. 2.4 : Gravimetric adsorption Unit.

a vacuum of 10^{-6} torr for 6 hours, cooled to 298K and exposed to the adsorbate vapour at the desired vapour pressure. The change in weight due to adsorption was measured at regular intervals on a cathetometer.

2.4.5 Thermal analysis :

Simultaneous TG-DTA analyses of all the as-synthesized crystalline phases were performed on an automatic derivatograph (SETARAM TG-DTA 92). The thermograms of the samples were recorded under the following conditions.

Weight of the sample = *30 mg.*
Heating rate = *10K/ min*
SENSITIVITY
TG = *25 mg*
DTG = *0.2 mv.*
DTA = *0.1 mv.*
Atmosphere = flowing air.

Preheated finely powdered alumina, fired at 1273K was used as the reference material.

2.4.6 Temperature programmed desorption of ammonia :

This technique was used to determine the surface acidity, and acid strength distribution of the samples. The experimental set up used in this study is shown in Fig 2.5. The catalyst sample (10-20 mesh,400 mg) was loaded in the silica reactor which was connected to a sorptometer. After activation at 673K (10^{-6} torr), the sample was cooled to room temperature and an adsorption isotherm of ammonia was determined, after which the physically sorbed ammonia was removed from the sample by evacuation and an ammonia adsorption isotherm was once again determined. The difference between the first and second isotherms gave a nearly constant value for chemisorbed ammonia. The sample was then evacuated at the same temperature and now connected to a conventional gas-chromatograph

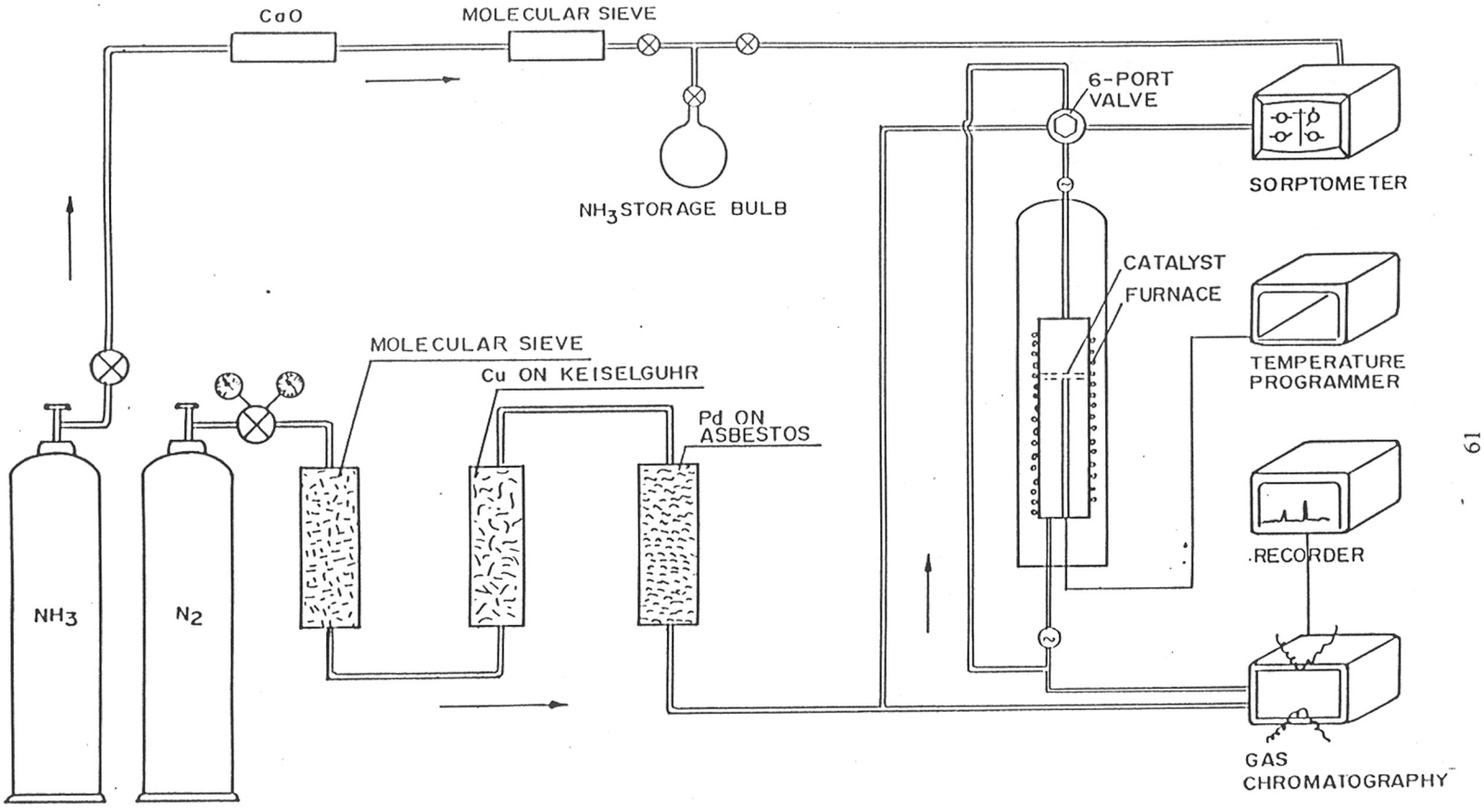

Fig. 2.5 : Temperature Programmed Desorption (TPD) apparatus.

(Shimadzu GC-RIA having a TCD and a six-port valve. The sample was heated at a rate of 10K min^{-1} in a flow of nitrogen (100 ml / min). The concentration of desorbed ammonia as a function of temperature was recorded upto 823 K.

2.4.7 Surface area measurements :

Omnisorb 100 CX unit (supplied by Coulter Corporation, USA) was used for the measurement of nitrogen adsorption to determine surface area. The samples were activated at 673K for two hours in high vacuum. After the treatment, the anhydrous weight of the sample was taken. The samples were then cooled to 74K using liquid nitrogen. After this, the samples were allowed to adsorb nitrogen gas. Finally the BET surface area was calculated using the t-plot method.

2.4.8 High Resolution Solid State MAS NMR Spectroscopy :

The high resolution solid state MASNMR spectra of ^{29}Si were obtained at 295 K in a Bruker MSL-300 spectrometer operating in the FT mode, using one cycle type measurements. Bloch decays were averaged over 2400 times before fourier transformation to get spectra with sufficient S/N. While acquiring the Si spectra, a 90 degrees pulse and a recycle time of 3s was found to be sufficient to give fully relaxed spectra. MAS was kept at 3.5 KHz. Chemical shifts in ppm were measured w.r.t. tetramethylsilane (TMS) as the external reference. The rotor (sample holder) was spun at a rate of 4.0 KHz. ^{27}Al MAS NMR spectra were obtained using 45 pulse with one second delay time, at the Lamor frequency of 78.0131 MHz with a spinning speed of 4 -5 MHz. Chemical shifts in ppm were measured w.r.t. aqueous 0.1N $AlCl_3$ as the external standard.

The high resolution MASNMR spectra of Ga were recorded at 295K on a Bruker MSL-400 spectrometer at the Lamor frequency of 121.99 MHz in a 100 KHz spectral

window. An excitation pulse (t pulse) of 1.0 μs and $t_{repetition}$ of 0.1s was adjusted with 50, 000 NS (number of scans) having spinning rate of 6000 Hz. The free induction decays were collected under MAS and typically 2000 transients were accumulated to give acceptable S/N. Before fourier transformation, the FID was apodized with a 100 Hz exponential line broadening.

The high resolution MASNMR spectra of ^{9}Be were recorded at 295K on a Bruker MSL-300 spectrometer at the Lamor frequency of 42.17 MHz. The data were collected using a pulse length of 2 μS, spectral width of 125 KHz and a relaxation delay of 1 sec. The powdered sample was packed in a 7.0 mm o.d zirconia rotor and spun at ~ 3.3 KHz. An aqueous solution (0.01M) of $BeSO_4$ was used as the reference for chemical shift. 1000 - 2000 transients were collected using a standard CYCLOPS pulse sequence for the zeolite samples. The raw FID'S were processed with a line broadening function of 100 Hz prior to Fourier transformation.

2.4.9 Infrared spectroscopy :

The infrared spectra were recorded with a PYE UNICAM SP3 300 spectrometer in the frequency range 4200-1300 cm^{-1} using the nujol method. This was done to study the fundamental region of the vibrations of the zeolite framework. KCN was used as an internal standard.

To study the vibrations in the hydroxyl region of the zeolite samples, i.e., in the range of 4000-1300 cm, self supported wafers were used. For in-situ studies, a cell in which the temperature can be varied from liquid nitrogen temperature to 773K was fabricated and used (Fig. 2.6). This cell was connected to a volumetric adsorption apparatus (Micromeritics, USA, Model : Accusorb-2000E). The spectra were recorded with a

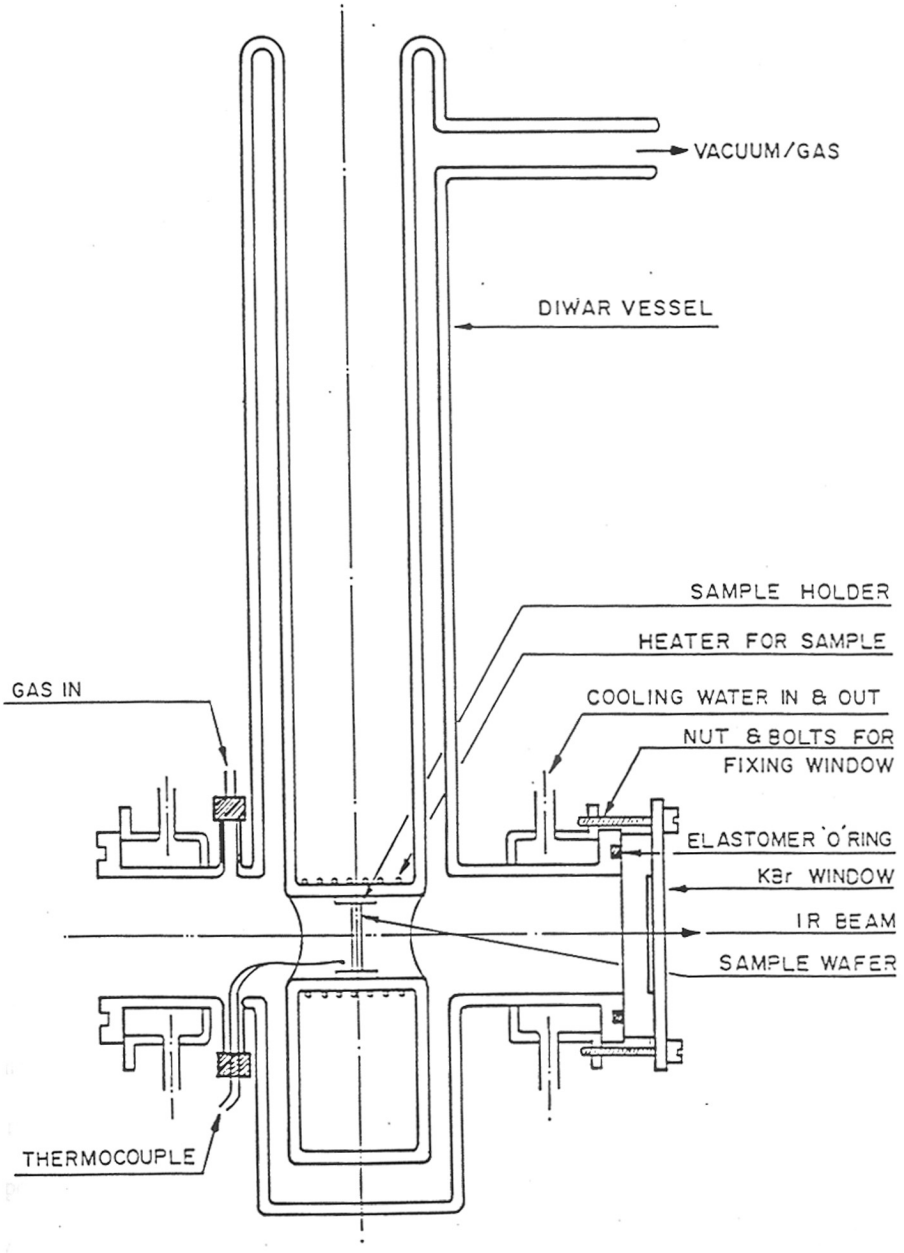

Fig. 2.6 : FTIR Transmittance Cell

NICOLET 60 SXB FTIR spectrometer. The sample was pressed under a pressure of 5 tons per sq.inch into a thin wafer (5-6 mg/cm) and mounted in a sample holder (SH). It was then placed inside the heating compartment of the cell (HC) and aligned in line with the ir beam. The cell was sealed at both the ends by KBr windows (KW) with the help of elastomer O rings. A thermocouple placed in close vicinity of the sample measured the temperature of the sample. Another side tube at the top of the sample measured the temperature of the sample. The side tube at the top of the cell was connected to the high vacuum system. Cold water was constantly circulated through the cooling coil provided near the KBr windows. The sample was heated to 673 K (at a heating rate of 5K/min), under vacuum and maintained at this temperature for approximately 6 hours and then cooled down to 323K in vacuum. The spectra were recorded by averaging over 500 scans with 2 cm^{-1} resolution. Vapours of pyridine were admitted in to the sample through the adsorption manifold of the system.

2.5 CATALYTIC MEASUREMENTS

The purity and source of all the reactants used during the present catalytic studies are presented in Table 5.1 and 5.2 (chapter V).

The as-synthesized alumino- and gallo-isomorphs of mordenite, beta and the beryllo-silicate analog of beta were tested for the catalytic activity in the isomerization of m-xylene. The reaction was carried out at atmospheric pressure using a glass reactor described in Section 2.5.1. The catalyst was always activated at 753K for 8h in flowing dry air, prior to the start of the run. The catalyst was then cooled to the reaction temperature in a flow of dry N_2. The exact reaction parameters used in different experiments are presented along with the data in the later chapters.

Another reaction, namely the alkylation of benzene with 1-hexene and long chain

olefins was carried out over a range of zeolites, both at atmospheric pressure (using a glass reactor described in section 2.5.1) as well as at higher pressures using a stainless steel (SS 316; 19 mm id) reactor (Catatest, Model BL-2, Geomecanique, France.) Both the reactors were fixed bed, down-flow types.

The catalyst was always activated in the manner already described above. Benzene was injected first for one hour at the reaction temperature prior to injection of the actual alkylation mixture (olefins + benzene). The exact reaction parameters used in the different experiments will be presented along with the data in Chapter V.

2.5.1 Atmospheric Pressure Reactor :

All the catalytic experiments were carried out in a fixed bed down-flow tubular reactor. The reactor consisted of a fused silica tube of 1.5 cm inner diameter (i.d.) and 30 cm length with a provision for feeding the carrier gas at the top. It had a thermowell which carried a thermocouple for sensing the reaction temperature. The zeolite powder was pressed into pellets in a hydraulic press with 1.5 cm die at pressures upto 10 ton sq.inch. These pellets were crushed gently and sieved to obtain 15-20 mesh size particles. 1g (on anhydrous basis) of catalyst was loaded in the centre of the reactor in such a way that the catalyst was placed between inert porcelain beads. The upper portion of reactor, serving as a vapourizer-cum-preheater was packed with inert porcelain beads. The reactor was placed in a two zone furnace (Fig 2.7). Before commencing the reaction, the catalyst was activated in a stream of dry air at 753 K for approximately 8h. The catalyst was then flushed with dry nitrogen and cooled to the reaction temperature. After fine adjustments of the temperature and gas flow rates to the required values, the feed was then injected into the reactor using a syringe pump (Sage instruments, USA, Model 352) at the required rate. The flow rates of

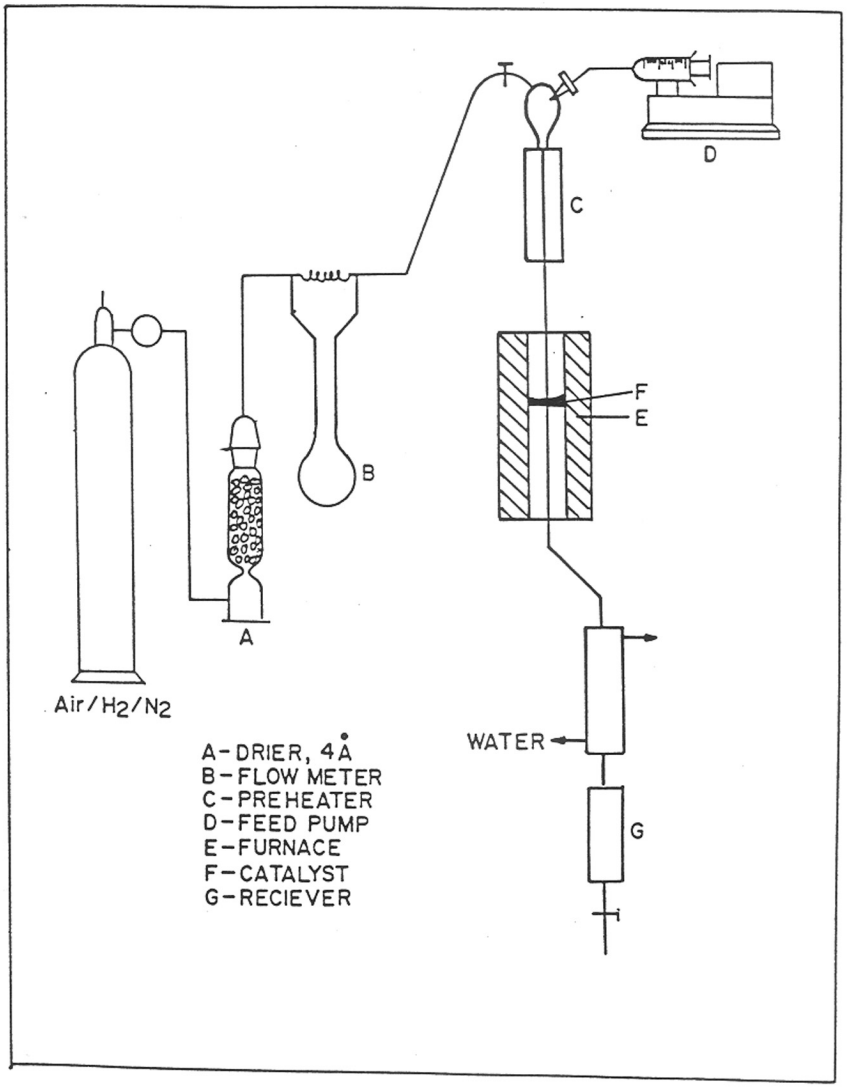

Fig. 2.7 : Fixed bed down flow reactors used for reactions in this study

gaseous reactants/carrier gases were controlled by needle valves and monitored by a calibrated flow meter.

2.5.2 High Pressure Reactor :

A high pressure reactor (Model BL-2) supplied by M/s Geomecanique, Paris, France, was used in this study. The reactor having a total volume of 220 ml was made of SS-316 and was 88.5 cm long with an inner diameter (i.d.) of 19 mm. It had a thermowell running all along the length of the reactor (o.d.= 6 mm). Five thermocouples could be inserted through the thermowell to measure the reactor temperature at different points. The furnace was made up of five shells (zones), whose temperatures could be independently controlled with five temperature controllers. Gases were introduced via mass flow controllers, while the outgoing gases were measured by a wet gas flow meter. About 60-80g (1.5x3 mm) catalyst was used in the high pressure benzene alkylation reactions. The catalyst was activated in flowing dry air at 753K, then purged with nitrogen, cooled to 373K and pressurized with N_2 to 6 bars. After adjusting all the parameters, the feed was injected at the desired rate. Samples were collected periodically (liquid as well as gas).

2.5.3 Product Analysis :

The products from xylene isomerization were analyzed using a Shimadzu Gas Chromatograph (G.C.Model FID Detector). The samples collected at fixed intervals were injected into the G.C. through the six-port valve for analysis. A two meter long stainless steel column (3mm, i.d) packed with Bentone-34 loaded with diisodecylphthalate (10%) was used for separation of the components of the products.

The products from the benzene alkylation reaction were analysed in a gas chromatograph (Hewlett Packard 5880A) equipped with a capillary column (50 m x 0.25

mm, cross-linked with methyl silicone gum). The products were identified by GC-MS (Shimadzu QCMS-QP2000A). Since the G.C. response to different compounds varied, standard samples were injected to determine the response factors. The product analyses were normalized using these G.C. response factors.

CHAPTER -3

PHYSICO-CHEMICAL CHARACTERIZATION OF MODIFIED ZEOLITE BETA AND MORDENITE

CHAPTER III

PHYSICO CHEMICAL CHARACTERIZATION OF MODIFIED ZEOLITES

A. ZEOLITE -BETA

3.1 [Ga]- AND [Be]- BETA BY DIRECT SYNTHESIS :

3.1.1 Synthesis :

The quality of [Ga] and [Be]- beta with respect to crystalline purity and uniformity of crystallite size largely depends on the source of silica. Under the conditions employed, highly crystalline material free from aluminum impurities was obtained when TEOS was used. The reaction gel compositions for samples 2, 3 and 4 (table 3.1) were adjusted as below :

Sample 2 : 30.0 SiO_2 : Ga_2O_3 : 18.22 (TEA)$_2$O : 2.98 Na_2O : 0.3 H_2SO_4 : 575.0 H_2O

Sample 3 : 60 SiO_2 : Ga_2O_3 : 36.33 (TEA)$_2$O : 0.14 H_2SO_4 : 5.95 Na_2O : 1147.0 H_2O and

Sample 4 : 150 SiO_2 : Ga_2O_3 : 90.8 (TEA)$_2$O : 0.06 H_2SO_4 : 14.84 Na_2O : 2867 H_2O

The yield of the product was about 70 % and the ratio SiO_2: Ga_2O_3 of the product was always less than that in the gel. The template concentration had to be increased considerably to obtain samples of higher SiO_2/Ga_2O_3 ratio. The chemical compositions of the calcined samples are given in the table 3.1.

3.1.2 X-RAY DIFFRACTION, SEM, TEM AND TG-DTA ANALYSIS :

The XRD patterns of samples 2, 3 and 4 for [Ga]- beta, 6, 7 and 8 of [Be]-beta and 9, 10, and 11 of deberyllated beta are presented in the fig 3.1 (curves a, b, c), 3.2 (curves e, f, g) and 3.3 (curves h, i, j) respectively were similar to those for [Al] - beta reported by Newsam

Table 3 . 1 : Chemical composition of the samples.

S. No	Sample	Unit Cell Composition
1	H-Al-β (60)	0.05 Na [2.1 AlO_2 : 61.9 SiO_2]
2	H-Ga-β (20)	0.06 Na [5.82 GaO_2 : 58.18 SiO_2]
3	H-Ga-β (56)	0.04 Na [2.20 GaO_2 : 61.80 SiO_2]
4	H-Ga-β (113)	0.02 Na [1.11 GaO_2 : 62.90 SiO_2]
5	DA-H-Ga-β (110)	0.01 Na [1.14 GaO_2 : 62.86 SiO_2]
6	H-Be-β (28)	0.02 Na [4.27 GaO_2 : 59.73 SiO_2]
7	H-Be-β (55)	0.03 Na [2.25 GaO_2 : 61.75 SiO_2]
8	H-Be-β (110)	0.02 Na [1.14 GaO_2 : 62.86 SiO_2]
9	DA-H-Be-β (115)	0.01 Na [1.10 GaO_2 : 62.90 SiO_2]
10	DF-H-Be-β (120)	0.01 Na [1.05 GaO_2 : 62.95 SiO_2]
11	DFK-H-Be-β (105)	0.01 K [1.20 GaO_2 : 62.80 SiO_2]
12	H-Al-M (25)	0.01 Na [6.40 AlO_2 : 41.60 SiO_2]
13	H-Ga-M (19)	0.01 Na [5.05 GaO_2 : 42.95 SiO_2]
14	DA-H-Ga-M (27)	0.05 Na [3.31 GaO_2 : 44.69 SiO_2]

Figures in brackets are Silica / Metal oxide ratios,

DA – Demetallation by acid,

DF – by $(NH_4)_2 SiF_6$

DFK - by $(NH_4)_2 SiF_6$ then K^+ and NH_4^+ ion exchange

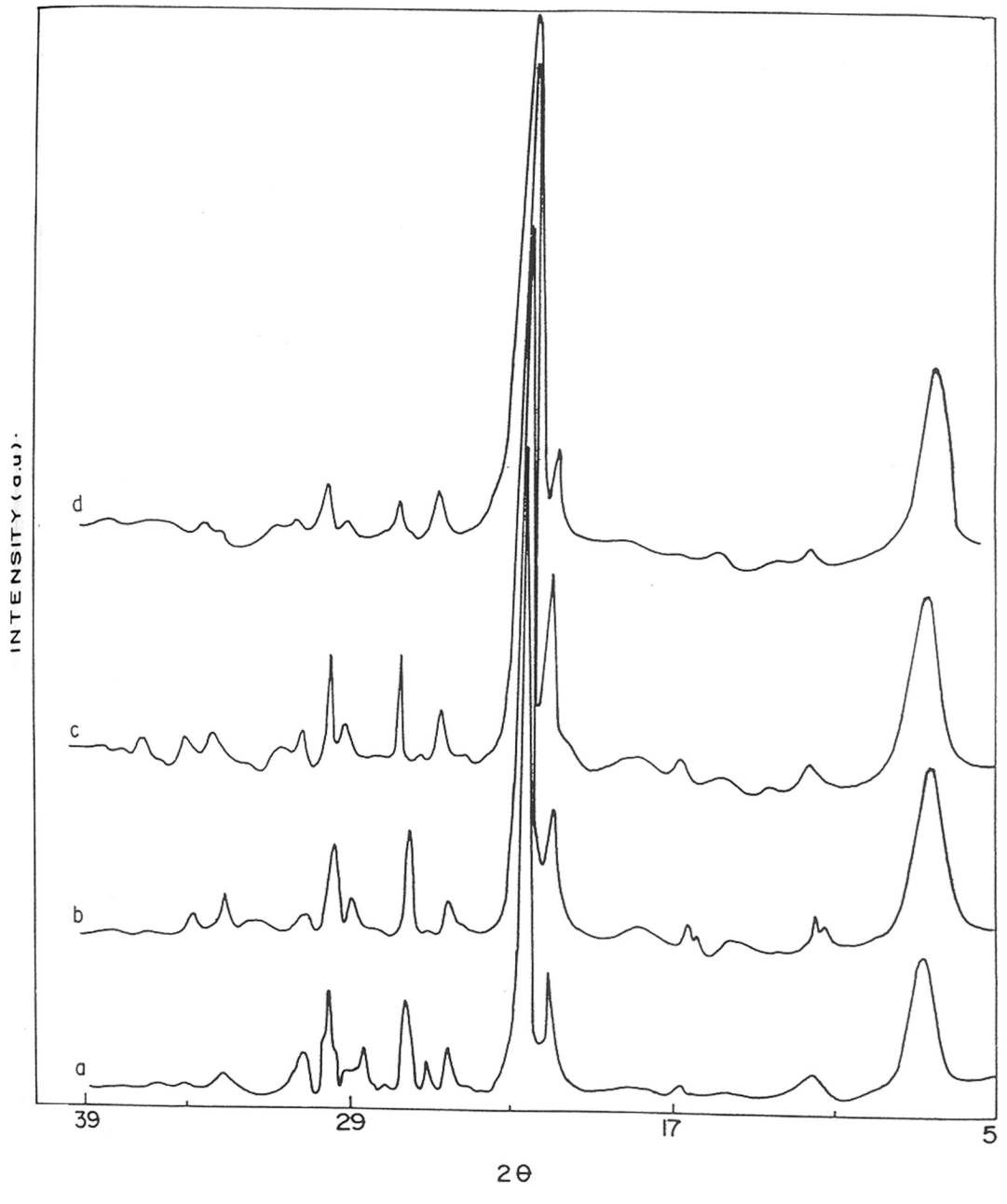

Fig. 3.1 : X-ray Diffraction patterns of H-Ga-β with SiO_2 / Ga_2O_3 ratios of 20, 56 and 113 [curves a, b and c respectively], and degallated H-Ga-β (110) [curve d]

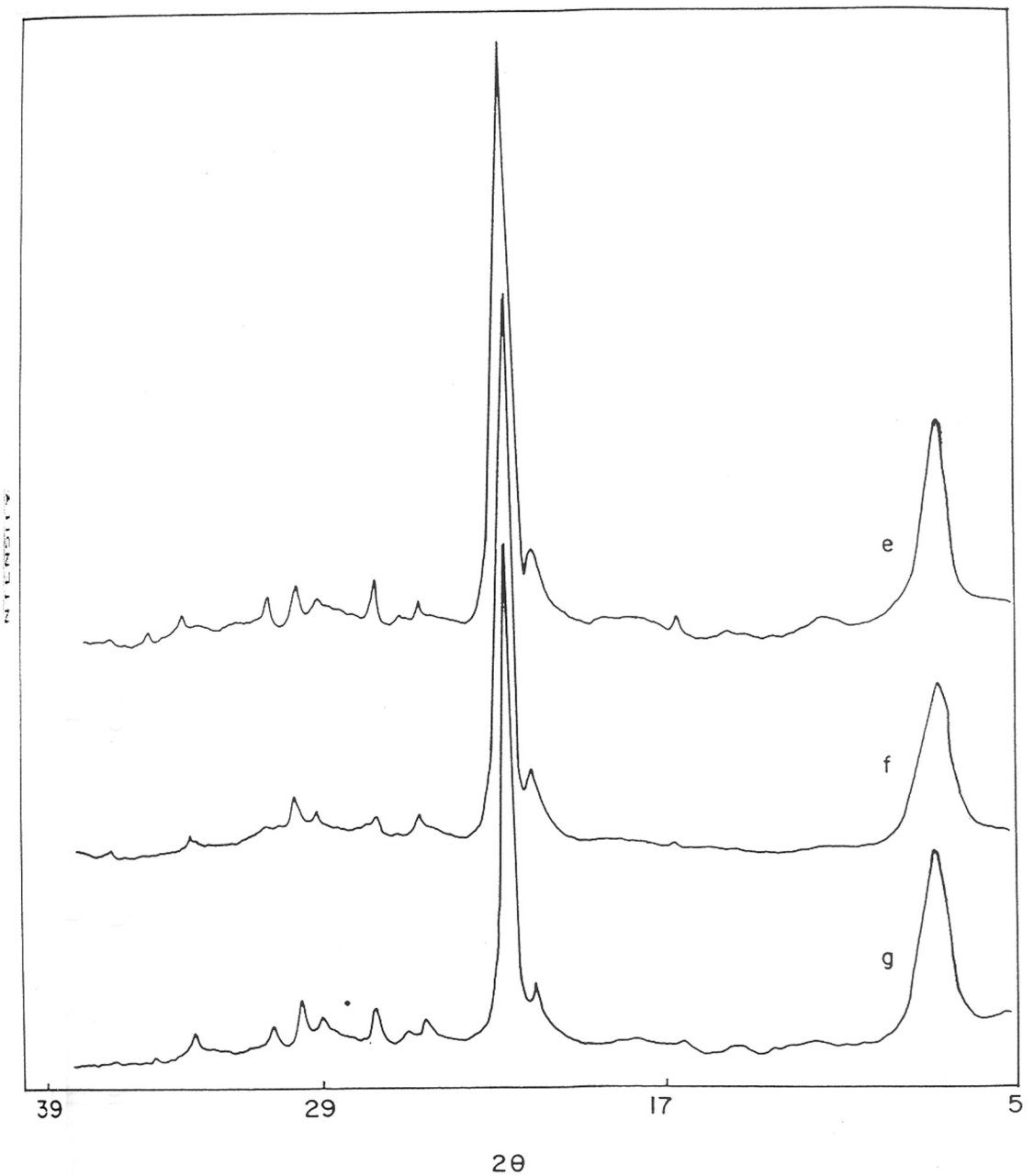

Fig. 3.2 : X-ray Diffraction patterns of H-Be-β with SiO_2 / BeO ratios of 28, 55 and 110 [curves e, f and g respectively]

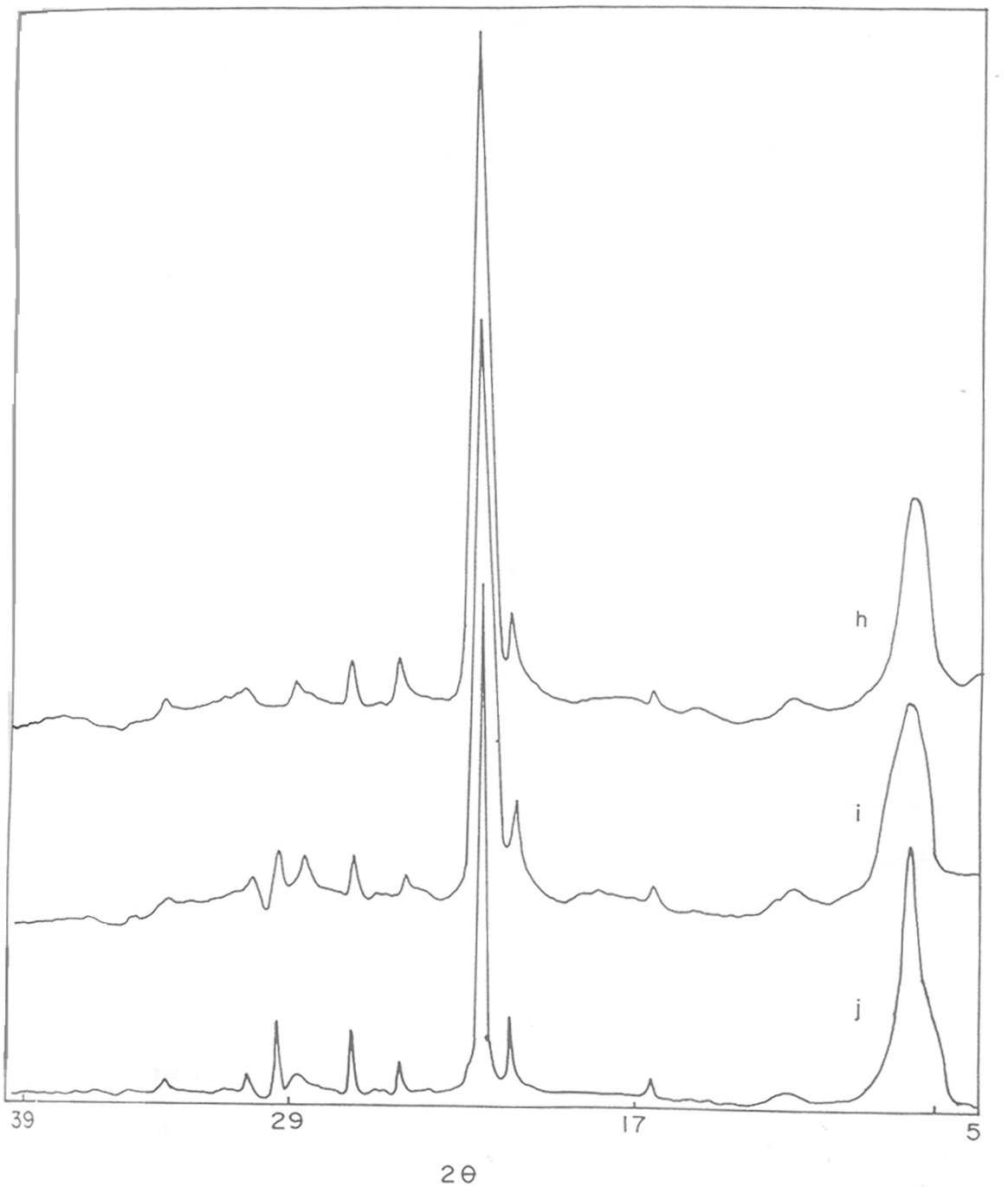

Fig. 3.3 : X-ray Diffraction patterns of deberyllated β zeolites; SiO_2 / BeO ratios of 115, 120 and 105 [curves h-j corresponding to samples 9, 10, 11 respectively of table 3.1]

et al[1]. It consisted of a combination of sharp and broad bands.

A systematic displacement of all the sharp lines towards lower 2θ values (higher d-spacings) is observed on isomorphous replacement of Al^{3+} by Ga^{3+}, whereas the displacement is towards higher 2θ values (lower d - spacings) in the case of Be^{2+} insertion. This is due to the longer Ga-O (1.823 A°) and shorter Be-O (1.63 A°) bond lengths compared to Al-O (1.75A°).

Newsam et. al[1] have identified two structural isomorphs A and B. which can be visualized by stacking together the layers of basic planes, which are either the left (L) or the right (R) handed. So for example, LLLL or RRRR stacking arrangements result in the left or right handed helical structures of polymorph A. An LRLR arrangement on the other hand results in the achiral structure of polymorph B. These stacking probabilities are energetically similar; so a real sample is likely to consist of an intimate mixture of all three isomers and hence does not have a chiral character. The first broad peak at around 7 degrees (2θ) in the XRD spectra of the assynthesized [Ga]- and [Be]- beta (samples 3 & 7) and the corresponding degallated and deberyllated samples (samples 5, 9, 10, 11) are shown in the fig. 3.4 (curves a -f). A distinguishable shoulder on the low angle side is observed in the spectrum of the as-synthesized [Ga]- beta, which is less pronounced in the spectrum of [Be]beta. After leaching out of Ga^{3+} and Si^{4+} insertion by treatment with $(NH_4)_2SiF_6$ solution, the shoulder becomes less visible, making the peak almost symmetrical. After leaching out of Be^{2+} by different methods, similar patterns were obtained as shown in fig. 3.4 (curves d - f). Newsam and Treacy[1] have showed by calculations that the shape of this first broad peak depends on the factor "a" which is the ratio of polymorph (A+B) to polymorph B in the sample. This factor depicts the change in the handedness in the stacking sequence. Thus the peak at low angle side and the shoulder at the high angle side correspond to the amount of polymorph B

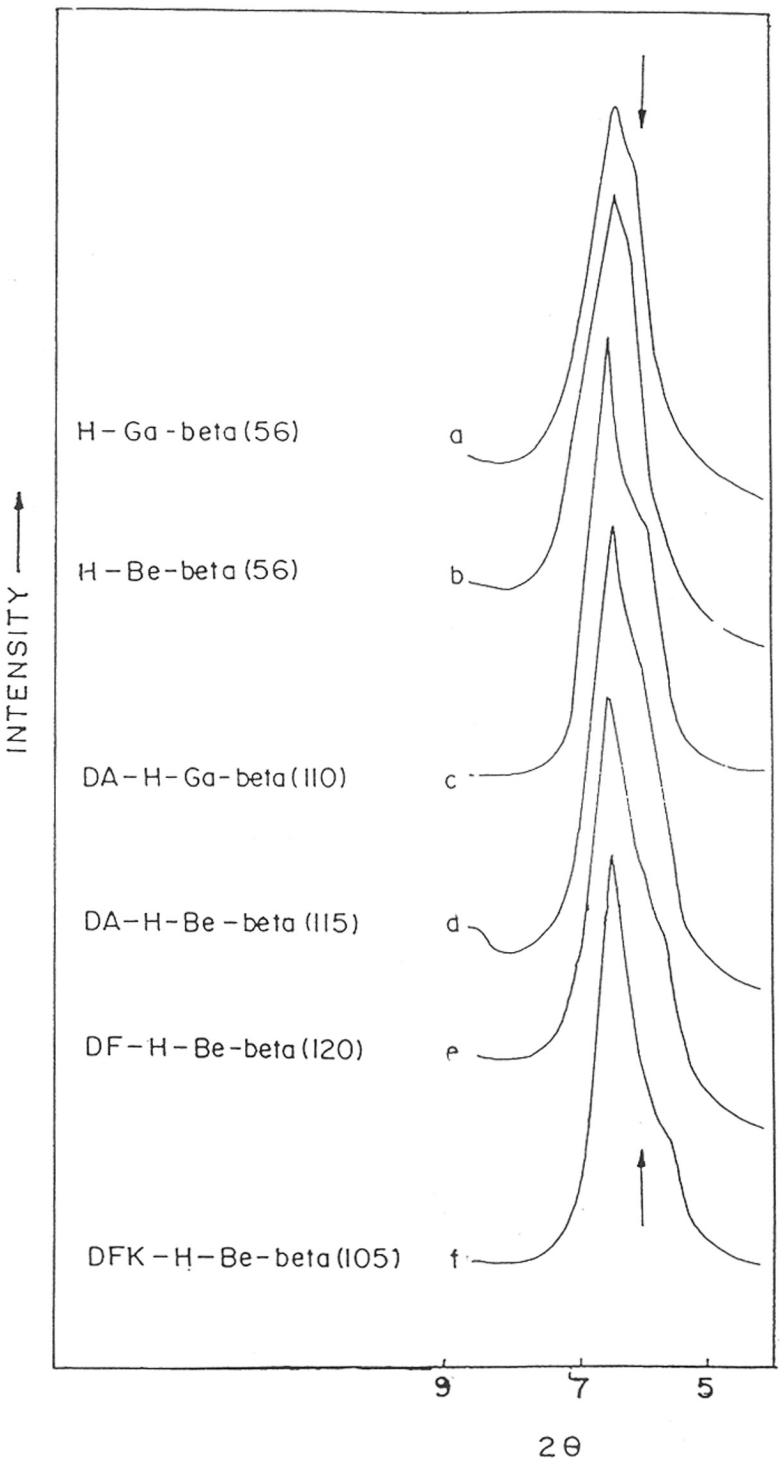

Fig. 3.4 : The low angle broad peak in the X-ray Diffraction pattern of Ga-β, Be-β, degallated and deberyllated -β [curves a-f corresponding to sample Nos. 3, 7, 5, 9, 10 and 11 respectively of table 3.1]

(monoclinic) and polymorph A (tetragonal) respectively. It follows that the assynthesized [Ga]-beta does not show any preference for A or B form, whereas the as-synthesized [Be]-beta sample contains more polytype B. Deberyllated samples show further enrichment of polytype B, which indicates that all the three methods of deberyllation selectively remove Be^{2+} from the framework of polytype A. Simultaneously structure healing through Si^{4+} insertion takes place which results in the formation of polymorph B. Our results corroborate the findings of Shen[2] et al. who have reported that the acid stability of polymorph A is less than that of polymorph B.

The SEM photographs for typical [Ga]- and [Be]- beta are shown in figs. 3.5 (a - c) and 3.6 (a - c) respectively. [Ga]-beta samples consisted of cuboid crystals of 0.4 - 0.6 μm in dimension, where as [Be]- beta samples consisted of cuboid to round crystals of 1.0 - 2.0 μm with a remarkable rough surface. These photographs also established the absence of amorphous material in the solid samples outside the pore system.

The topography of the particles was studied using a transmission electron microscope. Samples were examined by the side entry technique. Fig. 3.7 (a, b) shows typical images of [Be]- beta of the plane vertical to the page. The lattice fringe image of the particles are easily obtained, the 0.224 nm (111) plane spacing being well within the resolution limit, although the 0.196 nm (200) fringes are rarely observed and counted to give some estimate of the particle size. The fringe contrast within the particle is much improved and the internal structure is also more clearly reduced. The details of the stacking faults along the plane of the paper are clearly noticed as marked in the figure. This shows the lateral displacement by almost one third of the lateral distance. However, there seems to be much less defect density compared to the one described by Newsam et al. In the fig. 3.7 b, the channel size and side

A

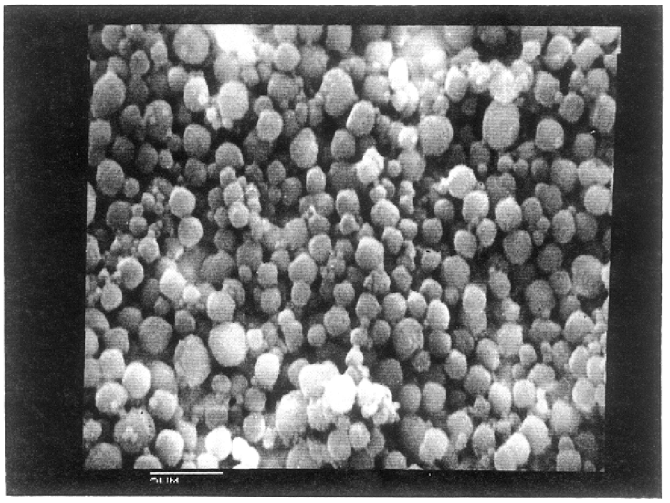

B

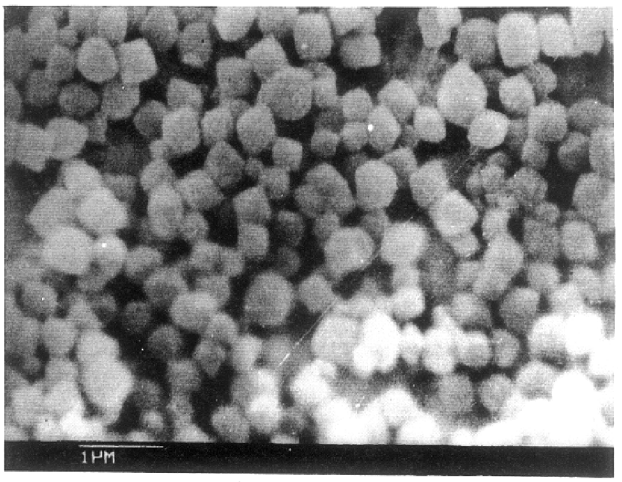

C

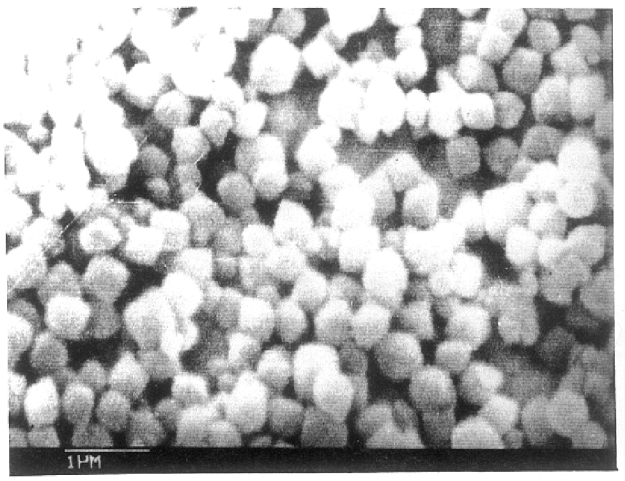

Fig. 3.5 : Scanning Electron Micrographs of Ga-β zeolites obtained from three different gel compositions, corresponding to sample Nos. 2, 3, 4, of table 3.1 [A, B and C respectively].

A

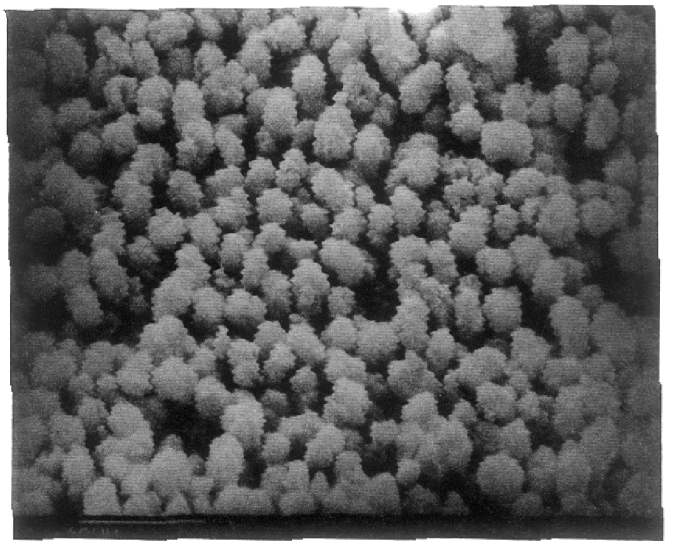

B

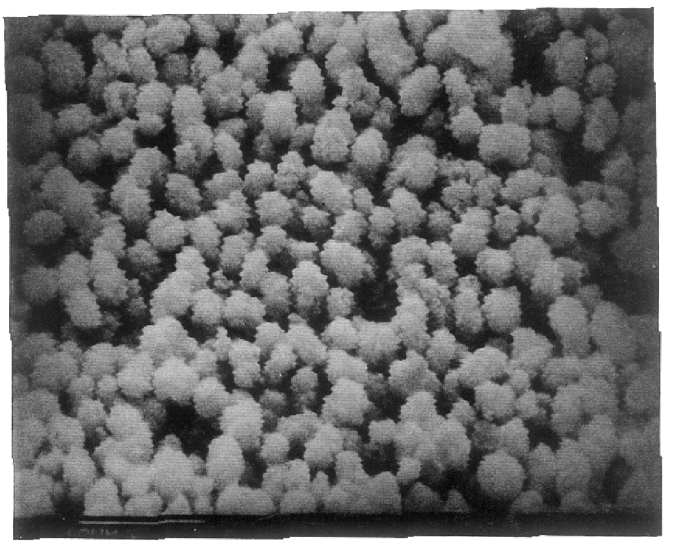

C

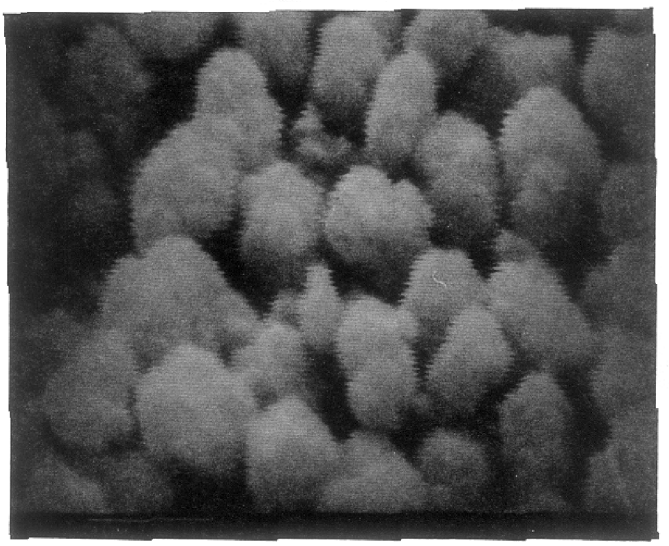

Fig. 3.6 : Scanning Electron Micrographs of Be-β zeolites obtained from three different gel compositions, corresponding to sample Nos. 6, 7, 8, of table 3.1 [A, B and C respectively]

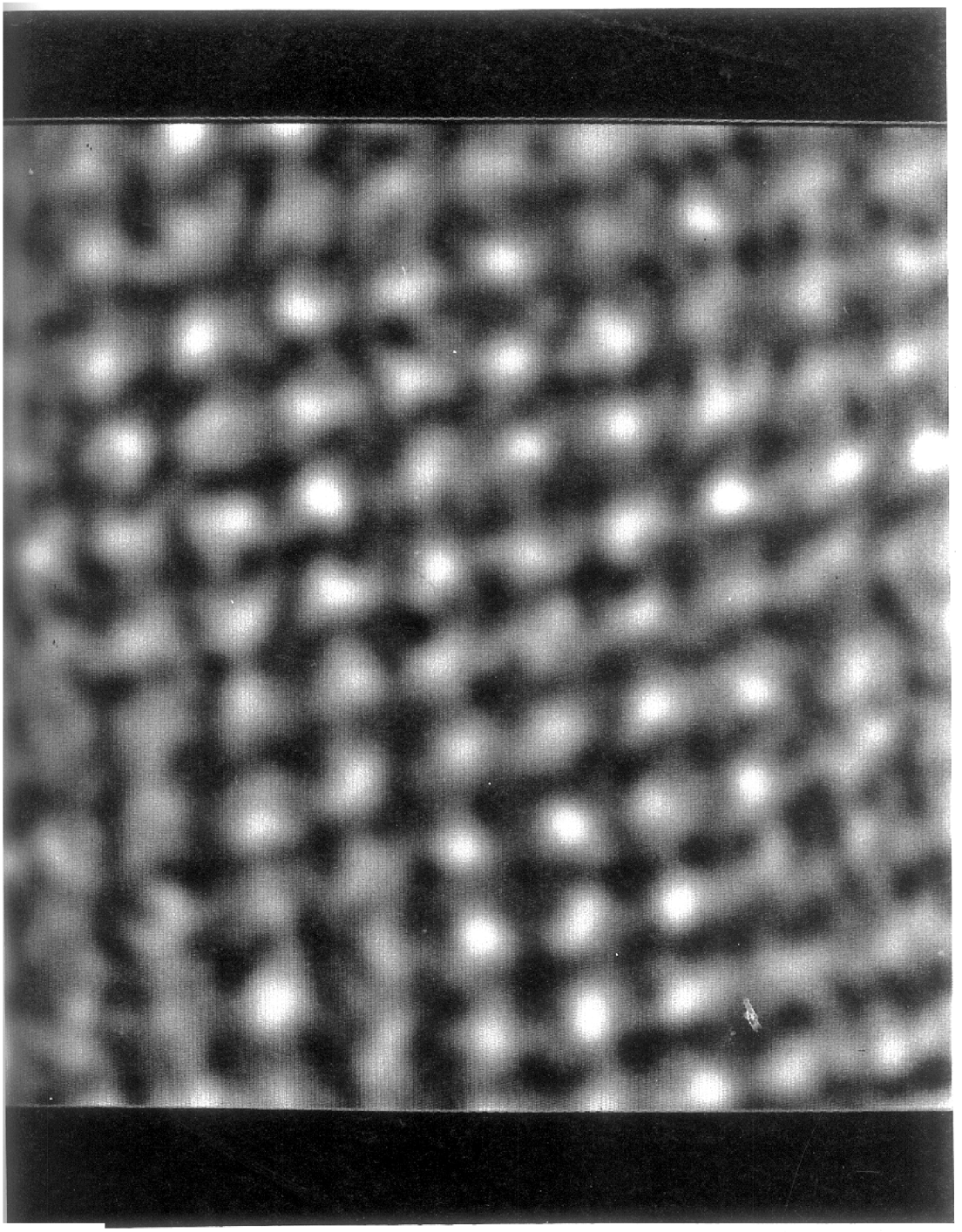

Fig. 3.7 (A) : Transmission Electron Micrograph of Be-β (20), corresponding to sample No. 6 of table 3.1.

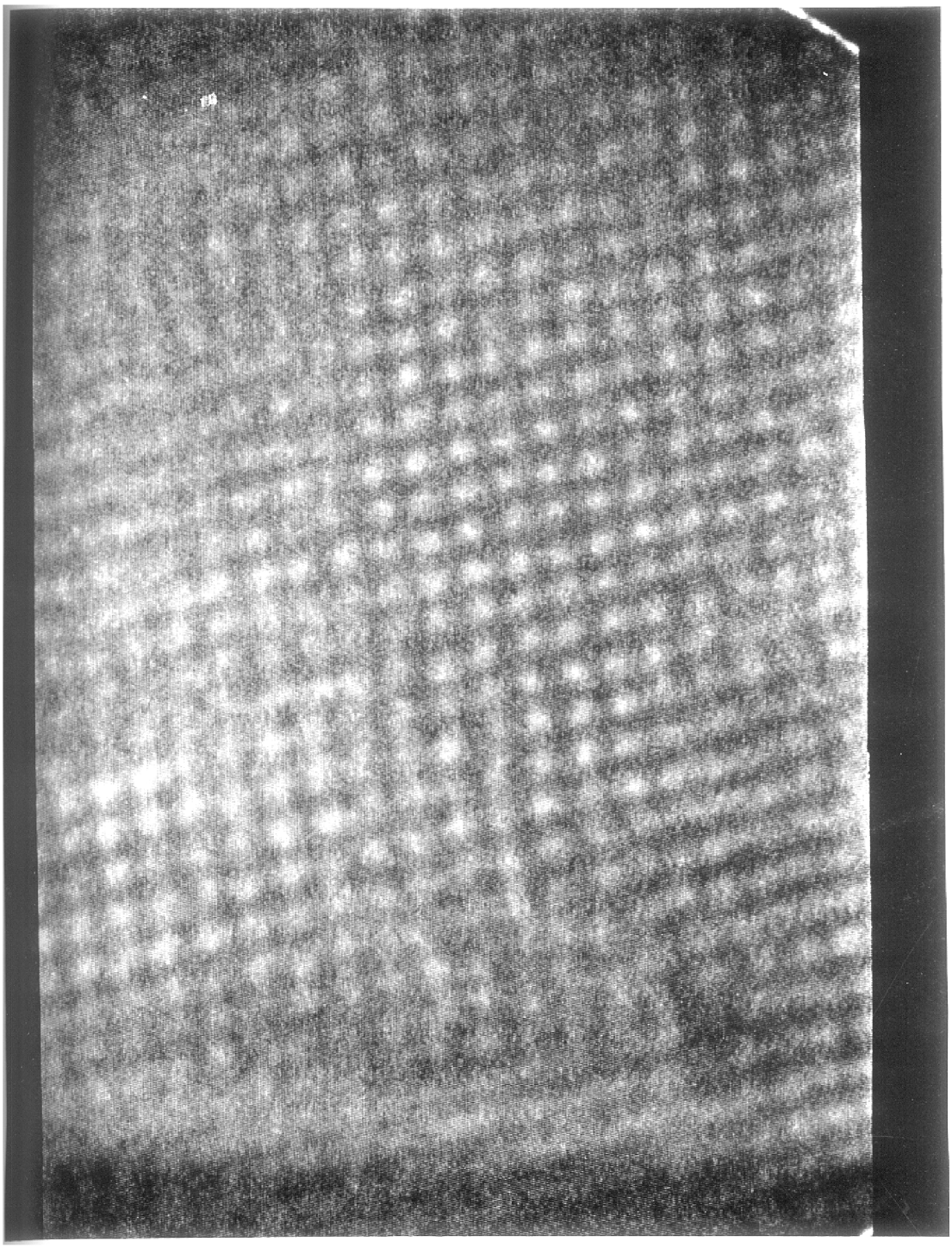

Fig. 3.7 (B) : Transmission Electron Micrograph of Be-β (20), corresponding to sample No. 6 of table 3.1.

pockets are clearly seen which is around 7.5 x 6.5 A° comparable to the literature value.

A typical thermogram of the as synthesized zeolite [Ga]- beta (20) and [Be]- beta (28) are shown in the fig. 3.8. In this, there are three distinct zones of exothermic weight loss in DTA / DTG curves of both [Ga]- and [Be]- samples with the peak maxima at 540, 613, 773 and 590, 673, 883 K, respectively. Perez–Pariente[6] et al. have reported three exothermic weight losses in the range 493 - 623, 623 - 773 and 773 - 973 K, receptively in the decomposition of as synthesized [Al] - beta. The first two exothermic weight losses can be assigned to the removal of TEA-OH and TEA^+ ions respectively. The last exothermic weight loss is assigned to the oxidative decomposition of residual coke formed by the decomposed template materials occluded in the zeolite channels. The higher temperature in this stage for [Be]-beta compared to [Ga]-beta can be attributed to the excessive deberyllation during the exothermic decomposition of template. Extra lattice beryllium species could block the channels of zeolite and inhibit the easy escape of decomposed gases from the template.

3. 1. 3 SOLID STATE MAS NMR SPECTROSCOPY :

The state of the hetero atom (Al^{3+}/ Fe^{3+}/ Ga^{3+}/ Be^{2+} etc.) in the framework of zeolite beta is very complex. In the case of Al^{3+}, Yang and Xu[4], using MAS NMR spectroscopy identified three forms of aluminum, -framework, -non-framework and transient state aluminum in the calcined [Al]-beta. Because the structure of zeolite beta is deformable, distortion and strain created during the decomposition of template partially displaces framework aluminum. Ga^{3+} cations in zeolites show an almost similar behaviour[5], whereas no information is available about the [Be]-beta zeolite. In the fig.3.9 ^{71}Ga MAS NMR spectrum of [Ga]-beta is depicted. The spectrum shows the presence of Ga in the tetrahedral position having a single broad peak at δ =149.6 ppm. No extra framework octahedral Ga was detected

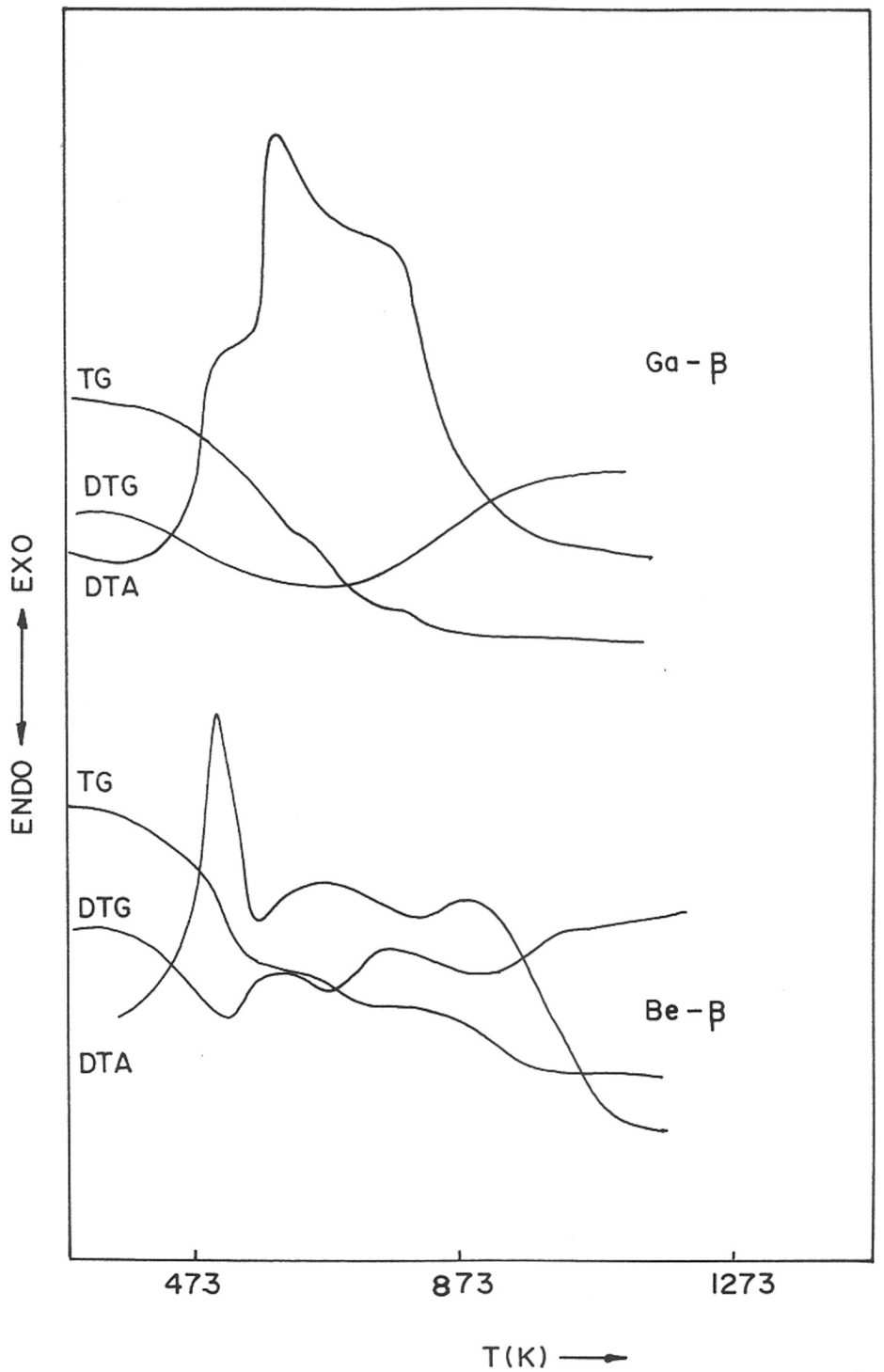

Fig. 3.8 : The thermograms of Ga-β-(20) and Be-β-(28).

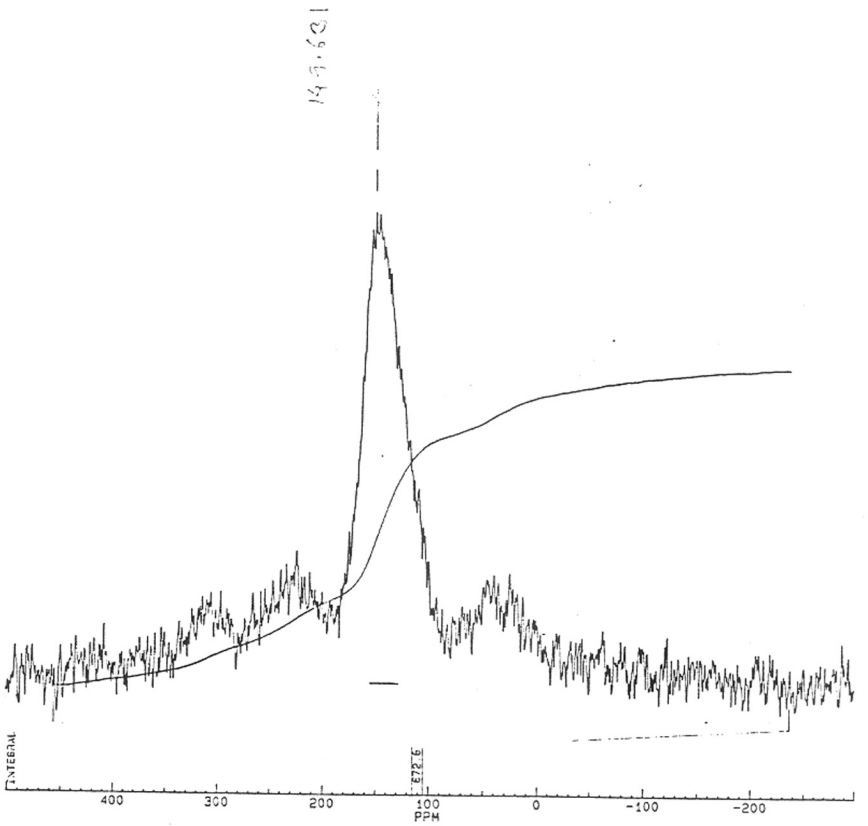

Fig. 3.9 : ^{71}Ga MAS NMR spectrum of Ga-β.

at δ =0 ppm.

In the fig. 3.10 (a-e), ^{29}Si MAS NMR spectra of as synthesized [TEA]-Be-beta (55), NH_4^+ form of sample 7 ([NH_4]-Be- beta), NH_4^+ form of sample 10 (DF–[NH_4]-Be-beta (120), K^+ exchanged sample 10, and NH_4 form of sample 11 (DFK–[NH_4]-Be-beta (105) are presented and the chemical shift values are tabulated in table 3.2. Four different components centered at δ = -89, -102.2, -109.5 and -112.9 ppm can be distinguished in ^{29}Si MASNMR spectrum of [TEA]-beta sample (fig. 3.10a). After it was calcined and NH_4^+ ion exchanged, noticeable changes are observed in these spectra (fig. 3.10b). The resonance line at -89 ppm totally disappears. The intensity of the -104 ppm resonance line strongly decreases, and that of the -111.3 and -115.5 ppm lines increase (fig. 3.10c). The change in the line position from -102.2, -109.5 and -112.9 to -104, -111.3 and -115.5 ppm indicates a decrease in the Be content in the zeolitic tetrahedral environment. When this sample is treated with $(NH_4)_2$ SiF_6, Be is leached out of the framework resulting in the shift of resonance lines further to -105.2, -111.7 and -115.5 ppm respectively. When this sample was ion exchanged with K^+ (sample 5, table 3.2). The positions of all these resonance lines were shifted to the low field side to -102.1, -109.8 and -114.1 ppm, respectively. This indicates the enrichment of the zeolite lattice with Be^{2+} in tetrahedral positions. According to Yang and Xu[4], because the framework of beta is deformable, distortion and strain is produced when it is exchanged with proton which have high electron affinity, leading to the breakage of the Al-O bond. On the other hand, when it is exchanged with other cations (e.g. Na^+) due to the deformability of the framework, extra lattice Al species which are still attached to the framework by one or two points (so called transient state Al) and even completely non framework Al go back into the framework. In case of [Be]-beta also, such transient Be species went back into the lattice on exchange with K^+ cations, shifting the ^{29}Si resonance lines to low field side in sample 5 of

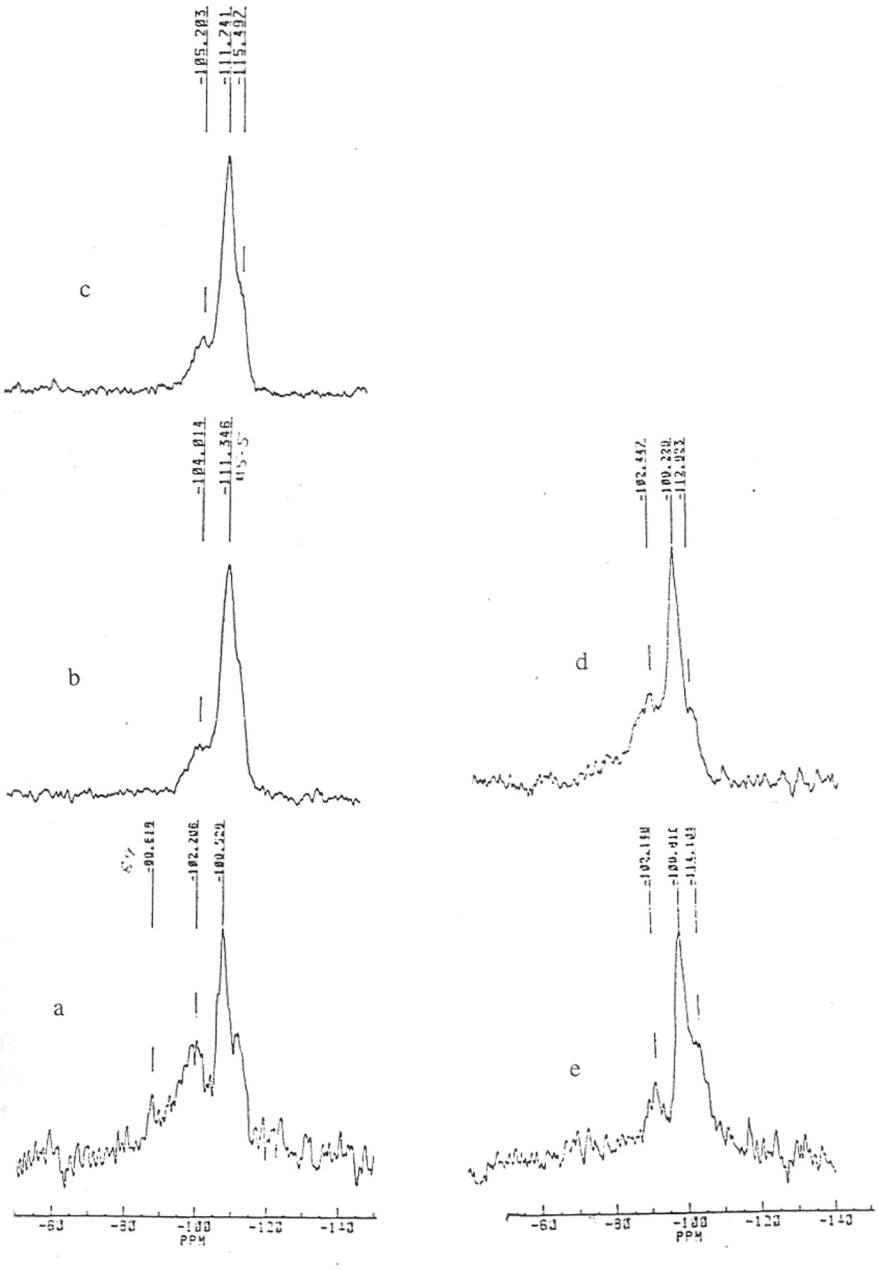

Fig. 3.10 : ^{29}Si MAS NMR spectrum of Be-β [curves a- e corresponding to sample nos. 7-11 respectively in table 3.1]

Table 3.2 Chemical Shifts in MASNMR of Be-β

S.No*	Sample	^{9}Be Resonance line (PPM)	^{29}Si Resonance line(PPM)
1	TEA-Be-β(56)	~ 2.57	-89, -102.2, 109.5, -12.9
	↓ Calcination ↓ NH_4^+ Exchange		
2	NH_4-Be-β(56)	~ 1.92	-104, 113.3, 115.5
	↓ $(NH_4)_2SiF_6$ ↓ Treatment		
3	NH_4-DF-Be-β(120)	~ 2.39	-105.2, 111.7, 115
	↓ K^+ Ion Exhange		
4	K.DF-Be-β(120)	~ 2.57	-102.1, -109.8, -114
5	TEA-Be-β(56)	~ 2.57	-102.4, 109.2, 112.9
	↓ $(NH_4)_2SiF_6$ ↓ Treatment ↓ K^+ Ion Exhange		
6	H-DFK-Be- β(105)	~ 1.93	-
7+	Beryllium Oxide	-2.3	-
8+	Beryllium Silicate having non-Zeolitic Structure	-3.47	-

Reference for 1-6, 0 ppm of 0.1m $BeSO_4$ solution, for 7 and 8, -1.73 ppm of 0.05m $BeSO_4$ solution.

Ref. 7

table 3.2.

In another variation in modification of [Be]-beta, wherein it was calcined and K^+ cation exchanged after treatment with $(NH_4)_2\ SiF_6$ (sample 6 in table 3.2), ^{29}Si resonance lines were observed at -102.4, -109.2 and -112.9 ppm, i.e. almost at the same position as for original as synthesized sample. These lines are assigned to positions of Si in (3Si 1Be) or (3Si 1OH), in (4Si 0Be) and in other non-equivalent Si positions occupying different structural sites in the zeolite[6].

^9Be MASNMR spectra are presented in fig. 3.11(a-e) and the resonance line positions are given in table 3.2. Romannikov et al.[7] have reported the chemical shift of ^9Be in ZSM-5 zeolite to be δ = -5.8 ppm relative to 0.05 molar solution of $BeSO_4$ in H_2O, set to δ = -1.73 ppm. Using this standard value of -1.73 ppm for 0.06 molar solution of $BeSO_4$, San et al[8] have reported tetrahedral ^9Be line to be at -5.0 ppm in their beryllated sample of ZSM-5 prepared by treatment with $(NH_4)_2\ BeF_4$ solution. This difference in chemical shift was attributed to the difference in the concentration of the reference $BeSO_4$ solution. In the spectrum of ^9Be in our samples, we have a very strong single line at -2.57 ppm with 0.1 molar solution of $BeSO_4$ set to 0 ppm. If it is set to -1.73 ppm, then the position will be at -4.3 ppm. This difference can also be attributed to the increase in the concentration of standard $BeSO_4$ solution in this case. To understand the state of Be species giving rise to the resonance line at -4.3 ppm, the following points may be noted.

1) Treatment of H ZSM-5 with (NH_4) BeF_4 solution inserts Be^{2+} in the lattice of the zeolite[9].

2) [Be]-ZSM-5 can also be prepared by direct hydrothermal synthesis using $BeSO_4$ solution.

3) All samples of modified beta prepared by treating with $(NH_4)_2SiF_6$ show an identical

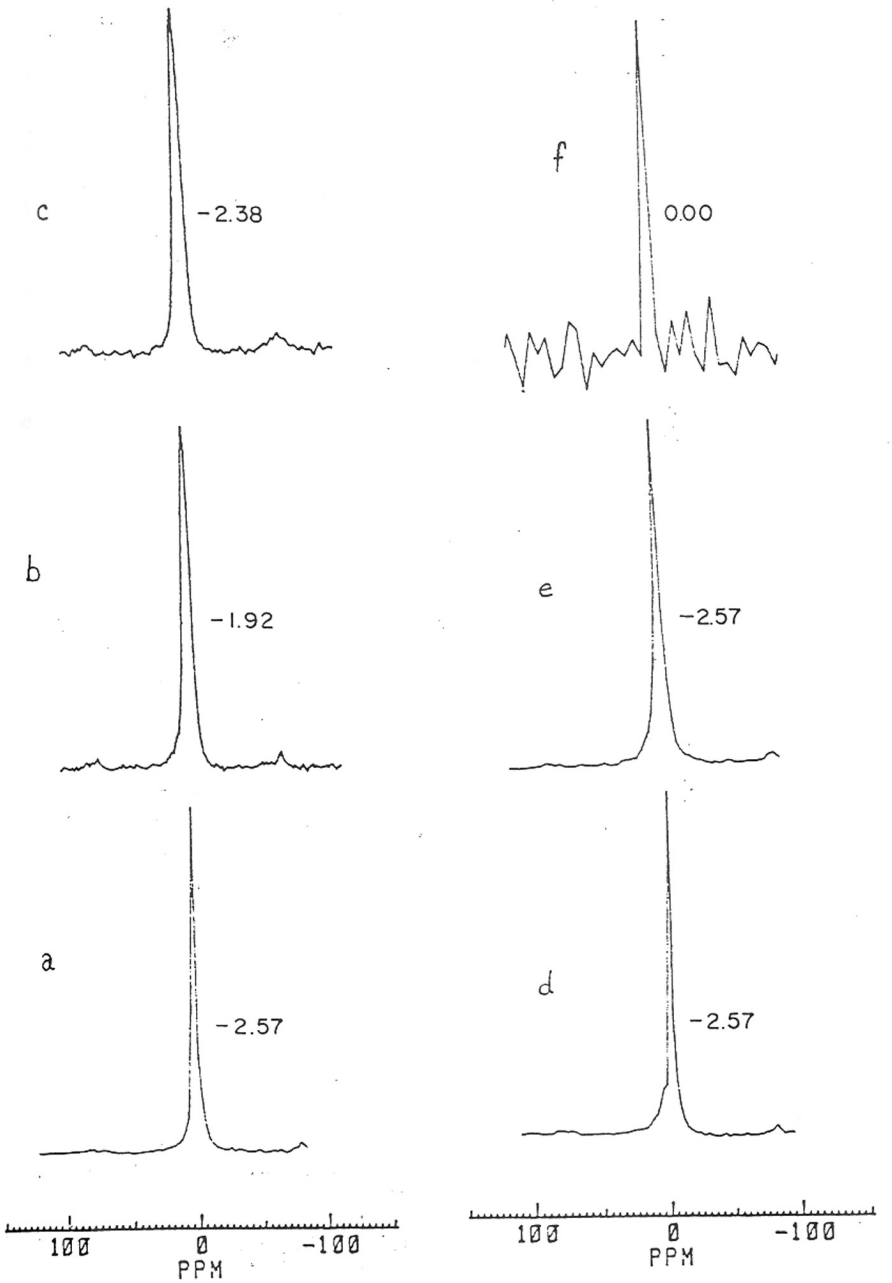

Fig. 3.11 : ^{9}Be MAS NMR spectrum of Be-β. [curves a- e, corresponding to sample nos. 7-11 respectively in table 3.1, and curve f, of 0.1 M $BeSO_4$ solution]

chemical shift of -4.3 ppm.

4) The chemistry of Be^{2+} insertion into zeolite beta parallels that reported by Han et al.[8] for ZSM - 5 zeolite, by Chang et al[9] for Al insertion and Skeels et al. for insertion of Si[10], Fe and Ti[11] into zeolite framework using the aqueous metal fluoride solutions.

5) Be^{2+} is most suited for isomorphous substitution in zeolite because the value of radii $(r)_r$ (0.35 and 0.42 A°) and electronegativities (x= 210 and 260) for Be^{2+} and Si^{4+} are nearly the same.

Therefore the spectrum of ^{9}Be with a line at -4.3 ppm should be attributed to Be^{2+} in framework positions. But, there is an exception in the case of $[NH_4]$-Be-beta (56) and H-DFK -Be-beta (105), samples 2 & 6 in table 3.2, respectively. They were not treated with $(NH_4)_2SiF_6$ after the calcination step in the procedure. The chemical shift values of these are -3.65 and -3.66ppm respectively, after correction for concentration difference in the standard solutions. The values are close to those for beryllium silicate having non zeolitic structure, reported by Romannikov[7] et al. So, in conclusion ^{29}Si and ^{9}Be MASNMR spectroscopic results show that Be^{2+} is in the framework of as-synthesized beta, it comes out on calcination in any stage of preparation and can be reinserted by treating with aqueous $(NH_4)_2SiF_6$ solution.

3. 1. 4 ADSORPTION OF WATER AND HYDROCARBONS :

On the basis of sorption results, Lok et al.[12] have shown that beta has an open structure with 12-ring windows. Bond et al[13] found that all the C_8-aromatics (xylenes, ethylbenzene) can enter the zeolite channels at room temperature. 1,3,5 trimethylbenzene enters the zeolite but tri-isopropyl and t-butyl analogs can not. Olson[14] et al. have used these

probe molecules to differentiate between the 12-ring and the 10-ring window zeolites. In table3.3, adsorption results on [Ga]- and [Be]-beta zeolites are presented. Pore volumes of fully crystalline materials determined by adsorption of cyclohexane, ethylbenzene, m-xylene, 1, 2, 4 trimethyl benzene are in the range 0.18 ± 0.02 ml/g of zeolite. Nitrogen pore volume indicates that there is no extra lattice debris in the pores of the pure zeolite samples.

3.1. 5 TEMPERATURE PROGRAMMED DESORPTION OF AMMONIA (TPD OF NH_3) :

The typical results of the T.P.D of NH_3 for [H]-Ga- and [H]-Be-beta zeolites are presented in fig. 3.12 (a-g). That for [H]-Al-beta(60) is also included (fig.3.12,d) for comparison. The curves a-c refer to [H]-Ga-beta samples 2,3 and 4 having SiO_2 : Ga_2O_3 ratios of 20, 56 and 113, respectively. The TPD curves are typical of high silica zeolites having low, medium and high temperature peaks called α, β and γ peaks respectively. The amount of NH_3 adsorbed was distributed under α, β and γ peaks by approximately measuring the area under the curves and are presented in table 3.4. The total amount of NH_3 adsorbed was found to be more than the number of Ga atoms per unit cell as some of the adsorbed NH_3 is physically adsorbed on sites like silanol groups. Only the last peak with the maximum around 623 K was found to correlate with the Ga content, acidity and catalytic activity. The temperature of this peak maximum (623 K) is lower than that for [Al]-beta of comparable Al content (650 K) which indicates that acid sites on [Ga]-beta are weaker than those on [Al]-beta. Brönsted acid sites associated with the bridged of –OH groups (Si (OH) Ga) are probably associated with both the 3622 cm^{-1} i.r band and the maximum at 623 K in the T.P.D spectrum of NH_3. Beyond 723 K, the rising portion of the T.P.D curve is due to the dehydroxylation of the surface OH groups as no NH_3 is detected in the desorbate and only

Table 3 . 3 : Adsorption Properties of modified Zeolites

S. No	Sample	Adsorption, (Wt. %) Water	C – H	M – X	E.B	1, 3, 5 TMB	1,4 DIPB	N_2 pore vol. ml/g
	Kinetic diameter Å	2.65	6.0	6.8	7.0	7.0	7.1	3.4
1	H-Al-β (60)	17.0	18.2	22.6	20.6	17.8	16.1	0.25
2	H-Ga-β (20)	19.0	17.3	21.3	20.0	16.4	17.6	0.23
3	H-Ga-β (56)	19.1	18.0	20.9	19.6	17.0	16.3	0.24
4	H-Ga-β (113)	18.3	18.7	21.04	18.7	16.5	15.6	0.22
5	DF-H-Ga-β (110)	17.4	19.2	19.6	19.0	18.0	17.2	0.23
6	H-Be-β (28)	18.1	17.5	18.6	18.6	16.0	16.3	0.20
7	H-Be-β (55)	18.3	18.1	19.0	19.1	17.0	17.1	0.21
8	H-Be-β (115)	18.8	18.0	20.1	20.2	16.3	17.2	0.20
9	DA-H-Be-β (115)	20.3	17.2	20.2	18.1	17.6	16.6	0.22
10	DF-H-Be-β (120)	20.4	19.6	20.3	19.6	18.2	18.2	0.24
11	DFK-H-Be-β (105)	20.6	19.3	21.0	20.6	17.6	18.7	0.25
12	H-Al-M (13)	17.0	9.0	-	-	-	-	0.17
13	H-Ga-M (19)	16.2	10.2	-	-	-	-	0.17
14	DA-H-Ga-M (27)	16.7	8.9	-	-	-	-	0.17

C-H = cyclohexane; M-X = m-xylene; E-B = ethylbenzene; 1, 3, 5 TMB = 1, 3, 5 trimethyl benzene; and 1, 4 DIPB = 1, 4 diisiopropylbenzene.

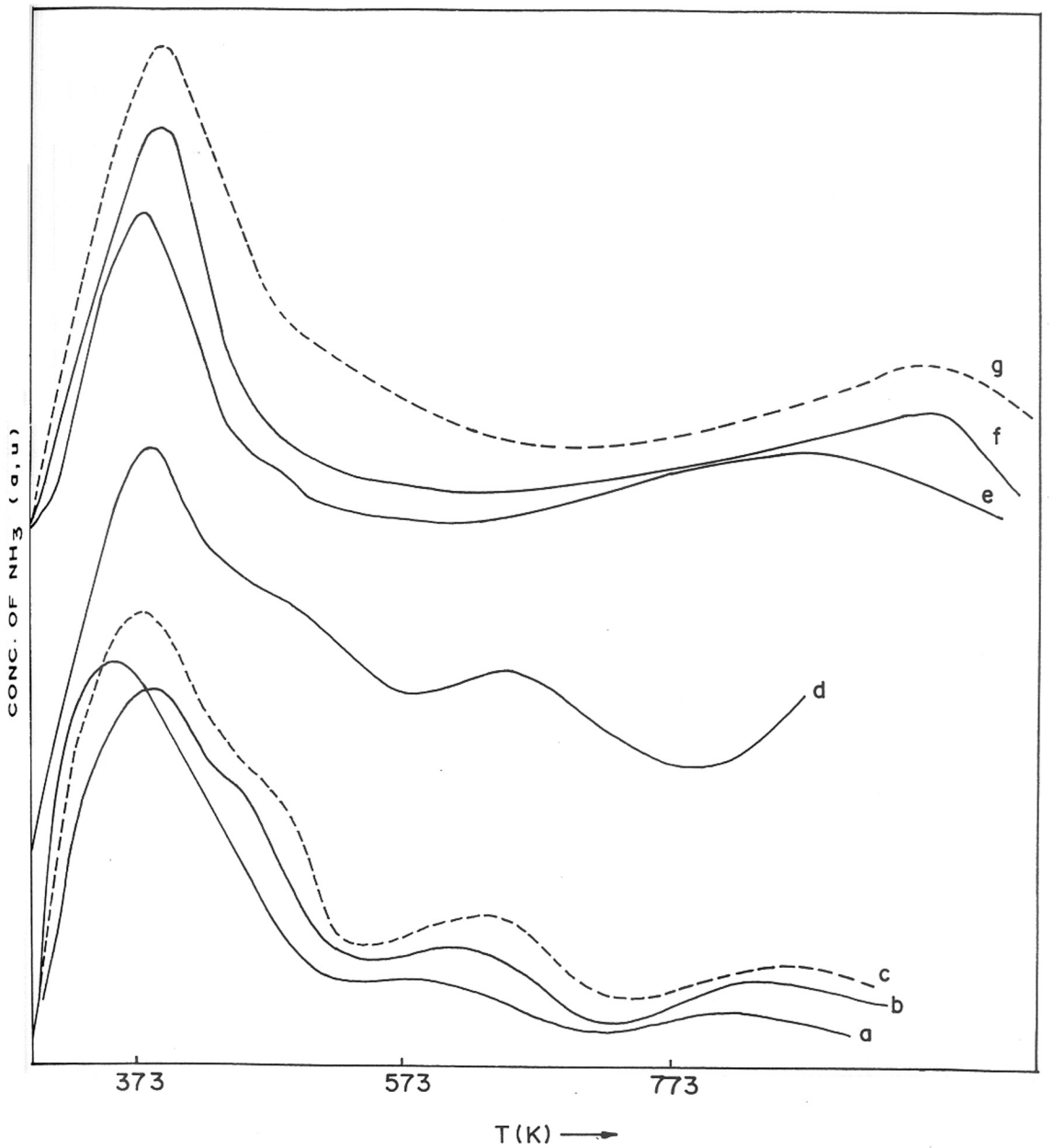

Fig. 3.12 : TPD curves of NH_3 from H-[Ga]- β - 20, 56, 113, (curves a, b and c), H-[Al]- β-60 (curve d) and H-[Be]- β-28, 55, 115 (curves e-g), respectively.

Table 3.4 : Temperature Programmed Desorption (TPD) of NH_3

Sr. No.	Sample	Peak Maxima (K)			NH_3 (mol /u.c)	
		∝ -peak	β -peak	γ peak	(∝ +β) peak	γ peak
1	Hal -β (60)	360	450	608	6.27	1.8
2	H- Ga -β (20)	390	450	623	7.10	3.3
3	H-Ga-β (86)	390	460	~ 600	5.40	1.7
4	H –Ga-β (113)	390	460	~590	4.4	0.77
5	DF-H-Ga-β (110)	380	~ 450	~ 600	3.9	0.85
6	H –Be-β (28)	395	~ 450	-	10.75	0.95
7	H –Be-β (55)	395	455	-	6.9	0.80
8	H –Be-β (115)	380	430	-	4.3	0.60
9	DA-H-Be-β (115)	395	-	-	3.3	0.70
10	DF-H-Be-β (120)	390	-	-	2.8	0.50
11	DFK-H-Be-β (105)	387	-	-	4.1	0.40
12	H-Al-M (13)	423	-	600	8.2	3.9
13	H-Ga-M (19)	420	-	580	6.3	2.3
14	DA-H-Ga-M (22)	430	-	620	4.6	1.6

H_2O is evolved. In an earlier study[15], we observed that in the case of [Al]-beta the strongly adsorbed NH_3 was desorbed at 640 K. Isomorphous substitution of Ga for Al, hence decreased the strength of the strong acid sites in the beta framework. Similar conclusions, were drawn by Simmons et al.[16] and Chu and Chang[17] for [Al]- and [Ga]-ZSM–5, respectively. The corresponding peak maxima were 655 and 635 K for [Al] and [Ga]-ZSM-5, respectively[17]. These results are in accordance with the conclusions drawn from the FTIR data concerning the effects of isomorphous substitution and framework structure on the relative acidity of the zeolites.

In fig. 3.12 (e-g) T.P.D of NH_3 curves for [H]-Be-beta samples 6, 7 and 8 of table 3.4 with SiO_2 : BeO ratios of 28, 55 and 115 are presented. Although the nature of curves in the low temperature region (<573 K) is similar to that for [Ga]-beta, a well defined high temperature γ peak is almost absent. This indicates that negligible amount of Brönsted acid sites associated with bridging hydroxyl groups Si(OH) Be are present in [H]-Be-beta zeolites. Even if Lewis acid sites are present, they seem to be weaker than those on [Al]- and [Ga]-beta zeolites. Though the total amount of NH_3 adsorbed are more than the amount of Be atoms per unit cell, most of the NH_3 desorbed below 573 K in the α and β peak region. The rising portion in the curves beyond 673 K is due to dehydroxylation, liberating only H_2O. In the study of MAS NMR described earlier, it was observed that calcination removes Be^{2+} from the lattice position and hence a decrease in acidity is expected.

3. 1. 6 INFRARED SPECTROSCOPY :

3. 1. 6. 1 Framework spectra :

The typical mid-infrared spectra determined by the KBr pellet technique for the as-synthesized forms of [Al]-beta (20), [Ga]-beta (20) and [Be]-beta (28) are shown in fig. 3.13 (a-c). The band positions are summarized in Table 3.5. We find that the frequency due to the asymmetric T-O stretching vibration (ν_{OTO}) which is sensitive to the external linkages of TO_4 tetrahedra and to the framework Si to hetero atom ratio shifts towards higher frequency for [Be]-beta and to a lower frequency for [Ga]-beta compared to [Al]-beta. This shift is attributed[18] to the change in the reduced mass of the -(Si-O-Be) and -(Si-O-Ga) harmonic oscillator compared to -(Si-O-Al). Figure 3.13 illustrates the difference in band positions in these samples. Szostak and Thomas[18] reported similar shifts due to isomorphous substitution of Al by Ga in the MFI system. This kind of frequency shift was also observed when [TEA]-Be-beta was calcined, NH_4^+ ion exchanged and then again calcined to get [H]-Be-beta as can be seen from the table 3.5.

3. 1. 6. 2 [TEA]-beta conversion to [Na]-beta :

FTIR spectra of [TEA]-beta (sample 3, SiO_2 / Ga_2O_3 = 56) after evacuation for 3h at 450, 575 and 675 K, respectively are shown in fig.3.14 (a-c). In the OH stretching region, absorption bands are seen at 3740, 3622 and 3540 cm^{-1}. The absorption below 3100 cm^{-1} region is due to C-H vibrations in the organic moiety. The sharp band at 3740 cm^{-1} is assigned to the isolated SiOH groups (terminal SiOH or extra framework silica species). This absorption appears at the same frequency (3740 cm^{-1}) in [Al]-beta[15], as well as [Al]- ZSM-5[19] and [Ga]- ZSM-5[17]. It is hence independent of both isomorphous substitution and framework structure. The broad band with a maximum at 3540 cm^{-1} also belongs to the same category. It

Table 3. 5 **Framework i.r vibration frequencies (ν, cm^{-1}) of typical Zeolites.**

[TEA]-Be-β (of Sample 6)	[TEA]-Al-β (Sample A)[15]	[TEA]-Ga-β (Sample 2)	H-Be-β (28) (Sample 6)
1222	1220	1220	1220
1170	1172	1170	1171
1095	1084	1070	1090
980 (Sh)	988 (Sh)	972 (Sh)	975 (Sh)
825	782	780	810
625	615 (Sh)	616	620
580	572	580	579
-	-	544	-
525	522	508	520
470	480	478	473
420	456	450	430

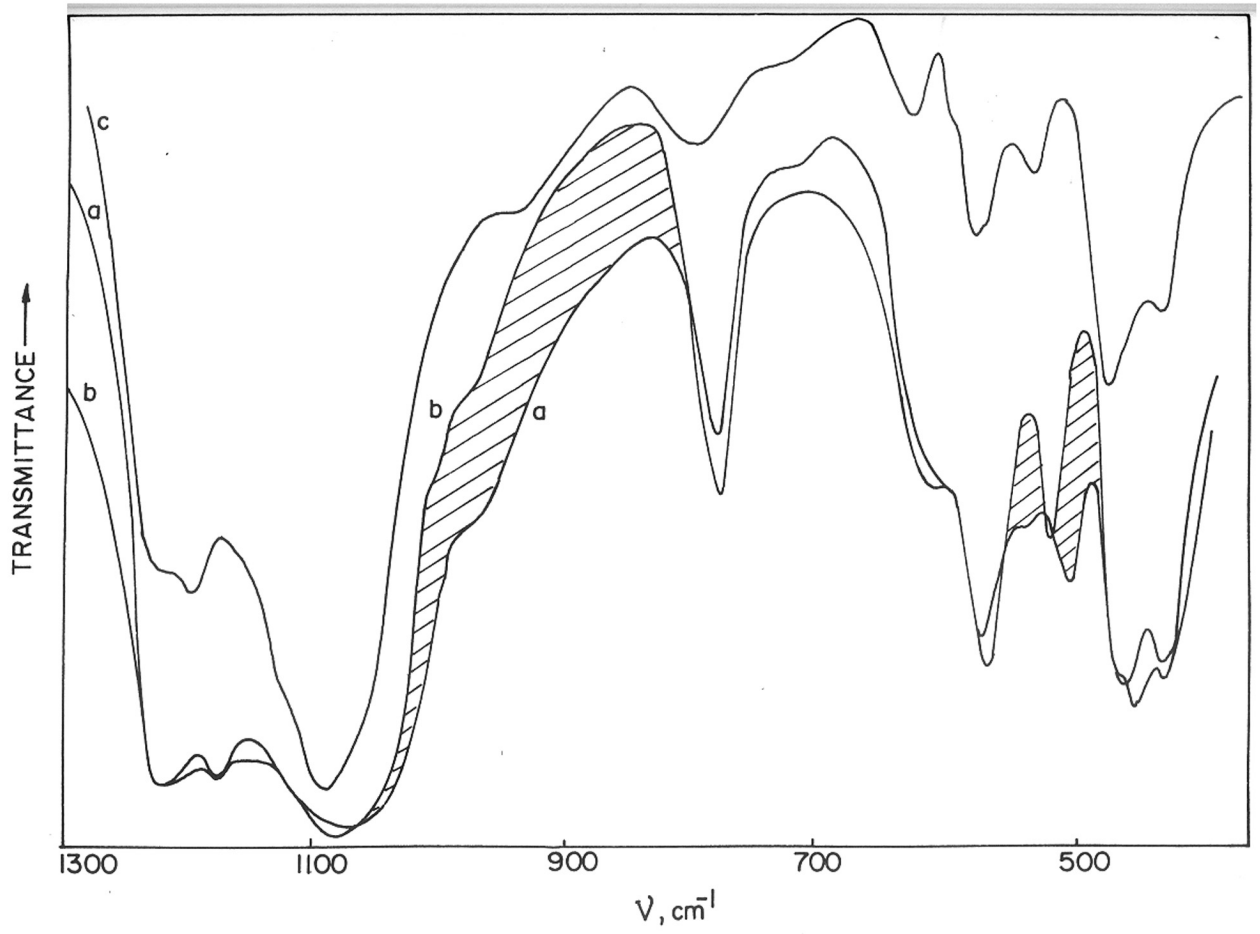

Fig. 3.13 : IR framework spectra of TEA[Al]- β (60), TEA-[Ga]- β (20) and TEA-[Be]- β (28)- curves a, b and c, respectively.

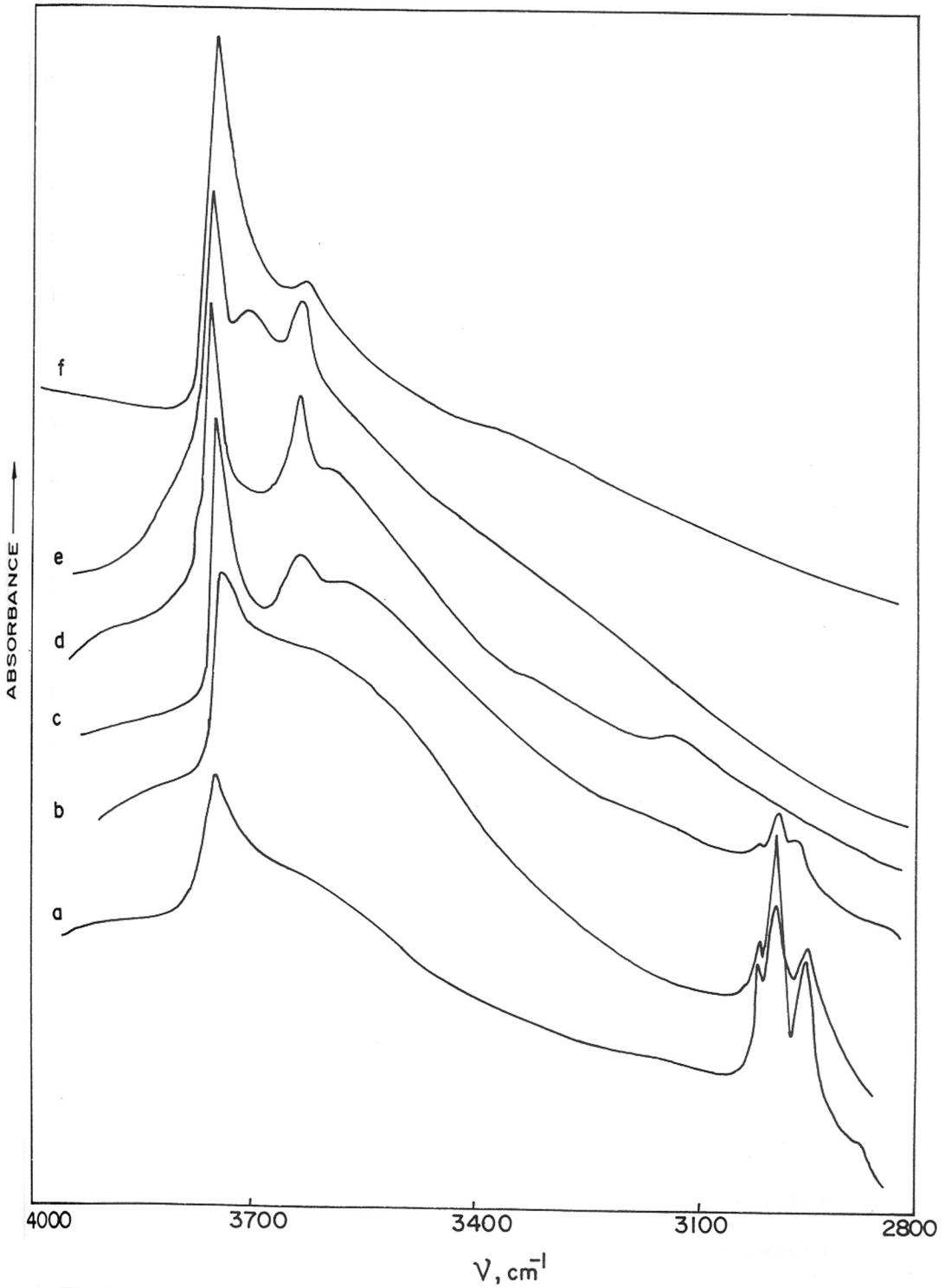

Fig. 3.14 : FTIR Spectra of [TEA]-Ga- β (56) treated in vacuum at 475, 575 and 675 K [curves a-c], in air and then in vacuum at 673, 723 and 823 [curve d-f] respectively

is associated with hydrogen-bonded SiOH groups. It appears at the same frequency(3540cm^{-1}) in both [Al]-beta and [Ga]-ZSM-5. The band at 3622 cm^{-1} is characteristic of [Ga]-beta and is assigned to the bridging hydroxyls (Ga-(OH)-Si). This band appears at 3602 cm^{-1} for [Al] -beta[15] and at 3620 cm^{-1} in the case of [Ga]-ZSM-5[17]. Thus isomorphous substitution (Ga for Al) has a greater influence on the O-H stretching frequency than does a change in the framework structure (from beta to MFI).

To investigate the concentration and the stability of the OH groups in samples free from occluded organics, a sample was heated in a flow of dry air at 673, 723 and 823 K and subsequently evacuated (10^{-6} torr) at the same temperature. The corresponding spectra of [Na]-beta are shown in the fig.3.14 (curves d-f). The concentration of bridging hydroxyls (3622 cm^{-1} band) decreases on evacuation above 673 K. The removal of organics is almost complete at 673 K. There is still some carbonaceous material on the sample evacuated at 673 K as could be inferred from its light grey colour, and a broad low intensity band around 3100 cm^{-1}. Hence, calcination in air between 673 and 723 K would remove most of the bridging hydroxyl groups. Similar results were obtained in the case of samples containing different amount of Ga except that, due to the lower concentration of Ga, the intensity of the 3622 cm^{-1} band was lower.

FTIR spectra of the samples during the conversion of [TEA]-Be-beta to [Na]-Be-beta was recorded in an identical manner and presented in fig. 3.15(a-f). After evacuation of [TEA]-Be-beta at 450, 575 and 675 K, (curves a-c respectively), a remarkable difference in the evolution of well defined bands are noticeable. The nature of the spectra is remarkably different from that of [TEA]-Ga-beta. In the OH stretching region, on vacuum calcination of [TEA]-Be-beta, only isolated silanol groups (3740 cm^{-1}) and hydrogen bonded hydroxyl groups (3540 cm^{-1}) appear. A weak shoulder at 3685 cm^{-1} appears, whereas bands of bridging

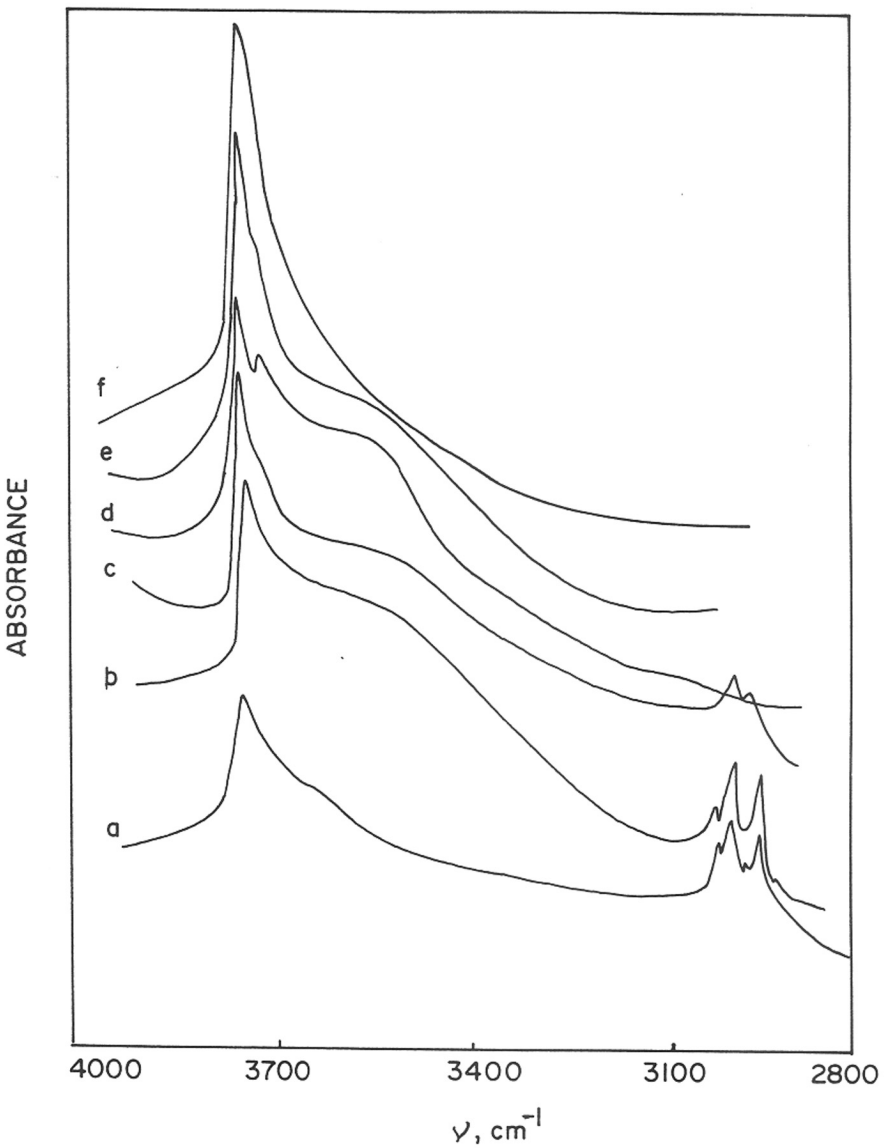

Fig. 3.15 : FTIR Spectra of [TEA]-Be- β (55) treated in vacuum at 475, 575 and 675 K [curves a-c], in air and then in vacuum at 673, 723 and 823 [curve d-f] respectively

hydroxyl groups Si-$(OH)_2$-Be expected at around 3650-3600 cm^{-1} is missing. But after air calcination at 675 K (curve d), the shoulder at 3685 cm^{-1} develops into a distinct band, which also disappears on further calcination in air (curve e and f). It should be noted here that this band disappears on adsorption of pyridine giving rise to Lewis acid sites but not Brönsted acid sites as described in the following section.

3.1.6.3 [NH_4]-beta conversion to [H]-beta :

Fig. 3.16 (a-e) depicts the changes in the i.r spectra of sample 3 (H-Ga-beta) in the NH_4 form on decomposition in situ in the i.r cell at 373, 473, 573, 673 and 773 K (curves a-e respectively) and subsequent evacuation. The bands at 3380, 3300 and 2950 cm^{-1} are due to N-H stretching vibrations and are eliminated at 673K. The band at 3622 cm^{-1}, characteristic of Ga-OH-Si groups grow in intensity with progressive deammoniation, reaches a maximum on evacuation at 673 K and decreases at higher temperatures. These results are consistant with those observed for [Na]-beta and indicate an optimal temperature in the range of 673 - 723 K for removal of organics as well as deammoniation. Identification of this temperature is an important step in the preparation of catalytically active [H]-beta. Calcination at a low a temperature may leave carbonaceous matter clogging the pores, whereas potential Brönsted acid sites may be eliminated at too high a temperature. Partial destruction of the framework structure and exit of metal cations like (Al or Ga or Be) from framework positions are additional hazards at higher temperatures.

FTIR spectra recorded during [NH_4]-Be-beta conversion to [H]-Be-beta are presented in fig. 3.17 (a-e). The existance of NH_4^+ cations is indicated only in the case of curve a, recorded at 373 K. In all the other spectra, weak bands of N-H stretching are seen at 3420, 3350 and 3310 cm^{-1}. The disppearence of these bands is associated with the appearance of

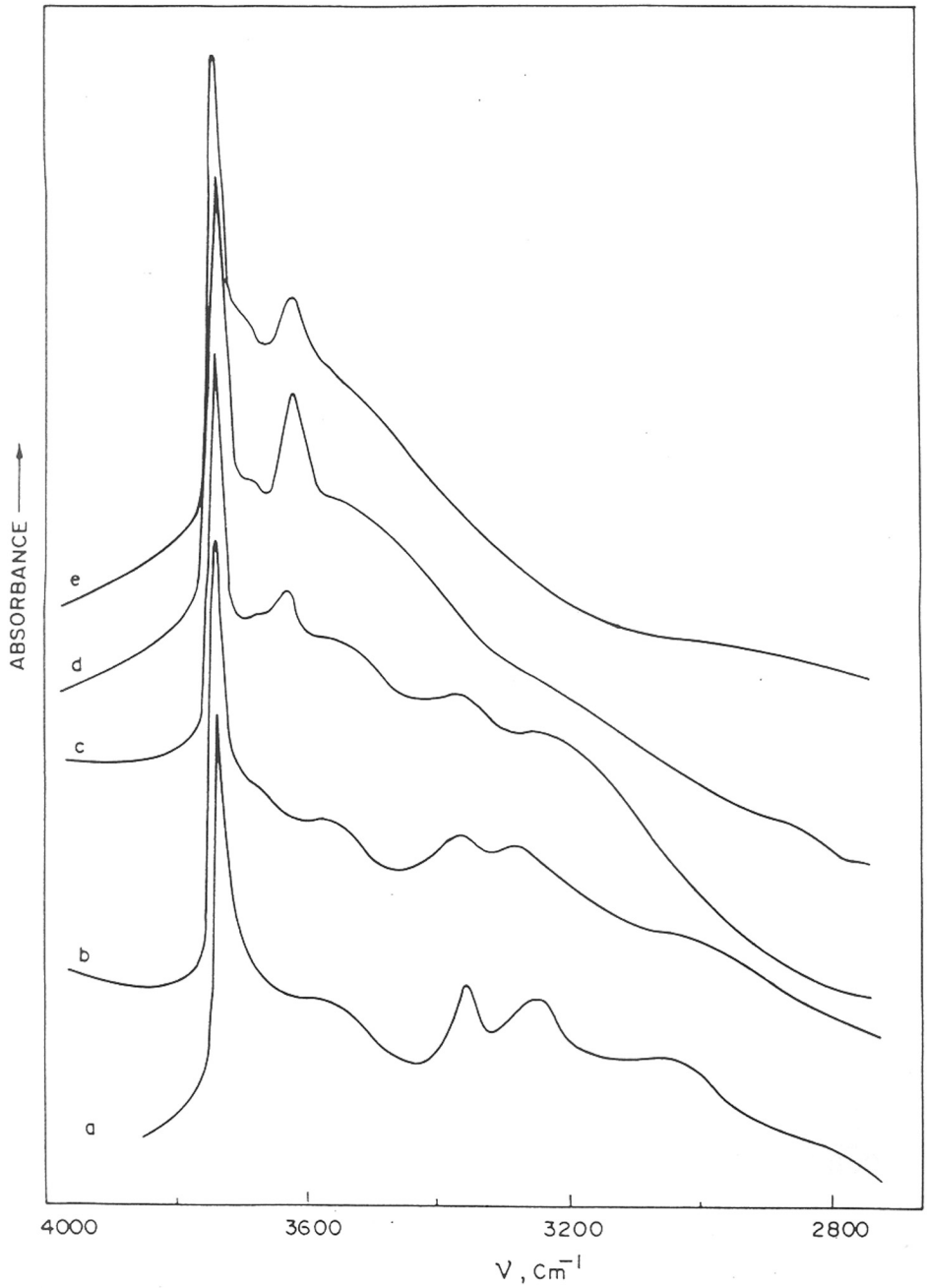

Fig. 3.16 : FTIR spectra of $[NH_4]$-Ga-β, treated in vacuum at 373, 473, 573, 673 and 773 K. [Curves a-e respectively].

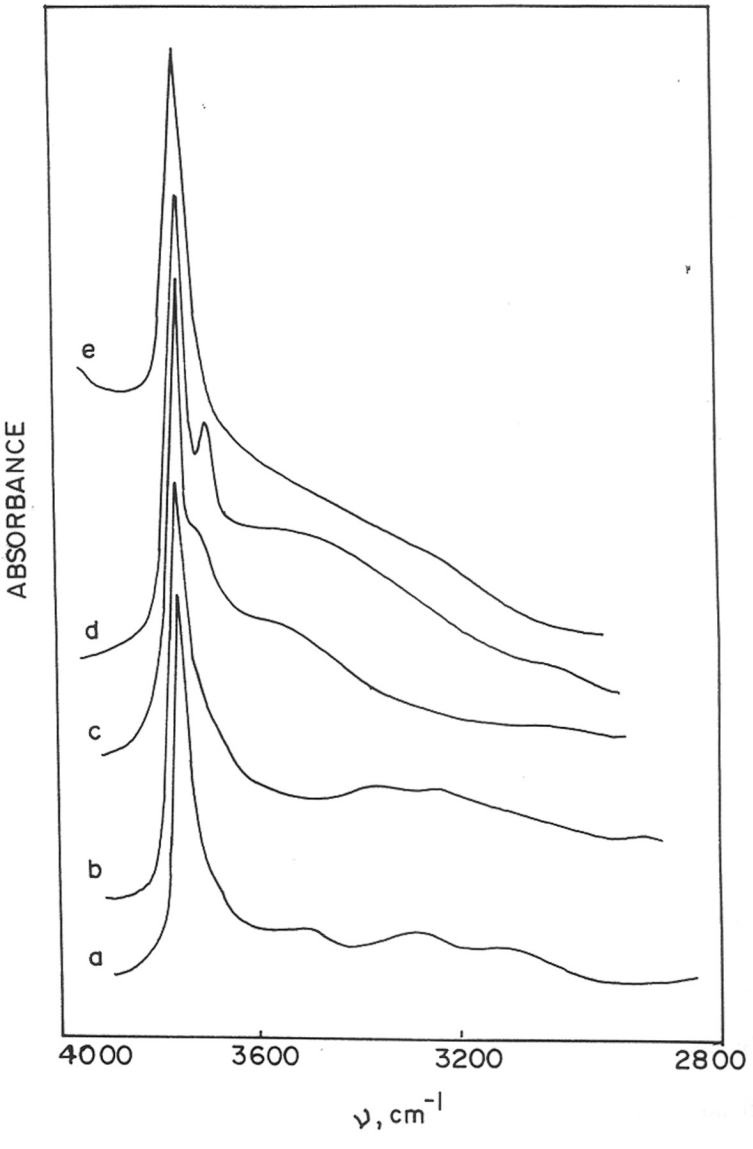

Fig. 3.17 : FTIR spectra of $[NH_4]$-Be-β treated in vacuum at 373, 473, 573, 673 and 773 K. [curves a-e respectively].

SiOH groups (3740 cm^{-1}), hydrogen bonded hydroxyl groups (3540 cm^{-1}) and a sharp band at 3685 cm^{-1}, the assignment of which is discussed in a later section. Any type of bridging hydroxyl groups (Si-OH-Be) is not seen. From MASNMR results it is known that H-Be-beta samples do not have lattice Be^{2+} ions. So they have no NH_4^+ exchange capacity. Small amounts of NH_4^+ ions remain weakly adsorbed on silanol groups and defect sites, which on decomposition evolve NH_3 gas which gets adsorbed on species responsible for the 3685 cm^{-1} band.

3. 1. 6. 4 [H]-beta conversion to D_2O, C_6H_6 -(H-beta):

To confirm that the absorption bands at 3740 and 3622 cm^{-1} are indeed due to (OH) groups situated at locations accessible to probe molecules and to assess the relative acidity of these (OH) groups, the shift in the (OH) frequency on adsorption of D_2O and benzene was evaluated. The results are given in table 3.6 [Ga]- and [Be]-beta evacuated at 673 K was exposed to vapours of D_2O or benzene at 423 K. After evacuation of excess vapours, the spectra were recorded. On admission of D_2O, the bands at 3740 and 3622 cm^{-1} disappeared while new bands at 2805 and 2750 cm^{-1} (due to surface OD groups) appeared. When H- bonded complexes of OH groups with weakly adsorbed bases (like benzene) are formed, the i.r bands of OH groups with acidic properties are shifted towards lower frequencies, the extent of shift being characteristic of the strength of the Brönsted acid sites[20-22]. On admission of benzene to [Ga]-beta, the band at 3740 was shifted to 3596 cm^{-1} and that at 3622 to 3300 cm^{-1}. On comparing the shifts induced by benzene adsorption on the absorption frequency of bridged hydroxyls (table 3.6), the relative strength of the acid sites of the zeolites may be classified as:

[Al]- ZSM-5 > [Al]-beta > [Ga]-beta > [Al]-Y > [Be]-beta

Table 3.6 : Frequency shifts (cm^{-1}) ν_{O-1} bands for hydroxyl groups after adsorption of D_2O and benzene.

Sample	$^{\nu}OH_{0-1}$ (cm^{-1})	$\Delta^{\nu}OH_{0-1}$ (cm^{-1})		Ref.
		D_2O	Benzene	
[Ga] - β	3740	935	144	Present study
	3622	897	322	-do-
[Be] - β	3740	930	130	-do
[Al] - β	3740	977	100	5
	3602	892	337	5
[Al] – Y	3640	-	300	20
[Al] -ZSM-5	3610	-	350	20

3. 1. 6. 5 Pyridine-[Ga]- and [Be]-beta :

Ever since the pioneering work of Parry[23], the i.r spectrocopy of adsorbed pyridine has been used as a characteristic tool to detect the presence of Brönsted and Lewis acid centers on solid surfaces. IR bands around 1640 and 1550 cm^{-1} are characteristic of protonated pyridinium ions and indicate the presence of Brönsted acid sites, where as bands at 1440-1450, 1595-1605 and 1630 cm^{-1} are characteristic of pyridine coordinately bound to Lewis acid sites[23]. When pyridine was adsorbed on [Al]-beta[15], bands at 1633 and 1546 cm^{-1} due to pyridinium ions and at 1618, 1500 and 1450 cm^{-1} due to coordinatively bound pyridine were detected. Fig. 3.18 (a-f) shows the i.r spectra of pyridine retained at 323, 373, 473, 573, 673 and 773 K, after adsorption of pyridine on [H]-Ga-beta at 298 K and subsequent evacuation at the above mentioned temperatures. As expected all the bands observed earlier for [Al]-beta are also observed confirming the presence of both Brönsted and Lewis acid sites in the gallium analog. An interesting difference between the two materials is the following. Although the concentration of the pyridinium ions on [Al]-beta decreased only beyond 673 K, their decrease started already at 573 K in the case of [Ga]-beta (Fig. 3.16); the bridging OH groups on the later are hence less stable than those on the Al analog. This observation is consistent with conclusions derived earlier from the TPD of NH_3 and spectra of OH groups.

The spectra of adsorbed pyridine on H-Be-beta (sample 11) at 373, 473 and 573 K are presented in the fig. 3.19 (a-c). The corresponding spectra of hydroxyl groups are presented in fig. 3.20 (a-c) as difference spectra. IR bands corresponding to Brönsted acid sites are negligible even at 373 K and only bands due to Lewis acid sites (1595, 1452 cm^{-1}) are seen. In the difference spectra shown in fig.3.20, as the adsorbed pyridine is desorbed at higher temperatures, an increase in the 3740, 3685 and 3540 cm^{-1} band intensities is seen which follows the decrease in Lewis acid sites. Isomorphous substitution of Be^{2+} in zeolite

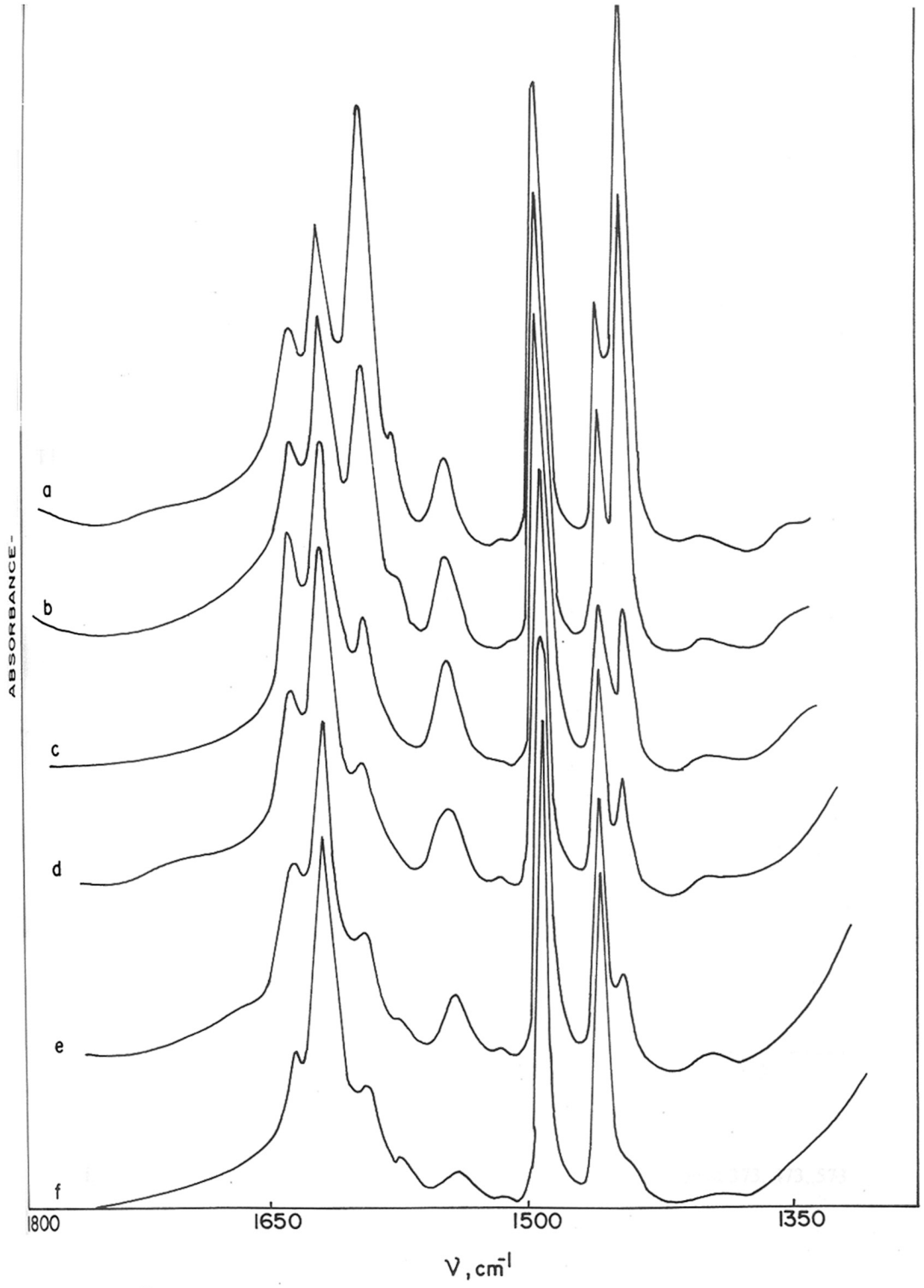

Fig. 3.18 : FTIR spectra of adsorbed pyridine retained after evacuation at 323, 373, 473, 573, 673, and 773 K on H-Ga-β [Curves a-f respectively].

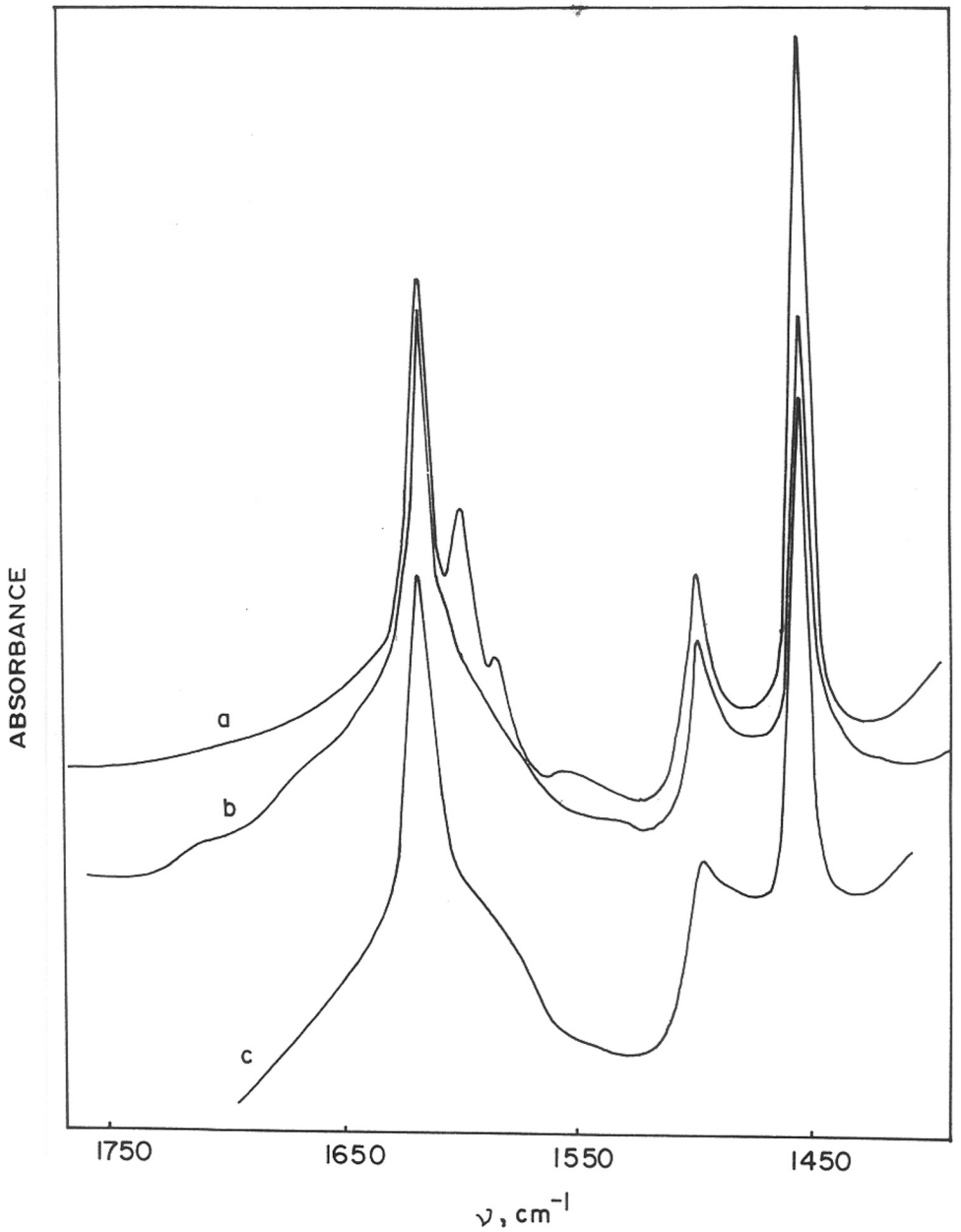

Fig. 3.19 : FTIR spectra of adsorbed pyridine retained after evacuation at 373, 473, 573 K.[Curves a, b and c respectively] on H-Be-β

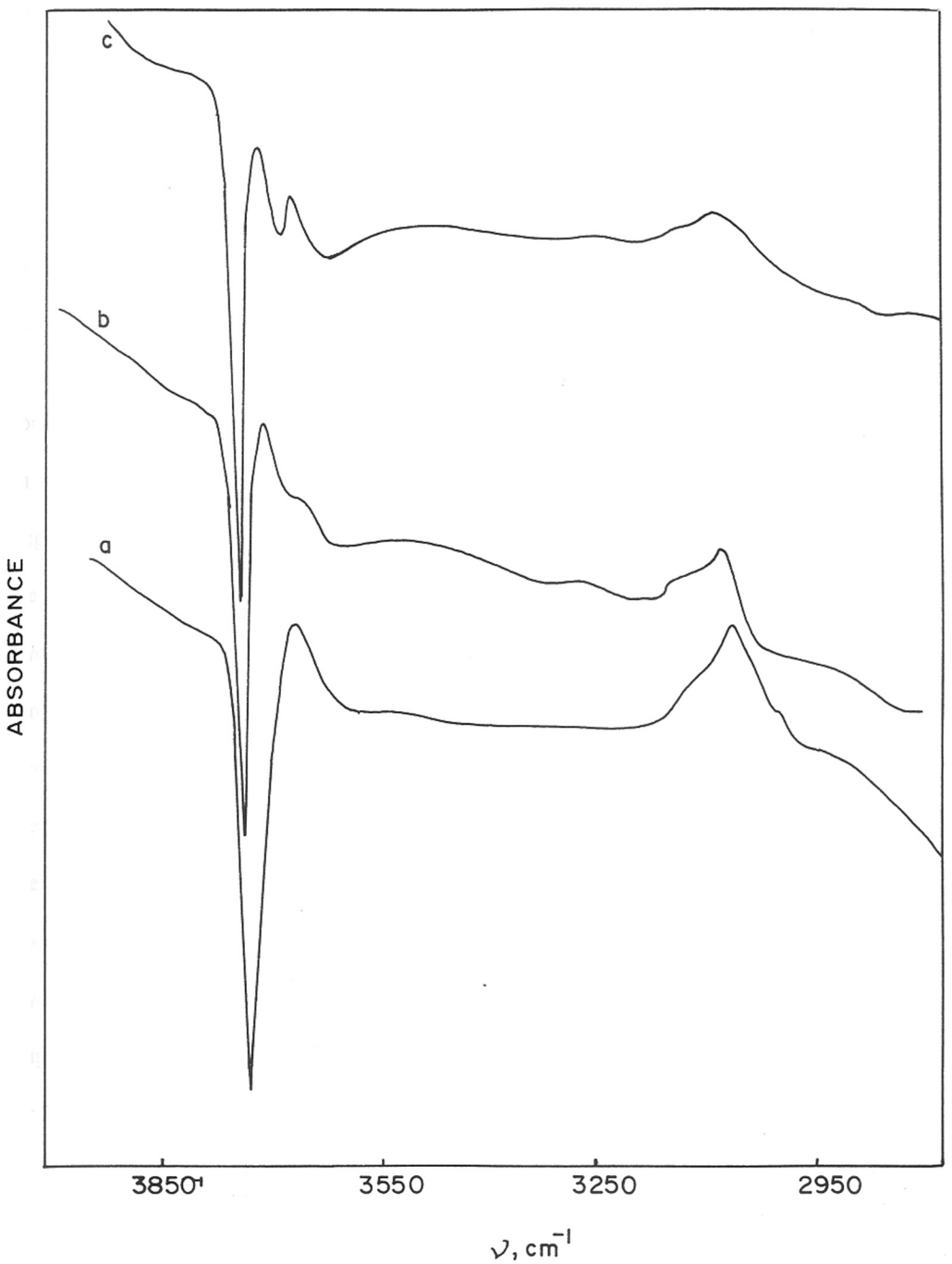

Fig. 3.20 : FTIR difference spectra of pyridine retained after evacuation at 373, 473, 573 K.[Curves a, b and c respectively] on H-Be-β

framework should result in bridging hydroxyl groups as shown below.

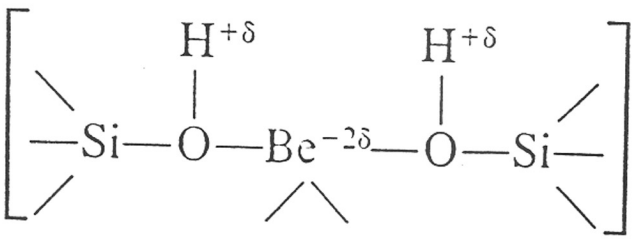

The tetrahedral environment is known to be thermodynamically the most favourable for Be^{2+} in oxide systems[25]. The isomorphous substitution of $(BeO_4)^{-6}$ for $(SiO_4)^{4-}$ is possible in many silicate minerals and some zeolites as well. The values of the radii and electro-negativity of Be^{2+} and Si^{4+} are very close, 0.35, 0.42 Å and 210, 260, respectively. The e/r of Be^{2+} (6.5) is higher than that of Al^{3+}(6.0). Therefore, the degree of protonation of bridging hydroxyl groups for Be^{2+} is to be expected to be higher than for Al^{3+}. Hence the strength of Brönsted acid sites in beryllium silicate zeolite should be higher than that of Al-silicate zeolite. Therefore bridging hydroxyl groups if at all are present in Be-beta, should have a frequency less than 3605 cm^{-1}, observed for Al-beta. Since Be^{2+} cations tend to hydrolyse[25], Be^{2+} cations in the framework may hydrolyse and come out of it and form extra lattice cation species or some kind of beryllium silicate species. Therefore, in the i.r spectrum of surface hydroxyl groups, band at 3685 cm^{-1} can be assigned to extra lattice Be species, this is supported by the MASNMR results. These species may most probably silica-beryllium debris or beryllium silicate.

3B ZEOLITE MORDENITE :

3.2 [Ga]-Mordenite

3. 2. 1 Synthesis :

The synthesis of Ga-mordenite was found to be reproducible only in a limited range of gel compositions. Synthesis of Ga-mordenite, with silica-sol as the source of silica was much easier, in the sense that slight variations in the addition sequence of the constituent reactants did not affect the final product. However, its synthesis with fumed SiO_2 as the silica source was rather critical. Pure, crystalline Ga-mordenite using fumed SiO_2 was obtained only when the SiO_2/Ga_2O_3 mole ratio of the reacting gel was in the range of 10-22. For SiO_2/Ga_2O_3 <20 only amorphous material was found after the reacting gel was subjected to crystallization. For SiO_2/Ga_2O_3 >22-25 dense phases like quartz were predominant. Moreover, a change in the addition sequence of the reacting constituents in an otherwise optimum gel composition and conditions also prohibited the formation of pure Ga-mordenite.

3. 2. 2 X-ray Diffraction :

The X-ray diffraction patterns of Al-mordenite (SiO_2/Al_2O_3 =13.3) and Ga-mordenite (SiO_2/Ga_2O_3 =19) and degallated mordenite (SiO_2/Ga_2O_3 = 27.0) appear similar (fig.3.21) and match very closely with that of Al-mordenite published earlier[26]. However, certain distinctively differing features can be seen among these diffractograms, inspite of general similarities. Firstly, as seen in fig.3.21, the peaks in the case of Ga-mordenite (curve b) and degallated mordenite (curve c) have noticeably lower intensities than the corresponding peaks in the Al-Mordenite sample (curve a). Secondly, isomorphous substitution of Ga for Al increases the "d" values (Table 3.7) and unit cell volume (Table 3.8).This is because the expected Ga-O bond length 1.823 Å is considerably longer than those of both Al-O (1.75 Å)

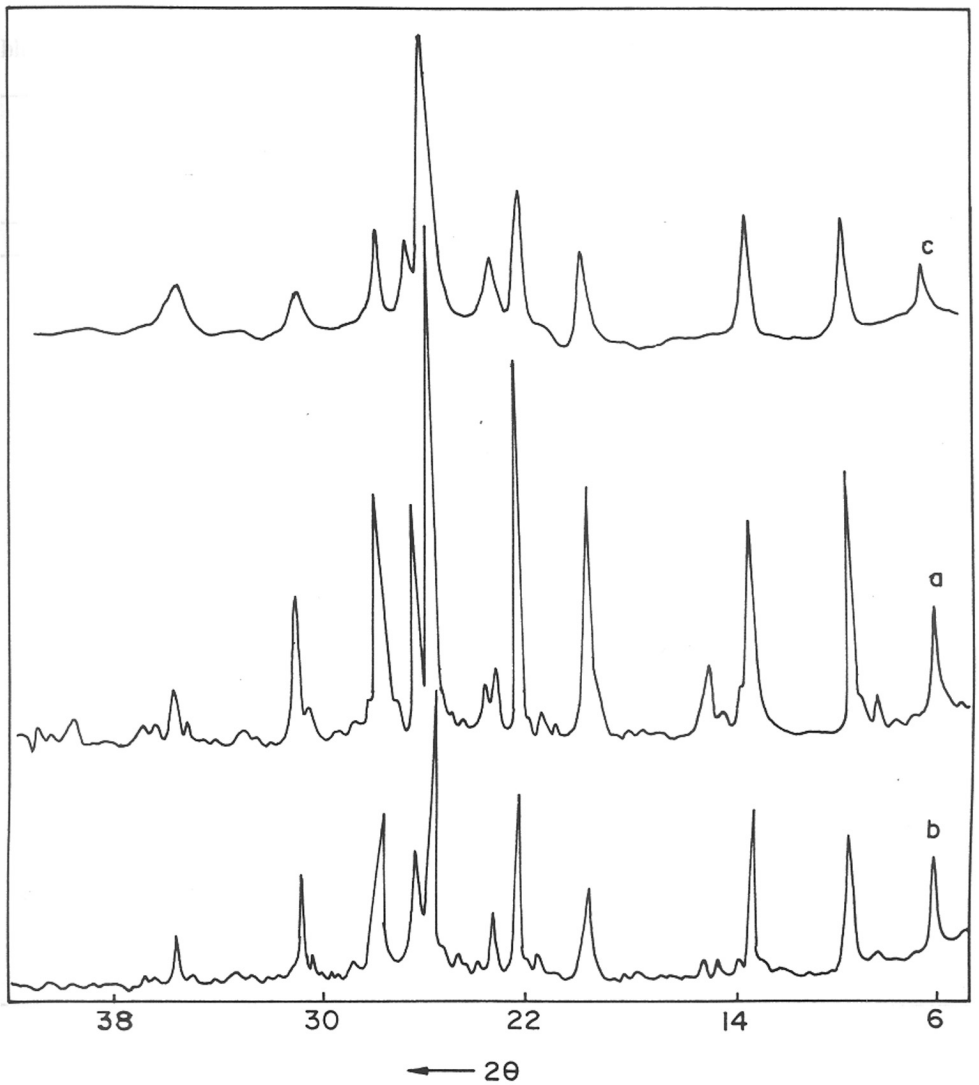

Fig. 3.21 : X-ray diffraction patterns of as-synthesized Al-mordenite, Ga-mordenite and degallated mordenite [curves a, b and c respectively]

Table 3.7 : XRD "d" Values of Alumino- and Gallo-Mordenite Zeolites

hkl	Mordenite (Al)		Mordenite (Ga)	
	d(nm)	I/I_o	d(nm)	I/I_o
110	13.503	0.242	13.562	0.423
200	9.054	0.541	9.051	0.478
111	6.553	0.415	6.573	0.535
330,400	4.507	0.512	4.514	0.349
150	3.969	0.775	3.984	0.641
241	3.808	0.154	3.834	0.198
202	3.453	1.000	3.468	1.000
350	3.373	0.475	3.383	0.479
511	3.213	0.484	3.219	0.620
402	2.878	0.293	2.888	0.261
352,442	2.503	0.113	2.515	0.109
004	1.886	0.090	1.879	0.096

Table 3.8 : Unit Cell Parameters of [Al]- and [Ga]- Mordenites

Sample	hkl	d(Å)	Unit Cell dimension (Å)			Unit Cell Volume $(Å)^3$
			a	b	c	
[Al]-Mordenite	352	2.503	18.067	20.284	7.491	2745.23
	402	2.858				
	241	3.808				
	111	6.553				
	241	3.808	18.060	20.278	7.497	2745.87
	511	3.213				
Average						2745.56
[Ga]-Mordenite	111	6.573				
	241	3.834	18.067	20.424	7.505	2769.348
	511	3.219				
	352	2.515				
	402	2.888	18.072	20.436	7.510	2773.5886
	241	3.834				
Average						2771.4683

and Si-O (1.61 Å) reflecting the increase in the mean T-O bond distances on gallium substitution. Thus, this lattice expansion is a direct result of incorporation of the larger Ga atoms in the framework positions of mordenite. On degallation, however the "d" values and unit cell volume decrease slightly as compared to the parent gallo-mordenite sample. The unit cell dimensions (Table 3.9) revealed an ortho-rhombic symmetry typical of mordenite. Further, as seen in fig.3.21, the X-ray diffraction patterns of degallated mordenite indicate a slight reduction in the intensities of the characteristic peaks although, the presence of some amorphous material is not visible in the background of the XRD pattern. This suggests that treatment with dilute acid solution brings about degallation without structural degradation, as evidenced in the product distribution in the xylene isomerization reaction (Chapter IV) and the surface area measurements.

3. 2. 3 Surface Area Measurement :

The amorphous content of zeolite samples was quantitatively estimated by the adsorption of argon using the t-plot method [27]. These measurements indicated that the surface area of the zeolitic part in the protonic form of the Al-mordenite was 572 m^2/g and its non-zeolitic content was 36 m^2/g. In the case of protonic Ga-mordenite, the surface area of the zeolitic content was 466 m^2/g and the non-zeolitic content was 102 m^2/g. The degallated-Mordenite had the surface area of the zeolitic content equal to 403 m^2/g. and of the non-zeolitic content was 76 m^2/g. Thus, these experiments revealed that the gallo-isomorph underwent greater structural degradation than its alumino analog.

3.2.4 Scanning Electron Microscopy :

The scanning electron micrographs of the as-synthesized Al-mordenite and Ga-mordenite samples, shown in the fig.3.22 indicate the absence of any amorphous material. These micrographs show that the two samples consisted of well-grown, round to slightly oval (sometimes hexagonal) single crystals of an average dimension of <2 μm and 1-2 μm respectively, as well as a few aggregates.

3.2.5 Thermal Analysis :

This technique, besides giving an insight into the behavior of the mordenite samples on heating, also helped establish the fact that the gallium species occupied tetrahedral framework sites in the gallosilicate (mordenite) lattice. The relative thermal behaviour of the as-synthesized [Al]-mordenite and [Ga]-mordenite and degallated mordenite samples are shown in the fig.3.23. The d.t.a. curve corresponding to [Ga]-mordenite appears to follow the same pattern as that of [Al]-Mordenite (fig.3.23, curves c, b, a respectively). The small weight loss observed at low temperatures in the t.g.a curve is due to the dehydration of water on the external surface or located in the pores not blocked by occluded templating ions. Subsequently, the major transformation and weight loss that occurs at higher temperatures is attributed mainly to the oxidative decomposition of the organic template. This is well reflected in the d.t.a curve exhibiting a characteristic exotherm. On substitution of Al by Ga, the decomposition temperature for TEA^+ cations changes from 872 and 735 K to 826 and 717 K, respectively. The weight loss at 872K (for [Al]-mordenite) and 826K (for [Ga]-mordenite) is attributed to the loosely occluded TEA^+ cations, whereas the same at temperatures 735K and 717K (for [Al]- and [Ga]- isomorphs, respectively) maybe considered to be due to the decomposition of organic ions which are strongly bonded and associated with aluminium/gallium acid sites in the channels [28].

A

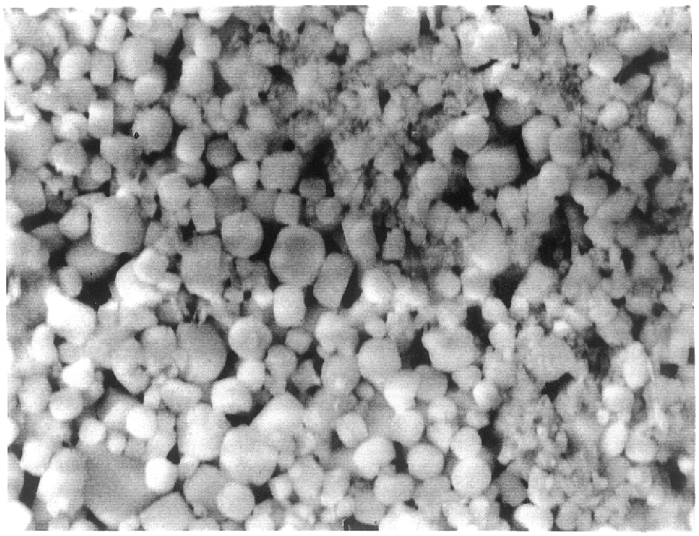

B

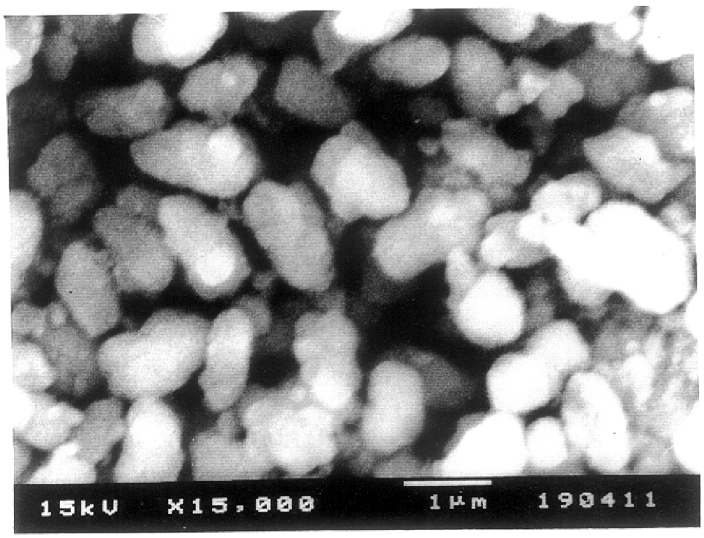

Fig. 3.22: Scanning elctron micrographs of A) alumino-mordenite and B) gallo-mordenite.

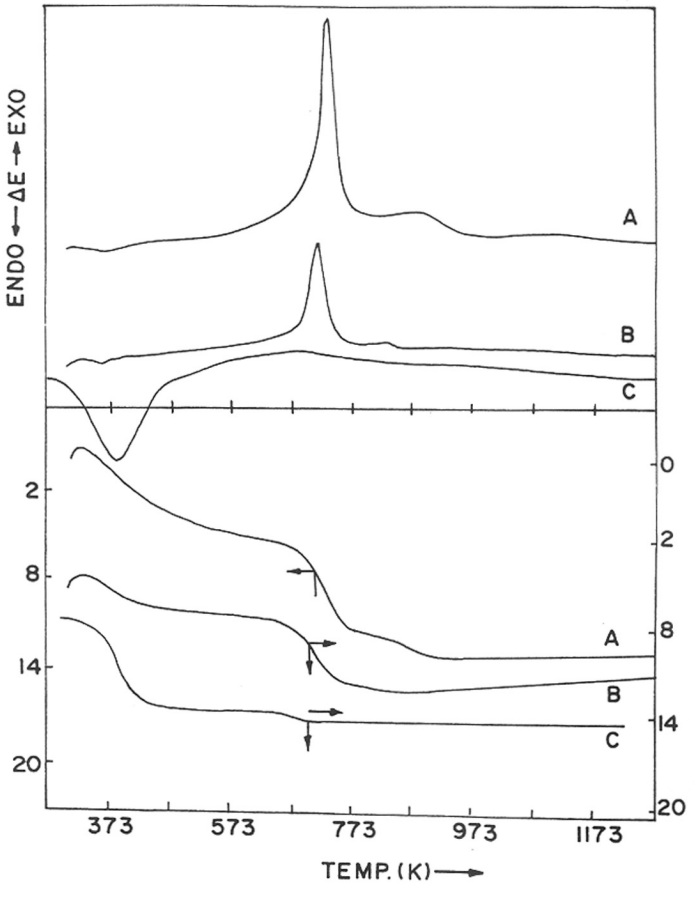

Fig. 3.23 : TG-DTA curves for Al-mordenite, Ga-mordenite and degallated mordenite [curves a, b and c respectively]

The d.t.a curve of corresponding degallated mordenite sample (fig.3.23, curve c) exhibits a different pattern. Here the weight loss upto ~ 380 K due to loss of water is apparent as a prominent endothermic peak. The exothermic weight losses corresponding to TEA^+ species are absent due to the absence of organic template.

3. 2. 6 : Adsorption Studies :

Adsorption measurements with molecules of different sizes give direct information about the dimensions of the pore systems in zeolites. Molecules whose kinetic diameters are less than the pore openings of the zeolites, can be sorbed by zeolites The kinetic diameters of a number of probe molecules have been compiled by Breck[29]. The adsorption of H_2O, n-hexane, cyclohexane, benzene, n-butylamine and the three xylene isomers, in the sodium form of [Al]-Mordenite, [Ga]-Mordenite and degallated mordenite are shown in Table 3. 9. It may be noted that the adsorption in gallo-mordenite is marginally lower than its aluminum analog. This may be due to either of the following factors or a combination of two or all of these factors, (1) the presence of large zeolite crystals (4-5 μm compared to 0.5-1.0 μm for the Al analog), (2) the migration of extra lattice gallium species to the surface, blocking the channels and (3) the occurrence of stacking faults in gallo-mordenites. The data indicate, however, that all the samples are large-pore mordenites.

3. 2. 7 FT.i.r. Spectroscopy :

The framework i.r. spectra in the region 200-1300 cm^{-1} of these mordenite analogs are shown in the fig.3.24. The values of the major absorption bands are compiled in Table 3.10 The assignments of these bands are already established[30,31]. The structure-sensitive range of the i.r. spectra shows prominent bands at 560-580, 640, 730 and 1080 cm^{-1} characteristic of a zeolite framework. On substitution of Al by Ga, the zeolite bands attributed to asymmetric and symmetric vibrations of the TO_4 (T = Si or Al) tetrahedra, are shifted to lower wave

Table 3. 9 : Adsorption of water and hydrocarbons

Adsorbed	[Na]-Al-Mordenite(13) (Si/Al = 6.65)	[Na]-Ga-Mordenite(18) (Si/Ga = 9.05, Si/Al>1000)	DAH-Ga Mordenite(55) (Si/Ga = 27.0, Si/Al>1000)
H_2O	10.2	9.5	8.5
n-hexane	7.1	6.5	6.0
Cyclohexane	10.2	8.9	8.0
benzene	10.6	9.0	8.6
n-Butylamine	6.7	5.5	3.5
p-xylene	8.3	7.2	7.0
m-xylene	7.7	6.9	6.5
o-xylene	8.0	6.8	6.3

Temp (K) = 298; $P/P_o = 0.5$

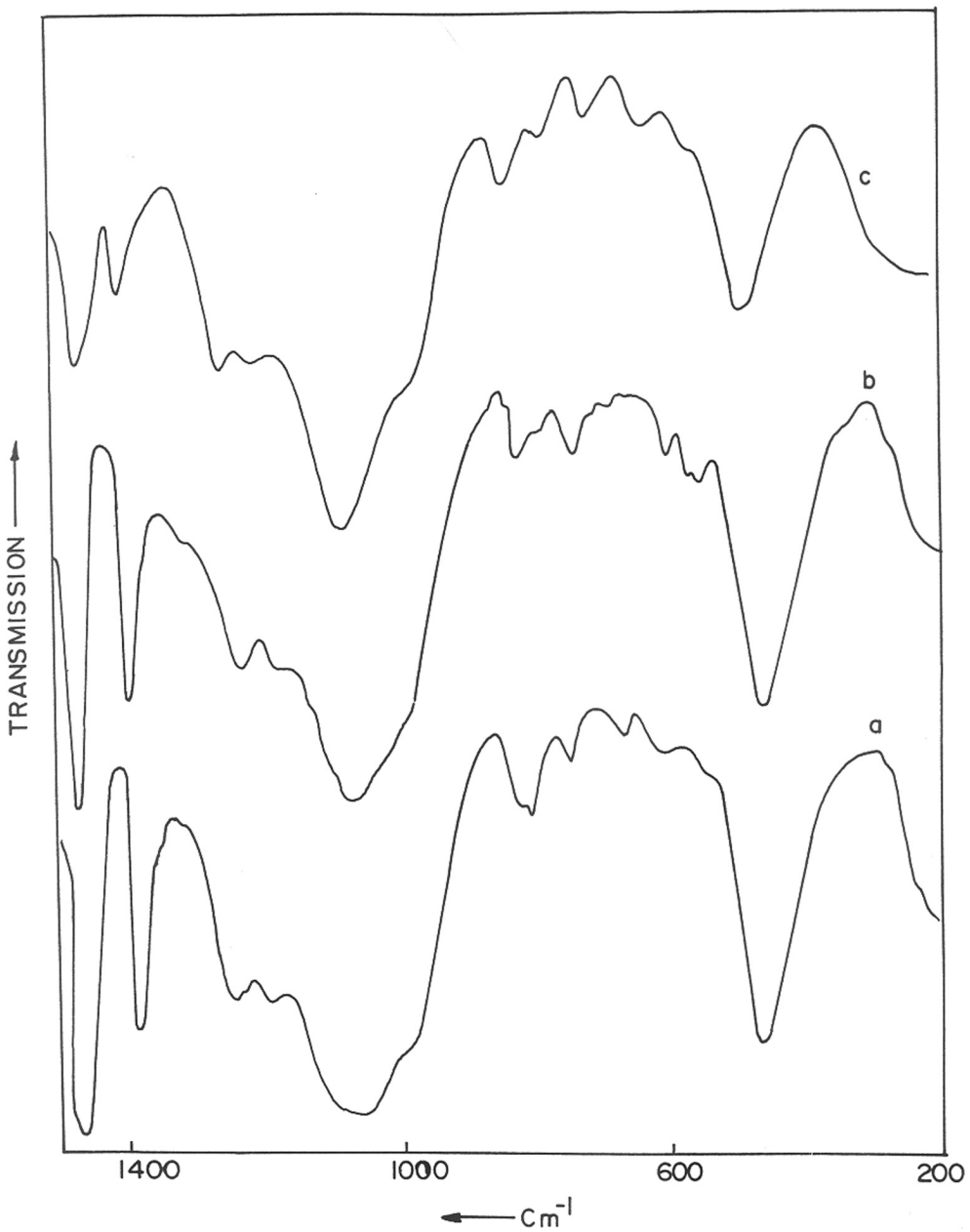

Fig. 3.24 : Framework i.r vibration spectra of Al-mordenite, Ga-mordenite and degallated mordenite [curves a, b and c, respectively]

Table 3.10 : Framework i.r vibration frequencies (ν, cm^{-1}) .

[Al]-Mordenite	[Ga]-Mordenite	DA-Ga-Mordenite
1235 w	1230 w	1231w
1080 s	1065 ms	1073ms
820 w	811 vw	815vw
786 vw	786 vw	785vw
730 w	722w	720 w
-	650 m	649 vw
606 vw	618 vw	615vw
460 ms	452 ms	455ms
375 vw	373vw	370w

numbers. For example, the band at 1235 cm^{-1} due to asymmetric stretching vibration[31] of Si-O-Al are shifted to 1230 and 1232 cm^{-1} in the case of the two gallo- isomorphs. The band at 1080 cm^{-1} due to symmetric streching vibrations of Si-O-Al is shifted to 1065 and 1073 in case of the gallo-isomorphs. Similarly, the band at 730 cm^{-1}, assigned to "isolated" AlO_4 tetrahedra in alumino-mordenite is shifted to 722 cm^{-1} and 720 cm^{-1} in [Ga]-Mordenite and degallated mordenite respectively. This is due to the substitution of Al by the heavier Ga atoms in the lattice of Mordenite.

The FTIR spectra of protonated mordenite samples [H]-Al-M (25), [H]-Ga-M(19) and DA-[H]-Ga-M (27) respectively) in the OH stretching region after evacuation for 4h at 673K are shown in fig.3.25. Well defined absorption bands are seen at 3740 and 3603 cm^{-1} for [Al]-Mordenite[curve a], and 3740 and 3616 cm^{-1} for [Ga]-Mordenite. The band at 3740 cm^{-1} is assigned to isolated Si-OH groups which may be either terminal or originating from extra framework silica. This particular band shows much higher intensity for the degallated samples. The degallation of the samples was done using dilute acid which creates silanol nests and this could be the cause of the generation of excess silanol groups which are evidenced in the higher intensity of the band characteristic of the silanol groups.

The band at 3603 cm^{-1} in [H]-Al-M(25) is attributed to the stretching vibrations of bridging hydroxyls (Al-OH-Si)[32,33]. Consequently, it may be said that the band at 3616 cm^{-1} in [H]-Ga-M (19) is characteristic of protonated gallo-mordenite and is assigned to bridging hyroxyls (Ga-OH-Si). The similar band was also observed at 3620 cm^{-1} for [Ga]-ZSM5 and at 3610 cm^{-1} for [Al]-ZSM-5. This band at 3620 cm^{-1} in the degallated samples in the fig.3.25 (curve c) shows a lower intensity indicating that degallation removes substantial Ga-OH-Si sites. The shift in the frequency from 3603 to 3616 cm^{-1} also suggests that the Ga(OH)Si sites are more covalent than the Al(OH)Si sites, therefore, these sites must be less acidic.

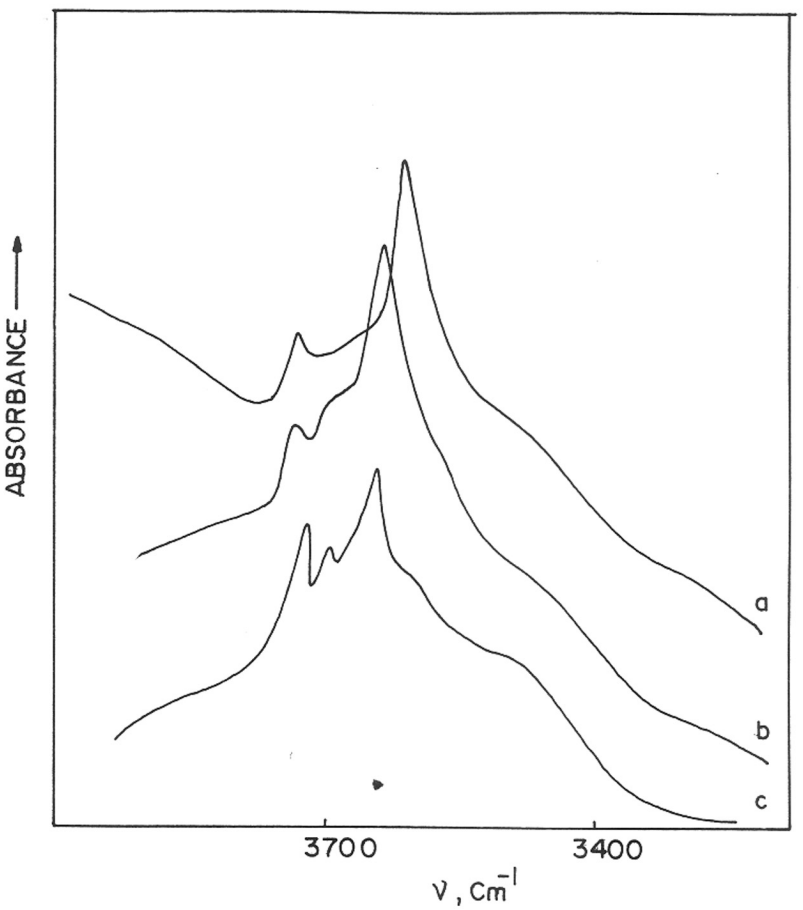

Fig. 3.25 : FTIR spectra of protonated Al-mordenite, Ga-mordenite and degallated mordenite [curves a, b and c, respectively]

In the fig.3.26 (curves A-E) the i.r.spectra of adsorbed pyridine on [H]-Al-M(25) at 323, 373, 473, 573 and 673 K are presented. Similar spectra for [H]-Ga-M(19) and for DA-[H]-Ga-M(27) are presented in fig.3.27 (curves a-e) and 3.28 (curves a-e) respectively. IR bands around 1640 and 1550 cm^{-1} are characteristic of protonated pyridine ions and indicate the presence of Brönsted acid sites while bands at 1440-1450, 1595-1605 and 1630 cm^{-1} are due to pyridine coordinatively bound to Lewis acid sites. When pyridine was adsorbed on [Al]-Mordenite, bands at 1632 and 1545 cm^{-1} due to pyridinium ions and at 1616, 1493 and 1451 cm^{-1} (fig.3.26) due to coordinatively bound pyridine are seen. The corresponding band positions for [Ga]-Mordenite, i.e. 1633 and 1548 cm^{-1} of pyridinium ions and 1620, 1500, 1450 and 1443 of coordinatively bound pyridine, thus confirm the presence of Brönsted and Lewis acid sites in the gallium analog (fig.3.27) of mordenite. In the fig.3.29 relative concentration of Bronstead and Lewis acid sites at different temperatures are plotted. It should be noted that the relative concentration of Lewis-to- Brönsted acid sites of [Ga]-Mordenite is higher than that of [Al]-Mordenite (fig.3.29). This may be attributed to relatively less thermally stable bridging OH groups in gallo-mordenite leading to dehydroxylation and giving rise to Lewis acid sites.

3. 2. 8: Solid State MAS NMR Spectroscopy :

The ^{29}Si and ^{27}Al MAS NMR spectra of [Al]-Mordenite and [Ga]-Mordenite are shown in fig. 3.30. This ^{29}Si spectra of both the samples can be resolved into three peaks : The peak at δ =100 ppm stems from Si(2Al) or Si(2Ga) configurations[34]. The peak at -105 ppm includes both Si(1Al) or Si(1Ga) configurations and SiOH defect groups. Finally, the peak at -110 ppm characterizes the Si(0Al) and Si(0Ga) configurations. The ^{27}Al MAS NMR spectrum of [Al]-Mordenite (fig.3.30) shows a single line at 50 ppm, corresponding to tetrahedral Al in the framework and suggesting the absence of extra lattice Al in the sample,

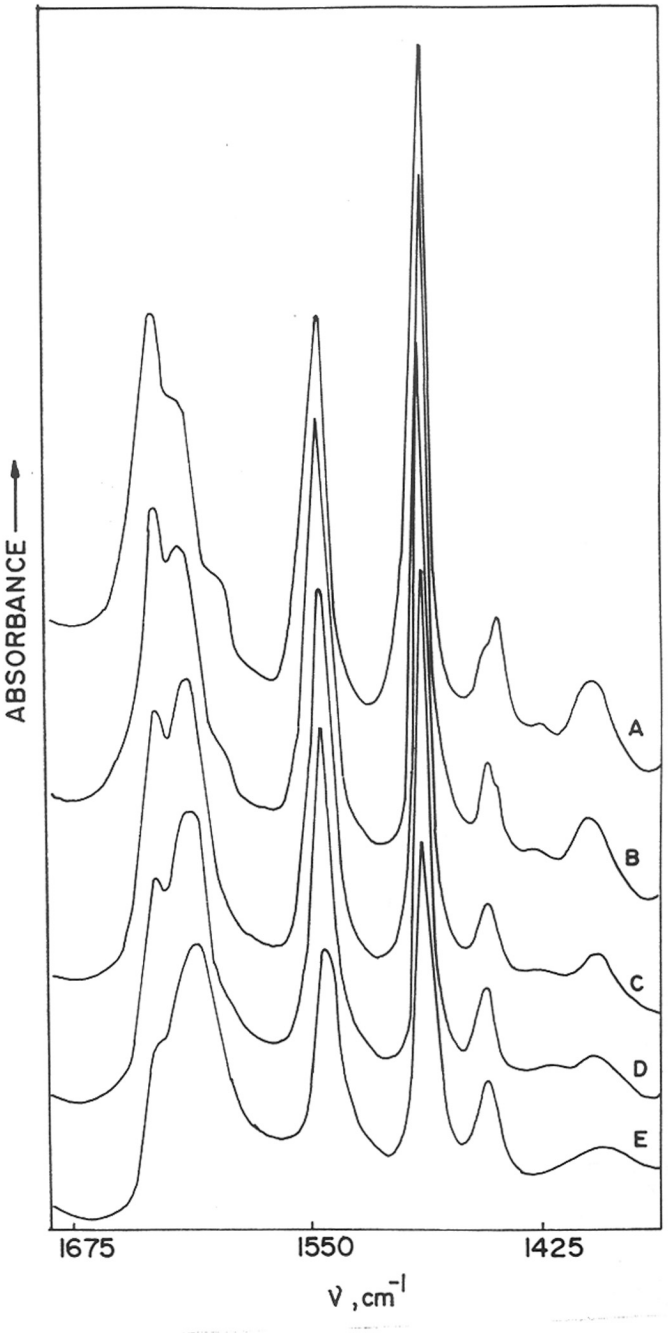

Fig. 3.26 : FTIR spectra of adsorbed pyridine retained after evacuation at 323, 373, 473, 573 and 673 K on Al-Mordenite (25) [Curves A-E respectively]

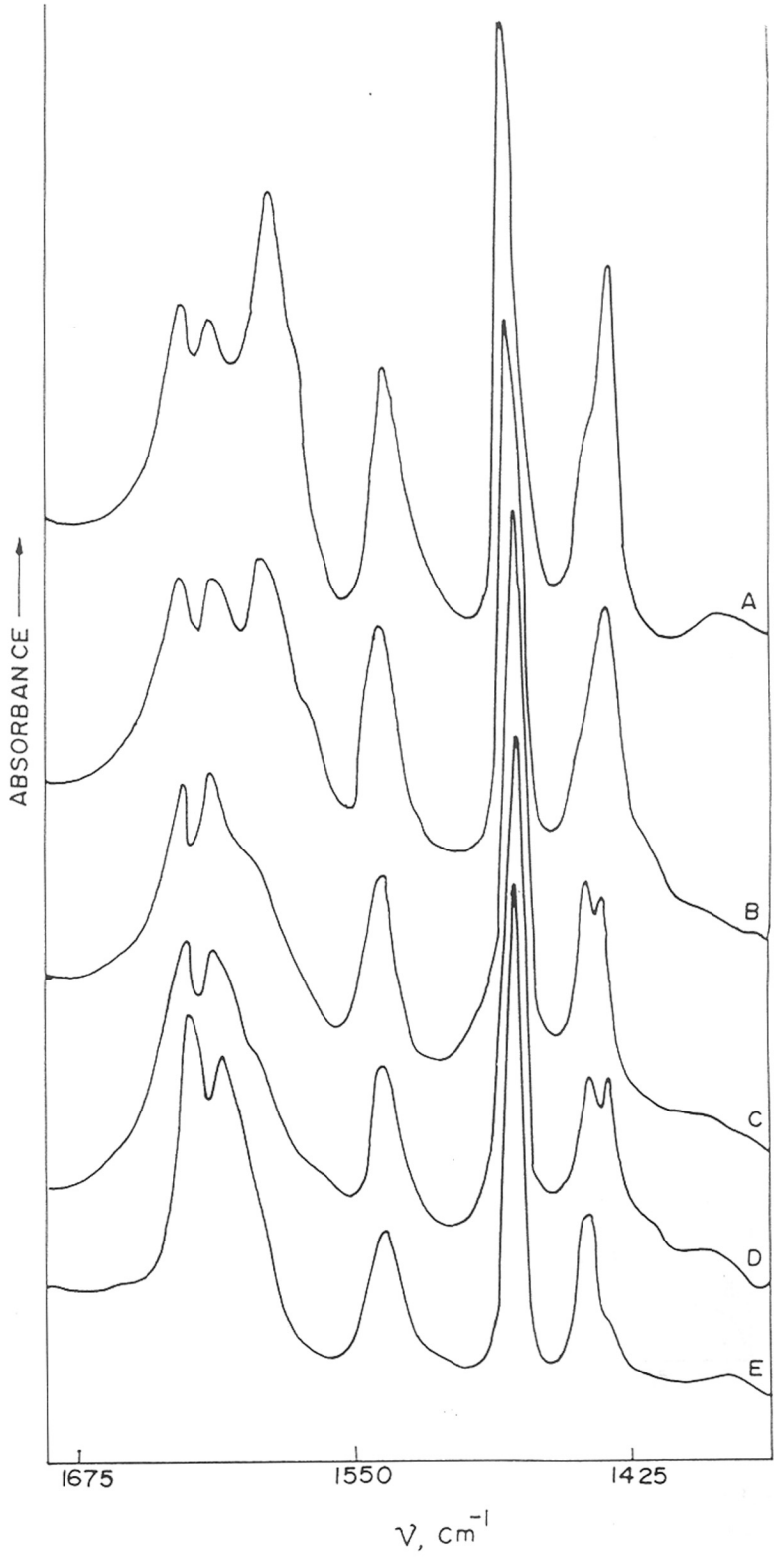

Fig. 3.27 : FTIR spectra of adsorbed pyridine retained after evacuation at 323, 373, 473, 573 and 673 K on Ga-Mordenite. [curves a-e, respectively]

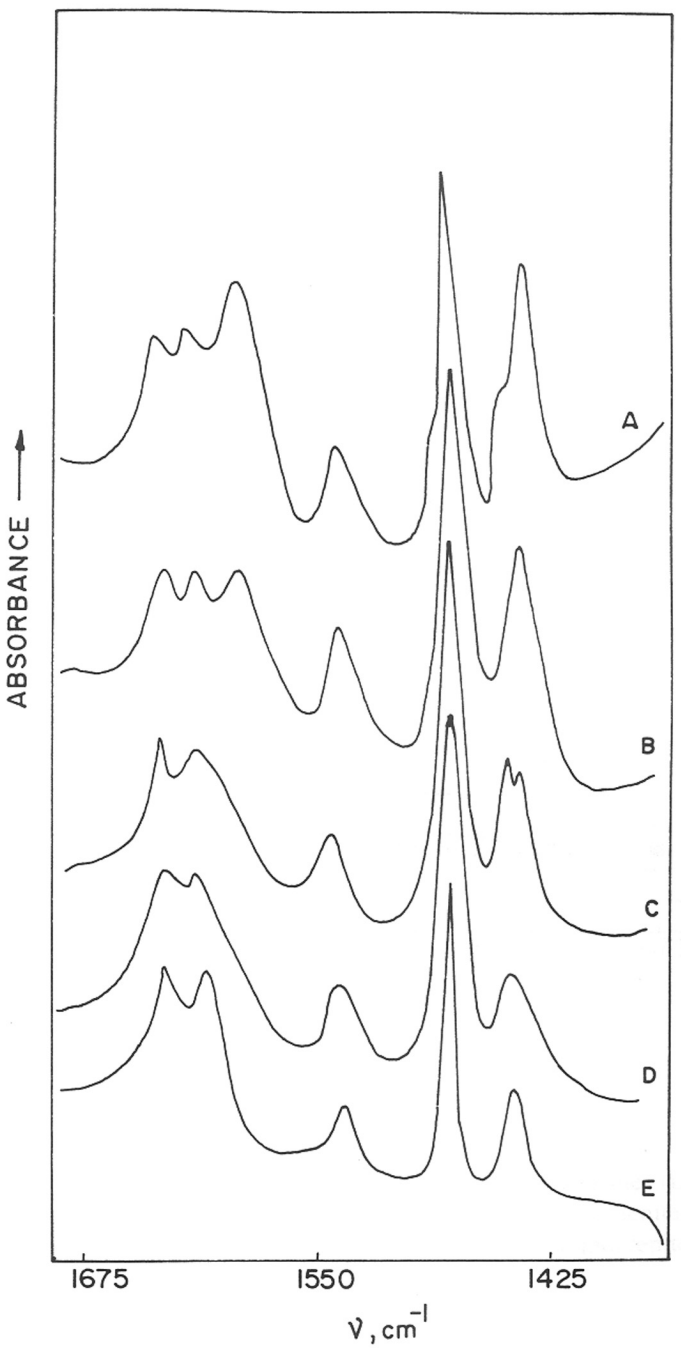

Fig. 3.28 : FTIR spectra of adsorbed pyridine retained after evacuation at 323, 373, 473, 573 and 673 K on degallated mordenite. [curves a-e, respectively]

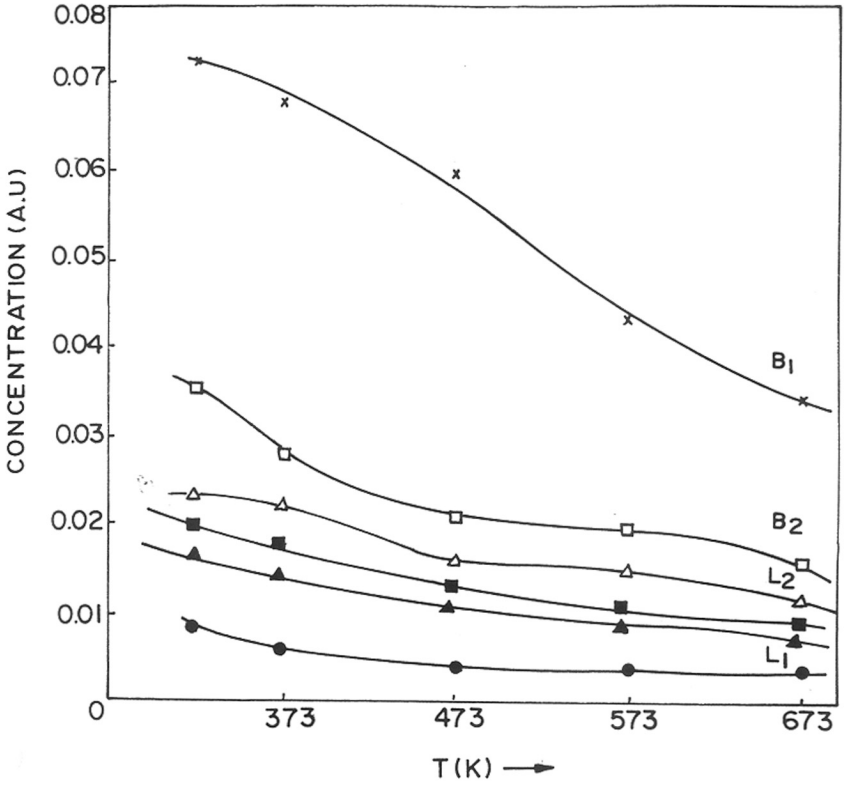

Fig. 3.29 : The concentration of Brönsted acid sites (B) and Lewis acid sites (L) versus temperature of desorption of chemisorbed pyridine on Al-mordenite [curves B1, L1], Ga-mordenite [curves B2, L2] and degallated Ga-mordenite [curves B3, L3], respectively.

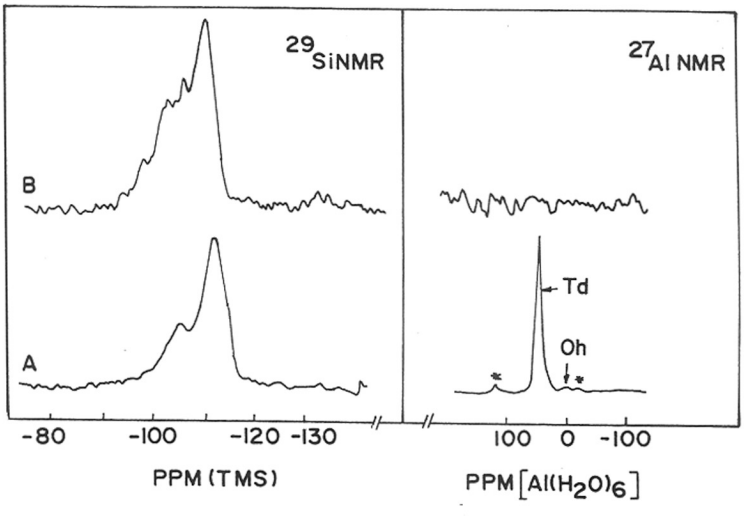

Fig. 3.30 : ^{29}Si and ^{27}Al MAS NMR of Al-mordenite and Ga-mordenite [Curves A and B respectively]

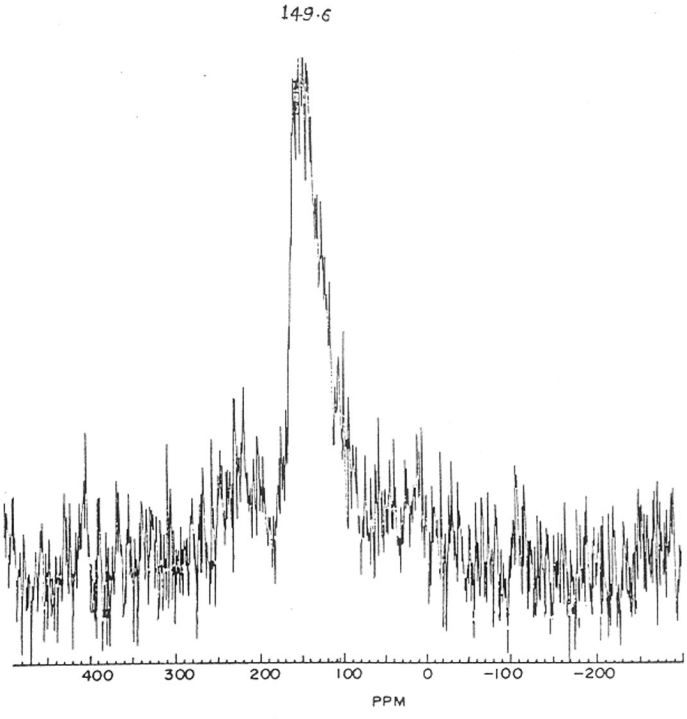

Fig. 3.31 : ^{71}Ga MAS NMR spectrum of Ga-Mordenite.

as there is no signal corresponding to any type of Al in the [Ga]-Mordenite. In the ^{71}Ga MAS NMR spectra of [Ga]-Mordenite shown in the fig.3.31, the characteristic signal of a tetrahedral Ga species[35] is seen as a single peak at 150 ppm. with no sign of any octahedral Ga.

3. 3 Conclusions :

In the hydrothermal synthesis of zeolite beta,the [Ga]- analog was obtained in the usual combination of polymorphs A and B whereas [Be]-analog formed enriched in thepolymorph B. But on leaching out of Ga and Be respectively from the framework by treatment with aqueous solutions of acid and ammonium florosilicate both of them become enriched in polymorph B.The Ga^{3+}cations were fairly stable in the framework of beta during calcination to remove template and NH_4^+-cations to obtain H^+-form whereas Be^{2+} cations completely came out of the framework during such treatment.However with controlled deberyllation of as-synthesized and Na^+-forms of the sample with $(NH_4)_2SiF_6$ solution,Be^{2+}cations remain in the framework until it was calcined to obtain H-beta.The Bronstead and Lewis acid sites both were observed on [Ga]-beta whereas only lewis acid sites were observed on [Be]-beta.The acid sites on [Ga]-beta were stronger than those on [Be]-beta.

A crystalline gallosilicate (SiO_2/Ga_2O_3 = 19.0,SiO_2/Al_2O_3 > 1000) with the framework structure of zeolite mordenite has been synthesized for the first time using tetraethylammonium bromide as a template. The Ga can be effectively removed from the same by acid leaching without affecting the crystallinity of the sample. Incorporation of Ga^{3+} ions into the lattice positions is confirmed by,

i) XRD (indicated by small lattice expansion),

ii) thermal analysis (shift of exothermic peak due to loss of occluded tetraethyl ammonium cations to lower temperature) and absence of exothermic peak in the degallated sample,

iii) FT.i.r. spectra of framework, surface hydroxyl groups and adsorbed D_2O, benzene and pyridine,

iv) ^{71}Ga MAS NMR spectra showing a single peak at 150 ppm,

v) SEM and adsorption results supporting the absence of amorphous matter both outside and inside the zeolite pore system of the gallo-mordenite and degallated mordenite.

On the basis of the above evidence, it is concluded that isomorphous substitution of Ga^{3+} for Al^{3+} in crystalline lattice of mordenite during synthesis has been demonstrated. However, on modification for further characterization by post-synthesis treatments, a part of the Ga^{3+} species migrate from the framework to non-framework positions.

REFERENCES :

1. Newsam, J.H., Treacy, M.M.S., Koetsier, W.T., and Gruyten, C.B., "Proc. Roy. Soc. Lond." **A 420** (1988) 373
2. Shen, J. P., Ma, J., Guo. J., Jinag, D.Zh. and Min, E.Ze., *Chinese chem. Lett.* **5** (12) (1994) 1075.
3. Perez-Pariente, Martins, J., Jacobs, P.H., *Appl-catal.* **31** (1987) 35.
4. Yang, C., and Xu, Gi, Zeolites, **19** (1997) 404.
5. Hegde, S. G., Abdulla, R.A., Bhat. R.N., and P.Ratnasamy., *Zeolites*, **12** (1992) 951.
6. Perez-Pariente, J., Sanaz, J., Forenes,V., and Corma,A., *J.catal.* **124** (1990) 217.
7. Romannikov, V. N., Chumachenko, L. S., Mastikhin, V. M., Ione, K. G., *J. Catal* **94** (1985) 508.
8. Han, S., Schmitt, K. D., Shihabi, D. S., and Chang, C. D., *J. chem. soc, chem. Comm.* (1993) 1287.
9. Chang, C. D., Chu. C. T. W., Mitale, J. N., Bridger, R. F. and Celverk, R. B., *J. Am. chem. Soc.*, **106** (1984) 8143.
10. Skeels, G. W., and Breck, D. W., in "Proce. Sixth Int. Zeolites conf"., ed. D.H. Olson and ABPSPO, Butter worth, survey (1984) 87.
11. Skeels and Flanigen, E. M., "ACS symp. Ser" **398** (1989) 420.
12. Lok, B. K., Cannan, T. R., and Massina, C. A., *Zeolites*, **3** (1983) 282.
13. Bond, A. E., Burgers, C. G. V., and Martin, D. E., U. S. patent No. 3799385 (1974) (assigned to BPPLL, U.K).
14. Olson, D. H., Kokatailo, G. T, Lawton, S. L. L., Meler, W. M.,*J.Phys. Chem.* **B5** (1981) 2238.
15. Hegde, S. G., Kumar, R., Bhat, R. N., and Ratnasamy, P., *Zeolites* **9** (1989) 23.

16. Simmons,D.K.,Szostak, R., Agarwal, P.K., and Thomas,T.L., *J.catal* .**106** (1987) 187.

17. Chu, C. T., and Chang, C. D., *J. Phys. Chem.* **89** (1985) 1569.

18. Szostak, R., and Thomas, T. L., *J. Catal.* **101** (1986) 549.

19. Wooley, G.L., Alemany, L. B., Dessau, R. M.,and Chester, A.W., *Zeolites*, **6**(1985) 14

20. Kustov, L. M., kazansky, V. B., and Ratnasamy, P., *Zeolites*, **7** (1987) 79.

21. Datka, J., *J. Chem. Soc. Faraday Trans.* **77** (1981) 511.

22. Coughan, B., Carroll, W., O'malley, P., and Nunen, J., *J. Chem. Soc., Faraday Trans,* **77** (1981) 1942.

23. Parry, E. P., *J. Catal.* **2** (1963) 371.

24. Mortera, C., and Cerrato, G., *Languimur,* **6** (1990)1810.

25. Everest, D. A., "The chemistry of Beryllium" Elsvier, Amsterdam, (1964).

26. Meier,W.M. *Z., Kristallogr.*, **115** (1961) 439.

27. Johnson,M.F.L., *J. Catal.*, **52** (1978) 425.

28. Kotasthane, A.N. and Shiralkar,V.P., *Thermochemica Acta*, **102** (1986) 37.

29. Breck,D.W., in *Zeolite Molecular Sieves, Structure Chemistry and Use* , New York : John Wiley and Sons, (1974) 320.

30. Pichat,P., Beaumont,R. and Barthomeuf,D., in : i) *Compt. Rendus. Sci. Acad. Sci C* : *Sci. Chim.*, **272** (1971) 612. ii) *J. Chem.Sco., Faraday Trans.I.* **70** (1974) 1402.

31. Tarte,P. *Spectrochim. Acta* **A 23** (1967) 2127.

32. Karge,H., *Z. Phys. Chem.*, **76** (1971) 133.

33. Eberly,P.E., Kimberlin,C.N. and Vaorheies, A., *J.Catal.*, **22** (1971) 419.

34. Engelhardt,G. and Michel,D. "High Resolution soild-state NMR of silicates and zeolites", John wiley, New York, (1987).

CHAPTER -4

m-XYLENE ISOMERIZATION OVER MODIFIED ZEOLITE BETA AND MORDENITE

CHAPTER IV

ISOMERIZATION OF META - XYLENE OVER MODIFIED BETA AND MORDENITE ZEOLITES.

4.1 INTRODUCTION :

The isomerization and disproportionation of m-xylene has long since been used as a tool to characterize the pore sizes of zeolites and to distinguish the medium pore zeolites from the large pore zeolites[1,2]. The shape and dimensions of the intracrystalline cavities in zeolites with ten- and twelve-membered rings is an important factor in determining the product selectivities in the conversion of m-xylene. The activity of zeolites in the isomerization and disproportionation of m-xylene also depends on their acidic strength. The nature of the metal ion (M = Al/Ga/B/Ti/ etc.) occupying the lattice position is an important factor that determines the acidity of the zeolites.

The rate of isomerization as well as the relative rate of disproportionation to that of isomerization was measured by Gnep[3,4]. The pore sizes of various medium pore zeolites were characterized using the para-/ortho-xylene (p-X/o-X) ratio[5]. Recent studies on m-xylene isomerization indicate that the test is useful in distinguishing medium pore zeolites but has limited application for characterization of large-pore zeolites[6,7]. The study of isomerization and disproportionation of m-xylene is of particular interest in establishing correlations between the intrinsic properties of zeolites, such as their pore structure, framework composition and relative acidity, with their catalytic activity and selectivity.

The isomerization of m-xylene over zeolites is accompanied by side-reactions such as disproportionation and demethylation. Relative to larger pore zeolites, the disproportionation reaction is greatly reduced over the medium pore ZSM-5. Moreover, ZSM-5 based catalysts

exhibit an enhanced selectivity for the formation of p-xylene (product shape selectivity). The preferential formation of p-xylene over the o-isomer is explained by the faster diffusion of the former through the pores of ZSM-5. The interconversion of xylenes takes place through 1,2-methyl shifts[2] as shown below :

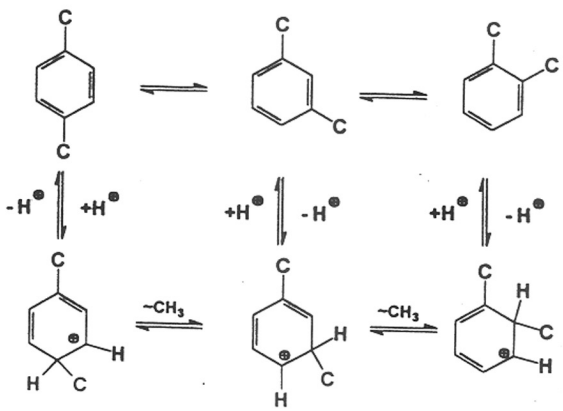

The selectivity for the disproportionation reaction relative to the isomerization reaction decreases with the decrease in the pore size of the zeolite, suggesting that the pore size of the zeolite is an important factor influencing selectivity[2].

In large pore zeolites the p-X/o-X ratio is always very close to the thermodynamic equilibrium value (1.0-1.4)[7]. The disproportionation of m-xylene is a bimolecular reaction which results in the formation of toluene and trimethylbenzenes, via 1,1-diphenylmethane type bulky transition states denoted as I, II and III which lead to the formation of 1,2,4 -, 1,3, 5- and 1, 2, 3-Trimethylbenzene (TMB)[8] , respectively as shown below :

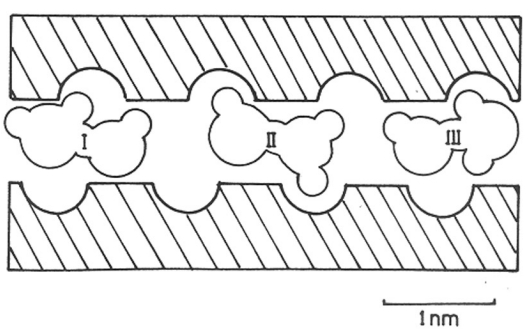

There are three important aspects of m-xylene isomerization which rank medium and large pore zeolites according to their pore openings and void space[9]. These parameters are :

i) The para-/ortho-xylene ratio which essentially ranks medium pore zeolites according to their product shape selectivity (PSS) properties.

ii) Isomerization/Disproportionation ratio which is based on the concept of restricted transition state shape selectivity (RTSS) and ranks zeolites according to their void space.

iii) 1, 3, 5-/1, 2, 4-trimethylbenzene ratio which distinguishes between medium and large pore zeolites.

During the present studies, m-xylene isomerization was used as a test reaction to characterize the relative acidities of the zeolites under investigation. The codes used for naming various samples have been listed in Table 4.1.

4.2 META-XYLENE ISOMERIZATION OVER MODIFIED BETA ZEOLITES:

4.2.1 Conversion of meta-xylene :

The effect of SiO_2/Ga_2O_3 and SiO_2/BeO (of the gallo- and beryllo-isomorphs of zeolite beta) on catalytic activity and selectivity in m-xylene isomerisation is shown in Tables 4.2 and 4.3. The activity (conversion of m-xylene) decreases with the increase in ratio. In the case of H-Ga-beta as the ratio increases from 17 to 113, conversion decreases from, 8.05 to 4.54. The degallated sample [DA-H-Ga-beta(110)] shows a further decrease (2.83%) due to extraction of Ga^{3+} cations from the lattice. A similar trend is also exhibited by the beryllo-isomorphs. The decrease in activity of the catalysts with decreasing Si/M ratio is due to the concomitant decrease in the number of Bronsted acid sites.

The results on the influence of reaction parameters like temperature and space velocity

Table 4 . 1 : Code-names used for various zeolite samples

Zeolite	Code – name*
Aluminum beta	H-Al-β (60)
Gallium beta	H-Ga-β(20)
	H-Ga-β (56)
	H-Ga-β(113)
Degallated beta	DAF-H-Ga-β(110)
[using $(NH_4)_2 SiF_6$]	
Beryllium beta	H-Be-β(28)
	H-Be-β(55)
	H-Be-β(115)
Deberyllated beta (Acid leaching)	DA-H-Be-β(15)
Deberyllated beta [using $(NH_4)_2 SiF_6$;	DF-H-Be-β(120)
starting with NH_4-Be-beta]	
Deberyllated beta [using $(NH_4)_2 SiF_6$;	DFK-H-Be-β(105)
starting with TEA-Be-beta]	
H-Al-Mordenite	H-Al-M(13)
H-Ga-Mordenite	H-Ga-M(19)
Degallated mordenite	DA-H-Ga-M(27)
(Acid leaching)	

* Numbers in brackets indicate silica/metal oxide ratios.

Table 4. 2 : Effect of SiO_2 / Ga_2O_3 on isomerization of m-xylene over gallo-isomorphs of zeolite beta.

Feed = m-xylene + H_2(1: 4 moles); WHSV=4 h^{-1}; Temp.= 523 K; TOS[a] = 4h.

Sample Code	H-Ga-β(20)	H-Ga-β(56)	H-Ga-β(113)	DA -H-Ga-β(110)
m-xylene conv. %	8.04	6.29	4.52	2.83
Products (Wt.%)				
Toluene	0.89	0.54	0.17	0.08
p-xylene	2.79	2.52	2.01	1.34
m-xylene	91.96	93.71	95.48	97.17
o-xylene	3.06	2.73	2.12	1.31
1, 3, 5-TMB[b]	0.38	0.13	0.07	0.03
1, 2, 4-TMB	0.85	0.37	0.15	0.07
1, 2, 3 - TMB	0.07	-	-	-
p-X/o-X	0.91	0.92	0.95	1.02
1, 3, 5-TMB/ 1, 2, 4-TMB	0.45	0.35	0.46	0.43
Disp/ Isom. Ratio[c]	0.2	0.08	0.05	0.03

a. TOS = Time on stream

b. TMB = Trimethylbenzene

c. Disp./Isom. = Σ TMB/p-X + o-X,(moles)

Table 4.3 : Effect of SiO_2/BeO on isomerization of m-xylene over H-[Be]-β(55) and deberyllated beta.

Feed = m-xylene + H_2 (1:4 moles); WSHV = $4h^{-1}$; TOS[a] = 4h.; Temp. = 623K

SiO_2 / BeO	H-Be-β (28)	H-Be-β (55)	H-Be-β (115)	DA-H-Be-β(115)	DF-H-Be-β (120)	DFK-H-Be-β (105)
m-xylene conv. %	4.69	2.84	2.89	1.64	1.94	2.12
Products (Wt.%)						
Toluene	0.12	0.10	0.11	0.04	0.04	0.06
p-xylene	2.00	1.16	1.15	0.72	0.87	0.97
m-xylene	95.31	91.16	97.11	98.36	98.06	97.88
o-xylene	2.42	1.42	1.51	0.83	0.97	1.02
1,3,5-TMB[b]	0.042	0.03	0.04	0.01	0.01	0.01
1, 2, 4-TMB	0.11	0.13	0.08	0.04	0.05	0.06
1, 2, 3-TMB	-	-	-	-	-	-
p-X/o-X	0.83	0.80	0.76	0.87	0.91	0.95
Disp/Isom[c].	0.05	0.05	0.04	0.03	0.028	0.030
1, 3,5-/1, 2,4-TMB	0.36	0.23	0.50	0.25	0.25	0.17

a. TOS=Time on stream

b. TMB=Trimethylbenzene

c. Disp./Isom.=ΣTMB/p-X + o-X(moles)

on the activity and selectivity are recorded in Tables 4.4 to 4.7. The temperature ranges were 498-598K for the gallo-isomorph H-Ga-beta(20) and 623-723K for the beryllo-isomorph [H-Be-beta(55)]. The space velocity (WHSV) values were varied in the range 4 to $15h^{-1}$ the case of H-Ga-beta-(20) and 4-$10h^{-1}$ in the case of H-Be-beta(55). These results indicate that conversion of m-xylene increases with increase in temperature. However, with an increase in WHSV the meta-xylene conversion decreases due to reduced contact time.

Table 4.8 depicts the effect of isomorphous substitution in zeolite beta. From the table it is seen that the gallo-isomorphs required higher temperatures (~ 498 K) as compared to the Al-analog (473 K) to attain similar m-xylene conversion levels. The beryllo-isomorph required still higher temperatures (648 K). In all the cases meta-xylene conversion decreased with time on stream.

4. 2. 2 para-Xylene/ortho-Xylene (p-X/o-X) ratio :

In the isomerization of m- xylene over 10-membered ring zeolites, p-xylene is formed preferentially due to its relatively faster diffusion through the zeolites pores. Earlier studies indicated that zeolite beta did not show shape-selectivity in the distribution of xylene isomers[8]. This is because of its large intracrystalline void space. The present studies on isomorphously substituted gallo-and beryllo-isomorphs also produced similar results.

From Tables 4.2 to 4.7 it is seen that the p-X/o-X ratio followed the thermodynamic equilibirium value (~1.0) closely. The p-X/o-X ratio is found to be independent of process conditions like temperature, WHSV and SiO_2/Ga_2O_3 or SiO_2/BeO ratios in conversions upto 25%. This tendency of following the thermodynamic equilibrium is characteristic for large pore zeolites and indicates the absence of diffusional constraints for xylenes in these isomorphs of zeolite beta. Variations in the p/o ratio between 0.8-1 are observed under the

Table 4 . 4 : Effect of temperature on m - xylene isomerization over H-Ga-β(20)

WHSV = 4 h^{-1}; TOS[a] = 4h; Feed = m-xylene + H_2(1:4 moles)

Temperature	498	523	548	573	598
m-xylene Conv. %	3.49	8.04	18.17	24.40	24.28
Products (Wt.%)					
Toluene	0.37	0.893	1.858	3.73	2.95
p-xylene	1.23	2.79	6.33	7.71	7.61
m-xylene	96.51	91.96	81.83	75.60	75.72
o-xylene	1.35	3.06	6.33	7.84	8.31
1, 3, 5-TMB[b]	0.16	0.38	1.01	1.42	1.37
1, 2, 4-TMB	0.30	0.85	2.34	3.32	3.58
1, 2, 3-TMB	0.07	0.07	0.31	0.38	0.46
Selectivity for isomerization[c]	0.74	0.73	0.69	0.63	0.65
p-X/o-X	0.91	0.91	1.00	0.98	0.92
Disp. / isom[d].	0.18	0.20	0.25	0.28	0.29
1, 3, 5-/1, 2, 4-TMB	0.53	0.45	0.43	0.43	0.38

a. TOS = Time on stream

b. TMB = Trimethylbenzene

c. Selectivity for Isomerization = p-X+o-X/m-xylene conv.

d. Disp./Isom. = ΣTMB/p-X+o-X (moles)

Table 4.5 : Effect of temperature on m-xylene isomerization over H-Be-β(55)

WHSV=4 h^{-1}; TOS[a] =4h; Feed = m-xylene + H_2 (1:4 moles); Temp = 623K

Temperature	623	648	673	698	723
m-xylene conv.%	2.84	5.27	9.53	16.63	27.27
Products (Wt.%)					
Toluene	0.10	0.13	0.24	0.35	0.06
p-xylene	1.16	2.83	4.49	8.10	13.36
m-xylene	97.16	94.73	90.47	83.37	72.73
O-xylene	1.42	2.17	4.49	7.61	13.01
1, 3, 5-TMB[b]	0.03	0.05	0.07	0.11	0.21
1, 2, 4-TMB	0.13	0.14	0.20	0.38	0.51
1, 2, 3-TMB	-	-	0.03	0.08	0.11
p-X/o-X	0.80	0.94	1.00	1.06	1.03
Disp / Isom[c].	0.050	0.031	0.029	0.027	0.028
1,3,5-/1,2,4-TMB	0.23	0.37	0.38	0.28	0.40

a. TOS = Time on stream

b. TMB = Trimethylbenzene

c. Disp./Isom. = Σ TMB/p-X + o-X,(moles)

Table 4 . 6 Effect of Space velocity on m-xylene isomerization over H-Ga-β(20)

Feed = m-xylene + H_2 (1: 4 moles); Temp. =573 K; TOS[a] = 4h.

WHSV (h^{-1})	4	8	15
m-xylene conversion	24.44	13.76	5.41
Product (Wt. %)			
Toluene	3.73	0.81	0.36
p–xylene	7.71	6.50	2.54
m–xylene	75.56	86.24	94.59
o–xylene	7.85	5.03	2.30
1, 3, 5–TMB[b]	1.42	0.46	0.09
1, 2, 4–TMB	3.33	0.88	0.1
1, 2, 3 – TMB	0.38	0.09	0.03
Selectivity for isomerization[c]	0.64	0.84	0.89
p-X/o-X	0.98	1.29	1.10
Disp./isom[d].	0.289	0.109	0.039

a. TOS = Time on stream

b. TMB = Trimethylbenzene

c. Selectivity for Isomerization = p-X+o-X/m-xylene conv.

d. Disp./Isom. = ΣTMB/p-X+o-X (moles)

Table 4.7 Effect of space velocity on m-xylene isomerization over H-Be-β (55)

Feed = m-xylene + H_2 (1: 4 moles) ; Temp. = 723K; TOS[a] = 4h

WHSV	4	6	8	10
m-xylene conv. %	27.27	12.97	8.22	7.50
Products (Wt.%)				
Benzene	0.01	0.01	0.01	0.01
Toluene	0.06	0.16	0.17	0.13
Ethyl benzene	-	0.01	0.01	0.01
p-xylene	13.36	6.40	3.86	3.60
m-xylene	72.73	87.03	91.78	92.50
O-xylene	13.01	6.01	3.93	3.58
1, 3, 5-TMB[b]	0.21	0.09	0.06	0.04
1, 2, 4-TMB	0.51	0.24	0.16	0.12
1, 2, 3-TMB	0.11	0.05	0.02	0.02
Selectivity for Isomerization[c]	0.97	0.97	0.95	0.96
p-X/o-X	1.03	1.06	0.98	1.00
Disp/Isom[d].	0.028	-	-	-

a. TOS = Time on stream

b. TMB = Trimethylbenzene

c. Selectivity for Isomerization = p-X+o-X/m-xylene conv.

d. Disp/Isom. = ΣTMB/p-X+o-X (moles)

Table 4 . 8 : Effect of Isomorphous substitution on m-xylene isomerization over beta zeolites

Feed = m-xylene + H_2 (1 : 4 moles); WSHV = h^{-1}; TOS[a] = 4h.

Zeolite	H-Al-β(28)	H-Ga-β(20)	H-Be-β(28)
Temperature	473 K	498 K	648 K
m-xylene Conv. %	5.60	3.47	5.27
Product (Wt.%)			
Toluene	0.60	0.37	0.13
p - xylene	2.30	1.23	2.30
m – xylene	94.40	96.53	94.73
o - xylene	2.20	1.35	2.52
1, 3, 5 - TMB[b]	0.10	0.16	0.02
1, 2, 4 - TMB	0.50	0.29	0.01
1, 2, 3 - TMB	-	0.06	-
Selectivity for isomerization[c]	0.80	0.74	0.95
p-X/o-X	1.05	0.91	0.91
Disp. / isom[d].	0.1	0.17	0.02
1, 3, 5-TMB / 1, 2, 4 –TMB	0.25	0.54	0.22

a. TOS = Time on stream

b. TMB = Trimethylbenzene

c. Selectivity for Isomerization = p-X+o-X/m-xylene conv.

d. Disp./Isom. = ΣTMB/p-X+o-X (moles)

specified reaction conditions (Table 4.2 - 4.7). However, since shape- selectivity for preferential formation of p-xylene is not expected in twelve-membered ring zeolites, it can be concluded that these variations are not caused by diffusion effects.

4. 2. 3 Disproportionation of m-Xylene :

In addition to isomerization, xylene molecules also undergo bimolecular disproportionation to toluene and trimethylbenzenes. It has been established earlier that in twelve-membered ring zeolites, disproportionation of m-xylene involves 1,1-diphenylmethane type transition states[10,11]. There are three possible transition states, leading to the formation of 1,2,4-; 1,3,5-; and 1,2,3-TMB. These diphenylmethane-type intermediate complexes are bulkier than both reactants and products. It has been suggested by Weisz[4] and Mavrodinova et al.[12,13] that the D/I selectivity in zeolites depends mainly on their intracrystalline void space. Besides pore size differences, several other explanations have been put forth to explain the differences in disproportionation/isomerization selectivity between large pore zeolites; and it has been established that disproportionation requires stronger acids sites than isomerization[6,14].

The present studies on m-xylene isomerization over isomorphously modified zeolites also indicate that D/I ratios are affected by the acidity of the zeolites. The following observations regarding disproportionation of m-xylene can be summarized from the data presented in this section :

i) Tables 4.2 and 4.3 indicate that disproportionation decreases as the SiO_2/Ga_2O_3 and SiO_2/ BeO ratios in the H-Ga-beta and H-Be-beta samples increase. This may be attributed to a decrease in the concentration of acid sites.

ii) It is also noticed that higher temperatures favour disproportionation in the case of H-[Ga]-beta zeolites. However, in the case of H-Be-beta (Table 4.5) it is seen that disproportionation decreases with increase in temperature even though the overall conversion increases. The reason for this behaviour is not clear. It could be that higher temperatures, Be^{2+} species get dislodged from the lattice and reduce the available void space. It is also known that Beryllium is very much less acidic than the gallium isomorph. Besides, as the beryllium-beta catalysts were not acidic enough, the D/I values are lower than over the Ga-isomorph (Tables 4.4 and 4.5).

iii) Table 4.6 indicates that in the case of H-[Ga]-beta (20), as the space velocity increases (from 4 to $15h^{-1}$) the disproportionation reaction decreases more than the isomerization reaction resulting in a decrease in the D/I ratio with WHSV. Apparently being a bimolecular reaction the disproportionation reaction is slower than the isomerization reaction and at high space velocities there is not sufficient time for the adsorbed molecules to interact.

iv) Table 4.8 demonstrates the effect of isomorphous substitution in beta zeolites on m-xylene conversion. Over H-[Al]-beta(28), the disproportionation reaction was less than over H-Ga-beta (20) even though one would expect a larger acidity in the former . The reason for the larger D/I ratio in H-[Ga]-beta could be the generation of strong lewis acid sites from the extra lattice Ga^{3+} species.

v) In fig. 4.1 the disproportionation / Isomerization ratios [D/I; equal to the molar ratio of trimethylbenzenes / (p-X + o-X)] are plotted as a function of time on stream. Unlike the isomerization of m-xylene, its disproportionation is controlled by the restricted transition state shape-selectivity (RTSS) exerted by the void space available around the active sites present in the zeolites. As seen in fig. 4.1, the D/I ratio increases with time on stream. The D/I values

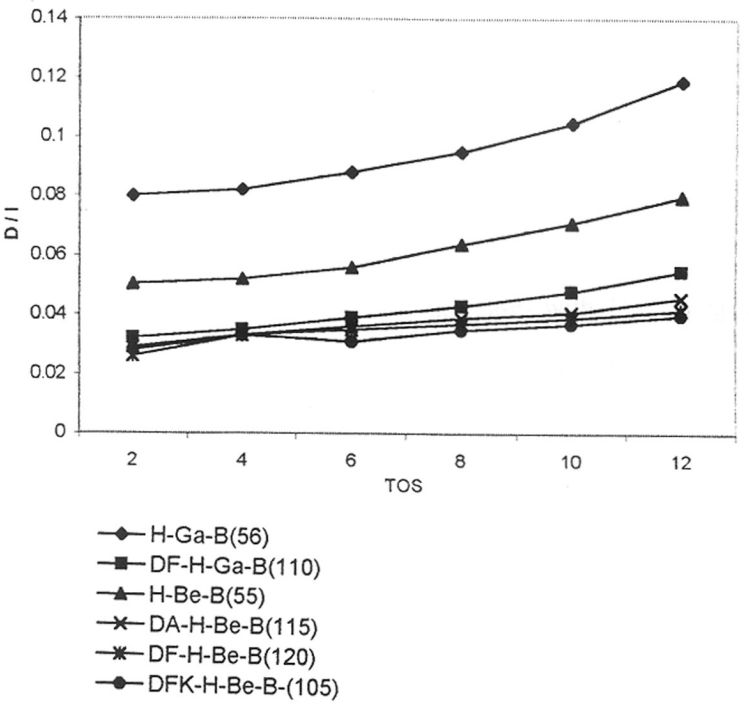

Fig. 4.1 : Effect of Time on Stream on Disproportionation/Isomerization ratio in m-xylene conversion over modified gallo and beryllo-isomorphs of beta at 523 and 623K respectively.
Feed= m-xylene + H_2 (1:4 moles), WHSV = $4h^{-1}$

increased from 0.085 to 0.15 (TOS = 2 to 12 hrs.) for the gallo-isomorph of beta while it was in the range 0.03 to 0.05 for the beryllo-isomorphs.

4. 2. 4: 1,3,5 - / 1,2,4-TMB ratio :

It has been demonstrated in section 4.1 that none of the three transition state complexes can be easily accomodated in the sinusoidal channels of zeolite beta. Nevertheless, among these three transition state complexes, the size of the complex required to produce the 1,2, 4-TMB isomer is smaller than that needed for 1,3,5 or 1,2,3-TMB.

Fig. 4.2 illustrates the influence of time on stream (TOS) on 1,3,5- / 1,2,4- TMB ratio over various isomorphs of zeolite beta. This ratio decreases with TOS, suggesting that pore size narrowing (pore blockage) may be taking place due to catalyst deactivation. Therefore the formation of bulky 1,3,5-TMB isomer is restricted due to spatial or diffusional constraints. The 1,3, 5- / 1,2,4- TMB ratio for the Ga-isomorphs broadly lie between 0.4 - 0.5, while those of the beryllo-isomorph are comparatively lower (0.2-0.3). This is due to the lower stability of Be^{2+} in lattice (most of the Be^{2+} species get dislodged during the calcination of the NH_4^+-form). This produces extra framework species which reduce the available void volume. The DA-H-Be-beta(115) sample exhibited much higher 1,3,5-/ 1,2,4- TMB ratio (0.4) in the initial stages of the run, as compared to the other modified Be-analogs.

4 . 3 m-Xylene isomerization over modified mordenties :

The isomerization and disproportionation of m-xylene has been carried out over the gallo-mordenite isomorph obtained by direct synthesis and the degallated sample. The results are compared with the Al-analog. The results are also compared with those of the isomorphously substituted beta zeolites already discussed in section 4.3.

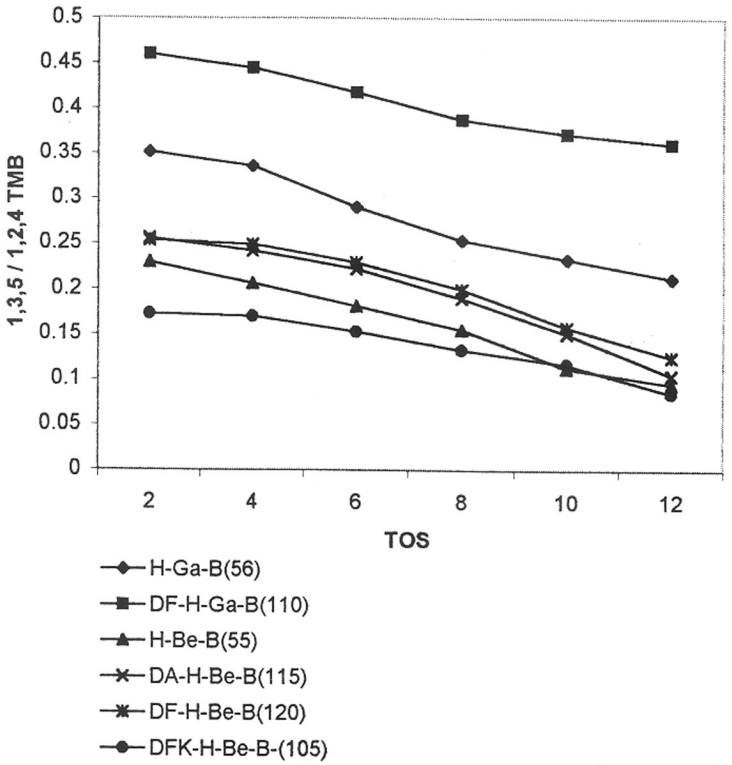

Fig. 4.2 : Effect of Time on Stream on 1,3,5-/1,2,4–TMB ratio in m-xylene conversion over modified gallo- and beryllo-isomorphs of beta at 523 and 623K respectively.
Feed = m-xylene + H_2 (1:4 moles), WHSV = $4h^{-1}$

4. 3.1 m-xylene conversion and p-xylene / o-xylene ratio :

Tables 4.9 and 4.10 illustrate the effect of temperature over H-Al-M(13.3) and H-Ga-M(19) respectively. The temperature range in the case of H-Al-M (13.3) was 433-473 K while in the case of H-Ga-M(19), the temperature range was 493-593 K. As seen in these tables. H-Ga-M(19) required a higher temperature to attain conversion levels comparable to H-Al-M(13.3).

The data presented in these two tables also illustrate that the p-xylene/o-xylene ratio tends to follow the thermodynamic equilibrium at higher temperatures, while at lower temperatures, p/o selectivity in isomerization is significantly lower.

4. 3. 2 Disproportionation of m-xylene :

The results of disproportionation of m-xylene are presented in fig. 4.3. Table 4.9 reveals that D/I ratio of H-Al-M(13.3) is 0.12 (at a m-xylene conversion of 30.68% at 473K), while on the H-Ga-M(19) sample, this ratio is 0.25 (corresponding to m-xylene conversion = 38.35 % at 573K; Table 4.10), which suggests a greater disproportionation reaction over H-Ga-M(19). When compared to the isomorphously substituted beta-zeolites, the analogous isomorphs of mordenite catalyzed the disproportionatoin reaction to a greater extent. This is attributed to the greater acidity of mordenite.

Fig. 4.3 demonstrates the effect of time on stream on the disproportionation activity of H-Al-M(13.3), H-Ga-M(19) and DA-H-Ga-M(27). The disproportionation is found to increase with TOS. The relatively higher disproportionation in the gallo-mordenites is attributed to the lower stability of the Ga^{3+} species in the lattice which results in partial migration of the Ga^{3+} ions from the lattice to non-lattice positions giving rise to additional Lewis acidity. The relatively lower acidity of the degallated sample DA-H-Ga-M(27) compared to the parent H-

Table 4.9 : Isometization of m-xylene over H-Al-mordenite(13.3)

WHSV = 3.5 h^{-1}; TOS[a] = 4h; Feed = m-xylene + H_2 (1: 4 moles)

Temperature (K)	433	453	473
m-xylene Conv. %	3.50	13.20	30.68
Products (Wt.%)			
Toluene	0.30	1.10	2.00
p-xylene	1.20	5.10	12.50
m-xylene	96.50	86.80	69.32
o-xylene-	1.80	5.70	12.80
1, 3, 5-TMB[b]	-	0.10	0.50
1, 2, 4-TMB	0.20	1.10	1.90
1, 2, 3-TMB	-	0.10	0.98
p-x/o-x	0.66	0.89	0.98
Disp. / isomerization[c]	0.06	0.11	0.12
1, 3, 5-/1, 2, 4-TMB	-	0.09	0.26

a. TOS = Time on stream

b. TMB = Trimethylbenzene

c. Disp./Isom. = Σ TMB/p-X + o-X,(moles)

Table 4.10 : Isomerization of m-xylene over H-Ga-mordenite (19.0)

WHSV = $3.5h^{-1}$; TOS[a] = 4h; Feed = m-xylene + H_2 (1:4 moles)

Temperature(K)	493	513	533	553	573	593
m-xylene conv.%	1.61	5.58	14.68	16.91	38.35	53.27
Products (Wt.%)						
Toluene	0.64	0.88	1.53	3.07	5.99	9.59
p-xylene	0.53	1.35	4.84	4.98	12.66	15.51
m-xylene	98.39	94.42	85.32	83.09	61.65	46.73
O-xylene	-	2.43	6.16	5.88	12.14	14.49
1, 3, 5-TMB[b]	0.05	0.06	0.10	0.22	1.41	2.92
1, 2, 4-TMB	0.39	0.85	2.03	2.27	0.507	8.49
1, 2, 3-TMB	0.02	0.01	0.02	0.04	0.62	1.12
p-X/o-X	-	0.55	0.79	1.04	1.07	0.70
Disp / Isom[c].	0.76	0.21	0.17	0.20	0.25	0.37
1,3,5-/1,2,4-TMB	0.13	0.07	0.05	0.09	0.23	0.34

a. TOS = Time on stream

b. TMB = Trimethylbenzene

c. Disp./Isom. = Σ TMB/p-X + o-X,(moles)

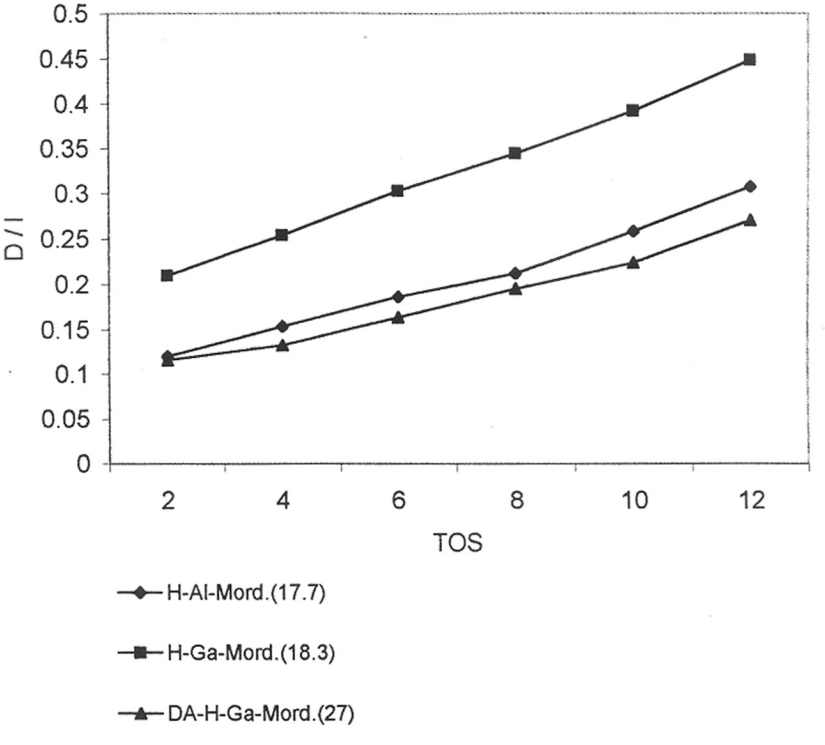

Fig. 4.3 : Effect of Time on Stream on D/I ratio in m-xylene conversion over alumino- and gallo-mordenites at 473 and 513K respectively.
Feed = m-xylene + H_2O (1:4 moles), WHSV = $3.5h^{-1}$

Ga-M(19) acounts for its lower disproportionation activity.

4. 3. 3: 1, 3, 5-/1, 2, 4-Trimethylbenzene (TMB) ratio :

Mordenite is a large pore zeolite like beta; nevertheless, differences in the m-xylene iomerization and disproportionation are observed between the two zeolites. The 12-MR pores of mordenite are criss-crossed with smaller 8-membered ring channels. The opening to the side channels alternate on both sides of the main channel and therefore it is difficult to locate all the methyl groups of the transition state complexes I and II (see section 4.1) in the side pockets[15]. In the case of beta, this sterical hinderance is less pronounced.

This feature is clearly reflected in fig. 4.4. The 1,3,5- / 1,2,4- TMB ratio values for H-Ga-beta(56) and DA-H-Ga-beta(110) are aproximately 17-20 % higher (in the initial stages of the run) then those obtained for H-Ga-M(19) and DA-H-Ga-M(27). Fig. 4.4 illustrates the effect of time on stream on the 1,3,5- / 1,2 4- TMB ratio. The values of this parameter are in the range of 0.26-0.18 for H-Al-M(13.3) and 0.07-0.06 for H-Ga-M(19). The lower value for the latter sample may be due to constraints imposed by extra framework Ga^{3+} speices. The extraction of Ga^{3+} from the framework decreases the crystallinity of the sample and causes pore blockages, which prevents the diffusion of 1,3,5-TMB besides decreasing the void space. The data obtained for DA-H-Ga-M(27) provides additional evidence in support of this conclusion. In the degallated sample, the exclusion of the extra framework Ga^{3+} species relaxes the diffusional constraint and also increases the void space to some extent and hence the values of 1,3,5-/1,2,4-TMB ratio (0.08-0.07) obtained are more than the values obtained for H-Ga-M(19).

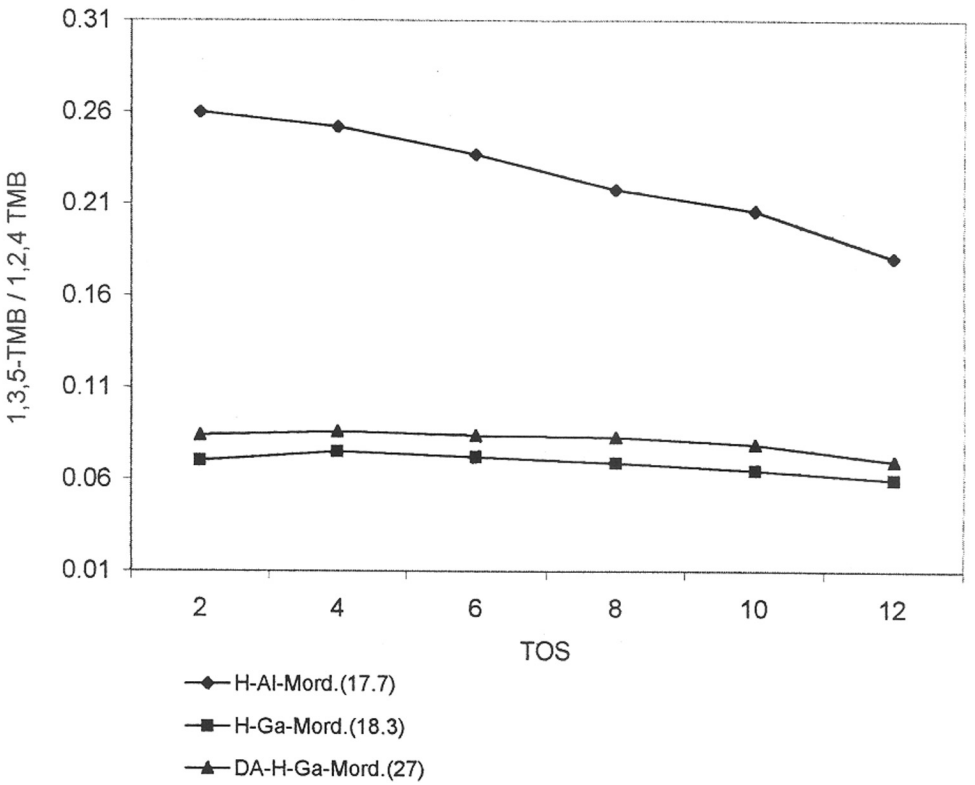

Fig. 4.4 : Effect of Time on Stream on 1,3,5-/1,2,4-TMB ratio in m-xylene conversion over alumino- and gallo-mordenites at 473 and 513K
Feed = m-xylene + H_2 (1:4 moles), WHSV=3.5h^{-1}

4.4 CONCLUSIONS :

The evaluation of the results of m-xylene isomerization studies in the present investigation indicates that subtle differences in the reaction are noticed depending upon the acidity and intracrystalline void space of zeolites. The disproportionation/isomerization (D/I) ratio in the conversion of m-xylene follows the order : H-Ga-M > DA-H-Ga-M > H-Al-M > H-Ga-β > H-Be-β > DF-H-Ga-β > DA-H-Be-β > DF-H-Be-β > DFK-H-Be-β. This order is more or less in agreement with the acidity trend exhibited by these zeolites. The 1,3,5-/1,2,4-TMB ratio which is used as a parameter to distinguish between medium and large pore zeolites, could be used in the present investigations to evaluate qualitatively the approximate intracrystalline void space. The results suggest the presence of extraneous materials (amorphous oxides) or extraframework species imposing diffusional constraints in varying degrees.

REFERENCES :

1. Csicsery, S. M., *J. Catal.*, **108** (1987) 433.
2. Olson, D. H., and Haag, W. O., in "Catalytic Materials : Relationship between structure and reactivity ". ACS. Synp. Ser. No. **248** (1984) 275.
3. Gnep, N. S., Tejada, J., and Guisnet, M., *Bull. Soc. Chin. Fr.*, **1** (1982) 5.
4. Dewing, J., *J. Mol. Catal.*, **27** (1984) 25.
5. Weisz, P. B., *Pure and Appl. Chem.*, **52** (1980) 2091.
6. Martens, J. A., Perez-Pariente, J., Sastre, E., et al. *Appl. Catal* , **45** (1988) 85.
7. Kumar, R., Rao, G. N., and Ratnasamy, P., *Stud. Surf. Sci. Catal.*, **49B** (1989) 1141.
8. Perez-Pariente, J., Sastre, E., Fornes, V., et al. *Appl. Catal.*, **69** (1991) 130.
9. Bhat, R. N., "Ph.D Thesis", University of Pune, (1991) 128.
10. Pines, H., and Arrigo, T., *J. Amer. Chem. Soc.*, **80** (1958) 4369.
11. Santilli, D. S., *J. Catal.*, **99** (1986) 327.
12. Mavrodinova, V., Penchev, V., et al. *Zeolites,* **9** (1989) 197.
13. Mavrodinova, V., Penchev, V., et al. *Zeolites*, **9** (1989) 203.
14. Jagannathan, K, Srinivasan, A., and Rao C. N. R., *J. Catal.,* **69** (1981) 418.
15. Meier, W. M., and Olson, D. H., "Atlas of Zeolite Structure Types, Structure Commision IZA", Polycrystal Book Service. Pittsburgh, (1978).

CHAPTER -5

ALKYLATION OF BENZENE WITH LONG CHAIN OLEFINS OVER MODIFIED LARGE PORE ZEOLITES

CHAPTER - V

ALKYLATION OF BENZENE WITH LONG CHAIN OLEFINS OVER MODIFIED LARGE PORE ZEOLITES

5.1 INTRODUCTION :

High silica large pore zeolites have been recognized as important catalysts in many industrial hydrocarbon processes. In fact, H-mordenite is being used in the isomerization of meta-xylene. Shape selectivity is one of the unique properties of medium and small pore zeolites, since these zeolites have pore dimensions similar to the kinetic diameters of simple organic molecules. Large pore zeolites, however, make it possible to carry out reactions involving bigger molecules, which cannot enter the pores in small or medium pore zeolites.

Zeolites make excellent catalysts for alkylation reactions, due to their exceptionally strong acidities. Commercial alkylation processes are generally based on acid catalysts[1-4]. The catalysts are acidic halides, proton acids, supported acids, etc. Due to the hazardous and corrosive nature of these conventional catalysts (eg. : $AlCl_3$, anhydrous HF, supported H_3PO_4, etc.) which cause severe environmental damage, the replacement of these catalysts by zeolites is a welcome change. A number of zeolite based catalysts for the alkylation of benzene are now in practice[5,6]. A new process that uses a solid acid catalyst for the manufacture of linear alkybenzenes (LAB) by the alkylation of benzene with linear olefins has recently been commercialized by UOP[7] . The new process replaces the conventionally used anhydrous HF as the catalyst. A typical industrial alkylation reaction using a zeolite is the production of ethyl benzene by the Mobil-Badger process using ZSM-5. However, other industrially important alkylation reactions like the manufacture of cumene[8] and linear alkyl benzenes[9] (LAB) from long chain olefins and benzene were till recently based on conventional catalysts

like solid phosphoric acid (SPC) and anhydrous HF respectively. Alkylation of benzene with long chain olefins (generally C_{10}-C_{13} olefins) leads to alkyl benzenes which on sulfonation produce surface active sulfonates.

This chapter presents the results of the studies on the catalytic properties of gallium and beryllium isomorphs of zeolite beta (prepared by direct synthesis) and that of Be-beta modified by post synthesis. Their activities have been compared with the aluminum analog. Similarly, the catalytic activity of Ga-mordenite has also been compared with its Al-analog. The alkylation reaction has also been carried out over a number of medium pore zeolites to compare their shape selectivity characteristics with those of the large pore zeolites. For comparison, the reaction has also been carried out over an amorphous SiO_2-Al_2O_3 catalyst.

5 . 2 MATERIALS AND METHODS :

Information regarding the reactants (feeds) used in the various experiments is compiled in Tables 5.1 and 5.2 . Besides, a number of zeolites and molecular sieves were used in these studies and their source and properties are presented in Table 5.3 . The details regarding the various procedures adopted in synthesis and modifications of the zeolites have already been discussed in section 2.2 of chapter II .

The details of the experimental set-up for the alkylation reactions have also been described in section 2.4 of the same chapter. The various reaction parameters used in the different experiments and the data obtained are discussed in the following sections.

5 . 3 RESULTS AND DISCUSSIONS :

Alkylation reactions are catalyzed by acids. The alkylation of aromatic rings is essentially an electrophilic substitution reaction and alkyl halides (Friedel-Craft) are generally used as catalysts . The mechanism of alkylation by Friedel-Crafts catalysts can be explained

Table 5.1 : Reactants used, their source and purity .

Feed	Source	Purity	Nature of impurities
Benzene	Loba Chemie, India	>99.9 % (AR)	-
1 - hexene	Aldrich Chem. Co USA	99 +%	hexane and its double bond isomers
1 - dodecene	Aldrich Chem. Co USA	95 %	dodecane and its double bond isomers
Linear Long chains Olefins (C_{10} - C_{13}) Olefins, Commercial alkylation (Feed).	Reliance Industries Ltd., Patalganga, India.	8.3 wt. % of Olefins	91.7 % of Paraffins

NOTE : The pure olefins and the olefin mixture were dried over silica-gel, while benzene was dried over molecular sieve - 4A prior to use.

Table 5 . 2 : Composition of mixed olefin feed.

Composition (wt. %)		
Carbon Fraction	Paraffins	Olefins
C_{10}	21 . 3	1 . 9
C_{11}	33 . 8	3 . 1
C_{12}	24 . 8	2 . 6
C_{13}	7 . 9	0 . 7

Table 5 . 3 : Characteristics of the zeolites used.

Zeolite	SiO_2 / Al_2O_3	Surface area (m^2/g) Zeolite	Non - Zeolite	Pore - System	Source
H-Y[1]	6 . 2	530	1.20	3-D; 0.74 nm openings 1.3 nm cages	Linde, USA
RE-Y[2]	5 . 1	775	37	- do -	PQ - Zeolites, Holland; RE exchanged
DAI-Y	10 . 4	644	5	- do -	Linde, USA Dealuminated
H-M (1)[3a]	17 . 7	598	1	1-D; 0.67 x 0.7 nm	Norton, USA
H-M (2)[3b]	43 . 9	568	66	- do -	Dealuminated
H-M (3)[3b]	99 . 2	538	85	- do -	- do -
H-Ga-M[4a]	18 . 3	456	88	- do -	Synthesized
H-β	35 . 0	500	191	3-D; 0.75 nm and 0.55 nm	PQ - Zeolites, Holland
H-Ga-β[4b]	56 . 0	351	109	- do -	Synthesized
H-Be-β[5]	28 . 6	384	173	- do -	Synthesized
DFK-H-Be-β[6]	105	317	192	- do -	Prepared
H-Eu-1	40 . 0	432	64	1-D; 0.58 x 0.41 nm (side pockets: 0.68 x 0.58 x 0.81 nm)	Synthesized
H-K–L[7]	6 . 1	350	3	1-D; 0.71 nm	Linde, USA
H-ZSM-12	111 . 5	342	55	1-D; 0.57 x 0.6nm	Synthesized
H-ZSM-5	39 . 4	413	7	2-D; 0.54 x 0.56 nm and 0.51 x 0.55 nm	United Catalyst India Ltd., India
Si–Al[8]	11 . 4		437	Av. Dia. ~ 2.7 nm	Prepared

* : Includes contribution from the external surface of zeolite crystallites and amorphous material.

1 : US-Y sample
2 : 70 % RE-exchanged from NH_4^+ - form; calcined to obtain H-form
3 : a) H-mordenite, b) Dealuminated mordenites.
4 : a) Gallium isomorph of mordenite b) Gallium-isomorph of beta
5 : Beryllium isomorph of beta
6 : Deberyllated isomorph of beta
7 : Exchanged with NH_4NO_3 to convert to H-form (50 % exchange)
8 : Amorphous SiO_2 -Al_2O_3

as follows. Alkylation is induced by the interaction of the acidic catalyst with the alkylating agents, leading to a highly polarized complex containing a carbocation[10].

$$RCH = CH_2 + HX + AlX_3 \rightleftharpoons [\, RC^+H - CH_3 \,]\,[\, AlX_4 \,]^-$$

The carbocation then attacks the aromatic substrate, forming an intermediate, which is transformed into the product by the loss of a proton.

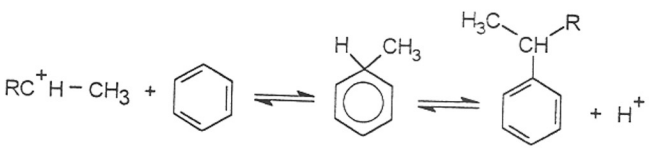

In case of olefins, a proton donor is needed for the formation of the carbocation under the acidic conditions used.

Zeolites are excellent alkylation catalysts because of the high strength of the proton acidity[11], hence they are used for the alkylation of aromatics with alcohols, olefins, etc. The mechanism of alkylation over zeolites is presented below.

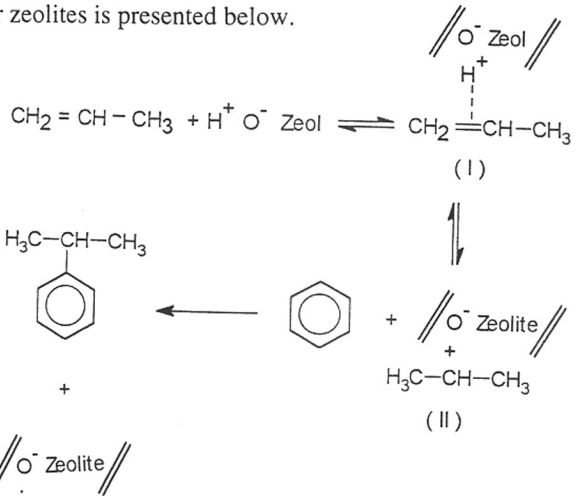

According to Venuto et. al.[12], the mechanism for alkylation involves the formation of

intermediate (I) which produces a secondary carbocation (II). This carbocation interacts with benzene to give cumene (in the example given above). Thus, with respect to olefins, the net reaction is the addition of the hydrogen of the aromatic hydrocarbon to the double bond (- C = C -) of the olefin .

5 . 3 . 1 Alkylation with 1-hexene over modified beta zeolites :

5. 3. 1.1 Product distribution:

The isomorphous substitution of Al by Ga and Be in the frame work of zeolite beta has already been demonstrated in Chapter (III).

The alkylation of benzene with 1-hexene leads to various products, whose composition change with time on stream, nature of the catalyst used, temperature, etc. The various products observed are :

i) saturated paraffins, namely n-hexane and its isomers, viz., 2-methyl pentane and 3- methyl pentane.

ii) i - hexenes, resulting from skeletal isomerization of the (- C = C -) bond of 1-hexene.

iii) alkylbenzenes with side chains less than C_6 resulting from the cracking of hexylbenzenes, or the alkylation of benzenes with the lighter cracked olefins (C_2 -C_4), accompanied by small concentrations of other heavier products.

iv) and, the n- and i-products of 2-hexylbenzene and 3-hexylbenzene. In general the concentration of the n-isomers is much greater than the iso-counterparts.

5. 3. 1. 2 Effect of SiO_2 / Al_2O_3 ratio :

The influence of the SiO_2 / Al_2O_3 ratio of H-beta catalyst on the product distribution is shown in the Table 5.4. The conversion of 1-hexene in all the cases under the conditions of the experiments was more than 99 % and independent of the SiO_2 / Al_2O_3 ratios.

Table 5 . 4 : Effect of SiO_2/Al_2O_3 ratio over H-Al-beta zeolites in the alkylation of benzene with 1- hexene.

Temp. = 413 K ; benzene/olefin mole ratio = 10 ; space velocity = 4 h^{-1} ; Time on stream = 4 h

Products (Wt. %)	H - Al - β (25)*	H – Al - β (35)*	H – Al - β (60)*
C_6 Compounds[a]	47 . 05	50 . 53	62 . 30
$<C_6$ Fraction[b]	15 . 32	12 . 56	5 . 19
Others[c]	2 . 08	2 . 10	1 . 16
i - 2 – hexylbenzene	3 . 52	3 . 15	1 . 76
2 – hexylbenzene	17 . 86	17 . 83	17 .14
i - 3 – hexylbenzene	2 . 35	2 . 03	1 . 18
3 – hexylbenzene	11 . 82	11 . 80	11 . 27
(2 ϕ / 3 ϕ)[d]	1 . 51	1 . 51	1 . 52
Total hexylbenzenes (%)	35 . 55	34 . 81	31 . 35
1- hexene conversion (%)	100	100	100

*. Numbers in brackets indicate SiO_2/Al_2O_3 ratios.

a . Isohexenes, n-hexane and isohexanes .

b . Cracked products; C_1 -C_5.

c . < C_6-alkylbenzenes and > C_6-alkylbenzenes.

d . The ratio of 2- hexylbenzene/3- hexylbenzene.

It is observed (Table 5.4) that with the increase in SiO_2/Al_2O_3 ratio from 25 to 60, the composition of the product also undergoes changes. Elimination of some of the acid sites in the H-beta (SiO_2/Al_2O_3 = 60) suppresses the formation of cracked products and enhances the yield of isomeric products. The decrease in SiO_2 / Al_2O_3 ratio decreases the total yield of phenyl hexanes (hexylbenzenes) to a small extent. This decrease in yield is mainly due to the decrease in the yield of the iso-hexylbenzenes. The 2-ϕ/3-ϕ ratio is also not influenced by the changes in SiO_2/Al_2O_3 ratio.

5. 3. 1. 3 Effect of temperature :

The influence of temperature was studied on the sample with an intermediate SiO_2 / Al_2O_3 ratio of 35. Temperature has a marked effect on the product distribution (Table 5.5). The conversion of 1-hexene was 100 % at all the three temperatures. At lower temperatures isomerization of 1-hexene to form iso-olefins was more pronounced while higher temperatures resulted in the formation of cracked products. The yield of the C_6 compounds decreased from 50.53% at 413 K to 16.67 at 453 K while the cracked products (< C_6 Fraction) increased from 12.56 (at 413 K) to 34.19 at 453 K.

The iso-hexylbenzenes increased with the increasing temperature especially in the case of the 2-ϕ isomer. The 2-ϕ/3-ϕ ratio increased with increasing temperature due to the greater amount of the 2-ϕ component present in the product. The increase in the 2-ϕ isomer yield at high temperatures is expected from thermodynamic considerations. The overall yield of the hexylbenzenes increases with temperature (34.81 at 413 K and 42.66 at 433 K) though the increase is less pronounced at 453K. It appears that the yield will decrease at still higher temperatures. These observations are again as expected from thermodynamic.

Table 5 . 5 : Effect of Temperature on the alkylation of benzene with 1-hexene over H-Al-beta (35).

SiO_2 /Al_2O_3 = 35; benzene /1-hexene mole ratio = 10; space velocity = 4 h^{-1}; Time on stream = 4 h

Product Distribution (Wt.%)	413 K	433 K	453 K
C_6 Compounds[a]	50 . 53	35 . 86	16 . 67
< C_6 Fraction[b]	12 . 56	18 . 95	34 .19
Others[c]	2 . 10	2 . 56	6 . 46
i - 2 hexylbenzene	3 . 15	5 . 12	5 . 17
2 – hexylbenzene	17 . 83	25 . 18	27 . 35
i - 3 hexylbenzene	2 . 03	2 . 93	2 . 76
3 – hexylbenzene	11 . 80	9 . 40	7 . 38
2ϕ / 3ϕ[d]	1 . 51	2 . 67	3 . 71
Total C_6 hexylbenzenes (%)	34 . 81	42 . 63	42 . 66
1- hexene conversion (%)	100	100	100

a . Isohexenes, n-hexane and iso-hexanes .

b. Cracked products; C_1-C_5.

c. < C_6-alkylbenzenes and > C_6-alkylbenzenes.

d. The ratio of 2-hexylbenzene/3-hexylbenzene.

5. 3. 1. 4 Effect of isomorphous substitution :

Table 5.6 compares the catalytic activity for H-Al-beta, H-Ga-beta, H-Be-beta and modified H-Be-beta zeolites.

The conversion of 1-hexene is 100 % over the H-Al-beta and decreases in the order : H-Al-beta > H-Ga-beta > H-Be-beta > modified H-Be-beta. It is noticed (Fig. 5.1) that the yield of hexyl benzenes in most over Ga-beta. It is also observed that the C_6 fraction is the least on Ga-beta due to maximum transformation into alkylbenzenes. The cracked products are higher over Al-beta suggesting it to be the most acidic of all the isomorphs. Apparently, Ga-beta possesses the optimum acidity to alkylate 1-hexene without cracking it or transforming it into saturates through H_2 transfer mechanisms.

Another reason for the greater shape-selectivity of the isomorphs could be their weak acidities leading to slow transformation of the 2-hexylbenzenes (or C_2 cation) formed initially into 3-hexylbenzenes (or C_3 cation). Interestingly, it is also noticed that there is hardly any skeletal isomerized products (i - hexylbenzenes) over the isomorphs.

However, an interesting feature of these catalytic studies is the alkylation reaction over modified H-Be-beta. When the reaction was carried out over the modified Be-isomorph, the change in the shape selectivity ($2\phi/3\phi$) with time on stream (TOS) (Fig 5.2) is much smaller than that observed over H-Be-beta (Table 5.3). Activity loss is also significantly less for modified Be-beta than for H-Be-beta.

5. 3. 1. 5 Effect of time on stream :

The activity of the H-Al-beta, H-Ga-beta, H-Be-beta and modified H-Be-beta catalysts was tested upto 10 hrs. The results are presented in fig. 5.3-5.6. The variation in the composition of the products arising out of isomorphous substitution has already been

Table 5 . 6 : Effect of isomorphous substitution in the alkylation of benzene with 1-hexene.

Temp. = 413 K , benzene/1-hexene mole ratio = 10; space velocity = 4 h^{-1};

Time on stream = 4 h.

Zeolite	H-Al-β	H-Ga-β	H-Be-β	H-Be-β (modified)
SiO_2 / M_2O_3* or MO^+	35*	56*	55*	105*
1- hexene conversion (%)	100	94 . 80	86 . 32	75 . 16
Product Distribution (wt%)				
C_6 Compounds[a]:	50 . 53	39 . 83	58 . 61	69 . 16
< C_6 – Fraction[b]	12 . 56	0 . 21	0 . 03	-
Others[c]	2 . 10	0 . 97	0 . 38	-
i - 2 hexylbenzene	3 . 15	-	-	-
2 - hexylbenzene	17 . 83	41 . 05	29 . 53	22 . 00
i - 3 hexylbenzene	2 . 03	-	-	-
3 – hexylbenzene	11 . 80	17 . 94	11 . 45	8 . 84
2 ϕ / 3 ϕ [d]	1 . 51	2 . 28	2 . 58	2 . 49
% Total C_6 – hexylbenzene	34 . 81	58 . 99	40 . 98	30 . 84

NOTE :

* $M_2O_3 = Al_2O_3/Ga_2O_3$,

+ MO = BeO

a . Isohexenes, 1-hexane and isohexanes .

b. Cracked products; C_1-C_5.

c. < C_6-alkylbenzenes and > C_6-alkylbenzenes.

d. The ratio of 2- hexylbenzene/3- hexylbenzene.

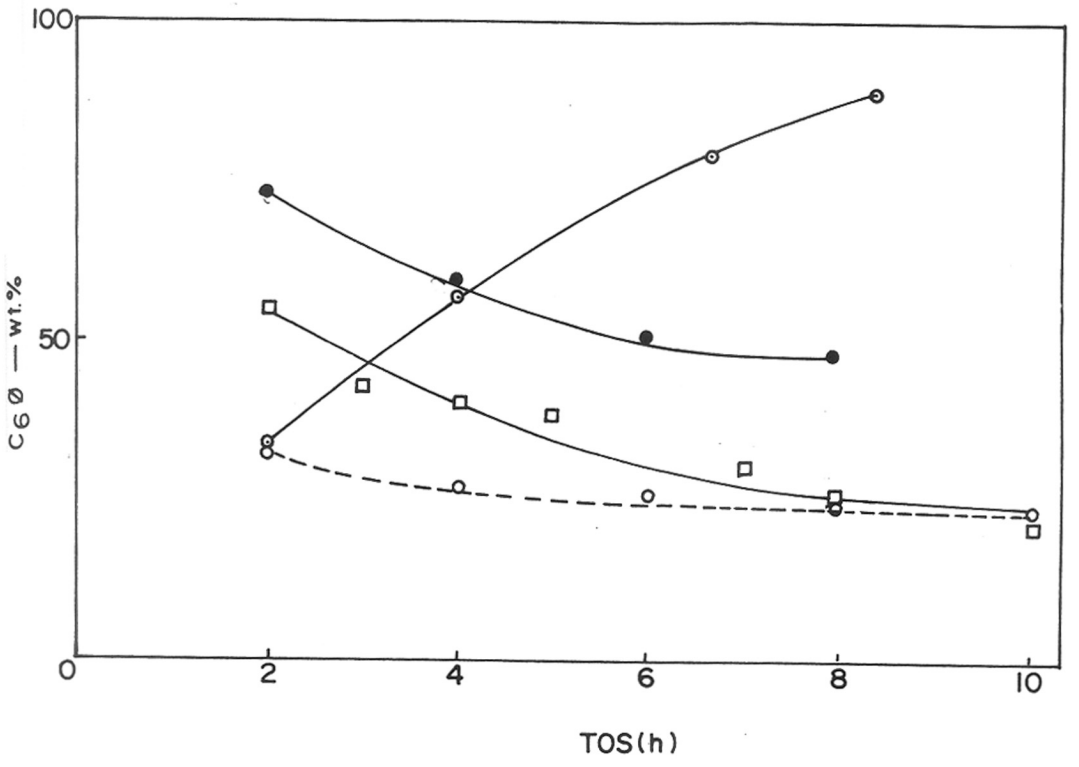

Fig. 5.1 : Effect of Time on Stream on the formation of C_6-phenylhexenes over different isomorphs of zeolite beta.
Benzene/1-hexene mole ratio=10. WHSV= $4h^{-1}$, Temp.=413K;
(⊙) H-Al-beta(35) ; (●) H-Ga-beta(56); (□) H-Be-beta(55) ;
(O) Deberyllated -Be-beta[DFK-H-Be-beta(105)].

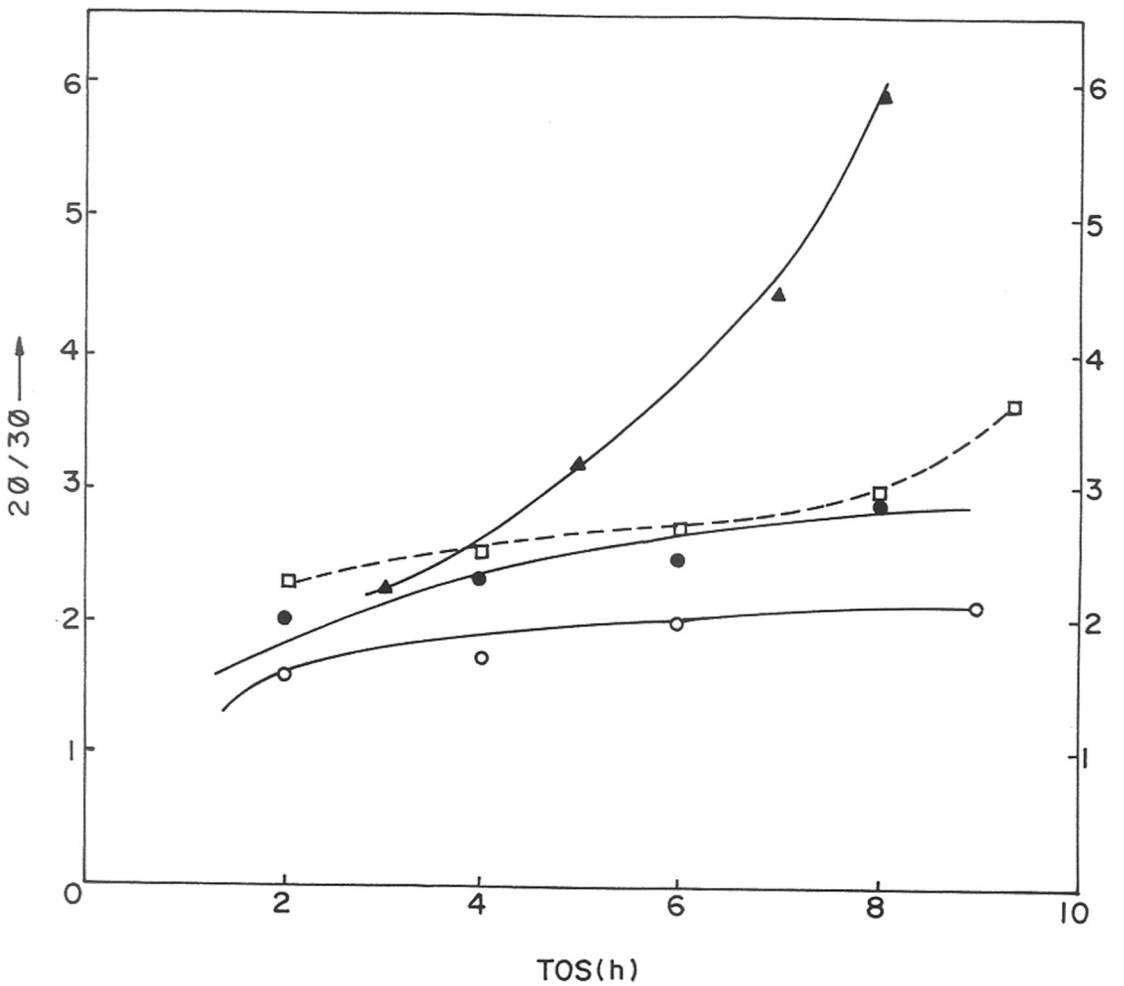

Fig. 5.2 : Effect of Time on Stream on shape-selectivity in the Alkylation of Benzene With 1-hexene over various isomorphs of H-beta.
Benzene/1-hexene mole ratio = 10. ;WHSV = $4h^{-1}$, Temp. = 413K;
(⊙) H-Al-beta(35) ; (●) H-Ga-beta(56); (Δ) H-Be-beta(55) ;
(□)Deberyllated-Be-beta(120)[DFK-H-Be-beta(105)].

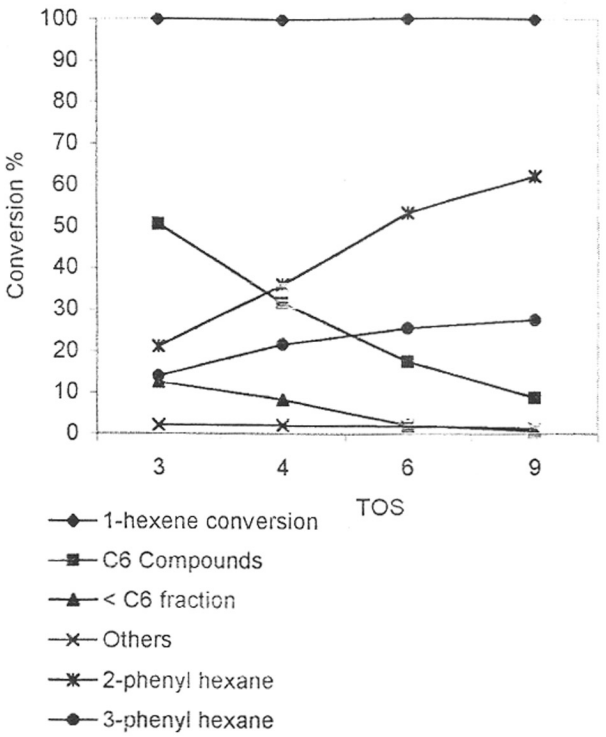

Fig. 5.3 : Effect of Time on Stream (TOS) on catalytic activity of H-Al-beta(35) in the Alkylation of benzene with 1-hexene.
Benzene/hexene mole ratio = 10. WHSV = $4h^{-1}$, Temp. = 413K;
SiO_2/Al_2O_3=35

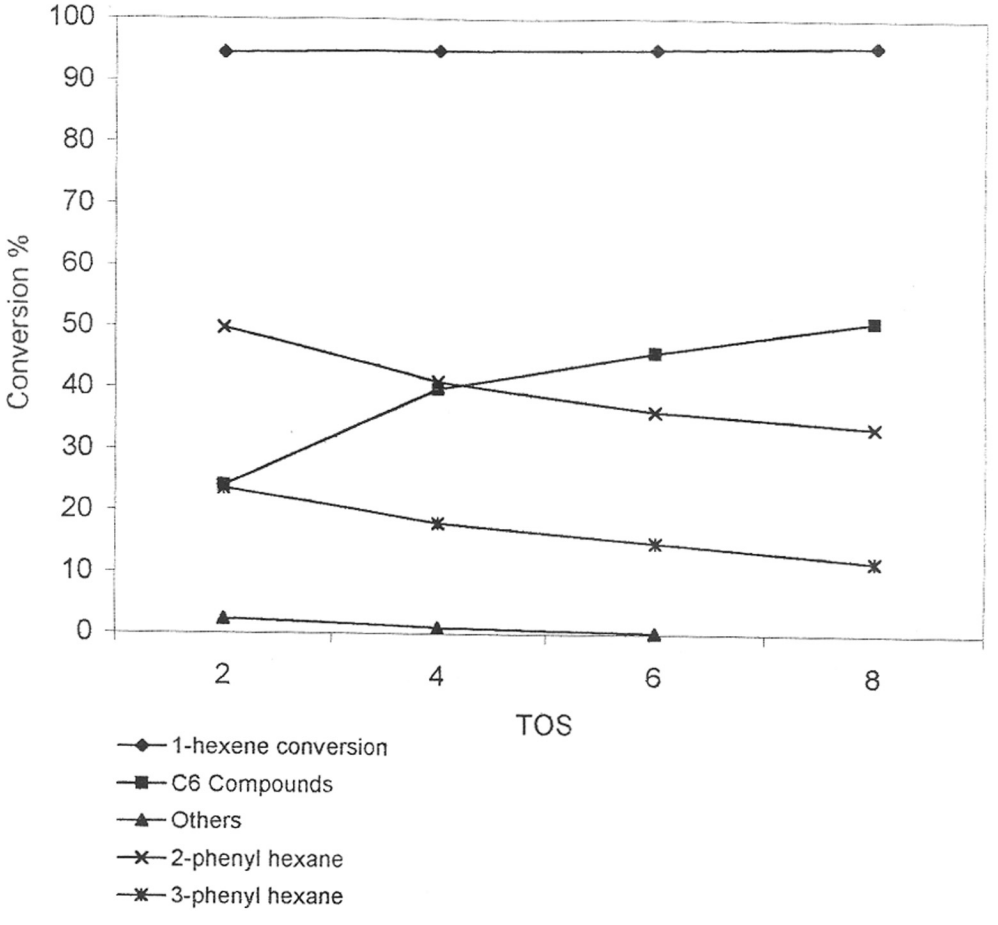

Fig. 5.4 : Influence of Time on Stream on the catalytic activity of H-Ga-beta(56) in alkylation of benzene with 1-hexene.
Benzene/1-hexene mole ratio= 10. WHSV= $4h^{-1}$, Temp.= 413K;
SiO_2/Ga_2O_3 =56

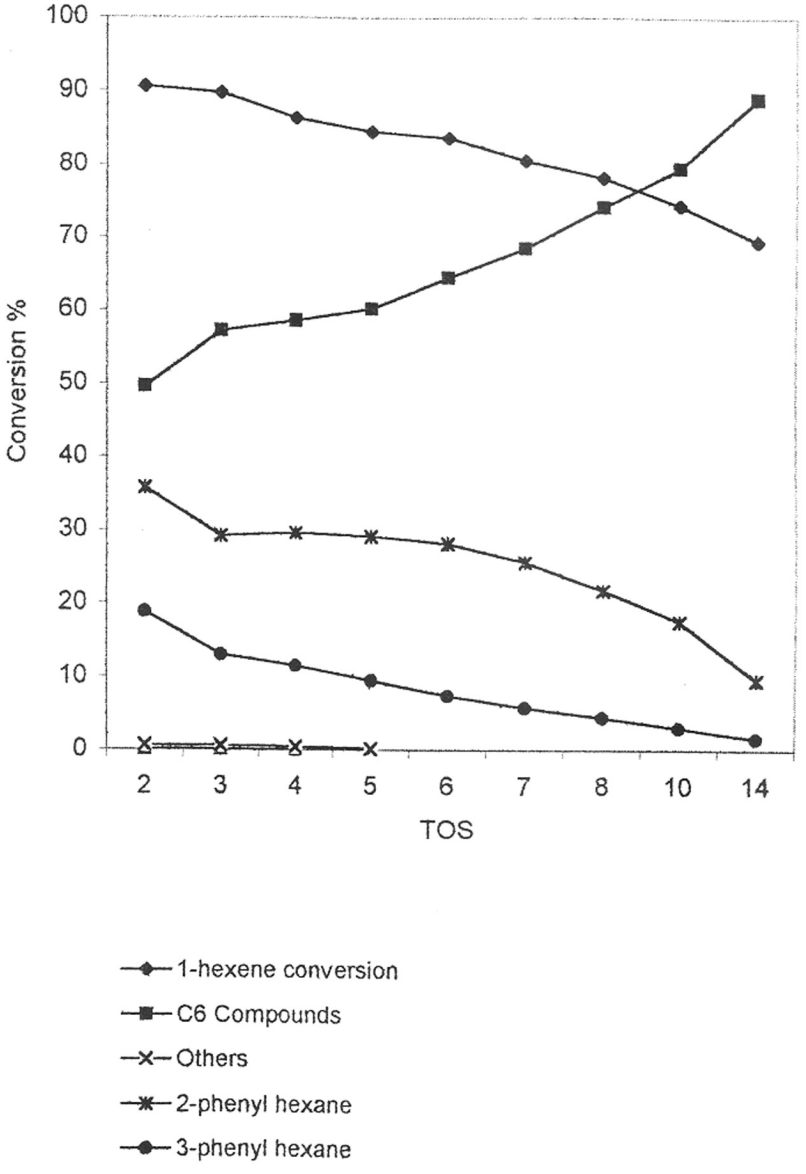

Fig. 5.5 : Effect of Time on Stream on the catalytic activity of H-Be-beta(55) in the alkylation of benzene with 1-hexene.
Benzene/1-hexene mole ratio= 10. WHSV= $4h^{-1}$, Temp.= 413K;
SiO_2/BeO =55

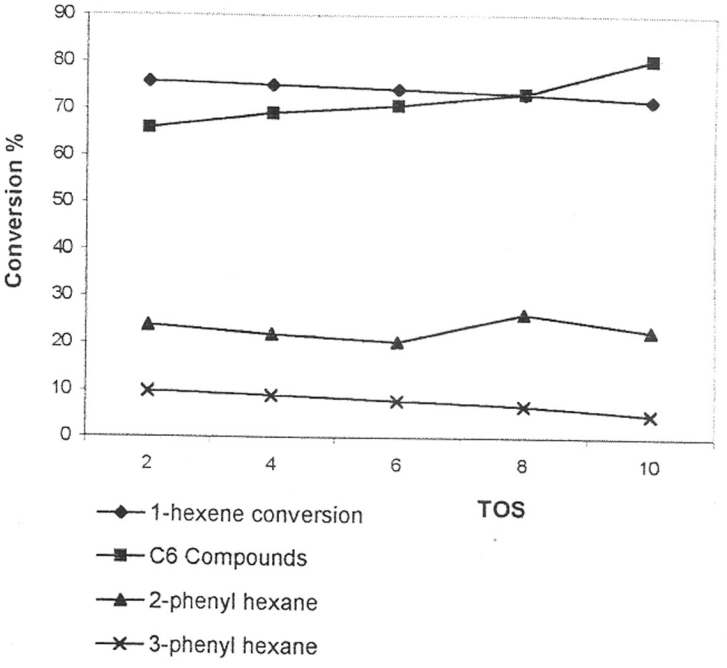

Fig. 5.6 : Effect of Time on Stream on the catalytic activity of DFK-H-Be-beta in alkylation of benzene with 1-hexene.
Benzene/1-hexene mole ratio= 10. WHSV= $4h^{-1}$, Temp.= 413K;
SiO_2/BeO =105

discussed in the previous section.

As seen in fig.5.3, deactivation rate is least in H-Al-beta. It exhibited total conversion of 1-hexene even upto 10 hours. on stream whereas in the case of un-modified H-Ga- beta and H-Be-beta (fig. 5.4-5.5), the conversion of 1-hexane decreased with time. The Be-isomorph is seen to deactivate most rapidly. However, the life of the catalyst improved considerably after modification of H-Be-beta (fig. 5.6) although olefin conversion was reduced due to a decrease in the acidity of the catalyst, consequent to a decrease in the framework Be^{2+} content.

As seen in fig. 5.2, shape selectivity increases with time on stream and the relatively smaller 2-phenyl isomer is favoured. Shape selectivity is lower in H-Al-beta. The comparatively higher shape selectivity (2ϕ/3ϕ ratio) which increases with time, in the as synthesized Ga- and Be-isomorphs is probably due to the deposition of extraneous materials inside the pores or at pore openings (Table 5.3).

Fig. 5.4 presents the variation of composition with time on stream in the case of H-Ga -beta. Although the conversion of 1-hexene does not vary much even upto 10 hours, there is a marked variation in the composition of the products. The initial activity and formation of hexylbenzenes is much higher when compared to the Al-analog. In H-Ga-beta there is a decrease in the production of hexylbenzenes and rapid deactivation (Fig 5.4). In the case of H-Al-beta (fig.5.3) which deactivates rather slowly, the production of alkylbenzene isomers increases with time on stream due to suppression of cracking.

5 . 3 . 2 Alkylation of benzene with 1-hexene over mordenites :

The isomorphously substituted gallo-mordenite catalyst, obtained by direct synthesis was tested for its catalytic activity in this alkylation reaction and compared with its Al - analog. The relevant physical characteristics of the catalysts used in the reaction have been presented in Table 5.3. The results of the alkylation experiments are presented below:

5. 3. 2. 1 Effect of temperature :

As found in the case of H-Al-beta (section 5.3.1), the conversion of 1-hexene was 100 % over the H-Al-mordenite catalyst at all temperatures. Similarly, eventhough there was no significant change in selectivity for formation of hexylbenzenes, their formation decreased slightly when the temperature was raised from 393 to 433 K and cracked products were favoured at the higher temperature (Table 5.7).

Similarly, as seen in Table 5.7 and 5.8, in the case of mordenite too, temperature affects isomer selectivity. It is observed that the 2ϕ/3ϕ ratio increases with an increase in temperature in the Al- as well as Ga-isomorphs. Also, for a particular temperature, as compared to H-Al mordenite, the 2ϕ/3ϕ ratios are higher for the Ga-isomorph. Temperature also affects the distribution of the other products. Over the H-Al-beta catalyst, it was seen that cracking into the C_1-C_5 fraction was significant. In the case of the H-Al-mordenite, it is observed that the C_1-C_5 components are practically absent in the product; instead cracked products resulting from cracking of alkylbenzenes (yielding < C_6 - alkyl benzenes) are predominant. It should be noted that <C_6-alkyl benzenes could also have been formed from the alkylation of benzene with the cracked olefins in the C_2-C_4 range.

Table 5 . 7 : **Effect of temperature on alkylation of benzene with 1-hexene over H-Al-mordenite.**

Sio_2 / Al_2O_3 = 17.7; Benzene / n- hexene mole ratio = 10; WHSV = $4h^{-1}$.

Temperature	393 K	413 K	433 K
Product Distribution (wt.%)			
C_6 – Compounds[a]	2 . 30	0 . 85	0 . 70
< C_6 – Fraction[b]	-	-	1 . 70
Others[c]	14 . 20	16 . 05	17 . 80
2 – phenylhexane	51 . 64	54 . 27	54 . 93
3 – phenylhexane	31 . 86	28 . 83	24 . 87
% Total C_6 – phenyl hexanes	83 . 50	83 . 10	79 . 80
2ϕ / 3ϕ[d]	1 . 64	1 . 88	2 . 20
% 1–hexene conversion.	100	100	100

a . Isohexenes, n-hexane and isohexanes .

b. Cracked products; C_1-C_5.

c. < C_6-alkylbenzenes and > C_6-alkylbenzenes.

d. The ratio of 2-hexylbenzene/3-hexylbenzene.

Table 5 . 8 : **Effect of temperature on alkylation of benzene with 1-hexene over H-Ga-mordenite.**

Sio_2 / Ga_2O_3 = 19.0; benzene / n-hexene mole ratio = 10; TOS = 5 hrs.

Temperature	393 K	413 K	453 K
Product Distribution (wt. %)			
C_6 – Compounds[a]	64 . 40	50 . 18	30 . 15
< C_6 – Fraction[b]	-	17 . 45	21 . 00
Others[c]	13 . 30	3 . 17	5 . 85
2 – phenylhexane	1 . 30	23 . 50	36 . 72
3 – phenylhexane	16 . 54	5 . 70	6 . 28
2ϕ / 3ϕ[d]	4 . 46	4 . 12	5 . 84
% Total C_6 - phenylhexanes	3 . 70	29 . 20	43 . 00
% 1-hexene conversion	97 . 3	97 . 92	99 . 00

a . Isohexenes, n-hexane and isohexanes .

b. Cracked products; C_1 - C_5.

c. < C_6 - alkylbenzenes and > C_6 - alkylbenzenes.

d. The ratio of 2-hexylbenzene/3-hexylbenzene.

5. 3. 2. 2 Effect of space velocity :

Fig. 5.7 demonstrates the effect of space velocity on Ga-H-mordenite (SiO_2 / Ga_2O_3 = 18.3). It is seen that at higher space velocities, 1-hexene conversion decreases due to a decrease in contact time. Similarly, selectivity to phenylhexanes also decreases at lower contact times (higher WHSV), along with a marginal increase in the concentration of the hexene isomers.

5. 3. 2. 3 Effect of isomorphous substitution :

The effect of isomorphous substitution of gallium, in place of aluminium in the mordenite framework, on the catalytic activity has been studied. The combined results of the studies on the effect of isomorphous substitution and time on stream (at two different temperatures) over both Ga - and Al -isomorphs of mordenite are presented in Fig. 5.7 to Fig. 5.11.

The product differences basically arise out of the difference in the relative acidities of the two isomorphs (acidity of Al-mordenite > acidity of Ga-mordenite) and also the relative stability of the Al^{3+} and Ga^{3+} cation in the zeolite framework. The Al^{3+} ion is more stable than the Ga^{3+} ion in the tetrahedral position in the zeolite framework. The H-Ga-mordenite sample exhibited a tendency to isomerize 1-hexene to i-hexenes, while isomerization was practically negligible in case of H-Al-mordenite, especially at lower temperatures. However, unlike in the case of H-Al-beta, where the formation of hexylbenzenes increased with time on stream, the mordenite system exhibited a different trend. Both H-Al- and H-Ga-mordenites exhibited greater initial activities but the H-Ga-mordenite sample deactivated rapidly. Also, H-Al-mordenite exhibited higher shape selectivity for the 2-phenyl hexane as compared to

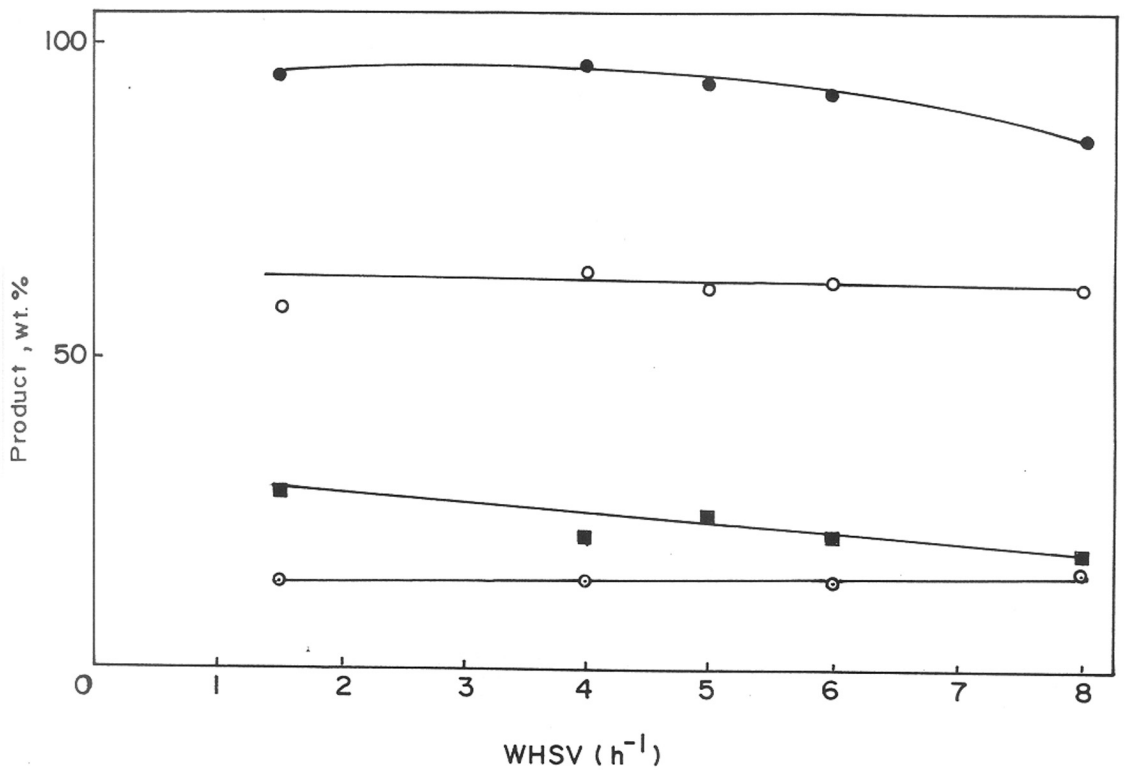

Fig. 5.7 : Effect of space velocity on Product Distribution in the alkylation of benzene with 1-hexene over H-Ga-mordenite.
Benzene/1-hexene mole ratio= 10. Time on Stream = 4h; Temp.= 413K; SiO_2/Ga_2O_3 =19; (●) 1-hexene conversion (%); (O) Isohexenes (wt.%); (■) C_6-hexylbenzene (wt.%); (⊙) Others (<C_6 alkylbenzenes and < C_6 alkyl benzenes-wt.%)

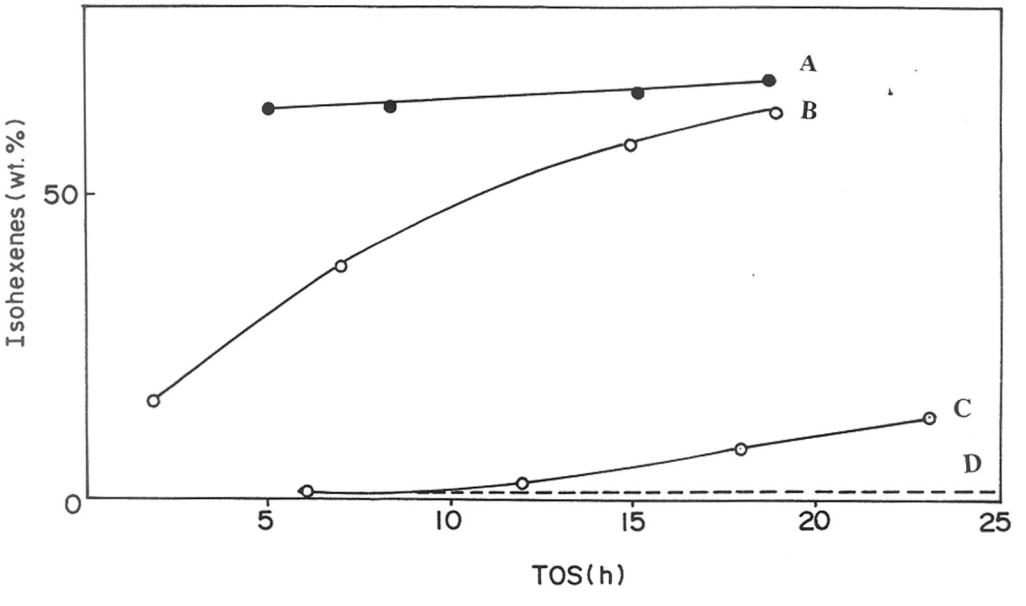

Fig. 5.8 : Effect of Time on Stream and Temperature on isomerization of 1-hexene Over alumino- and gallo-mordenite.
Benzene/1-hexene mole ratio= 10. WHSV= $4h^{-1}$; SiO_2/Ga_2O_3 =19 SiO_2/Al_2O_3 =17.7; (A) H-Ga-mordenite (temp. = 393K); (B) H-Ga-mordenite (temp. = 453K); (C) H-Al-mordenite (temp.= 533K); (D) H-Al-mordenite (temp. = 393K)

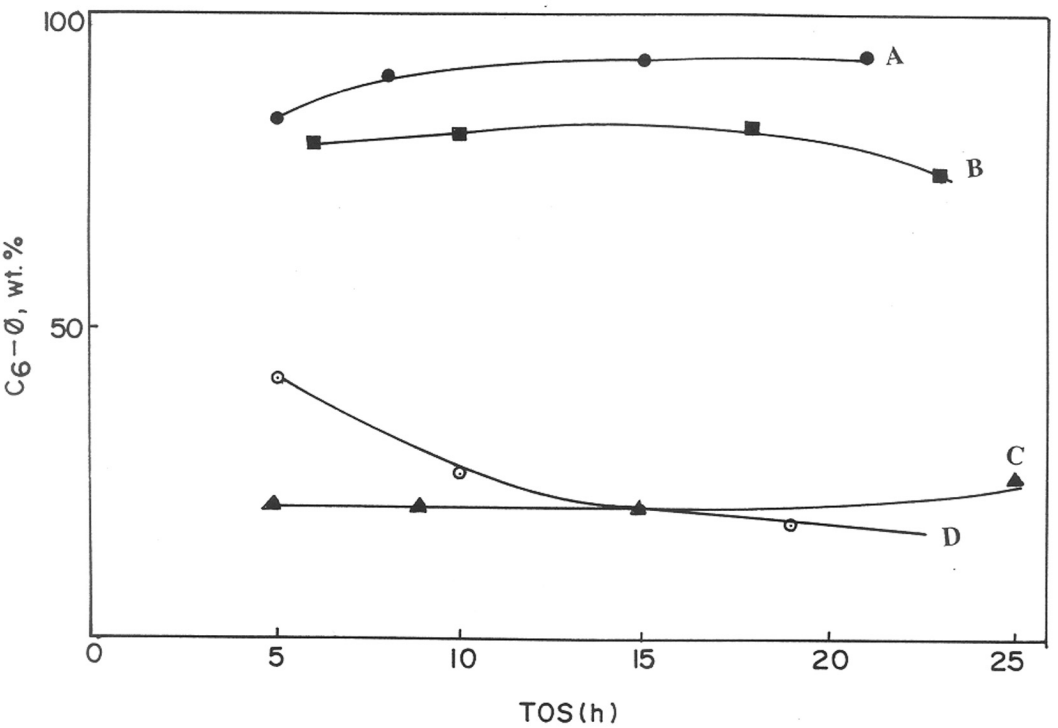

Fig. 5.9 : Effect of Time on Stream and Temperature on formation of C_6-hexylbenzenes over alumino- and gallo-mordenite
Benzene/1-hexene mole ratio= 10. WHSV= $4h^{-1}$; SiO_2/Ga_2O_3 =19
(A) H-Ga-mordenite (temp. = 393K); (B) H-Ga-mordenite (temp. = 453K); (C) H-Al-mordenite (temp.= 533K); (D) H-Al-mordenite (temp. = 393K)

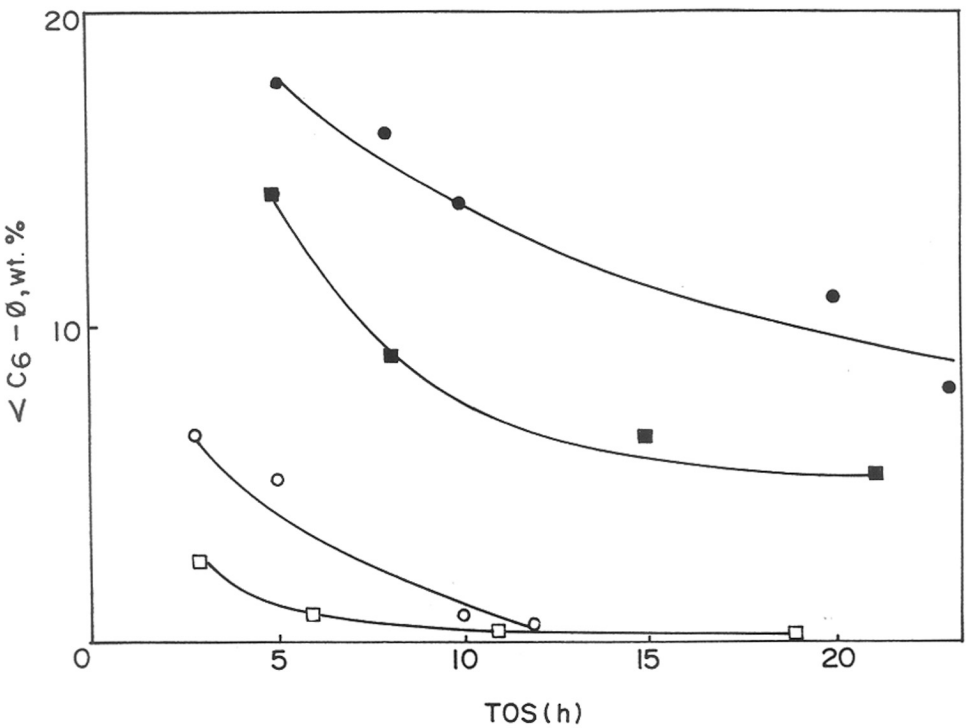

Fig. 5.10 : Effect of Time on Stream and Temperature on formation of Cracked alkylbenzenes in the alkylation of Benzene with 1-hexene over alumino- and gallo-mordenite
Benzene/1-hexene mole ratio= 10. WHSV= $4h^{-1}$; SiO_2/Ga_2O_3 =19
SiO_2/Al_2O_3 =17.7; (●) H-Al-mordenite (temp. = 433K); (■) H-Al-mordenite (temp. = 393K); (○) H-Ga-mordenite (temp.= 453K); (□) H-Ga-mordenite (temp. = 393K)

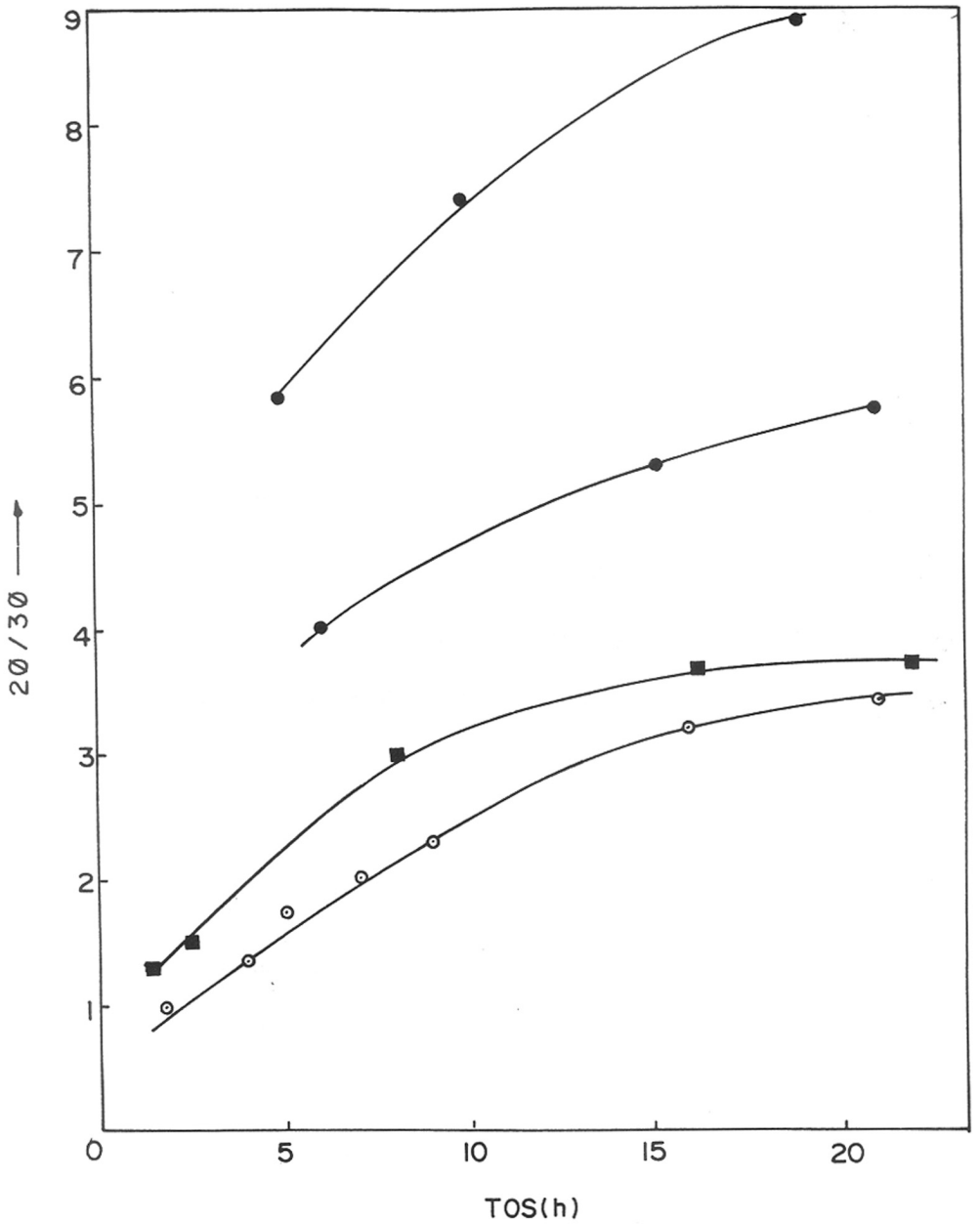

Fig. 5.11 : Effect of Time on Stream and Temperature on the shape-selectivity in the formation of C_6-alkybenzenes over alumino- and gallo-mordenite Benzene/1-hexene mole ratio= 10. WHSV= $4h^{-1}$; SiO_2/Ga_2O_3 =19 SiO_2/Al_2O_3 =17.7; (A) H-Ga-mordenite (temp. = 453K); (B) H-Ga-mordenite (temp. = 393K); (C) H-Al-mordenite (temp.= 433K); (D) H-Al-mordenite (temp. = 393K).

H-Al-beta, especially at higher temperatures. This may be attributed to the unidimensional pore system of mordenite. On the whole, the gallo-isomorphs of beta and mordenite show similar trends in the catalytic activity.

5 . 4 Comparative studies of alkylation of benzene with long chain linear olefins over medium and large pore zeolites:

The alkylation of benzene with 1-hexene, 1-dodecene and a mixture of C_{10} - C_{13} olefins (alkylation feed used in LAB manufacture) was carried out over a number of zeolites.

5. 4. 1 Alkylation with 1-hexene:

Table 5.9 presents the results of alkylation of benzene over a number medium and large pore zeolites. The large pore zeolites (12 membered rings) were H-Y, H-B, H-M, H-L and ZSM-12. The medium pore zeolites (10 membered rings) were EU-1 and ZSM-5. For comparison purposes an amorphous SiO_2 - Al_2O_3 was also used.

When alkylation was carried out with 1-hexene, the 2-ϕ and 3-ϕ isomers were found to be produced, (Table 5.9). The 1-ϕ isomer (wherein the phenyl group is attached to the terminal carbon) was not detected due to the lower stability of the primary carbenium ion compared to the secondary carbenium ions[13]. The 3-ϕ isomer is produced by the isomerization of the C_2 - carbenium ion $(C_2)^+$ to the C_3-carbenium ion $(C_3)^+$ which occurs rapidly even at relatively low temperatures over even weak acid sites.

As the stability of $(C_2)^+$ and $(C_3)^+$ ions are nearly the same, it is expected that 2-ϕ and 3-ϕ isomers must be formed in nearly the same proportion; i.e., the ratio of the 2-ϕ hexane to 3-ϕ hexane (2-ϕ/3-ϕ) should be ~ 1. However, as seen in Table 5.9, this ratio is always >1 for all zeolites and even silica-alumina. This is due to the competitive nature of the alkylation and

Table 5 . 9 : Alkylation of benzene with 1-hexene over different medium and large pore zeolites.

Zeolite	TOS (h)	Conversion (wt. %)	$<C_6$ Fraction[a]	C_6 – compounds[b]	Other[c]	$C_6\phi$[d]	$2\phi/3\phi$	Δ[e]
Si–Al	4	94.66	20.13	62.27	5.68	11.81	1.91	11.3
	8	81.29	1.11	61.62	12.27	24.35	2.39	
ZSM–5	4	94.39	12.29	48.56	18.20	20.95	12.00	-
	13	94.58	37.7	58.05	16.28	21.89	8.13	41.1
H-EU-1	2	95.75	2.46	46.68	4.01	46.85	5.70	18.3
	14	96.19	0.94	58.05	3.63	46.68	7.65	
H-K–L	3	83.44	0.16	72.99	1.83	25.02	1.84	2.0
	19	70.78	-	86.11	0.33	13.56	2.16	
ZSM–12	4	98.39	0.13	11.17	4.76	83.94	2.66	1.2
	19	92.90	0.12	12.28	2.80	84.82	2.84	
H–Y	2	100.00	29.46	5.85	31.82	32.87	1.40	0.66
	5	100.00	11.69	2.71	15.65	69.95	1.42	
D-Al–Y	4	93.55	17.76	13.91	5.10	63.23	1.26	0.90
	15	65.01	8.01	26.36	2.72	62.91	1.36	
RE–Y	4	92.20	0.31	15.54	3.11	81.04	1.20	0.50
	17	54.33	-	39.74	1.21	59.05	1.26	
H-β	3	100.00	12.56	50.53	2.10	34.81	1.50	9.70
	9	100.00	0.60	8.72	1.27	89.41	2.08	
H-M(1)	4	100.0	10.06	62.80	5.90	21.24	1.30	12.9
	18	96.94	0.48	57.93	1.80	39.79	3.10	
H-M*	5	100.00	17.06	43.23	18.24	21.47	2.14	14.2
	20	97.99	0.60	6.04	8.20	85.16	4.27	
D-Al–M	4	66.36	0.61	1.15	8.95	89.29	3.37	6.00
	19	61.51	0.54	5.69	3.50	90.27	4.27	

Conditions : Temp. (K) = 413, * 433; Press (Mpa) = 0.1; WHSV (h^{-1}) = 4.0;

Benzene/ hexene mole ratio = 10

a . Cracked products, C_1- C_2.

b . Isohexenes, n-hexane and i-hexanes.

c . Mostly $<C_6$ - alkylbenzenes and heavier material.

d . n - and i - products ; n - ϕ > > i -ϕ ; mostly monoalkylbenzenes.

e . Δ = change in $2\phi/3\phi$ ratio per hour x 100.

olefin isomerization reactions and the lack of any skeletal isomerization of the alkylbenzenes at the conditions of the reaction. Therefore, even before the equilibration of the hexene isomers (or carbenium ions) is achieved, alkylation of the reactant 1-hexene to the 2-phenyl isomer takes place to some extent.

The values of the 2-ϕ/3-ϕ ratios in the case of the large pore zeolites are mostly close to 1. However, ZSM-12 has a 2-ϕ/3-ϕ = 2.66. The isomorphously substituted Ga-beta and Be-beta and Ga-mordenite show 2-ϕ/3-ϕ >1 which has alrdy been discussed in the previous sections. In the case of ZSM-12 (2-ϕ/3-ϕ = 2.66), the shape selectivity could be due to its highly puckered ring system leading to a smaller pore-opening (0.57x 0.6nm). It is surprising to note that even in the case of silica-alumina which possess an average pore diameter much larger (~ 2.7nm) than those of the zeolites, the 2-ϕ content is large (2-ϕ/3-ϕ = 1.91). This could be due to its lower acid strength when compared to the zeolites and hence the slower isomerization of the C_2 carbenium ion.

In the case of the two medium pore zeolites, EU-1 and ZSM-5, the 2-ϕ /3-ϕ ratios are much larger (5.7 and 12.0, respectively) indicative of the shape-selectivity of these zeolites. It is however, interesting to note that EU-1 which has a much smaller pore opening than ZSM-5 leads to a smaller 2-ϕ /3-ϕ ratio. Apparently, product shape-selectivity (which is determined by the size of the pore opening) is not the only important factor in determining the 2-ϕ/3-ϕ ratios. The presence of large side pockets in EU-1 (Table 5.3) provides enough space for the bimolecular alkylation reaction which leads to the formation of the bulkier 3-ϕ isomer. In ZSM-5, apparently bimolecular reactions are sterically more hindered[14]. Thus, the above results indicate that both product and transition state selectivites may be playing a role in determining the 2-ϕ/3-ϕ ratios in the case of zeolites.

The change of the 2-ϕ/3-ϕ ratio during run is presented in column 8, Table 5.13. In the case of DAI-Y, the change in negligible (0.9 units). The magnitude of the above changes are related to the size and type of the pore systems. The 3-dimensional pore systems (Y and beta) produce smaller changes. Mordenite with a undimensional pore system leads to a larger change in the 2-ϕ/3-ϕ ratio with increasing duration of run. However, the change in the ratio of both L, posssesing a larger pore diameter (0.71nm) and ZSM-12. possessing smaller pore openings (0.57 x 0.6nm) is similar (2.0 and 1.2 respectively).

The selectivity for the 2-ϕ isomer increases in the case of EU-1, while it decreases rapidly in the case of ZSM-5. The decrease in the formation of the bulkier 3-ϕ isomer over EU-1 is due to probably the blockage (or non-accessibility) of the side-pockets wherein such isomers may be formed preferentially. The decrease in the 2-ϕ isomer formation over ZSM-5 is probably due to the progressive blockage of the pore-openings and the increased contribution of the external surface to the reaction with duration of the run.

The initial activity and deactivation rate (decrease in conversion with time) of different zeolites is found to be again different (column 3, Table 5.9). The large pore zeolites Y and mordenite have higher initial activities and also deactivate rapidly. While the rapid deactivation of Y is attributed to its larger acid site density, the deactivation of mordenite is due to its unidimensional pore system. The medium pore zeolites, EU-1 and ZSM-5, both possess low initial activities and deactivation rates. Similiarly, they also possess low selectivities for hexyl-benzenes (colum 6 Table 5.9). Again, the selectivites for hexylbenzenes production do not change significantly in the case of the above two zeolites.

Zeolite Y and ZSM-12 exhibit good selectivites for hexylbenzene formation both

initially and after a TOS of 15-19 h, while H-beta and H-M (1) exhibit high selectivities only after many hours on stream. The dealuminated mordenite D-Al-M, on the other hand, has good selectivites both when TOS = 4 and 19 h.

The shape-selectivities of zeolites is accentuated by the presence of extraneous materials inside the pores or at the pore-openings. The presence of extraneous materials inside the pores is often detected by the adsorption of hydrocarbons and NMR-methods[15]. The amorphous content of the zeolite samples was quantitatively estimated by the adsorption of argon using the t-plot method[16]. However, how much of this amorphous material affects the pore openings or the pore-dimensions is not easy to determine. Zeolite-beta contains substantial anounts of amorphous materials (Table 5.3). It is also found that their 2-ϕ/3-ϕ ratios are much higher. Similarly, the dealuminated mordenite, D-Al-M, also contains amorphous materials and has a larger 2-ϕ/3-ϕ ratio than H-M (1). However, eventhough RE-Y is more amorphous than DAl-Y, the 2-ϕ/3-ϕ ratios are similar in the two zeolites due to the larger and more open pores in the FAU-system.

5 . 4. 2 ALKYLATION WITH 1-DODECENE :

The results of the alkylation studies carried out with 1-dodecene are presented in Table 5.10. The studies were carried out at a pressure of 0.6 Mpa and a temperature of 408 K at which conditions benzene remains in the liquid phase. Also a low space velocity (WHSV = 0.8 h^{-1}) was used . Under the above conditions, catalyst deactivation was much smaller, 100% conversion being observed for upto about 20 hours for most of the catalysts . The lower deactivation noted at 0.6 Mpa is probably due to the solvent action of liquid benzene dissolving away the deactivating components from the catalyst surface. Under the above conditions, the yields of the C_{12}-alkylated products (ϕ-dodecanes) were also high, the selectivities being > 80 % in the case of RE-Y, SiO_2 - Al_2O_3 and beta.

Table 5.10 : Alkylation of benzene with 1-dodecene

Catalyst	C_{12} - alkyl benzene distribution, (wt. %)$^{+}$						
	2-ϕ	3-ϕ	4-ϕ	5-ϕ	6-ϕ	2-ϕ / 6-ϕ ratio	2-ϕ / 3-ϕ ratio
Si-Al	33 . 4	21 . 9	14 . 8	15 .6	14 . 2	2 . 4	1 . 5
RE-Y	17 . 6	19 .1	19 . 8	22 . 0	21 . 5	0 . 8	0 . 9
H-β	39 . 1	26 . 4	18 . 9	10 . 8	4 . 8	8 . 2	1 . 5
H-M (2)$^{++}$	563 . 7	35 . 4	0 . 9	Tr	-	70 . 7**	1 . 8
H-M (3)$^{++}$	65 . 8	34 . 2	Tr	-	-	-	1 . 9
HF *	16 . 7	16 . 4	17 . 5	24 . 1	25 . 3	0 . 7	1 . 0

Conditions : Temp. (K) = 408 ; Press (Mpa) = 0.6 ; WHSV (h^{-1}) = 0.8 ; Benzene : Olefin (mole) ratio = 10 ; Conversion of Olefin ~100 % ; Data obtained at 10h on stream)

+ . Includes iso-phenyl compounds .

++. Conversion incomplete.

* : C_{12}–alkyl benzene fraction from commercial LAB : liquid phase reaction; WHSV indeterminate.

** : 2-ϕ/: 4-ϕ ratio .

As discussed in the earlier section, based on the relative stabilities of the different secondary carbenium ions, one would expect the isomer content to increase with the C-number. This is found to be so in the case of both HF and RE-Y. Apparently, RE-Y is non-shape selective even during alkylation with a large molecule like dodecene. Beta and mordenite, which were both non-shape selective or weakly shape-selective during alkylation with 1-hexene, now exhibit marked shape-selectivites with dodecene. Olson has also observed differences in isomer distribution in dodecyl benzenes during studies using HF, H_2SO_4 and $AlCl_3$[2].

The shape-selectivity effect, as expected, is much larger for the unidimensional mordenite system than for beta; in fact, mordenite is so shape-selective that the 6-ϕ isomer is not detected at all. Further, both H-M (2) and H-M (3) deactivated more rapidly than the other zeolites, the selectivity for the C_{12} alkyl benzenes being less than 10% at the above conditions. Interestingly, silica-alumina is found to produce relatively more of the 2-ϕ and 3-ϕ isomers when compared to HF or RE-Y. Apparently, as discussed earlier, acidity differences are probably responsible for this behaviour.

5 . 4. 3 ALKYLATION WITH MIXTURE OF OLEFINS (C_{10} - C_{13}) :

The results of alkylation with a commercial mixed olefin feed (C_{10} - C_{13}) are presented in Table 5.11 The comparison of the feed according to the C-fractions is also presented in the table. Due to the large number of isomeric olefins in each carbon fraction, and the difficulty in separating and identifying them, estimation of the individual components has not been carried out.

The results are found to be similar to those reported earlier. SiO_2-Al_2O_3 and H-beta, H-Y and H-M produce more 2-ϕ isomers than RE-Y and HF. As expected, shape-selectivity in the case of H-M and H-beta increases with the C-number of the fraction. It is to be noted that

Table 5.11 : Alkylation of benzene with a mixture of (C_{10}-C_{13}) olefins^{+}

Product	Product distribution, (wt.%)						
	Catalyst						
C_n	n-ϕ	H-M (1)*	H-β	H-Y	RE-Y	Si-Al	HF**
C_{10}	2	22.5	8.0	4.7	2.9	4.9	5.0
	3	7.2	3.5	2.8	2.8	3.4	3.5
	4	6.3	2.9	2.6	3.5	2.5	3.0
	5	13.1	2.5	2.6	5.0	3.0	3.1
C_{11}	2	38.5	16.1	11.4	7.9	12.0	5.9
	3	8.8	10.1	7.3	7.4	8.0	5.8
	4	tr	7.8	6.4	7.9	5.7	6.4
	5	-	2.1	6.2	8.8	5.9	8.4
	6	-	3.1	3.1	3.9	2.7	4.3
C_{12}	2	3.6	10.5	10.9	6.1	11.8	5.7
	3	tr	7.1	7.3	6.6	8.0	5.7
	4	-	5.2	6.2	7.0	5.4	6.1
	5	-	2.9	6.4	2.3	5.7	8.4
	6	-	1.3	6.4	2.3	5.2	8.8
C_{13}	2	-	6.7	4.0	2.3	4.5	2.9
	3	-	4.3	2.8	2.3	4.5	2.9
	4	-	2.2	2.4	2.8	2.0	3.2
	5	-	1.9	2.6	3.2	2.0	4.3
	6	-	0.8	2.6	3.0	2.0	4.7
	7	-	1.0	1.3	1.2	0.8	2.0
2-ϕ (%)		64.6	41.3	31.0	19.2	33.2	19.6

Conditions : Temp. (K) 408; Press.(Mpa) = 0.6; WHSV (h^{-1}) = 0.8; Benzene : Olefin (mole) ratio = 10

\+ . Composition of feed (wt.%) : Olefins (total) 8.3; C_{10} = 1.9; C_{11} = 3.1; C_{12} = 2.6 ; Paraffins (C_{10} , C_{11} , C_{12} and C_{13}) constitute the rest.

* . Conversion incomplete.

** . Composition of parent olefin mixture not known; Commercial LAB product; liquid phase reaction; WHSV indeterminate.

the end-phenyl (C_6 ,C_7) isomers of the C_{11} and C_{13}-alkylbenzenes are present in smaller quantities due to the lower alkylation probability (half) at the central carbon atoms.

At the conditions of the study, the conversions of the olefins over the samples [except H-M (1)] were 100%. The selectivity for alkylbenzenes were also very high, being > 90 % for all the catalysts [except H-M (1)].

5 . 5 CONCLUSIONS :

These studies suggests that large pore zeolites can be used beneficially for the alkylation of benzene to obtain linear alkyl benzenes. From the data presented in the previous sections it can be concluded that :

1. The composition of the products varies with reaction parameters but desired products can be obtained under optimized reaction conditions.

2. The activity and shape–selectivity of the catalysts changes considerably on isomorphous substitution of one element by another in the zeolite lattice.

3. The comparative studies over various large and medium pore zeolites indicate that : a) Zeolite Y does not exhbit shape–selectivities favouring the formation of the less bulky 2-ϕ isomer during alkylation.

   b) The other wide pore zeolites like, beta, mordenite and ZSM-12, however, exhibit shape-selectivities favouring the formation of the less bulky 2-ϕ isomer. Morever, the shape-selectivities in mordenite and beta become more pronounced with increasing C-number of the alkane.

4. The life of mordenite catalysts apparently improves on dealumination.

5. Shape-selectivity for the reaction probably arises from the fact that rate of alkylation may be greater than that of isomerzation. The other possibility could be due to product

diffusion control which leads to the preferential formation of the 2-ϕ isomer.

6. Finally, we can also conclude that both acidity or rather the acid site density and microporosity may be the factors influencing the rate of deactivation.

REFERENCES :

1. Pujado, P. R. in "Handbook of Petroleum Refining Process", Ed. Meyers, R. A., Mc Graw-Hill, Inc., New York, (1986).
2. Olson, A. C., "Ind. Eng. Chem", **52** (1960) 833.
3. Canfield, R. C., Cox, R. P. and McCarthy, D. M., "Chemical Engineering Progress", (Aug. 1986) 36.
4. Berna, T., Jose, L., Moreno, D. and Alfonso, EP Appl.O 353, 813 (1991).
5. Dwyer, F. G., "Catalysis of Organic reactions", ed. , W. R. Mosa, Marcel Dekker, New York, (1981) 39.
6. Petrochemical Handbook, "Hydrocarbon processing", (March 1997) 107.
7. Fritsch, T., Ozmen, S., Raghram, Banerji, A., Bernai, J., and Moreno, A., Paper presented at the 3rd. CESIO International Surfactants Congress, London, (June 1-5, 1992).
8. Petrochemical Handbook, "Hydrocarbon processing", **70** (1991) 152 .
9. Vora, B. V., Pujado, P. R., Imai, T., and Fritsch, T. R., Paper presented in " Recent advances in the detergent industry ", Society of Chemical Industry, Univ. of Cambridge, England, (26 – 28 March, 1990).
10. Patinkin, S. H., and Friedel, B. S., in the Fiedel –Crafts and Related Reactions, ed. G. A. Olah, Vol. II, Part I, Interscience , New York (1964) 1
11. Poutsma, M. L., in "Zeolites Chemistry and catalysis" ed. Rabo, J. A, American Chemical society, Washington, (1976) 437.
12. Venuto, P.B ; Hamilton, L.A. ; Landis, P. S.; and Wise, J. J.; *J.catal.*", **5** (1966) p.81
13. Corma, A., Aguada, A. L., Nebot, I., and Tomas, F., *J. Catal.*, **77** (1982)159.

14. Olson, D. H., and Haag, W. O., "Am. Chem. Soc. Symp. Ser.", **248** (1984) 275.

15. Corma, A., and Nieman, J., "Proc. Akzo. Catal. Symp; Fluid catalytic Cracking", Scheveninger, The Netherlands, (1991) 217.

16. Johnson, M. F. L., *J. catal*, **52** (1978) 425.

SUMMARY

SUMMARY

This thesis is a study of modifications in large pore zeolites. The studies include synthesis, Physico-chemical characterization and evaluation of the catalytic properties of the zeolites beta and mordenite.

The work was primarily aimed at the Isomorphous substitution of Ga^{3+}- and Be^{2+}- ions in the lattice of zeolite beta and Ga^{3+}- ions in the lattice of mordenite by hydrothermal synthesis and further modifications to make active catalysts.

Preliminary experiments were carried out by varying various synthesis parameters such as reactivity of silica its source template concentration, alkalinity, water content, SiO_2 / Ga_2O_3 or SiO_2 / BeO ratio and temperature, and optimum conditions were found.The [Ga]-beta samples were obtained in 13-15 days at 393 K, with tetraethylorthosilicate (TEOS) as the silica source, whereas the synthesis of Al-beta using TEOS required only 6-7 days at 393K . The typical gel composition was $60SiO_2 : Ga_2O_3 : 36.33\ (TEA)_2O : 1.14\ H_2SO_4 : 5.95\ Na_2O : 1147\ H_2O$. Thus crystallization time for [Ga]-beta was almost twice that required for [Al]-beta using the same silica source. Similarly, crystalline [Be]-beta was obtained using TEOS as the source of silica. The typical gel composition was $60SiO_2 : BeO : 36.33\ (TEA)_2O : 5.95Na_2O : 1147\ H_2O$. However, syntheses of pure form of [Be]-beta required much lower temperature (353K) and highly crysrtalline samples could be obtained in two weeks. The difference between the Si:Ga and Si:Be ratio in the starting gel and the final product increased with increasing silicon content. Both the gallo and beryllo-silicate analogs of zeolite beta were obtained in the purest form, since they were synthesized using tetraethyl orthosilicate, which was free from Al impurities .

Another novel isomorphously substituted gallosilicate analog of mordenite was successfully synthesized during the course of the present study . An Al-mordenite sample was

also synthesized for comparison. Synthesis was carried out hydrothermally using sodium silicate, as the source of silica at 453 K in 4-5 days . The typical reactive gel compositions were $7.5Na_2O:Al_2O_3$: 30 SiO_2:3 TEABr:054 H_2O for Al–mordenite and $7.5Na_2O:Ga_2O_3$:30 SiO_2: 3 TEABr :1054 H_2O for Ga mordenite respectively. Fumed silica was used as the source of silicon for the synthesis of Ga mordenite to obtain an Al-free material, at a lower temperature (413K) in 7 days.

The beryllosilicate analog of zeolite beta and gtallosilicate analogs of zeolite beta as well mordenite were further modified by post-synthesis methods. The Be-beta was deberyllated by treatment with aqueous solution of $(NH_4)_2SiF_6$ and by acid leaching. During deberyllation with $(NH_4)_2SiF_6$ the sample was used in as-synthesized form containing the organic template instead of the NH_4^+ form. This procedure produced a more crystalline material.

All the samples were characterized by XRD, SEM, TG-DTA, TPD of NH_3, FT–IR spectroscopy, MAS NMR spectroscopy, adsorption and catalytic reactions. On the basis of these results the following conclusions could be drawn :

1. The XRD patterns of the gallo- and beryllo-silicate beta were similar to those of [Al]-beta. A systematic displacement of all sharp lines towards lower 2θ values (higher d-spacings) was observed on isomorphous replacement of Ga^{3+} for Al^{3+}, whereas the displacement was towards higher 2 θ values (lower d-spacings) in the case of [Be]-beta. This suggests that the unit cell dimensions of zeolite beta increase on isomorphous replacement of Al^{3+} by Ga^{3+} due to the longer [Ga]-O bond compared to Al-O bond.In the case of [Be]–beta, the unit cell dimensions decrease slightly on isomorphous replacement of Al^{3+} by Be^{2+}, due to the relatively shorter Be-O bond, similarly, the XRD patterns of [Ga]-mordenite and Al-mordenite were identical. The

intensity of the major peaks in the XRD patterns of [Ga]-mordente was lower when compared to its Al-analog. The modified beta samples were highly crystalline and showed appropriate lattice variations. A remarkable observation on Be-Beta was that unlike the Al- and Ga–analogs, it was made up of a larger amount of polymorph B than polymorph A.

2. SEM revealed that the gallosilicate beta samples were made up of crystals of 0.4 - 0.6 μm and were more or less cubic. Beryllosilicate beta samples too consisted of cubic crystals .

3. The pore volume of Na-[Ga]-beta was about 0.21 ml/g. and that of Na-[Be]-beta was about 0.20 ml/g. The pore volume of Na-[Ga]-mordenite was found to be 0.17 ml/g.

4. The framework i.r spectrum (in the 400-1300cm $^{-1}$ region) of gallo- and beryllo-silicate-beta was compared with that of [Al]-beta having nearly the same silica to metal oxide ratio. The bands due to the external linkages of TO_4 tetrahedra shifted to lower wave numbers for [Ga]-beta compared to [Al]-beta.This shift is attributed to a change in the reduced mass of the -$(Si\text{-}O\text{-}Ga)_n$-harmonic oscillator compared to $(Si\text{-}O\text{-}Al)_n$– moiety.

In the case of [Be]-beta, the corresponding bands overlapped with other modes of vibration and ir shifts were not clearly observed in this case .

Similarly, the framework spectra in the region (400-1300 cm^{-1}) of [Al]-mordenite and [Ga]-mordenite indicated a similar trend. On introduction of [Ga], most of the bands were shifted to lower wavenumbers consistent with isomorphous substitution.

5. FT-IR spectra of the as-synthesized (containing TEA-template), calcined and NH_4^+ forms of [Ga]-beta and [Be]–beta were recorded and compared with that of [Al]-beta . In the case of H-beta , it was found that isomorphous substitution of (Ga for Al) had an even greater influence on the O-H stretching frequency than a change in the framework structure from beta to MFI . FTIR spectra of calcined samples ([Al]–beta, [Ga]–beta and [Be]-beta) indicated that the optimum temperature for calcination in air should to be around 730, 723 and 673K, respectively. At these temperatures most of the carbonaceous material was removed without excessive elimination of the bridging hydroxyl groups. However the bridging hydroxyl groups disappeared even at this temperature (673K) in the case of [Be]-beta. Similarly, the results of the ir spectra of the Na^+- and NH_4^+-[Ga]-beta were consistent with those observed for the Na^+- and NH_4^+-[Al]-beta and indicated an optimum temperature in the range of 673- 723K, for removal of organics as well as deammoniation. Analogous resultswere obtained for modified samples. Similar studies were also carried out on Al- and Ga-mordenite zeolites.

The samples were also characterized by the i.r spectra of adsorbed pyridine. The results of pyridine adsorptions not only confirm the presence of Bronsted and Lewis acid sites, but also indicated that the relative concentration of Lewis to Bronsted acid sites in [Be]- and [Ga]-zeolites was higher than that of the [Al]-analog.

The FTIR studies on the adsorption of D_2O and benzene helped to establish the relative acid strength of beta compared with ZSM-5 and Y. On comparing the shifts induced by benzene adsorption on the absorption frequency of bridged hydroxyl groups, the relative strengths of the acidity of the zeolites may be arranged as : $[Al]_{(350)}$ -ZSM-5 >$[Al]_{(337)}$ - beta >$[Ga]_{(322)}$ - beta > $[Al]_{(300)}$ - Y > $[Be]_{(290\ cm^{-1})}$-beta.

6. The results of the t.p.d of NH_3 in the case of the gallo- and beryllo-silicate beta indicated that the isomorphous substitution of Ga or Be for Al decreased the strength of the strong acid sites in the beta framework, lowering the relative acidity of the zeolites which is in the order : [Be]-beta < [Ga]-beta < [Al]-beta .

7. The thermal stabiltiy of beta zeolites was found to be in the order :

[Be]-beta < modified [Be]-beta < [Ga]-beta < [Al]-beta

Similarly in the case of the mordenite system, the thermal stability of [Ga]-mordenite was less than that of [Al]-mordenite .

8. The solid state MAS NMR of ^{27}Al, ^{71} Ga and ^{9}Be spectra show that negligible amounts of octrahedral extraframework metal species are present in the beta samples. The MAS NMR spectra of ^{9}Be cation in [Be]-beta was studied on samples in different stages of preparation . It was possible to retain Be^{2+} cation in the lattice by controlled treatment up to the NH_4^+-form. On calcination of NH_4^+-form to obtain the H-form Be^{2+} was found to come out of the lattice. Similarly, the ^{29} Si and ^{27}Al spectra of [Al]-mordenite indicated the presence of negligible amounts of octahedral Al. Also, the ^{71} Ga MAS n.m.r spectrum showed the presence of Ga in tetrahedral positions in the [Ga]-mordenite sample.

9 The meta-xylene isomerization reaction was used as a tool to characterize the acidities of the Ga- and Be-isomorphs of beta as well as the gallomordenite zeolites. The p-xylene/o-xylene ratio in m-xylene conversion over both the isomorphs of beta Ga- and Be-isomorphs) was nearly equal to the equlibrium value. This indicated the lack of constraints for the diffusion of xylene isomers in zeolite beta. The isomerisation/ disproportionation (I/ D) ratio for Ga - Beta was found to be close to that of [Al]-beta

and in the range found for other large pore zeolites like mordenite. However, for Be-beta under comparable conversion conditions, isomerization activity was more than disproportionation .The activities of various isomorphs of beta was found to be in the order: modified Be-beta < Be-beta < Ga-Beta < Al-Beta as expected as per the order of acidities.

Similar results were obtained for the mordenite system. However, in Ga-mordenite dispropotionation was found to be more than in Al-mordenite, because of extra lattice Ga cations in the pores giving rise to increase in Lewis acidity.

Zeolite beta did not exhibit significant shape selectivity in the alkylation of benzene with long chain linear olefins. However the Ga- and Be-isomorphs resulted in increased selectivity for the 2-phenyl isomer, but deactivated rapidly. The modified berylloisomorph showed relatively low activity due to its low acidity, but deactivation was comparatively less. Mordenite exhibited more shape selectivity in this alkylation reaction compared to the other large pore zeolites. The gallomordenite sample exhibited higher initial activity but deactivated rapidly. No significant influence of the SiO_2/Al_2O_3 ratio (in beta zeolite) could be observed in this alkylation reaction.

LIST OF PUBLICATIONS

1. FT i.r. spectroscopic study of gallium beta.
S.G. Hegde; R.A. Abdulla; R.N. Bhat and P. Ratnasamy.
Zeolites, 12 (1992) 951.

2. Synthesis and characterization of a gallosilicate analog of zeolite mordenite.
A.J. Chandwadkar; R.A. Abdulla; S.G. Hegde and Janos B-Nagy
Zeolites, 13 (1993) 470.

3. Shape selective alkylation of benzene with long chain alkenes over zeolites.
S. Sivasanker; A. Thangaraj; R.A. Abdulla and P. Ratnasamy.
New Frontiers in Catalysis, Proceedings of the 10th International Congress on Catalysis, 19-24 July 1992, Budapest, Hungary. Elsevier Science Publishers B.V. (1993).

4. Synthesis and characterization of iron containing zeolite ZSM-5.
A.J. Chandwadkar; R.A. Shaikh; R.A. Abdulla; B. S. Rao; P.P. Bakare and R.F. Shinde.
Polish Journal of Appl. Chem ., XXXVII, 3-4 (1993) 161.

PATENT

1. A Process for the preparation of a crystalline gallosilicate catalyst composite Material.
P. Ratnasamy; A.J. Chandwadkar and R.A. Abdulla.767/DEL/91.